

Full-scale Tests on Stability of Cantilevered Steel Girders

by

Maha Essa

A thesis submitted in partial fulfillment of the requirements for the degree of

Master of Science

in

Structural Engineering

Department of Civil and Environmental Engineering

University of Alberta

© Maha Essa, 2024

ABSTRACT

Cantilever–suspended-span construction, commonly referred to as Gerber girder systems, is a popular roof-framing system for large single-storey buildings in North America. This system consists of a series of simply-supported girders in the principal framing direction that extend beyond the column as cantilevers, with the portion of the girder between the supports referred to as the back span. Due to the continuity of the cantilever segment over the column support, this system offers several advantages such as ease of erection, reduced moments and lower deflections in comparison to simply-supported beams. Despite these advantages, it has become clear following several collapses in Canada and the United States that the stability response of these systems is complex and in need of further investigation. Moreover, designers use disparate methods for these systems due to the lack of special design guidelines in the U.S. and Canadian steel design standards, despite the wide use of Gerber systems in practice.

To improve the understanding of the stability response of these systems, a full-scale physical testing program was developed consisting of 14 A992 W410×85 single-overhanging girders, with back span and cantilever lengths of 9.14 m and 1.83 m, respectively. The test specimen matrix was developed based on numerical simulations conducted by Esmaeili et al. (2021), which was used to evaluate the influence of various parameters on the LTB capacity of steel cantilevered girders. The design of the test setup was based largely on preliminary FEA simulations of the test specimens which provided the anticipated loads and displacements in the tests. The experimental results for capacity and displacements of each test girder were analyzed, considering the effect of influential parameters such as loading and bracing conditions, residual stresses, and initial geometric imperfections. Finally, the moment resistances obtained from the experiments for each

test girder were compared against resistances predicted by the CISC (Lasby 2019) design procedure.

To my father, Dr. Hesham Essa,
my biggest inspiration.

ACKNOWLEDGEMENTS

This research was funded by the CISC Centre for Steel Structures Education and Research (the Steel Centre). Financial support in the form of scholarships from the University of Alberta, DIALOG, and the Canadian Institute of Steel Construction is gratefully acknowledged, as well as the generous donation of test girders and ancillary testing segments by Supreme Group.

To Greg Miller and Cameron West, thank you for using your time and practical expertise to provide significant assistance throughout the physical testing program. To my supervisors, Dr. Robert Driver and Dr. Ali Imanpour, and colleague and Ph.D. candidate Vahab Esmaeili, thank you for sharing valuable insights and guidance. Finally, to the fellow students and professors of the Steel Centre, thank you for the many constructive discussions shared throughout this project.

TABLE OF CONTENTS

1	INTRODUCTION.....	1
1.1	Background.....	1
1.2	Statement of Research Problem.....	3
1.3	Objectives and Scope.....	4
1.4	Organization of Thesis.....	5
2	LITERATURE REVIEW.....	6
2.1	Critical Moment of Back Span.....	6
2.1.1	<i>CSA S16-19 (2019).....</i>	<i>7</i>
2.1.2	<i>AISC 360-22 (2022).....</i>	<i>8</i>
2.1.3	<i>Yura and Helwig (2010).....</i>	<i>9</i>
2.2	Critical Moment of Cantilever.....	10
2.2.1	<i>Nethercot (1973).....</i>	<i>10</i>
2.2.2	<i>Trahair (1983).....</i>	<i>11</i>
2.2.3	<i>Essa and Kennedy (1994).....</i>	<i>12</i>
2.2.4	<i>CISC.....</i>	<i>13</i>
2.2.5	<i>Andrade et al. (2007).....</i>	<i>13</i>
2.3	Previous Experimental Investigations on Lateral–Torsional Buckling.....	14
2.3.1	<i>Fukumoto et al. (1980).....</i>	<i>14</i>
2.3.2	<i>Dux and Kitipornchai (1983).....</i>	<i>15</i>
2.3.3	<i>Kubo and Fukumoto (1988).....</i>	<i>15</i>
2.3.4	<i>Ji et al. (2019).....</i>	<i>17</i>
2.3.5	<i>Essa and Kennedy (1993).....</i>	<i>17</i>
2.3.6	<i>Venter (2016).....</i>	<i>22</i>
2.4	Summary.....	23
3	TEST CHARACTERISTICS.....	25
3.1	Numerical Model.....	25
3.2	Test Specimen Selection Criteria and Matrix.....	28
3.2.1	<i>Lateral Bracing Conditions.....</i>	<i>28</i>
3.2.2	<i>Loading Conditions.....</i>	<i>34</i>

3.2.3	<i>Cross-sectional Properties</i>	37
3.2.4	<i>Configuration of Overhangs</i>	38
3.2.5	<i>Test Matrix</i>	41
3.2.6	<i>Range of Inelastic Behaviour</i>	45
3.3	Initial Geometric Imperfections	45
3.3.1	<i>Cross-section Measurements</i>	46
3.3.2	<i>Global Geometric Measurements</i>	49
3.4	Material Properties	53
3.5	Residual Stresses	56
4	EXPERIMENTAL PROGRAM	61
4.1	Test Setup	61
4.1.1	<i>Gravity Load Application</i>	62
4.1.2	<i>Boundary Conditions</i>	69
4.1.3	<i>Lateral Bracing Conditions</i>	71
4.2	Instrumentation	74
4.3	Girder Installation and Test Procedure	80
5	EXPERIMENTAL RESULTS AND DISCUSSION	82
5.1	Experimental Girder Capacities	82
5.1.1	<i>Experimental Range of Inelastic Behaviour</i>	84
5.1.2	<i>Effect of Residual Stresses</i>	85
5.1.3	<i>Effect of Lateral Bracing</i>	86
5.1.4	<i>Effect of Loading Condition</i>	88
5.2	Displacement Results	90
5.2.2	<i>Load–Deflection Behaviour</i>	98
5.2.3	<i>Effect of Initial Geometric Imperfections on Deflection</i>	103
5.3	Stress Results	106
5.4	Experimental Errors	112
5.5	Comparison of Test Results with CISC Design Procedure	115
6	CONCLUSIONS AND RECOMMENDATIONS	127
6.1	Summary	127
6.2	Conclusions	128

6.3 Recommendations for Further Research	129
REFERENCES.....	131
APPENDIX A: MATERIAL PROPERTY PLOTS.....	135
APPENDIX B: MEASURED INITIAL GEOMETRIC IMPERFECTIONS	142
APPENDIX C: EXPERIMENTAL LOAD-DEFLECTION CURVES.....	157

LIST OF TABLES

Table 2-1: Summary of Kubo and Fukumoto (1988) test girders	16
Table 3-1: Geometrical properties of selected profiles for numerical study	27
Table 3-2: Variation of κ_1''' and κ_1' considered in test program	36
Table 3-3: Flange local slenderness ratio and ratio of moments of inertia for selected wide-flange sections in numerical simulation	37
Table 3-4: Test specimen mean dimensions	48
Table 3-5: Mean cross-sectional properties of W410×85	49
Table 3-6: Mean initial imperfections in experimental studies	52
Table 3-7: Maximum initial geometric imperfections in test specimens	53
Table 3-8: Specimens and their corresponding heats	54
Table 3-9: Mechanical properties of test specimens from tension coupon tests	56
Table 5-1: Experimental girder capacities	84
Table 5-2: Deflections at midspan of back span at peak load	93
Table 5-3: Deflections at cantilever tip at peak load	94
Table 5-4: Deflections at midspan of back span at post-buckling	95
Table 5-5: Deflections at cantilever tip at post-buckling	96
Table 5-6: Comparison of lateral deflection and twist at cantilever tip at buckling to initial sweep and twist for girders which failed by LTB	105
Table 5-7: Summary of compression flange longitudinal stresses at buckling	110
Table 5-8: Comparison of moment resistances from experimental results and CISC (2019)	124

LIST OF FIGURES

Figure 1-1: Gerber system.....	1
Figure 1-2: Bending moment diagrams associated with conventional and Gerber roof girders...2	2
Figure 1-3: Conceptual LTB curve	3
Figure 2-1: Loading and restraint conditions of test specimens (Essa and Kennedy 1993)	21
Figure 3-1: Typical overhanging girder investigated in numerical study (symbol \circ represents point of lateral support)	26
Figure 3-2: Typical roof framing under a schematic load pattern.....	28
Figure 3-3: Test specimen loading and restraint conditions	32
Figure 3-4: Effect of lateral bracing condition on flexural capacity of single overhanging girders.....	34
Figure 3-5: Load configuration	35
Figure 3-6: Effect of load pattern on nominal flexural capacity for C(T)–B(T) group	36
Figure 3-7: Effect of cross-sectional properties on the flexural capacity of cantilevered girders for C(T) - B(T) group	38
Figure 3-8: Effect of overhangs on the flexural capacity of cantilevered girders for C(T)–B(T) group.....	41
Figure 3-9: Loading and restraint conditions of test specimens (symbol \circ represents point of lateral support).....	44
Figure 3-10: Initial imperfection measurement locations along test girder	46
Figure 3-11: Cross-section measurements of test specimens.....	47
Figure 3-12: Sweep distribution for LRC2-0.80	50
Figure 3-13: Camber distribution for LRC2-0.80	51
Figure 3-14: Initial twist distribution for LRC2-0.80	52
Figure 3-15: Identification and location of tension coupons.....	55
Figure 3-16: Cutting locations for residual stress measurements for W410×85	57
Figure 3-17: Sections for residual stress measurements after cold-sawing	59

Figure 3-18: Residual stress distribution of W410×85.....	60
Figure 4-1: Model of experimental test setup (test specimen shown in blue).....	62
Figure 4-2: Cardinal directions on plan view of test setup	62
Figure 4-3: Gravity load mechanism at laterally braced load points	64
Figure 4-4: Test frame setup	65
Figure 4-5: Gravity load mechanism at unbraced cantilever tip	66
Figure 4-6: GLS and load collar setup at the cantilever tip.	67
Figure 4-7: Load collar components	69
Figure 4-8: Vertical support detail	70
Figure 4-9: Vertical support in the longitudinal direction.....	71
Figure 4-10: Bracing bracket used at load points with Acetal sheet.....	72
Figure 4-11: Cylindrical Acetal on test girder flange	72
Figure 4-12: Bracing detail	73
Figure 4-13: Instrumentation plan (LRC 1 and 4 shown).....	75
Figure 4-14: Miller-West Glider	76
Figure 4-15: Instrumentation setup at midspan of back span.....	77
Figure 4-16: Instrumentation setup at cantilever tip for LRC 2.....	77
Figure 4-17: Strain gauges mounted to top flange at second load point on back span	78
Figure 4-18: Strain gauges mounted to bottom flange at fulcrum support	79
Figure 4-19: Strain gauge mounted to top flange at fulcrum support	79
Figure 5-1: Load collar assembly change in LRC1-0.38	83
Figure 5-2: Downward deflection on back span and upward deflection at cantilever for LRC4-0.80 at the end of the test.....	91
Figure 5-3: Downward deflection at cantilever for LRC5-0.25 at the end of the test	91
Figure 5-4: Cross-sectional view of cantilever tip at end of LRC2-0.38 test.....	92

Figure 5-5: Load–lateral deflection curve at midspan of back span for LRC1-0.80100

Figure 5-6: Load–lateral deflection curve at midspan of back span for LRC1-0.25101

Figure 5-7: Load–lateral deflection curve for cantilever tip for LRC1-0.80101

Figure 5-8: Load–lateral deflection curve for cantilever tip for LRC1-0.25102

Figure 5-9: Load–vertical deflection curves for LRC1-0.80.....102

Figure 5-10: Load–vertical deflection curves for LRC1-0.25.....103

Figure 5-11: Strain gauges on bottom flange of fulcrum support (strain gauges shown in red)
.....107

Figure 5-12: Strain gauges on top flange of back span (strain gauges shown in red).....107

Figure 5-13: Load applied at cantilever tip versus longitudinal flange strains at bottom flange at
fulcrum support for LRC2-0.38108

Figure 5-14: Load applied at cantilever tip versus longitudinal flange strains at bottom flange at
fulcrum support for LRC2-0.25108

Figure 5-15: Load collar bending during loading LRC1-0.38 Retest113

Figure 5-16: Bending moment gradient under a 0.25 load ratio117

Figure 5-17: Assumed bending moment diagram for cantilever check by CISC method118

LIST OF SYMBOLS

A	=	Area of cross section using measured cross-sectional dimensions
b	=	Flange width
C_b	=	Moment gradient factor in AISC 360-22
C_{b-YH}	=	Moment gradient factor according to Yura and Helwig (2010)
C_w	=	Warping torsional constant
d	=	Section depth
d'	=	Depth of the girder between centres of flanges
E	=	Elastic modulus
F_{cr}	=	Critical stress
F_y	=	Yield stress
G	=	Shear modulus
h	=	Web depth
I_x	=	Major axis moment of inertia
I_y	=	Minor axis moment of inertia
I	=	Interaction factor in calculating elastic critical moment when cantilever segment is critical (Essa and Kennedy 1994)
J	=	St. Venant torsional constant
k	=	Distance between outside of the flange thickness to the web where the radius ends
k_2	=	Distance between edge of web and the end of the radius
L	=	Length of the unbraced segment
L_c	=	Length of cantilever segment of overhanging beam
L_b	=	Length of back span of overhanging beam; unbraced length
L_p	=	Limiting laterally unbraced length for the limit state of yielding
L_r	=	Limiting laterally unbraced length for the limit state of inelastic lateral-torsional buckling
M_0	=	Moment causing the largest bottom flange compressive at the end of unbraced length (Yura and Helwig 2010)
M_1	=	Moment at opposite end of M_0 (Yura and Helwig 2010)
M_A	=	Factored moment at one-quarter point of the unbraced segment
M_B	=	Factored moment at mid-point of the unbraced segment

M_b	=	Theoretical critical elastic moment of back span of overhanging beam
M_C	=	Factored moment at three-quarter point of the unbraced segment
M_{CL}	=	Moment at the middle of the unbraced length (Yura and Helwig 2010)
M_c	=	Theoretical critical elastic moment of cantilever segment of overhanging beam
M_{cr}	=	Theoretical critical elastic moment
M_{max}	=	Maximum factored moment in the unbraced segment; maximum moment
M^L_{max}	=	Local maximum bending moment along the back span
M_{Fmax}	=	Larger bending moment at the supports
M_{Fmin}	=	Smaller bending moment at the supports
M_n	=	Nominal moment resistance (largest moment along length of overhanging girder)
M_p	=	Plastic moment resistance
M_r	=	Factored moment resistance
n	=	Number of point loads on the back span plus 1
P_b	=	Point load on back span
P_{max}	=	Larger point load on the cantilever tips
P_{min}	=	Smaller point load on the cantilever tips
q_i	=	Magnitude of uniformly distributed load on back span
q_{max}	=	Magnitude of larger uniformly distributed load on cantilever segment
q_{min}	=	Magnitude of smaller uniformly distributed load on cantilever segment
s	=	Joist spacing
S_x	=	Elastic section modulus about the major axis
S_y	=	Elastic section modulus about the minor axis
t	=	Flange thickness
w	=	Web thickness
Z_x	=	Plastic section modulus about the major axis
ε	=	Longitudinal strain
κ'_1	=	Ratio of local maximum bending moment along the back span to the larger bending moment at the supports
κ'_2	=	Ratio of smaller bending moment at the supports to larger bending moment at the supports
κ''_1	=	Ratio of distributed load on the back span to the larger distributed load on the cantilever segments
κ''_2	=	Ratio of smaller distributed load on the cantilever segments to the

		larger distributed load on the cantilever segments
κ_1'''	=	Ratio of the load applied on the back span to the load applied on the cantilever tip
σ	=	Longitudinal stress; residual stress
σ_y	=	Yield stress
ϕ	=	Resistance factor in CSA S16-14
ϕ_b	=	Resistance factor for flexure in AISC 360-22
ω_2	=	Moment gradient factor for CSA S16-19

1 INTRODUCTION

1.1 Background

Cantilever-suspended-span construction, also known as the Gerber system, is a common steel roof framing scheme for large single-storey buildings in North America. This system, as shown in Figure 1-1, consists of a series of simply-supported steel girders in the principal framing direction that extend beyond the column as cantilevers, with the portion of the girder between the supports referred to as the back span. Drop-in spans (also known as suspended spans) are supported in alternate bays at the cantilever ends, and steel open-web steel joists (OWSJs) are used most commonly as the secondary framing members. Due to the continuity between adjacent bays, negative moments—where the top flange is in tension—are introduced at the supports, and therefore lower magnitudes of positive moments—where the bottom flange is in tension—are required to be resisted by the girder, as shown in Figure 1-2. As a result of these balanced moments, Gerber girders allow for a more efficient design—where lighter and shallower girders are adequate to carry the same loads as compared to simply-supported spans, which do not feature continuity over the vertical support. Furthermore, the system avoids costly and complex moment connections, making it faster to erect, and results in lower deflections than those seen in conventional roof girders (Rongoe 1996).



Figure 1-1: Gerber system

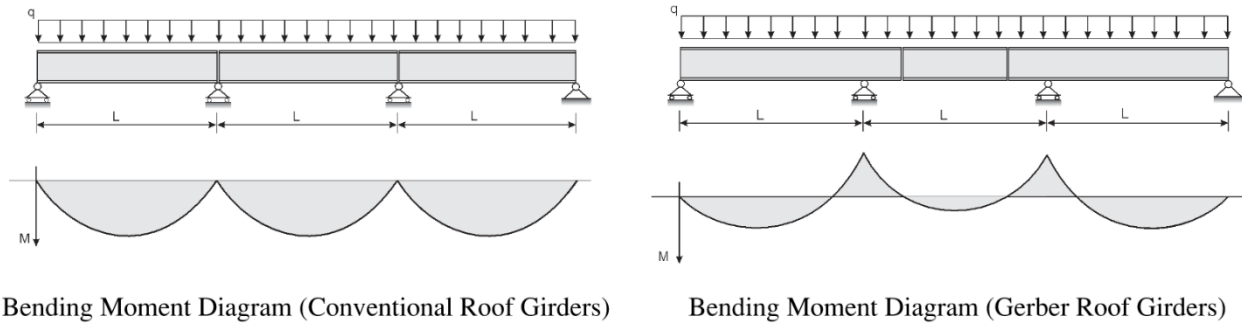


Figure 1-2: Bending moment diagrams associated with conventional and Gerber roof girders

Lateral-torsional buckling (LTB) is a potential type of girder failure characterised by simultaneous lateral movement and cross-sectional rotation (twist) under flexural bending. This can occur when the compression flange is either completely unbraced or braced at relatively large intervals along its length, and it may occur before the girder is able to reach its full cross-sectional capacity. Since continuous bracing of a member is not economically feasible, it is important to consider the potential for LTB failure in the design of any system that involves steel girders, as it can lead to structural collapse.

When a member's factored moment resistance, M_r , is plotted against its unbraced length, L , an LTB curve is obtained which showcases three distinct regions of bending resistance, as shown in Figure 1-3. The first of these is elastic LTB, which indicates that the member will regain its original shape upon removal of the applied load. Elastic LTB is observed primarily in slender girders with relatively long unbraced lengths. On the other hand, inelastic LTB means that the member will retain its deformed shape upon unloading, due to partial cross-section yielding occurring prior to the onset of instability, usually seen in members with intermediate stockiness. Lastly, stocky members with relatively short unbraced lengths reach their full cross-sectional capacity prior to the onset of LTB.

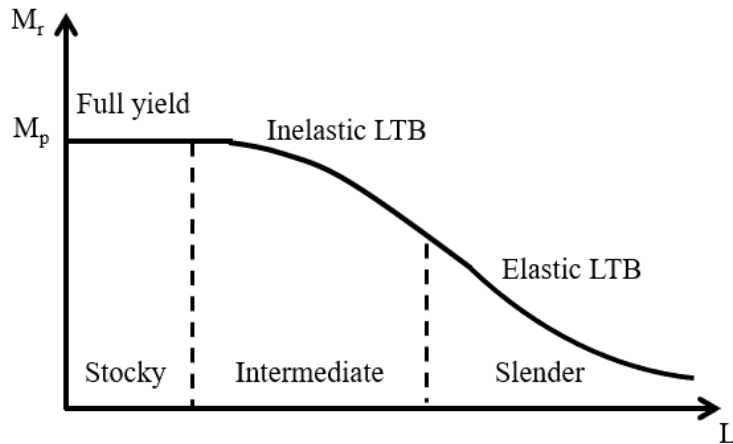


Figure 1-3: Conceptual LTB curve

If sufficient bracing is provided at discrete locations along a girder, it may be able to reach its full cross-sectional capacity prior to losing its flexural load-carrying ability. In this case, the location of maximum bending moment along the span of the girder reaches the plastic moment of the cross-section, and a plastic hinge is formed at this location as long as local buckling is precluded. Since the cross-section has fully yielded at this stage, plastic hinge formation results in significant deformation at the location of maximum bending moment. The experimental study presented herein investigates lateral bracing conditions that result in a failure mode of either inelastic LTB or reaching the full cross-sectional capacity.

Overhanging girders used in Gerber systems differ from built-in cantilever girders in the sense that warping is prevented at the root of built-in cantilevers. On the other hand, the girder is not fully prevented from warping at the root of the cantilever segment of an overhanging girder, and the extent of the effect of this warping on the stability of the system greatly depends on the flexural stiffness of the adjacent span.

1.2 Statement of Research Problem

Despite the advantages and widespread application of the Gerber system in steel buildings in North America, current steel design standards in Canada (CSA 2019) and the United States (AISC 2022) provide little guidance on the design of Gerber systems. The collapse of the roof in a

supermarket in Burnaby, BC in 1988 (Closkey 1988), as well as more recent collapses in Texas in 2011, Halifax in 2015, and Montreal in 2019 (Metten 2019) showed that a reevaluation of the stability response of these systems—specifically the LTB resistance and insight into various bracing strategies—is of crucial importance, and highlighted the need for a unified design method for these systems. The common factor in all these collapses was the assembly at the beam-column location, specifically the omission of a bottom chord extension and web stiffener at this location. The prediction of the LTB response in this system relies on the consideration of a variety of parameters, including loading and bracing conditions. The effects of these parameters can be realized from the results of full-scale physical testing of overhanging girders subject to different bracing and loading conditions. The experimental data obtained from these tests will be instrumental in developing a practical design method in the framework of the Canadian steel design standard for overhanging girders.

1.3 Objectives and Scope

The objective of this M.Sc. research project is to expand on the existing database on the capacity and behaviour of steel cantilevered girders under various loading and restraint conditions on the cantilever tip and back span, which will improve the understanding of their stability response and aid in the introduction of a practical and efficient design method for these systems. The study presented herein investigates evenly spaced joists provided to either the top flange or both the top and bottom flanges on the tip of the cantilever and along the back span, as well as the effect of various load patterns.

The experimental program includes physical tests of 14 full-scale ASTM A992 W410×85 (Class 1) single-overhanging girders. This is the first phase of a larger experimental program where double-overhanging girders as well as various cross-sections will also be tested. To achieve the objective of the research presented herein, the following tasks are required to be completed:

1. Conducting a literature review to understand the current database on the stability of steel cantilevered girders;
2. Identifying parameters most influential on the LTB capacity of cantilevered girders;
3. Developing a test matrix that includes the most influential parameters;

4. Developing an experimental test setup that accommodates the expected deflections under loading;
5. Performing 14 full-scale girder tests;
6. Analyzing the obtained moment resistance and deflection behaviour;
7. Discussing the effect of various loading and restraint conditions on the moment resistance and deflection behaviour; and
8. Comparing the test results with the Canadian Institute of Steel Construction (CISC) design procedure.

1.4 Organization of Thesis

This M.Sc. thesis is organized into six chapters. Chapter 1 presents background information on Gerber girders and their failure modes, including LTB and full cross-sectional strength. A literature review of past experimental research on LTB, as well as existing design methods for overhanging girders, is covered in Chapter 2. Chapter 3 presents the test specimen matrix and the selection criteria for this matrix based on numerical studies, as well as the measured initial geometric imperfections, material properties, and residual stresses of the girders used in the test program. An overview of the test setup is presented in Chapter 4, including the instrumentation used and the procedures followed for each individual full-scale test. The results—in terms of moment capacities, deflections, and measured longitudinal stresses—of these tests are then shown and discussed in Chapter 5, also highlighting the effect of various influential parameters on the obtained girder moment capacities and any experimental errors, as well as a comparison with the CISC design method for overhanging girders. Chapter 6 provides the key conclusions of this study and presents recommendations for future research in this area. Appendix A provides the measured initial geometric imperfections, while Appendix B provides the stress–strain curves obtained from standard coupon tests for each of the girders in the test program. Finally, the load–deflection curves for each of the test girders can be found in Appendix C.

2 LITERATURE REVIEW

This chapter presents an overview of relevant studies on the lateral–torsional buckling (LTB) capacity of overhanging girders. Various investigations performed by previous researchers, both numerical and experimental, are discussed, and methods of determining the LTB resistance in both the Canadian (CSA 2019) and American (AISC 2022) design standards are presented.

2.1 Critical Moment of Back Span

To assist in understanding the stability response of the Gerber system, it is necessary to analyze the current methods for calculating the theoretical elastic or inelastic critical moment of the back span of an overhanging girder. This analysis will provide insight into the stability of the system.

Essa and Kennedy (1994) proposed a method for determining the overall elastic buckling resistance of an overhanging beam, consisting of both a back span segment and cantilever segment, based on interaction buckling. Interaction buckling accounts for the beneficial effect of the less critically loaded segment restraining elastically the more critically loaded segment in an overhanging beam. This interaction method assumes that the back span of the overhanging beam is unrestrained and unloaded between supports, and that a concentrated load is applied at either the top flange or shear centre of the cantilever tip. The supports are assumed to be fork supports, where lateral deflections and cross-sectional twist are prevented, while allowing the section to warp.

Since the effects of warping restraints provided by the cantilever segment to the back span in the case where the back span is more critical was found to be insignificant (Trahair 1983), the overall buckling resistance of the overhanging beam in the case where the back span is critical can be taken as the resistance of the back span (Essa and Kennedy 1994).

A closed-form solution to the governing differential equations representing the critical elastic buckling moment of a simply-supported doubly-symmetric member was proposed by Timoshenko and Gere (1961). Ignoring any beneficial effect from the cantilever segment, Essa and Kennedy

(1994) proposed that the elastic critical moment of the back span of an overhanging beam can be calculated as:

$$M_b = \frac{\omega_2 \pi}{L_b} \sqrt{EI_y GJ + \left(\frac{\pi E}{L_b}\right)^2 I_y C_w} \quad 2-1$$

where L_b is the length of the back span, E is the elastic modulus, I_y is the minor-axis moment of inertia, G is the shear modulus, J is the St. Venant torsional constant, C_w is the warping torsional constant, and ω_2 is the LTB modification factor, which adjusts the resistance to account for the effect of various bending moment gradients on the back span.

The following sections highlight various available methods of calculating the LTB modification factor, as well as approaches to account for the extent of yielding in order to determine the nominal bending resistance of a given member.

2.1.1 CSA S16-19 (2019)

The Canadian steel design standard, CSA S16-19 (CSA 2019), prescribes the LTB modification factor intended to be used in Equation 2-1, given as:

$$\omega_2 = \frac{4M_{max}}{\sqrt{M_{max}^2 + 4M_A^2 + 7M_B^2 + 4M_C^2}} \leq 2.5 \quad 2-2$$

where M_{max} is the absolute value of the maximum moment along the back span, M_A is the absolute value of the moment at the one-quarter point of the back span, M_B is the absolute value of the moment at the midpoint of the back span, and M_C is the absolute value of the moment at the three-quarter point of the back span.

Upon calculation of the elastic LTB capacity (Equation 2-1), the standard requires determination of whether elastic or inelastic LTB is taking place before calculation of the nominal bending resistance. If elastic LTB governs, characterized by an elastic LTB capacity less than two-thirds of the plastic moment of Class 1 or 2 doubly-symmetric sections, the nominal bending resistance is calculated by multiplying the theoretical elastic buckling moment in Equation 2-1 by a

resistance factor (Equation 2-3). On the other extreme, stockier beams do not experience LTB before reaching their cross-sectional strength, and therefore the factored bending resistance is taken as the plastic moment (Equation 2-5) multiplied by a resistance factor. For beams that are neither stocky nor slender, inelastic LTB governs, and the capacity is represented by an empirical equation (Equation 2-4) which was developed to fit the results of previous tests on rolled I-beams (Baker and Kennedy 1984, Dibley 1969). However, this resistance is limited to the plastic flexural moment of the section multiplied by a resistance factor.

$$\text{If } M_b \leq 0.67M_p: M_r = \phi M_b \quad 2-3$$

$$\text{If } M_b > 0.67M_p: M_r = 1.15\phi M_p \left[1 - \frac{0.28M_p}{M_b} \right] \leq \phi M_p \quad 2-4$$

$$\phi M_p = \phi Z_x F_y \quad 2-5$$

where M_b is the critical elastic moment of the back span, M_p is the plastic moment capacity of the section, M_r is the factored moment resistance of the section, ϕ is a resistance factor (equal to 0.90 in CSA S16-19), Z_x is the plastic section modulus, and F_y is the nominal yield stress.

2.1.2 AISC 360-22 (2022)

Kirby and Nethercot (1979) presented a general expression for an LTB moment gradient modification factor, C_b , which is applicable to a variety of bending moment gradients along the unbraced length of a beam. The Specification for Structural Steel Buildings, AISC 360-22 (AISC 2022), prescribes a modified version of this factor, calculated as follows:

$$C_b = \frac{12.5M_{max}}{2.5M_{max} + 3M_A + 4M_B + 3M_C} \quad 2-6$$

where the moment parameters are the same as those defined for Equation 2-2.

This modification factor is to be used in the LTB resistance for doubly-symmetric compact I-shaped members bent about their major axis which, similar to CSA S16-19, is classified by the

standard into elastic LTB (Equation 2-7), inelastic LTB (Equation 2-8), or cross-section capacity (Equation 2-9).

$$\text{If } L_b > L_r: M_r = \phi_b M_n = \phi_b F_{cr} S_x \leq \phi_b M_p \quad 2-7$$

If $L_p < L_b < L_r$:

$$M_r = \phi_b M_n = \phi_b C_b \left[M_p - (M_p - 0.7 F_y S_x) \left(\frac{L_b - L_p}{L_r - L_p} \right) \right] \leq \phi_b M_p \quad 2-8$$

$$\text{If } L_b \leq L_p: M_r = \phi_b M_p = \phi_b F_y Z_x \quad 2-9$$

where L_b is the unbraced length, L_r is the limiting unbraced length for the limit state of inelastic LTB, L_p is the limiting unbraced length for the limit state of yielding, ϕ_b is the resistance factor, S_x is the elastic section modulus about the major axis, and F_{cr} is the critical stress.

The C_b modification factor can also replace ω_2 in the calculation of the elastic moment resistance in Equation 2-1, which would provide an identical solution to that obtained by Equation 2-7.

2.1.3 Yura and Helwig (2010)

Studying the effect of reverse-curvature bending on a beam with restraints provided only to the top flange, analogous to a typical back span of an overhanging girder, prompts the challenge of determining the actual unbraced length of a beam which experiences both positive and negative bending moments. Yura and Helwig (2010) confirmed that, although the inflection point represents the theoretical switch from compression to tension in the flange, this inflection point does not act as a point of bracing, and treating it as such is unconservative for many common scenarios.

Yura and Helwig (2010) performed various finite element simulations to propose several LTB modification factors for beams with reverse curvature bending, with either one or two inflection points along the span. Two cases were investigated: unbraced beams, where no intermediate bracing was provided along the length of the beam and loading was applied at the centroid of an I-shape, and gravity-loaded beams braced continuously on the top flange with load applied at the

top flange. For the case of bracing provided continuously on the top flange, the critical moment is calculated using the following LTB modification factor, which can then be used in Equation 2-1.

$$C_{b-YH} = 3.0 - \frac{2}{3} \left(\frac{M_1}{M_0} \right) - \frac{8}{3} \left[\frac{M_{CL}}{(M_0 + M_1)^*} \right] \quad 2-10$$

where M_0 is the moment causing the largest bottom flange compressive stress at the end of the unbraced length, M_1 is the end moment at the opposite end, and M_{CL} is the moment at the middle of the unbraced length. In the case where M_1 is positive, causing the top flange to be in compression, M_1 should instead be taken as zero in the term marked by the (*) in Equation 2-10.

Equation 2-10, however, only applies to beams with continuous bracing provided to the top flange under the gravity load. It could therefore be unconservative for use in a beam under discrete lateral bracing, such as the back span of a typical overhanging girder in a Gerber system, depending on the brace spacing. For the case of an unbraced beam along the back span, C_b is calculated using Equation 2-6.

2.2 Critical Moment of Cantilever

2.2.1 Nethercot (1973)

Nethercot (1973) studied the behaviour of single cantilevers and overhanging beams through finite element analyses, varying the level of load application, type of loading, and the restraint conditions present at the tip of the cantilever. An effective length concept, introduced first by Trahair (1963) and later adopted by design recommendations of the Structural Stability Research Council (SSRC) Guide to Stability Design Criteria for Metal Structures (Galambos 1988), is presented as follows:

$$M_{cr} = \frac{\pi}{k_b L} \sqrt{EI_y GJ + \left(\frac{\pi E}{k_b L} \right)^2 I_y C_w} \quad 2-11$$

where k_b is the effective length factor, presented as a table based on the type of loading, level of load application, and type of end restraint.

The effective length factors presented by Nethercot are valid only for the case of a cantilever span with an equal back span and an unloaded, unrestrained back span between supports. Kirby and Nethercot (1979) later restricted the effective length of the cantilever to not be less than the length of the back span; otherwise, Equation 2-11 would yield unconservative results.

2.2.2 *Trahair (1983)*

Built-in cantilever beams refer to cantilever spans where one end is fixed against rotations and deflection in all directions. The main difference between a built-in cantilever segment and an overhanging beam is the warping restraint at the support; while warping is prevented at the support in a built-in cantilever, an overhanging beam allows for a degree of warping, which also depends on the relative stiffness of the back span.

Trahair (1983) presented solutions for the buckling of built-in cantilevers under various loading, namely end moment, point load, and distributed load. Point loading was investigated under top flange, shear centre, and bottom flange loading, and it was found that the bending resistance of the members increased significantly when this loading was provided at the bottom flange. Trahair also found that the built-in cantilever model provided overestimations of the buckling resistance of an overhanging segment. Instead, cantilevers with supports that allow warping were investigated, and it was found that the capacity of the overhanging beam did not rely heavily on the degree of warping rigidity provided at the supports. A method based on interaction buckling was presented to obtain the elastic LTB resistance of a beam with two overhanging segments at each end of the back span, taking into account the buckling of the back span and cantilever segments separately. However, the only loading scenario considered in the study was a concentrated load applied at the tip of the cantilever.

2.2.3 *Essa and Kennedy (1994)*

In the case where the cantilever segment is more critical, Essa and Kennedy (1994) proposed that the elastic buckling resistance of the overall beam, M_{cr} , can be calculated as:

$$M_{cr} = M_c + I(M_b - M_c) \quad 2-12$$

$$\text{For top flange loading: } M_c = 1.5 \frac{GJ}{d} \quad 2-13$$

$$\text{For shear centre loading: } M_c = \frac{4}{L_c} \sqrt{EI_y GJ} \quad 2-14$$

where d is the depth of the cross-section, L_c is the length of the cantilever segment, I is an interaction factor which is a function of the ratio of the back span to the cantilever span, M_c is the elastic critical moment of the cantilever segment, and M_b is the critical elastic moment of the back span.

If M_b is less than M_c , the elastic critical moment of the cantilever segment is the same as M_c since the back span is more critical and the cantilever does not receive additional restraint from the back span. In this case, the overall buckling resistance of the overhanging beam can be taken as the resistance of the back span.

Equations 2-12 to 2-14 can be used for cantilevers that are free to warp at the fulcrum and apply to either a free or laterally restrained top flange at the cantilever tip (Essa and Kennedy 1994).

The interaction factor is determined as:

For cantilevers with no bracing:

$$I = -0.08 + 0.18 \left(\frac{L_b}{L_c} \right) - 0.009 \left(\frac{L_b}{L_c} \right)^2 \quad 2-15$$

For cantilevers with top-flange lateral bracing at the tip:

$$I = 0.064 + 0.162 \left(\frac{L_b}{L_c} \right) - 0.009 \left(\frac{L_b}{L_c} \right)^2 \quad 2-16$$

2.2.4 CISC

The Canadian Institute of Steel Construction (CISC) (1989) presented a design procedure for Gerber roof framing applications based on the recommendations of the SSRC Guide (Galambos 1988) on the design of overhanging beams which considers the back span separately from the cantilever segment. The critical elastic moment of the back span is calculated using the Roeder and Assadi (1982) equation for continuous top flange lateral bracing, and the resistance of the cantilever portion of the overhanging beam is calculated by accounting for lateral restraint and load height provided to the tip of the cantilever, and the effect of the continuity of the cantilever segment over the column, using the effective length concept introduced by Kirby and Nethercot (1979).

A more recent publication from CISC, Design Module 8 on Single-Storey Building Design (Lasby 2019), also requires treating the cantilever and back span segments separately. However, two checks are done for the back span: one for the maximum positive moment and one for the maximum negative moment. The check for the maximum positive moment on the back span calculates the critical elastic moment using the unbraced segment between lateral restraints on the back span subjected to the most critical bending moment gradient (i.e., closest to uniform bending). The critical elastic moment for the back span under maximum negative moment is calculated assuming the entire length of the back span as the unbraced length, obtaining a moment gradient factor considering loading along the entire back span. Lastly, the cantilever is checked under negative bending moment using the Essa and Kennedy (1994) interaction method, which assumes the entire length of the back span is unbraced. While Essa and Kennedy (1994) only assume the girder is unloaded between supports when calculating the critical elastic moment of the back span for use in the interaction equation, CISC (Lasby 2019) uses a conservative approach of assuming the back span is under uniform bending moment.

2.2.5 Andrade et al. (2007)

Andrade et al. (2007) investigated analytically and proposed equations for the elastic critical buckling moment of both doubly and singly symmetric I-section cantilevers that were either fully built-in (i.e., warping prevented at the support), or free to warp at the support. The loading

considered in the study included either a uniformly distributed load or a concentrated vertical load at the cantilever tip, as well as both shear centre loading and loading applied at either of the flanges. The effect of an adjacent span was therefore considered in the study by investigating a cantilever which is free to warp at the support, but the effect of the stiffness of such an adjacent span on the LTB capacity of the cantilever segment was not considered.

The authors found that the cantilevers which were free to warp at the support exhibited lower buckling capacities than those which were restrained from warping. The difference in capacity was small for long cantilevers and/or beams with stocky cross-sections, where the warping torsion generated during buckling was concluded to have a negligible effect on the buckling capacity. On the other hand, the difference in capacity between the free-to-warp and warping restrained beams became larger for shorter cantilevers and/or slender cross-sections. For these beams, warping torsion was concluded to have a large effect on the buckling capacity of the beam.

2.3 Previous Experimental Investigations on Lateral–Torsional Buckling

This section presents an overview of previous experimental programs that investigated the LTB response of steel W-shaped beams.

2.3.1 Fukumoto et al. (1980)

Fukumoto et al. (1980) tested 25 rolled girders of nominally identical shapes for each group of three different lengths (2.6 m, 2.0 m, and 1.5 m), totaling 75 tests. The experimental study aimed to investigate the effect of various beam parameters, such as geometric and material properties, on the obtained buckling strength. All girders were simply supported and tested under a concentrated vertical load applied at the top (compression) flange at midspan. End supports formed a torsionally pinned support, where twist was prevented but warping was allowed. Residual stress and material property measurements were recorded, as well as initial geometric imperfections such as initial out-of-straightness about the major and minor axes and the angle of twist. The study found that the parameter which had the largest influence on the variation of the ultimate strength is the plastic

moment of the member, which takes into account actual yield stresses and geometric imperfections impacting the cross-sectional dimensions.

2.3.2 *Dux and Kitipornchai (1983)*

Dux and Kitipornchai (1983) conducted a series of experiments on nine simply supported laterally continuous I-beams to investigate the influence of a moment gradient on the inelastic LTB resistance. The beams were tested in three groups of three, with each group having a different moment gradient. The loading configurations present in each of the three groups was: 1) a single concentrated load at midspan, 2) one concentrated load at a quarter of the length of the beam, and an equal concentrated load at three quarters of the length, and 3) two unequal concentrated loads applied at the same locations as in case 2. Each of the load points, as well as the end supports, was restrained both laterally and torsionally, and loading was applied at the top flange. Measurements of geometric imperfections and material properties were also included in the experimental study.

The experimental results show that the LTB capacity is a function of the moment gradient, where beams with a less severe moment gradient were able to sustain loads which resulted in a maximum moment very close to the plastic moment of the section, while the beams loaded under a uniform moment buckled earlier.

2.3.3 *Kubo and Fukumoto (1988)*

Kubo and Fukumoto (1988) investigated experimentally the interaction between local and overall LTB of thin-walled W-shaped beams. This experimental program consisted of 22 W-shaped beams of four different cross-sections with spans between 1.5 and 3.35 m, chosen specifically to allow for inelastic LTB to take place. Table 2-1 shows the ranges of W-shape dimensions and material properties investigated in the study, where d is the cross-section depth, b is the flange width, t is the flange thickness, w is the web thickness, E is the elastic modulus, and F_y is the yield stress.

Table 2-1: Summary of Kubo and Fukumoto (1988) test girders

Property	Range
d (mm)	200 – 300
b (mm)	125 – 150
t (mm)	4.17 – 4.42
w (mm)	2.92 – 3.15
E (GPa)	211 – 215
F _y (MPa)	262 – 316

Tests for residual stresses and initial geometric imperfections were conducted on sections cut from the original test members prior to beginning the tests. Since all the cross-sections used in the experiments were built-up sections using high frequency resistance seam welding, it was found that this method of constructing a built-up section resulted in large residual stresses. Additionally, the seam-welded girders in this study exhibited smaller initial geometric imperfections compared to fillet-welded beams in previous studies. Material properties, such as the yield and ultimate strengths, were found to be smaller for thicker plates compared to thinner plates.

The loading of all test specimens consisted of a single vertical load applied to the top flange at the midspan of the beams. The restraints in the tests consisted of preventing lateral deflection and twist at the end supports of the test girders, while still allowing the beam to warp. No bracing was provided to the beam at the load point, but a pair of transverse stiffeners were attached to the web at this location.

A comparison was conducted between the experimental results for the ultimate capacity and the capacities predicted by design standards, particularly the European Convention for Constructional Steelwork (1981), the American Institute of Steel Construction (1986), the American Iron and Steel Institute Specification (1986), and the Canadian Standards Association (CSA 1984). It was found that the ultimate capacity of W-shaped beams that experienced local flange buckling, failing by a combination of local flange and lateral–torsional buckling, was greatly reduced compared to the ultimate capacity of five of the 22 specimens which did not experience local flange buckling prior to reaching its ultimate capacity. Furthermore, the aforementioned design approaches were

found to be in good agreement with the ultimate capacities observed from the results of the experimental study, and the calculated elastic vertical deflections agreed with the experimental results to a reasonable degree.

The experimental results were used to propose an interaction equation, which reasonably estimated the interaction between local and lateral–torsional buckling.

2.3.4 Ji et al. (2019)

Ji et al. (2019) conducted large-scale experimental testing on seven simply-supported welded girders with unbraced lengths of 9.75 m, all predicted to fail in inelastic LTB. The supports were torsionally pinned, meaning twist was prevented but warping was allowed. Eight evenly-spaced identical vertical loads were applied at the top flange level along the length of the girders to simulate a uniformly distributed load. Initial geometric imperfections were measured for each girder, and residual stresses were measured in a companion research project.

The moment resistances obtained from the large-scale tests were compared to predictions by CSA S16-14 (CSA 2014), adjusted to account for load height, and it was found that the predictions match reasonably with the test results for girders with initial lateral out-of-straightness values less than $L/3300$.

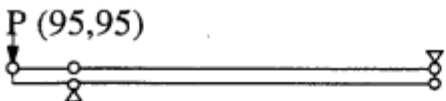
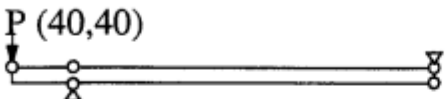
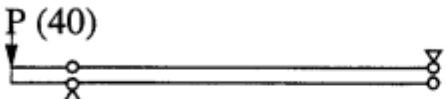
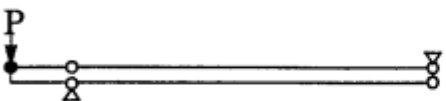
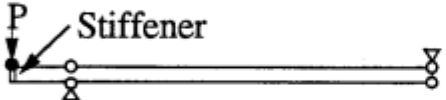
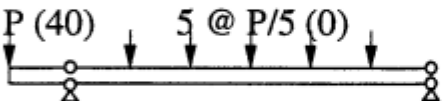
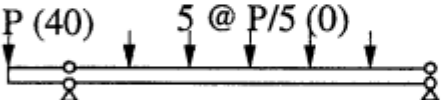
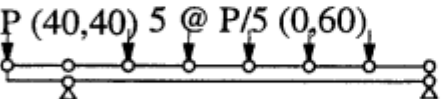
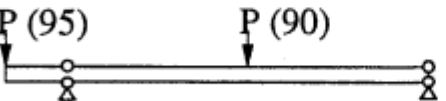
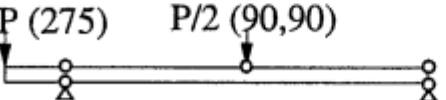
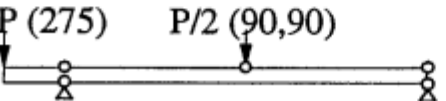
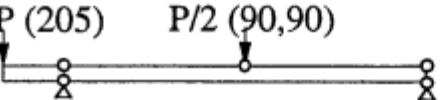
2.3.5 Essa and Kennedy (1993)

Essa and Kennedy (1993) investigated the effect of distortional buckling on the LTB capacity of hot-rolled W-shaped steel sections. The investigation was done through an experimental program as well as the development of a finite element model which was used to model the specimens tested in the experimental program. The finite element model is able to predict the distortional buckling capacity of steel beams under any combination of loading and restraint conditions.

In the experimental study, the authors performed 33 full-scale tests using 11 W-shaped steel single-overhanging girders, seven of which were W360x39 sections and four were W310x39 sections,

both providing reasonable span-to-depth ratios for cantilever-suspended-span construction.

The specimens all consisted of a 7.31 m simply supported back span with one 1.22 m cantilever extension. Various loading scenarios were investigated: the back span was tested under five concentrated loads, one midspan load, and no loads, while the cantilever was tested under one concentrated load at the tip. The effect of load height at each of these locations was also investigated, as well as the effect of adding stiffeners. Both lateral and torsional restraints, either independently or simultaneously, were included in the study, simulated in the tests by using thrust bearings, longitudinal and lateral rollers, and knife edges to achieve the desired degrees of freedom in each of the tests. Figure 2-1 shows the various loading and restraint conditions of the test specimens in the experimental study.

Test no.	Loading and restraint diagram	Section	Beam designation
1		W360x39	3B
2		W360x39	3B
3		W360x39	3B
4		W360x39	3B
5		W360x39	3C
6		W360x39	3A
7		W360x39	3A
8		W360x39	3A
9		W360x39	3K
10		W360x39	3K
11		W360x39	3K
12		W360x39	3K

a) Tests 1 through 12 (Essa and Kennedy 1993)

Test no.	Loading and restraint diagram	Section	Beam designation
13		W360x39	3K
14		W360x39	3K
15		W360x39	3K
16		W310x39	3V
17		W310x39	3V
18		W310x39	3V
19		W310x39	3V
20		W310x39	3T
21		W310x39	3T
22		W310x39	3T
23		W360x39	3G
24		W360x39	3G

b) Tests 13 through 24 (Essa and Kennedy 1993)

Test no.	Loading and restraint diagram	Section	Beam designation
25		W310x39	3P
26		W310x39	3P
27		W310x39	3P
28		W360x39	3H
29		W360x39	3H
30		W360x39	3H
31		W310x39	3M
32		W360x39	3D
33		W360x39	3D

1219 3657 mm

- Lateral restraint
 - Torsional restraint
 - || Web stiffener
 - △▽ Reaction
- (a,b) Height of load application and height of lateral restraint above top flange, mm, if applicable
- Lateral and torsional restraint

c) Tests 25 through 33 (Essa and Kennedy 1993)

Figure 2-1: Loading and restraint conditions of test specimens (Essa and Kennedy 1993)

The finite element model developed by the authors, which is able to model web distortion, residual stresses, and inelastic behaviour was found to be in very good agreement with the experimental results, giving a mean test-to-predicted ratio of 0.99. It was also found that the effect of web distortion on the capacity of W-shaped beams was more significant for beams with deeper cross-sections and thinner webs. This effect becomes even more pronounced in members that are braced torsionally along one flange and when the load is applied high above the shear centre. Stiffeners were found to effectively eliminate web distortion, which increases the buckling capacity.

It was also found that open-web steel joists, when properly welded to supporting members, provide both lateral and torsional restraint to the top flange, improving the resistance of the member by forcing the beam into a distortional buckling mode, which results in a higher buckling load compared to when only lateral restraint is provided to the girders in their experimental study. With all other aspects of the tests constant, it was found that the specimens with lateral restraint supplied to the column at the cantilever root have buckling loads up to 30% higher than those where no such restraint is provided. Furthermore, it was concluded that experimental results rely heavily on the level of restraint provided and are very sensitive to unwanted restraint or friction from reaction and load devices in the test setup.

2.3.6 Venter (2016)

Venter (2016) conducted physical experiments, as well as finite element (FE) investigations, to determine the elastic buckling capacity for a total of four built-in cantilevers and 20 single-overhanging beams. The beams tested were IPE_A100 beams—the smallest available cross-section, which reduced material cost—with a constant cantilever (and overhang) length of 2.5 m. The experimental study included both top flange and shear centre loading and ranging back-span-to-overhang ratios of 0.5 to 2.5, in increments of 0.5. Loading consisted of a single point load applied at the tip of the cantilever for both the built-in cantilever and overhanging beam tests. At the supports, the overhanging beams were restrained both laterally and torsionally, but allowed to warp. Tests on the material properties were conducted, and the initial geometric out-of-straightness was also documented. Twist and camber were not measured. It should be noted that this study excluded inelastic buckling or loading beyond the buckling capacity to investigate the post-

buckling response.

The results of the experiments displayed a scatter in the buckling loads in comparison to the FE predictions, where the buckling capacities in the tests were higher than predicted. The author attributed this variation to larger cross-sectional dimensions in the test specimens compared to nominal values, which would increase the torsional stiffness in the beam. Incidental friction at the support due to surface contact between the beam and the rollers at the support were also found to increase the buckling moment of the test beams, compared to FE analyses where the models had perfect boundary and loading conditions.

It was observed through the experimental study that as the length of the back span increased with respect to the length of the cantilever, the difference between the critical moments for shear centre and top flange loading decreased. It was also observed that, for top-flange loading, the critical moment increased between the built-in cantilevers (with an L_b/L_c ratio equal to zero) and $L_b/L_c = 1.0$, then decreased as L_b/L_c increased past 1.0.

2.4 Summary

Interaction methods of calculating the critical moment of an overhanging girder require treating the back span and cantilever segments separately, calculating the critical moment of each segment and then using the lower capacity as the overall capacity of the overhanging girder. However, the moment gradient factor used in calculating the critical moment of the back span, as proposed by past researchers, is shown to be conservative for cases typically observed in a Gerber system, such as discrete lateral bracing provided along the back span. Furthermore, calculations for the capacity of the cantilever portion of an overhanging girder rely on effective length factors which are restricted to very specific and limited loading and restraint conditions. To this day, there remains a relatively small amount of experimental data on the stability response of steel overhanging girders. Previous experimental programs on LTB were either on only simply supported girders, did not include cross-sections large enough to be used in typical Gerber construction today, or were only model experiments, therefore not capturing important data such as geometric imperfections or residual stresses. The numerical and experimental work conducted by Essa and

Kennedy (1993) provided an initial database for the stability response of steel cantilevered girders used extensively in Gerber systems. The work presented herein aims to expand on this database, by testing a wider range of practical loading and restraint conditions commonly encountered in typical cantilever-suspended span construction.

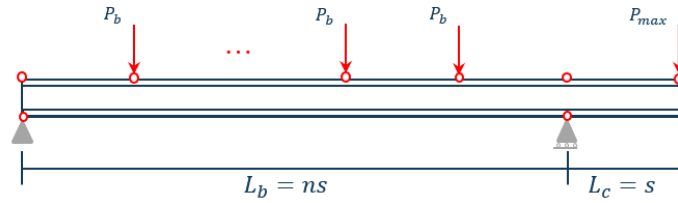
3 TEST CHARACTERISTICS

As part of the larger research program, a numerical model (Esmaeili et al. 2021) has been developed for overhanging girders. This numerical model was used to identify influential parameters affecting the lateral–torsional buckling (LTB) capacity of steel cantilevered girders and was also employed to develop the test specimen matrix. The primary goals were to select specimens and configurations that incorporated the various identified parameters to examine their effects on the stability of overhanging girders and to expand on the existing cantilever test database provided by Essa and Kennedy (1993). This chapter presents the development of the test specimen matrix, as well as methods of measuring initial geometric imperfections, material properties, and residual stresses.

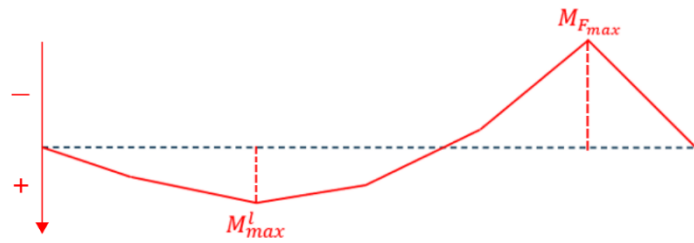
3.1 Numerical Model

A finite element model (Esmaeili et al. 2021) has been developed in the Abaqus program (Dassault Systèmes 2017) for overhanging girders. In flexural tests of overhanging girders, the possibility of distortional buckling, where the girder cross-section undergoes distortion and deflection simultaneously, can significantly influence the capacity of these girders, in addition to the global buckling limit state. The finite element model is capable of considering such buckling modes, as well as material and geometric nonlinearities, initial geometric imperfections, and residual stresses.

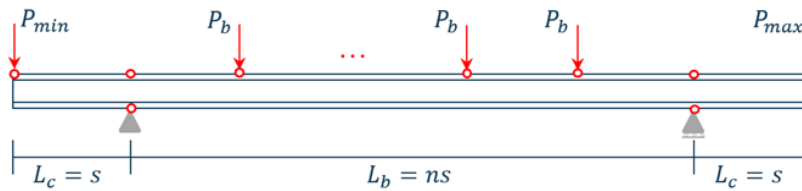
A typical overhanging girder considered in the numerical study is shown in Figure 3-1. In this figure, P_b refers to the point loads on the back span coming from secondary members such as open-web steel joists, P_{max} and P_{min} are the larger and smaller point loads at the cantilever tips, respectively, L_b represents the length of the back span, L_c is the length of the cantilever, s is the joist spacing, n equals the number of point loads on the back span plus 1, M_{max}^L is the local maximum bending moment along the back span, M_{Fmax} and M_{Fmin} represent the bending moments at the two supports, and κ'_1 and κ'_2 are defined as the ratios of M_{max}^L to M_{Fmax} and M_{Fmin} to M_{Fmax} , respectively.



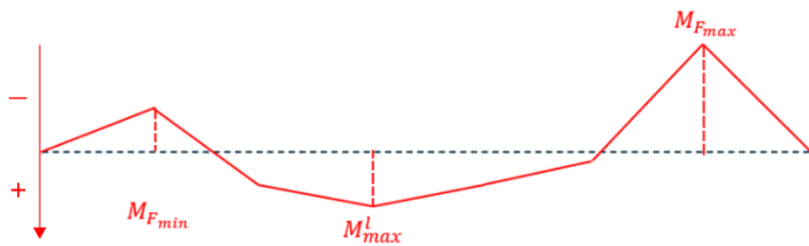
a) Configuration for single overhanging girder



b) Bending moment diagram for single overhanging girder



c) Configuration for double overhanging girder



d) Bending moment diagram for double overhanging girder

Figure 3-1: Typical overhanging girder investigated in numerical study (symbol \circ represents point of lateral support)

Numerical simulations of 266 overhanging girders, including 245 single-overhanging girders and 21 double-overhanging girders, were conducted. Seven standard steel wide-flange sections (W-

shapes) were included in the simulations, the cross-sectional properties and class (CSA 2019) of which are presented in Table 3-1. The specified yield stress of the material is 345 MPa conforming to both CSA G40.21 Grade 345WM (CSA 2013) and ASTM A992 (ASTM 2020). For all girders in the study, the length of the back span, L_b , is 9.0 m and the length of the cantilever, L_c , and joist spacing, s , are both equal to 1.8 m. The girders in the numerical study also included two full-depth web stiffeners, one at each support.

Table 3-1: Geometrical properties of selected profiles for numerical study

Cross-section	Flange Class	Web Class	$\frac{b}{2t}$	$\frac{h}{w}$	$\frac{I_x}{I_y}$	$\frac{L_b}{d}$
W410×85	1	1	5.0	34.8	17.5	22
W460×52	1	1	7.0	56.4	33.4	20
W460×60	1	1	5.8	53.6	32.0	20
W460×97	1	1	5.1	37.5	19.5	19
W460×144	1	1	6.4	31.5	8.7	19
W530×66	1	1	7.2	56.4	41.0	17
W530×82	2	1	7.9	52.8	23.5	17

In Table 3-1, $b/2t$ and h/w are the flange and web slenderness ratios, respectively, where b is the flange width, t is the flange thickness, w is the web thickness, and h is the clear depth of the web, giving rise to the flange and web classes; I_x/I_y is an index of the difference between the strong- and weak-axis geometric stiffnesses of the girder, and L_b/d is the span-to-depth ratio of the back span. A Class 1 flange and web has a $b/2t$ less than or equal to 145 divided by the square root of the yield strength and h/w less than or equal to 1100 divided by the square root of the yield strength, respectively.

Phenomena such as live loads or drifting snow require the consideration of the effect of pattern loading when studying the stability of Gerber systems. In these situations, adjacent bays may experience different intensities of loads. Figure 3-2 depicts a typical roof framing under a schematic load pattern considered in the analytical study. In this figure, q_i refers to the distributed load on the back span; q_{max} and q_{min} represent the larger and smaller distributed loads on the adjacent bays, respectively; and κ_1'' and κ_2'' are defined as the ratios of q_i to q_{max} and q_{min} to q_{max} ,

respectively.

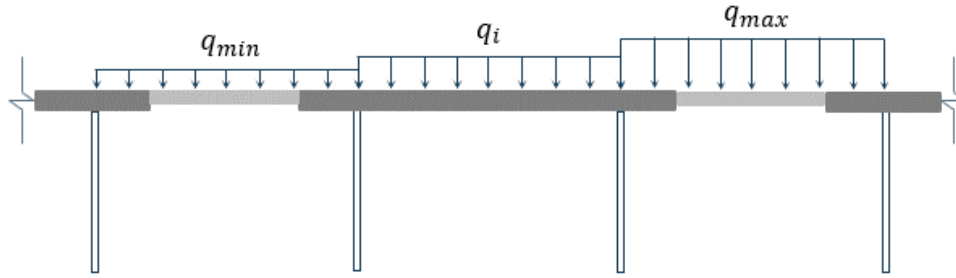


Figure 3-2: Typical roof framing under a schematic load pattern

To develop the Gerber stability database, the following range is considered for κ_1'' .

$$\kappa_1'' = \{2.00, 1.60, 1.30, 1.00, 0.77, 0.63, 0.50\} \quad 3-1$$

While a range was also considered for κ_2'' in the numerical study, the experimental study presented herein considers only single-overhanging girders where κ_2'' is equal to zero.

3.2 Test Specimen Selection Criteria and Matrix

Numerical simulations conducted by Esmaeili et al. (2021) were used to evaluate the influence of various parameters on the LTB capacity of steel cantilevered girders. The parameters with the highest influence, according to the numerical simulations, were considered in selecting the test specimens. The selection criteria are presented herein and include the lateral bracing conditions, loading conditions, cross-sectional properties, and configuration (single or double overhang). The final test matrix is presented, as well as the range of expected inelastic behaviours seen in the tests.

3.2.1 Lateral Bracing Conditions

Although the connection of an open-web steel joist (OWSJ) to the top flange of a Gerber girder in practice is known to provide a lateral as well as a torsional restraint to the flange, Esmaeili et al. (2021) took the conservative route of neglecting the effect of torsional restraint from the OWSJs in the numerical simulations and, therefore, it is not explored as part of this test matrix. In a typical Gerber system, there are two possible sources of loading at the cantilever tip: the first is the load

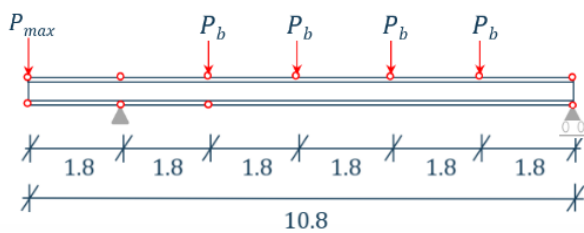
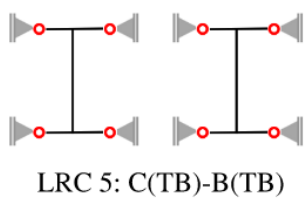
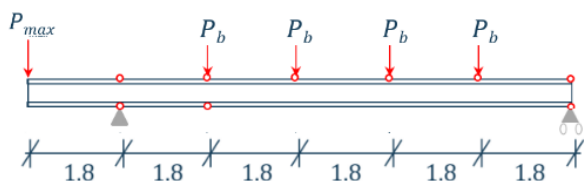
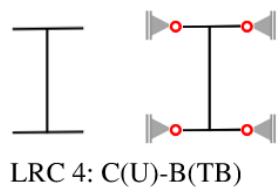
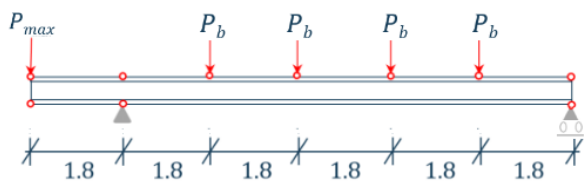
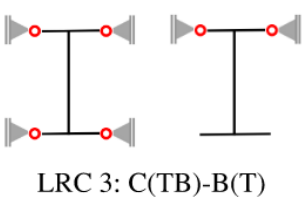
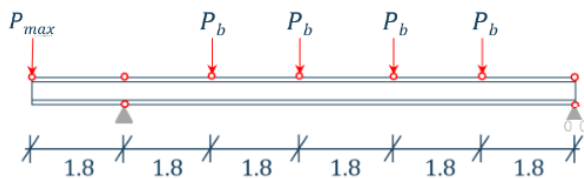
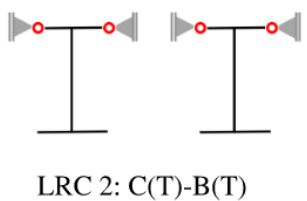
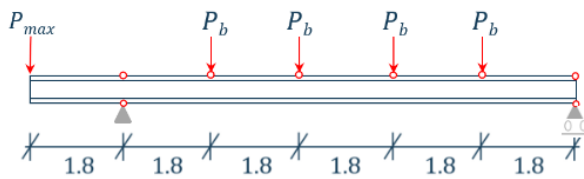
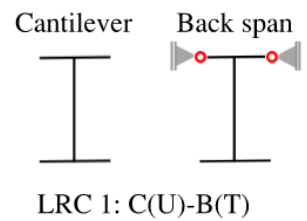
coming from the drop-in segment, transferred through a shear connection, and the second is from the presence of an OWSJ framing into the top flange of the girder at the cantilever tip. If there is no OWSJ framing into the girder at this location, the cantilever tip is considered unbraced, and the load applied at the cantilever tip comes entirely from the shear connection with the drop-in segment, which is applied at or near the shear centre. It is important to note that the numerical simulation results presented in this chapter consider shear centre loading for an unbraced cantilever tip and top flange loading for cases where the cantilever tip is braced. The lateral bracing condition present at the cantilever tip of a Gerber girder, as well as the presence of a bottom chord extension on secondary members off the column line, were included in the test matrix by categorizing the test specimens into five distinct groups according to the loading and restraint conditions (LRCs), as shown in Figure 3-3. Figure 3-3 also shows the cross-sectional view depicting the restraints provided to the cantilever tip and back span load location closest to the fulcrum (interior) support. The naming scheme of the groups is as follows:

- LRC 1: C(U)–B(T): cantilever tip is unbraced and back span is laterally restrained at the top flange;
- LRC 2: C(T)–B(T): cantilever tip is laterally restrained at the top flange and back span is laterally restrained at the top flange;
- LRC 3: C(TB)–B(T): cantilever tip is laterally restrained at both the top and bottom flanges and back span is laterally restrained at the top flange;
- LRC 4: C(U)–B(TB): cantilever tip is unbraced and back span is laterally restrained at the top flange at all load locations, with an additional lateral restraint provided to the bottom flange at the first load point from the fulcrum (interior) support; and
- LRC 5: C(TB)–B(TB): cantilever tip is laterally restrained at both the top and bottom flanges and back span is laterally restrained at the top flange at all load locations, with an additional lateral restraint provided to the bottom flange at the first load point from the fulcrum (interior) support.

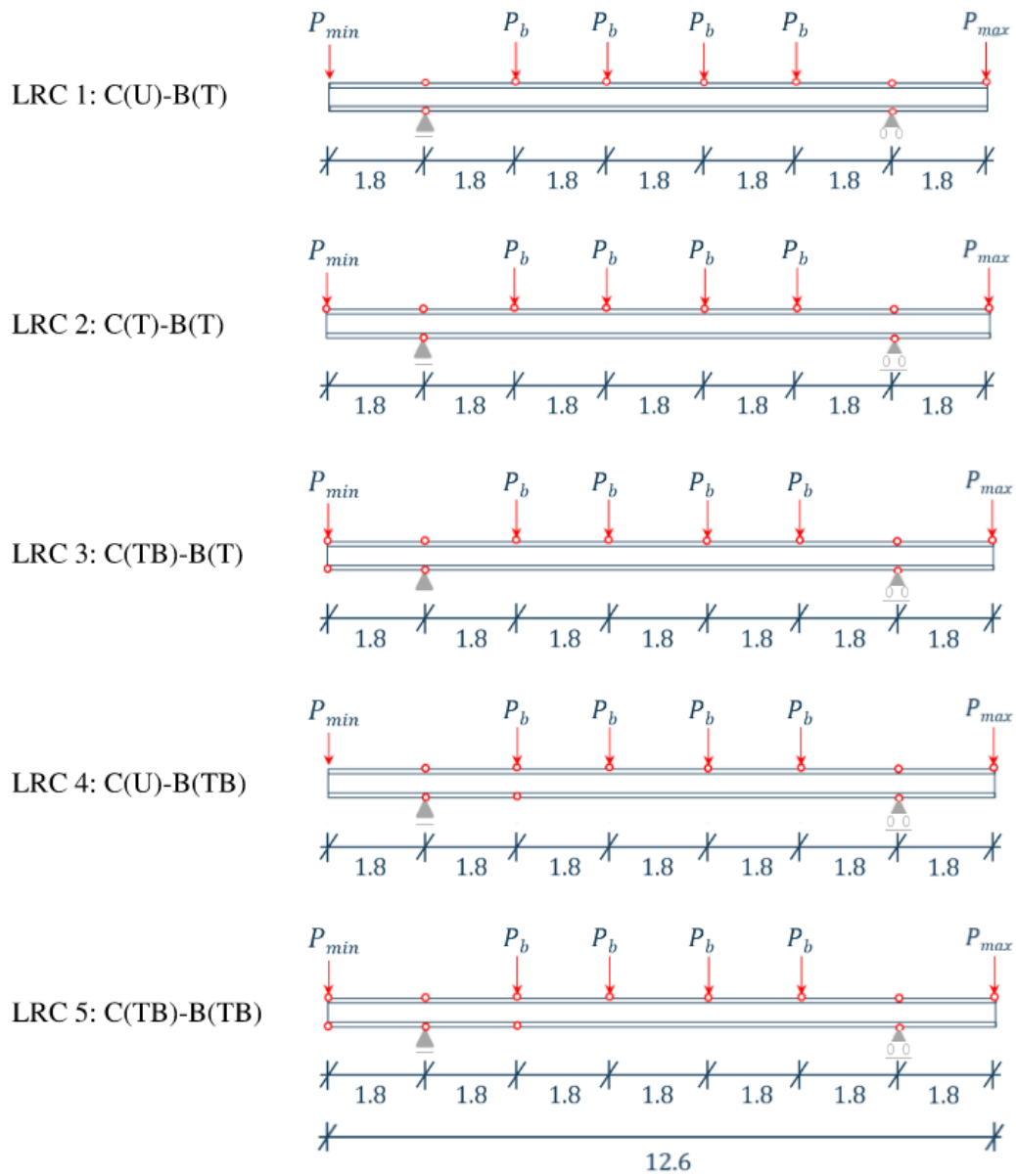
It should be noted that a restraint condition of C(T)–B(TB) (where the cantilever tip is laterally restrained at the top flange and back span is laterally restrained at the top flange at all load locations, with an additional lateral restraint provided to the bottom flange at the first load point from the fulcrum support) was not investigated. This is due to the fact that, under loading

conditions where the cantilever tip undergoes LTB and in the absence of a bottom flange brace at the cantilever tip, the most effective way to stabilize the overhanging girder and increase the LTB capacity is to first brace the bottom flange of the cantilever tip, rather than adding a bottom flange brace to the back span and keeping the cantilever tip bottom flange unbraced. Upon the addition of a bottom flange brace at the cantilever tip, additional stability can then be obtained by adding a bottom flange brace to the back span load location closest to the fulcrum. A restraint condition of C(TB)–B(T) therefore takes priority over C(T)–B(TB) in the test matrix.

To assess the impact of the various restraint conditions on the capacity of the cantilevered girders, the numerical model was used to analyze the effect of different L_b/d ratios, where L_b represents the length of the back span and d is the depth of the section, on the nominal moment resistance of the girder, M_n (taken as the maximum bending moment exhibited along the length of the overhanging girder) for the test specimen groups introduced above. This was achieved by varying κ_1'' values, specifically investigating values of 0.625, 1.00, and 1.60. The results of the numerical analysis are summarized in Figure 3-4.



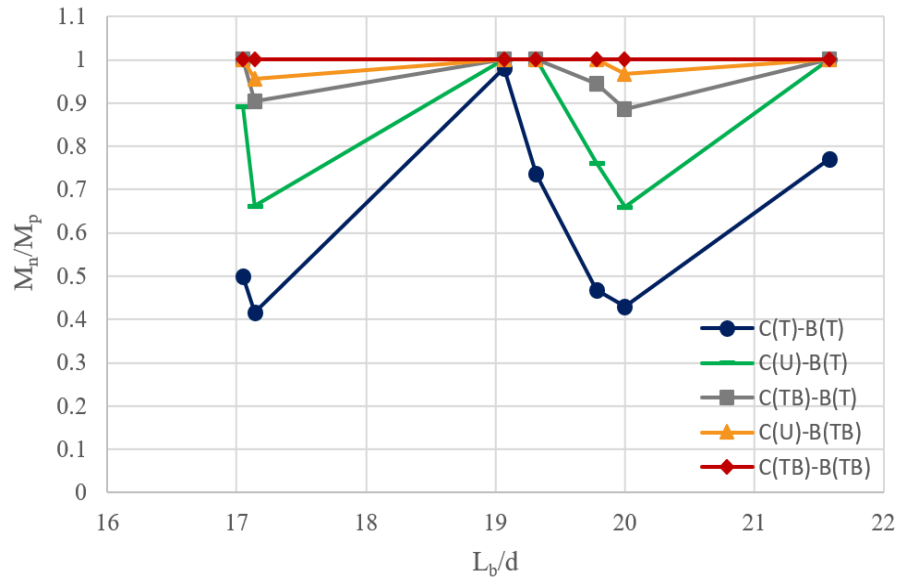
a) Single-overhanging girders (units in m)



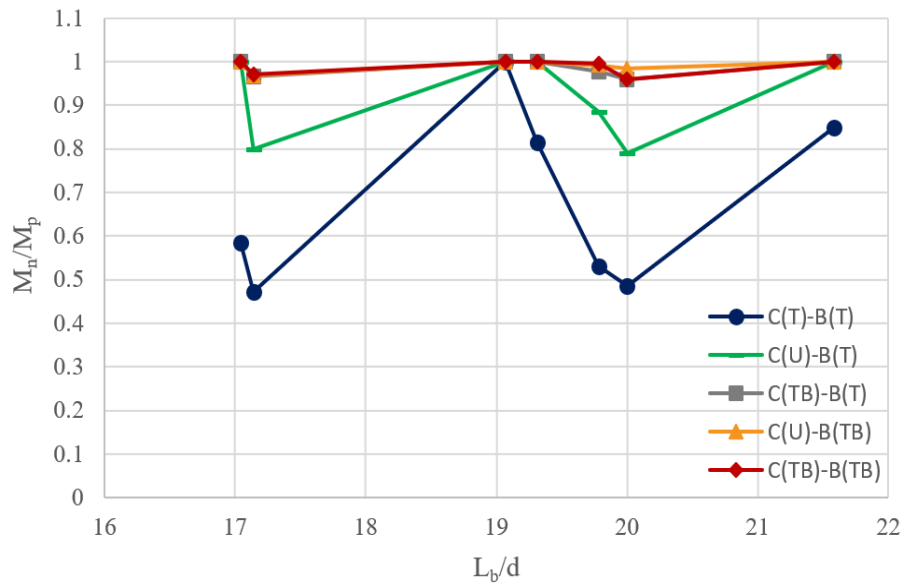
b) Double-overhanging girders (units in m)

• Lateral Restraint

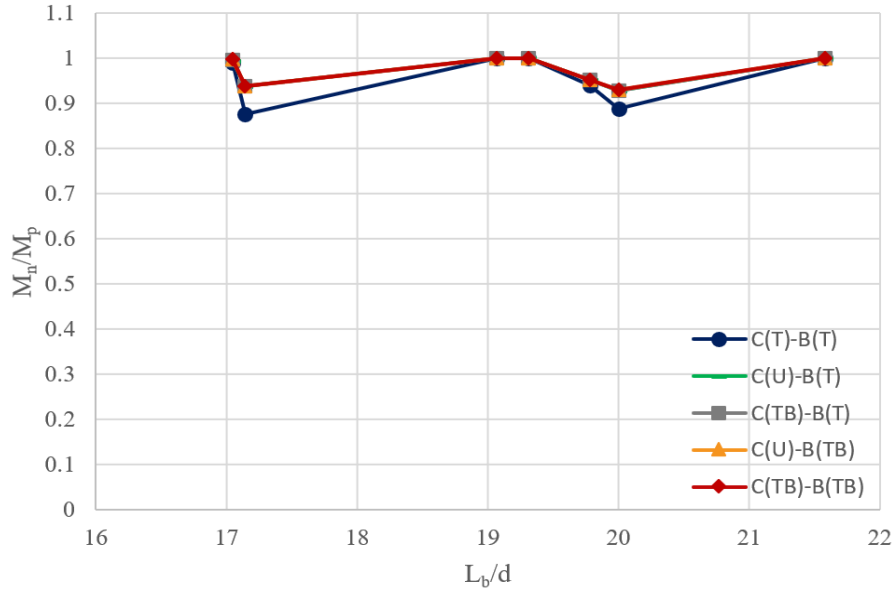
Figure 3-3: Test specimen loading and restraint conditions



a) $\kappa_1'' = 0.625$



b) $\kappa_1'' = 1.00$



c) $\kappa_1'' = 1.60$

Figure 3-4: Effect of lateral bracing condition on flexural capacity of single overhanging girders

The plots provided in Figure 3-4 illustrate the relationships between lateral bracing conditions and their impact on the system's capacity, as detailed below:

- Bottom chord extensions at the bracing location off the column line resulted in significantly higher capacities compared to models where only the top flange is braced along the entire back span.
- The C(T)–B(T) restraint case, where no bottom chord extensions are present on either the cantilever tip or back span, exhibited the lowest capacity.

The substantial variation in capacity with varying bracing conditions necessitated the inclusion of various lateral bracing conditions in the test matrix, as presented in Figure 3-3.

3.2.2 Loading Conditions

In a typical Gerber frame, the continuity of the girder over the column causes a negative moment, meaning that the bottom flange of the girder experiences compression. The length of the bottom

flange under compression and the location of inflection points depends on the bending moment gradient, and therefore on the loading condition, as depicted earlier in Figure 3-1 and quantified by the ratio κ'_1 . For this reason, it is important to evaluate the system under pattern loading, which is reproduced in this experimental study by testing the girders in each of the test specimen groups under different load ratios.

The selected load configuration in this experimental study considers a girder with a length of 10.97 m between the centerline of the load at the cantilever tip to the centerline of the support at the opposite end of the girder. The loading of the test specimens involves four point loads at 1.83 m intervals on the 9.14 m long back span, designated as P_b , as well as a point load applied at the tip of the 1.83 m long cantilever, called P_{max} , as shown in Figure 3-5. Each load point is assigned a node number from 1 through 5, and Node 4 represents the location of theoretical maximum positive moment along the back span. As lateral bracing also had to be provided at the load points, therefore requiring columns to be mounted on either side of the girder at the load points, the spacing of the load points was limited by the available holes in the laboratory strong floor, which are spaced in a 0.61 m (2 ft) grid pattern and are used to anchor the columns.

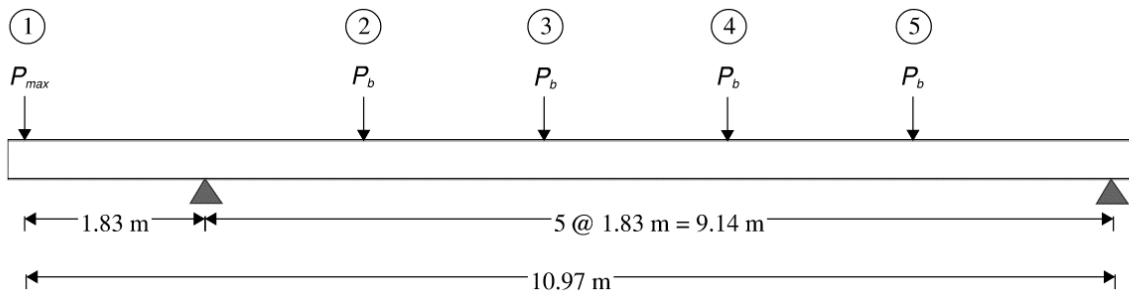


Figure 3-5: Load configuration

In each of the lateral bracing groups introduced in Section 3.2.1, a distinct load of P_{max} is applied on the cantilever tip. The load on the back span, P_b , is then varied as a fraction of P_{max} until a desired bending moment gradient is achieved. This is quantified by the ratio κ'''_1 , which is the ratio of P_b to P_{max} , and can take on three values in the test matrix: 0.80, 0.38, or 0.25. While a 0.50 load ratio was initially considered part of the test matrix, it was found not feasible to be simulated in the lab, due to the fact that the cantilever tip is expected to deflect upward under this load ratio,

which requires the release of hydraulic pressure at the actuator on the cantilever, while maintaining the load ratio itself required increasing hydraulic pressure. Table 3-2 summarizes the variation of κ_1''' considered in this experimental study, as well as their corresponding κ_1' values.

Table 3-2: Variation of κ_1''' and κ_1' considered in test program

κ_1'''	κ_1'
0.80	-2.00
0.38	-0.73
0.25	-0.35

The importance of testing different loading patterns is highlighted in numerical simulations (Esmaeili et al. 2021), which were used to analyze the influence of various load patterns, quantified by κ_1'' in the context of the numerical simulations, on the nominal flexural capacity of the girder. This effect is shown for three different cross-sections in the C(T)–B(T) lateral bracing group in Figure 3-6.

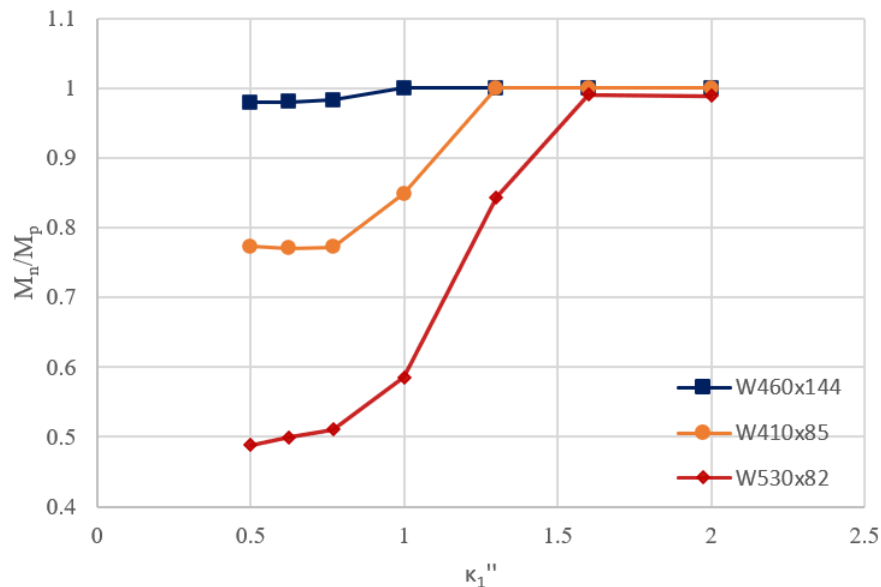


Figure 3-6: Effect of load pattern on nominal flexural capacity for C(T)–B(T) group

The plots provided in Figure 3-6 can be used to observe the relationships between load patterns and the capacity of cantilevered girders, as detailed below:

- Increasing κ_1'' past a value of 1.00, indicating a higher load on the back span than on the

cantilever, leads to a rapid increase in the flexural moment capacity for two out of the three beams investigated.

- The increase in flexural moment capacity as the load on the back span increases relative to the cantilever is due to the local maximum moment on the back span reaching the plastic moment capacity of the cross-section rather than the girder experiencing LTB.

3.2.3 Cross-sectional Properties

Three cross-sections included in the numerical study are a W410×85, W310×44.5, and W460×113. The W410×85 section complies with the Class 1 section width-to-thickness ratio limits, and the W310×44.5 and W460×113 profiles meet Class 2 section requirements. These will expand on the existing cross-sections in the Gerber stability database, a W360×39 and W310×39, tested by Essa and Kennedy (1993).

Numerical simulations showed that two dimensionless parameters are particularly influential on the LTB capacity of overhanging girders: the flange width-to-thickness ratio, $b/2t$, and the ratio of the strong- to weak-axis moments of inertia, I_x/I_y . Table 3-3 presents these ratios for each cross-section.

Table 3-3: Flange local slenderness ratio and ratio of moments of inertia for selected wide-flange sections in numerical simulation

Gerber Girder	$b/2t$	I_x/I_y
W410×85	4.97	17.5
W310×44.5	7.41	11.6
W460×113	8.09	8.78

Numerical simulation results show the significance of cross-sectional properties on the flexural capacity of overhanging girders. The variation of the flexural capacity as I_x/I_y changes for the C(T)–B(T) lateral bracing group are shown in Figure 3-7. This relationship is highlighted for different loading conditions, specifically investigating κ_1'' values of 0.625, 1.00, and 1.60.

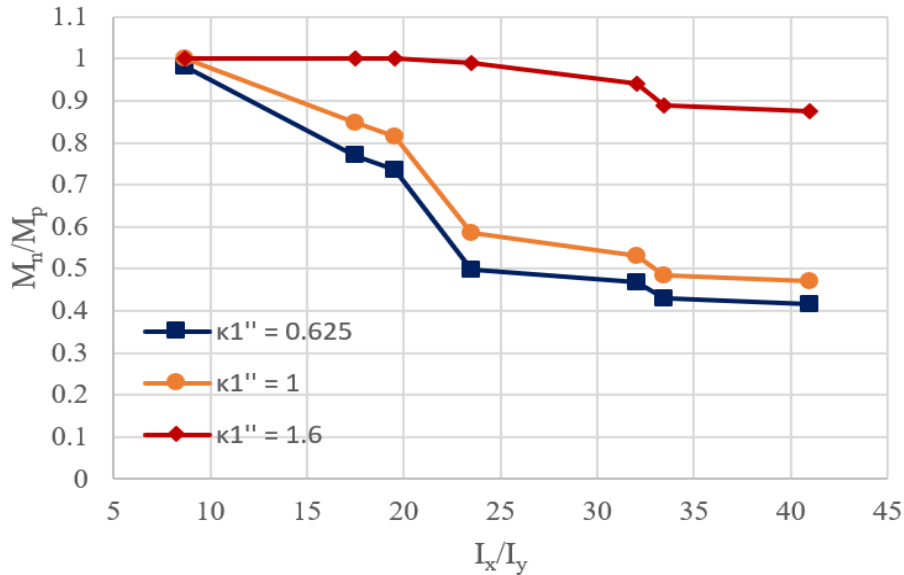


Figure 3-7: Effect of cross-sectional properties on the flexural capacity of cantilevered girders for C(T) - B(T) group

Important relationships between the capacity of the sections and the cross-sectional properties arise from analyzing the plots in Figure 3-7, such as:

- The capacity of the system decreases as the I_x/I_y ratio increases. Increasing the I_x/I_y ratio, indicating that the moment of inertia about the weak axis is decreasing relative to the moment of inertia about the strong axis, causes the system to be more susceptible to LTB.
- When the magnitude of the distributed load on the back span becomes larger than the magnitude of the distributed load on the cantilever (i.e., when κ_1'' becomes larger than 1.00), the influence of the cross-sectional properties on the nominal moment capacity diminishes due to the capacity approaching the fully plastic moment.

3.2.4 Configuration of Overhangs

The larger experimental study associated with this research program will incorporate both single and double overhanging girders. In practice, both configurations are used in Gerber systems depending on the location of the cantilever segment in the structural layout. While end spans typically consist of single overhanging girders, interior spans use girders which run continuously

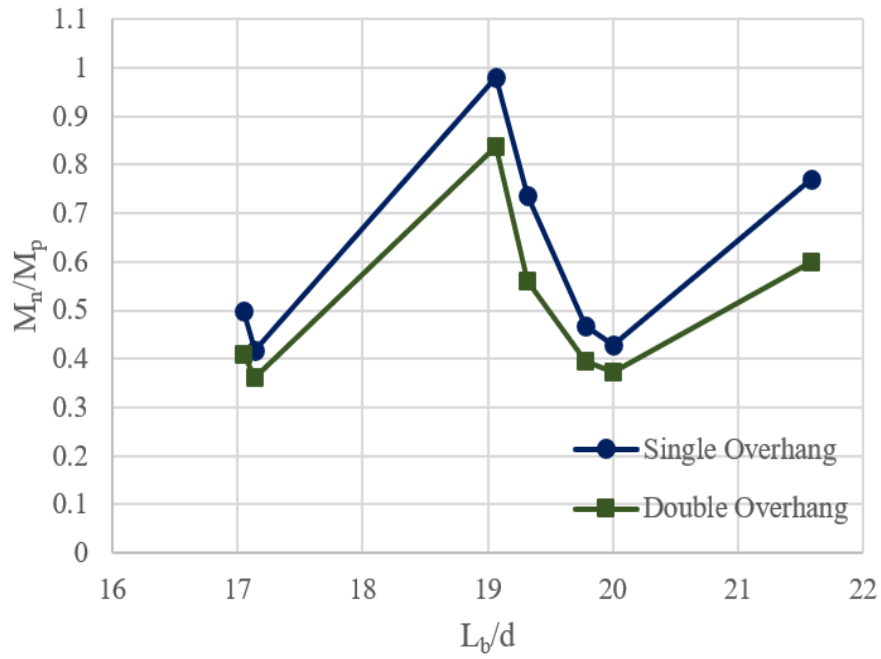
over two columns in a double overhanging configuration, connecting to drop-in segments on either end. Therefore, it is necessary to understand the stability response of both configurations of overhanging girders.

The test specimens consist of single overhanging girders with a total length of 10.97 m, between the centreline of the end support to the centreline of the load at the cantilever tip, and double overhanging girders with a total length of 12.80 m between the centrelines of the loads applied at each cantilever tip. These lengths effectively produce a full-scale Gerber system within the constraints of the laboratory's physical testing capacity.

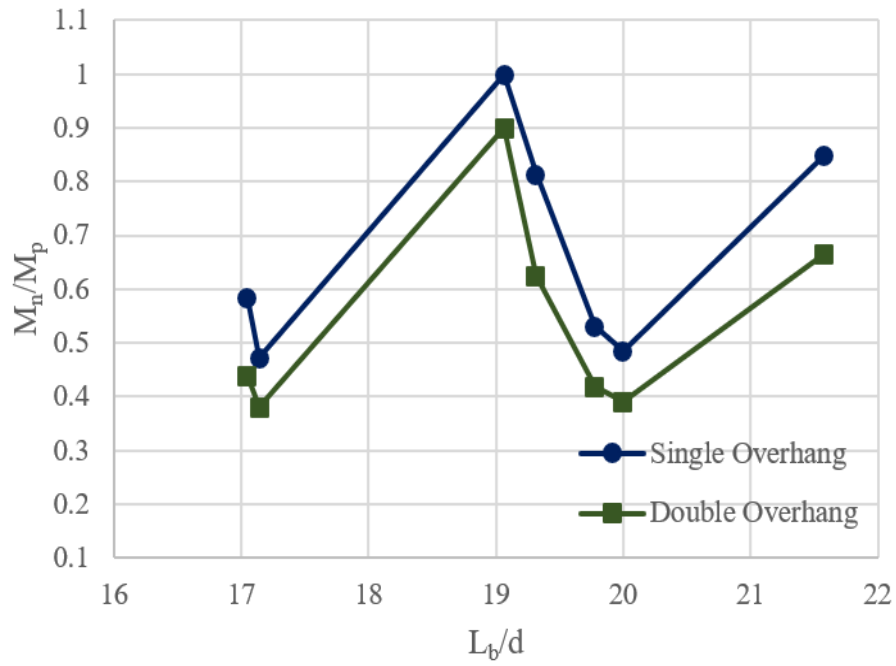
The numerical model was used to assess the effects of different L_b/d ratios, where L_b is the length of the back span (constant at 9.0 m) and d is the depth of the cross-section, on the nominal moment capacity of the girder, M_n , for both single and double overhanging girders. Different loading conditions were investigated, specifically κ_1'' values of 0.625, 1.00, and 1.60. The results of the analyses for the C(T)–B(T) group are shown in Figure 3-8.

The plots provided in Figure 3-8 can be used to observe important relationships between the overhang configuration and the capacity of overhanging girders, such as:

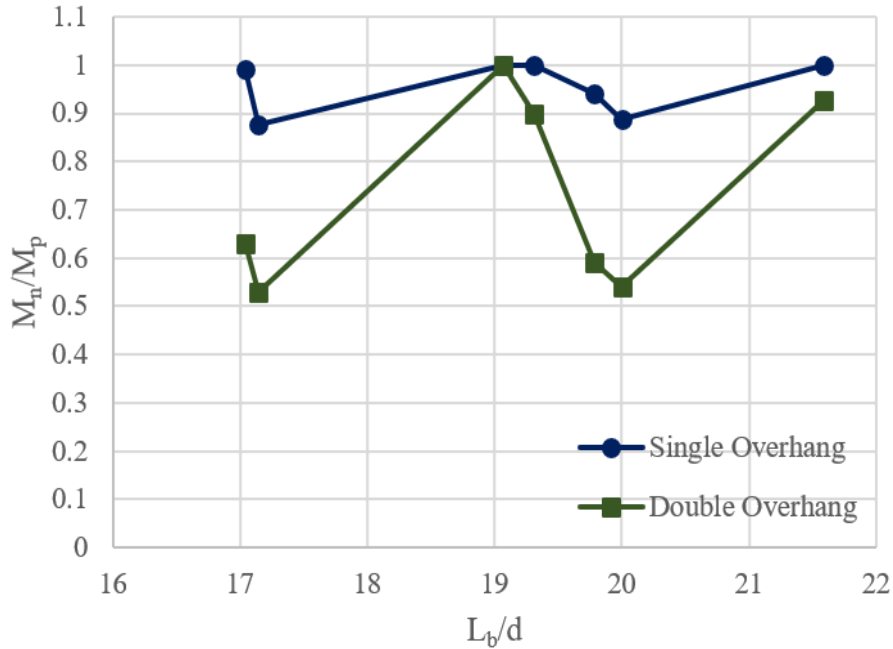
- The additional cantilever on double overhanging girders decreases the moment capacity of the girder for the same load ratio.
- The smaller capacities observed for a given double overhanging girder results from smaller κ_1' ratios for the same κ_1'' values as a single overhanging girder.
- The peaks in the charts correspond to cross-sections with smaller I_x/I_y values, which are consequently stronger than the rest of the sections in terms of weak-axis stiffness.



a) $\kappa_1'' = 0.625$



b) $\kappa_1'' = 1.00$



c) $\kappa_1'' = 1.60$

Figure 3-8: Effect of overhangs on the flexural capacity of cantilevered girders for C(T)–B(T) group

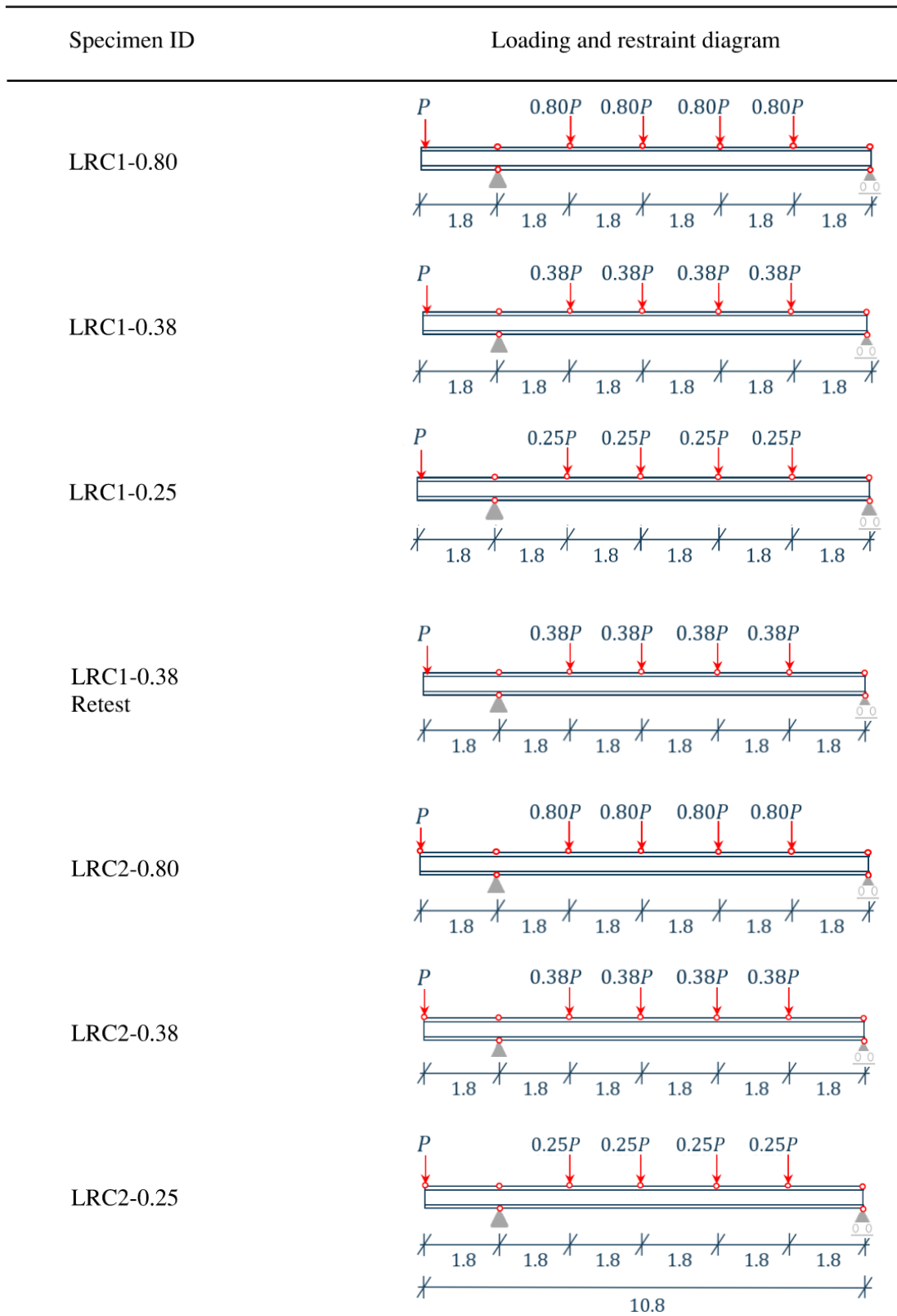
3.2.5 Test Matrix

The experimental study presented herein consists of 14 single-overhanging test girders, as presented in Figure 3-9. All 14 girders are W410×85 sections and come from three different heats of steel. One heat provided 8 of the 14 girders, while the other two heats provided 3 girders each. Four ancillary girders were also ordered, one from each of the three heats to perform material property tests, and one extra from the same heat of steel as 8 of the test girders to perform residual stress measurements. All test girders include two full-depth web stiffeners, one at each support. Although the unstiffened web crippling and yielding capacities of the test girders at the support locations exceeded the maximum reactions expected in the tests, it is considered good practice to include web stiffeners at column locations for increased resistance to local instabilities (CISC 1989). Moreover, lessons learned from past failures of the Gerber system such as those in British Columbia in 1988 (Closkey 1988), Texas in 2011, Halifax in 2015, and Montreal in 2019 (Metten 2019) necessitates the use of web stiffeners at column locations to prevent web crippling and

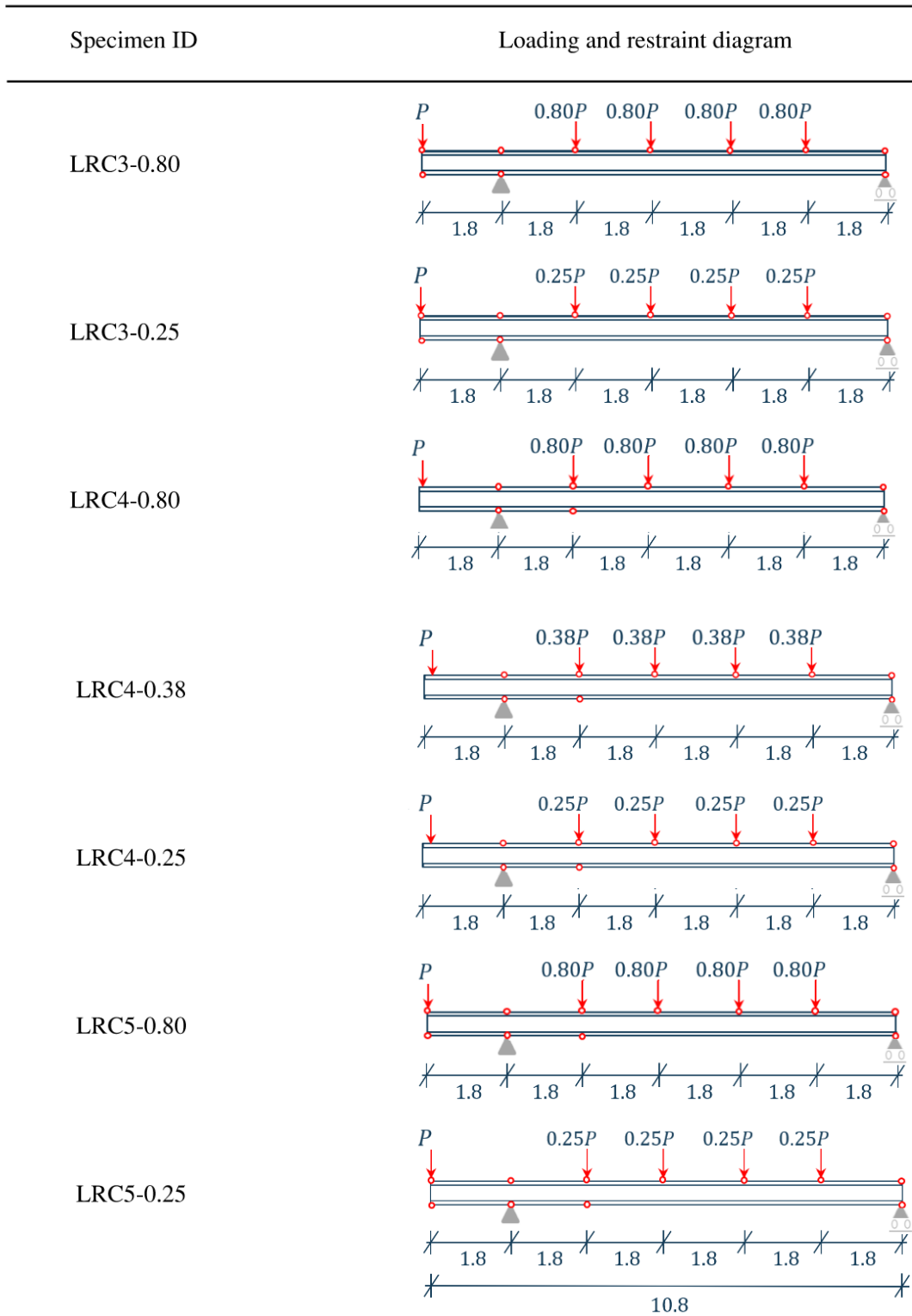
ensure proper alignment of the girder-column assembly. For this M.Sc. thesis, girders for each test are referred to by an alphanumeric specimen identification (ID) that indicates the loading and restraint condition (LRC) as well as the load ratio (κ_1''' value) which is induced in the test. The naming convention is 'LRC' (for loading and restraint condition) followed by: LRC number according to Figure 3-3 – ratio of the load applied on the back span to the load applied on the cantilever tip (κ_1'''). The reason for performing LRC1-0.38 Retest is explained in Chapter 5.

All girders were 11.43 m long, spanning 10.97 m between the centerline of the support and the centerline of the load applied at the cantilever tip. An additional length of 0.228 m was provided on either end of the girder for configuration in the test frame.

It should be noted that in Gerber construction typically seen in practice, the load is transferred from the suspended span to the cantilever tip of the overhanging girder through a shear connection. Part (or all, in the case of an unbraced cantilever tip) of the load on the cantilever tip is therefore applied at or near the shear centre. In the test specimen matrix of this experimental program, cantilever tip loads are applied at the top flange for all lateral bracing cases for ease of implementation in the laboratory, representing a more critical loading condition due to the destabilizing effect top flange loading has on the cross-section.



a) Test specimens in LRCs 1 and 2



b) Test specimens in LRCs 3 through 5

Figure 3-9: Loading and restraint conditions of test specimens (symbol \circ represents point of lateral support)

3.2.6 Range of Inelastic Behaviour

According to CSA S16-19 (CSA 2019), the limits for inelastic LTB for a Class 1 or 2 section is $0.67 < M_{max}/M_p < 1.0$, and this experimental study focuses on either LTB in the inelastic range or reaching the plastic moment capacity of the cross-section, with M_{max}/M_p values ranging between 0.65 to 1.04. As shown in Figure 3-1, there are two possible maximum moment ratios for each specimen: a maximum positive moment ratio (the local maximum moment on the back span), M_{max}^L/M_p , and a maximum negative moment ratio (the maximum moment experienced at the fulcrum), M_{Fmax}/M_p . Some of the loading and restraint conditions (LRCs) are expected to reach their fully plastic capacity, resulting in plastic hinge formation either at the location of maximum positive moment on the back span or maximum negative moment at the fulcrum and an M_{max}/M_p equal to (or greater than, due to the effect of material strain hardening) 1.00. Some LRCs are more likely to reach their full plastic capacities than others, with LRCs 3 and 5 having the most occurrences of plastic hinge formation.

Plastic hinge formation occurs where a cross-section has fully yielded, which results in large deformations at the location of the plastic hinge. Therefore, when the maximum positive moment ratio reaches 1.00, a plastic hinge forms at the location of local maximum moment on the back span. Since this coincides with a load point which is laterally braced in the test setup, it is therefore expected that the largest lateral deflection will occur at a location adjacent to the point load. Similarly, when the maximum negative moment ratio reaches 1.00, the plastic hinge forms at the fulcrum, which sees the largest negative moment. Since this location is also laterally braced in the test setup, it is expected that large lateral deflections will occur at the cantilever tip.

3.3 Initial Geometric Imperfections

As initial geometric imperfections are known to greatly influence LTB resistance of steel beams, they were measured for each girder tested in the experimental program. As shown in Figure 3-10, both cross-section imperfections and global geometric imperfections were measured at seven equally spaced points, which corresponded with the points of load application and vertical supports. The centerlines of the top and bottom flanges were marked at each of the seven locations

prior to measuring the geometric imperfections.

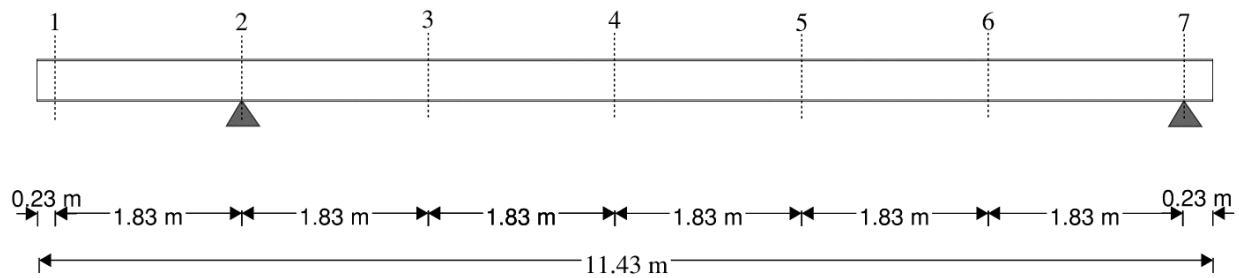


Figure 3-10: Initial imperfection measurement locations along test girder

3.3.1 Cross-section Measurements

To assess initial cross-sectional imperfections and obtain the dimensions of each girder, cross-section measurements were taken prior to testing at the seven stations. Figure 3-11 shows a schematic diagram of the dimensions measured on each cross-section. Table 3-4 summarizes the mean dimensions at the seven stations in Figure 3-10 for each of the test specimens. Redundant measurements (two of each) of a given dimension at a given station were critical to reduce inaccuracies in the measurement instrumentation and human error. Measuring tape was used to measure the section depth, d . Calipers were used to measure the flange thickness, t , and the flange width, b . The web thickness, w , was measured using an ultrasonic thickness measurement device. Fillet dimensions k_1 , which is the distance between the extreme surface of the flange and the end of the fillet radius, and k_2 , the distance between the edge of the web and the end of the radius, were measured using calipers only at the ends of the girders (rather than at the seven stations). For all girders, the differences between the measured and nominal cross-sectional dimensions are small and are within the allowable tolerances set by CSA G40.20-13 (CSA 2013).

According to CSA G40.20-13, the cross-sectional area of a structural-size shape is not to vary more than 2.5% from its nominal value (CSA 2013). Table 3-5 shows the cross-sectional area, A , major and minor axes elastic moduli (S_x and S_y , respectively), major axis plastic modulus, Z_x , and major and minor axes moments of inertia (I_x and I_y , respectively), based on the mean measured cross-sectional dimensions of the W410×85. In accordance with the SSRC Guide (Ziemian 2010),

the contribution of fillets to these cross-sectional properties was taken into account. Table 3-5 also presents the ratio of the measured to nominal cross-sectional properties, with the nominal value also taking the fillets into account. The measured cross-sectional area had the highest deviation from nominal, but still remained under 2.5% difference, while all other ratios were very close to 1.00.

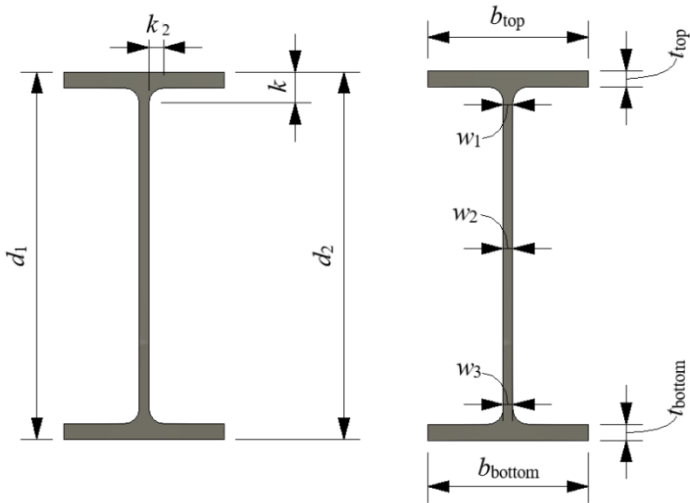


Figure 3-11: Cross-section measurements of test specimens

Table 3-4: Test specimen mean dimensions

Specimen ID	d (mm)	b (mm)	t (mm)	w (mm)	k (mm)	k_2 (mm)
LRC1-0.80	417	182	18.2	11.6	38.8	21.3
LRC1-0.38	417	182	17.9	11.5	38.3	22.1
LRC1-0.38 Retest	418	182	18.0	11.7	38.6	23.7
LRC1-0.25	418	182	18.0	11.6	36.2	21.3
LRC2-0.80	416	182	17.8	11.5	39.8	20.6
LRC2-0.38	418	182	17.9	11.6	41.0	21.8
LRC2-0.25	419	181	18.0	11.8	38.7	21.7
LRC3-0.80	419	181	17.9	11.5	37.1	19.9
LRC3-0.25	418	181	17.8	11.7	33.8	20.8
LRC4-0.80	419	183	18.0	11.7	39.2	20.4
LRC4-0.38	417	182	18.2	11.5	36.8	21.1
LRC4-0.25	417	182	18.0	11.6	35.4	22.5
LRC5-0.80	419	182	18.0	11.7	41.2	21.2
LRC5-0.25	418	183	17.9	11.6	37.8	20.8

Table 3-5: Mean cross-sectional properties of W410×85

Cross-Sectional Property	Measured	Measured/Nominal
A (mm ²)	11341.9	1.02
S_x (mm ³ ×10 ³)	1571.1	1.01
S_y (mm ³ ×10 ³)	199.4	1.00
Z_x (mm ³ ×10 ³)	1799.2	1.01
I_x (mm ⁴ ×10 ⁶)	328.2	1.01
I_y (mm ⁴ ×10 ⁶)	18.1	1.00

3.3.2 Global Geometric Measurements

The distance between the centre of the end support assembly and the centre of the bearing at the cantilever tip was taken as the length, L , of the test specimens. The distance between these points was measured three times using a Fluke 414D distance-measuring laser and averaged to obtain the length. The length of the extension of the girder past the cantilever load point and past the centre of the end support assembly was also measured. Measurements for initial out-of-straightness imperfections such as sweep (lateral out-of-straightness), camber, and twist were taken at the seven stations along the girder with the girder on level pedestals on the strong floor. Sweep and camber were measured at the top and bottom flanges, while twist was measured at the web.

Initial sweep of a given flange, done for both the top and bottom flanges, was determined based on measurements of the deviation of flange tips from a fine line which was stretched tightly along the girder length and held in place with magnets at each end of the girder. The flange centerline was marked along the girder, and the fine line was positioned such that it passed through the flange centerline at stations 1 and 7. The deviation of the flange tip to the fine line from the marked flange centerline was then measured at the remaining five stations. A positive sweep is taken as bowing towards the west side of the laboratory, looking at a plan view with the cantilever tip facing north.

The sweep distribution for specimen LRC2-0.80 is shown in Figure 3-12, and sweep distributions for all test specimens can be found in Appendix B. For the specimens listed in Table 3-4, the minimum and maximum initial sweeps (in mm) were found to be $L/3200$ and $L/1200$, respectively, in the top flange, and $L/4600$ and $L/1300$, respectively, in the bottom flange. The mean values of sweep for the top and bottom flanges were $L/1800$ and $L/2100$, respectively. According to CSA G40.20-13 (CSA 2013), the maximum initial lateral out-of-straightness for girders where there is no specified sweep is $L/1000$, and all specimens are within this limit.

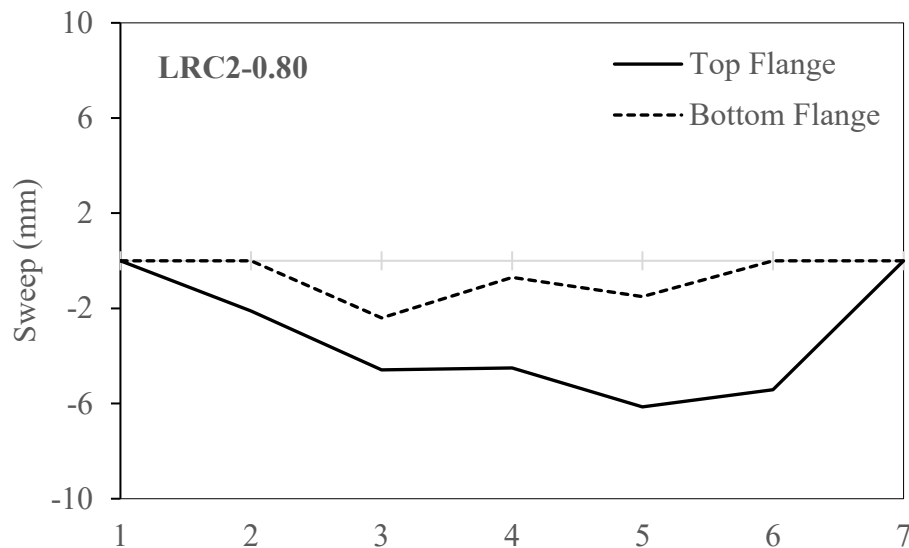


Figure 3-12: Sweep distribution for LRC2-0.80

Initial camber was determined using the self-levelling Fluke 180LG line laser level, which provided a continuous horizontal reference line above the respective flange for which camber was to be measured. The vertical deviation between the flange surface and the laser was measured at the seven stations. Using the measured vertical deviation at stations 1 and 7, combined with the horizontal distance between these two points, the slope between stations 1 and 7 was calculated (which represented the slope of the laboratory strong floor). The sloped line between stations 1 and 7 then allowed for the calculation of the camber at the remaining 5 stations along the girder by taking the difference between the vertical deviation for each of the 5 stations and the sloped line, with a negative camber corresponding to a sag. The camber distribution for specimen LRC2-0.80 is shown in Figure 3-13, and camber distributions for all test specimens can be found in

Appendix B. The minimum and maximum cambers (with units of mm) in all test specimens were found to be $L/2000$ and $L/900$, respectively, for the top flange, and $L/3700$ and $L/900$, respectively, for the bottom flange. The mean values of camber for all test specimens for the top and bottom flanges were $L/1400$ and $L/1500$, respectively. CSA G40.20-13 (CSA 2013) specifies a maximum initial camber of $L/1000$, and therefore there were two specimens which slightly exceeded this limit. These specimens were LRC1-0.80, which had a maximum bottom flange camber of $L/900$, and LRC5-0.25 with a maximum top flange camber of $L/900$.

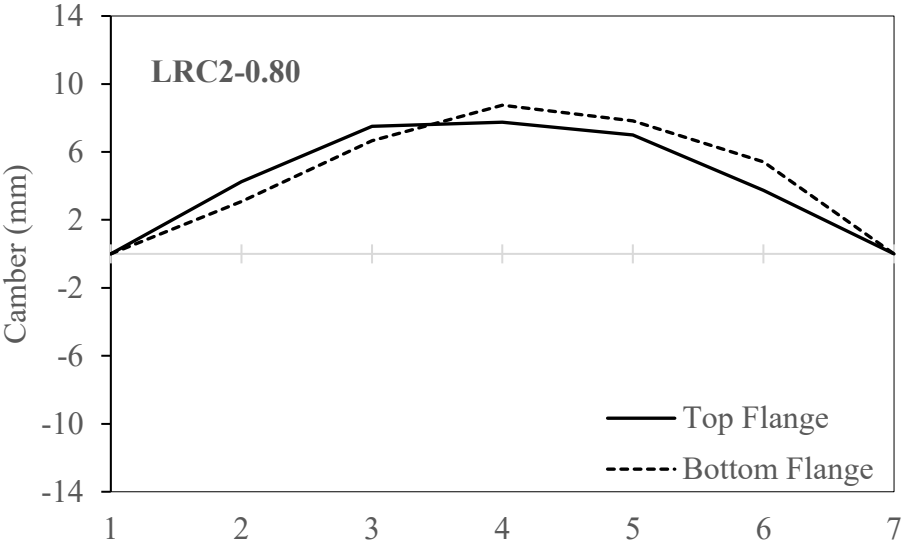


Figure 3-13: Camber distribution for LRC2-0.80

Initial twist was measured using a Mitutoyo Pro 360 digital protractor. A perfectly vertical web is taken as zero twist, where the digital protractor reads zero degrees. Measurements were taken on either side of the web at the seven stations, and deviation, in either direction, from the perfectly vertical web is taken as the test girders' initial twist. A positive twist value refers to clockwise rotation when looking at the girder from the end vertical support. Figure 3-14 shows the twist distribution for specimen LRC2-0.80; twist distributions for all test specimens can be found in Appendix B. The mean twist measured in the test girders was 0.2° . It should be noted that CSA G40.20-13 (CSA 2013) does not specify a limit on the tolerance for initial twist.

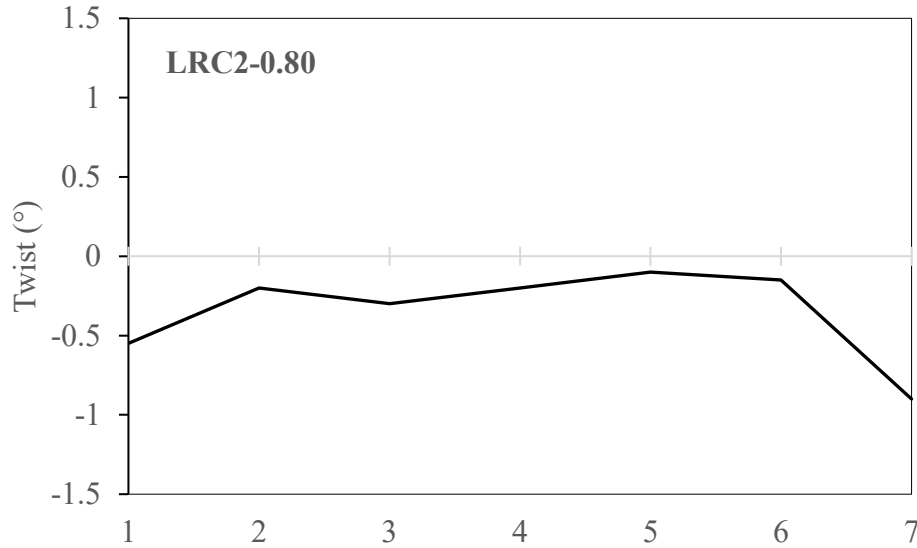


Figure 3-14: Initial twist distribution for LRC2-0.80

Table 3-6 shows a comparison between the mean maximum measured initial sweep and twist in this study and from previous experimental studies. The imperfections measured for the test girders of this study are larger overall, with the mean sweep and twist being larger than the mean seen in previous investigations. Table 3-7 summarizes the initial geometric imperfections measured for all test specimens, reported as the maximum value measured among the seven stations.

Table 3-6: Mean initial imperfections in experimental studies

	Number of Girders	Length, L (mm)	Sweep (mm)	Twist (°)
Current study	14	10,970	$L/1900$	0.2
Fukumoto et al. (1980)	75	1500 – 2600	$L/12,500$	0.08
Dux and Kitipornchai (1983)	9	5000 – 11,000	$L/3600$	0.01
Essa and Kennedy (1993)	11	9000	$L/2000$	1.2

Table 3-7: Maximum initial geometric imperfections in test specimens

Specimen ID	Length, L (mm)	Length / Sweep		Length / Camber		Twist (°)
		Top Flange	Bottom Flange	Top Flange	Bottom Flange	
LRC2-0.80	10981	-1788	-4575	1417	1255	-0.9
LRC2-0.38	10976	-1413	-1999	1463	998	0.7
LRC2-0.25	10975	-1742	-3976	1463	1756	0.3
LRC3-0.80	10979	-1821	-1540	1689	3658	0.6
LRC3-0.25	10979	-1212	-3277	1156	1568	0.4
LRC5-0.80	10984	-2554	-2255	1998	2031	0.5
LRC5-0.25	10975	3247	4480	-878	-1116	0.3
LRC4-0.80	10980	2278	1388	-1464	-1938	0.9
LRC4-0.38	10978	-1861	-3347	-1098	-1220	0.9
LRC4-0.25	10975	1539	1541	1291	1186	0.7
LRC1-0.80	10977	-1800	-2484	1126	941	-0.5
LRC1-0.38	10975	1929	1266	1219	1186	0.6
LRC1-0.38 Retest	10975	2512	1424	-1220	-1220	-0.6
LRC1-0.25	10977	-1678	-2601	1568	1514	-0.2

3.4 Material Properties

An additional 0.762 m (2.5 ft) long W410×85 segment from each of the three heats of steel as the test specimens was obtained for measurements of material properties. These segments were cut from the ends of one of the 12.192 m (40 ft) long original girders, which were cut to 11.430 m (37.5 ft) for the test specimens. Table 3-8 shows the heats associated with each of the girders used

in the tests. An extra 0.762 m long W410×85 segment was also ordered from the heat of steel which supplied 8 out of 14 of the girders (Heat 1) in order to measure residual stresses. Residual stress data are not available for girders from Heats 2 and 3.

Table 3-8: Specimens and their corresponding heats

Specimen ID	Heat Number
LRC2-0.80	Heat 1
LRC2-0.38	Heat 1
LRC2-0.25	Heat 1
LRC3-0.80	Heat 1
LRC3-0.25	Heat 1
LRC5-0.80	Heat 1
LRC5-0.25	Heat 1
LRC4-0.80	Heat 2
LRC4-0.38	Heat 3
LRC4-0.25	Heat 3
LRC1-0.80	Heat 1
LRC1-0.38	Heat 3
LRC1-0.38 Retest	Heat 2
LRC1-0.25	Heat 2

Mechanical properties determined using the standard coupon test (ASTM International 2023) included the mean flange and web static yield and ultimate stresses, as well as the elastic modulus

for each heat of the W410×85 cross-sections used in the full-scale tests.

From each of the three girders, a total of six tension coupons, two from each flange and two from the web, were cut from their corresponding parts into standard dog-bone specimens as outlined in ASTM A370-23 (ASTM International 2023), identified and shown schematically in Figure 3-15. The two web coupons were cut 50 mm away from the middle of the web in either direction, while the four flange coupons were cut 10 mm away from the edge of each flange. For the W-shape used in the tests, both the flange and web thicknesses conformed to sheet-type specimens with 50 mm gauge lengths. The cross-sectional area of each of the coupons was measured using calipers prior to conducting the material property tests.

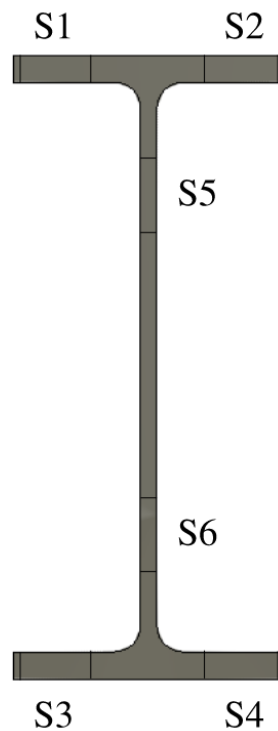


Figure 3-15: Identification and location of tension coupons

The tension coupons were tested in a uniaxial load frame, where a tensile strain rate of 0.3 mm/min was exerted as the coupons remained in the elastic region, which was then increased to 5 mm/min after taking static yield stress measurements. A mean value of the static yield stress was obtained using three readings taken on the yield plateau, and the static ultimate stress was read at the approximate maximum stress for each coupon. The elastic modulus, E , was obtained from a graphic plot of the stress–strain curve, where a linear regression trendline was used to determine

the slope of the curve in the elastic range. The results for each of the three heats of steel, with web and flange separated, are shown in Table 3-9. The engineering stress–strain curves for the tension coupons can be found in Appendix A. In the tension coupon tests, the flange yield stresses were consistently found to be lower than the web yield stresses, occasionally falling below the minimum specified yield stress for ASTM A992 steel of 345 MPa. The ultimate stress, F_u , was also consistently found to fall short of the minimum specified value of 450 MPa, with a mean among all 18 coupons of 440 MPa. However, the web yield strengths were found to be higher than the flange yield strengths, and the mean of all web and flange yield strengths was found to be 350 MPa, which is slightly higher than the nominal value of 345 MPa.

Table 3-9: Mechanical properties of test specimens from tension coupon tests

Heat Number	Mean Flange Yield Stress, F_y (MPa)	Mean Web Yield Stress, F_y (MPa)	Flange Ultimate Stress, F_u (MPa)	Web Ultimate Stress, F_u (MPa)	Modulus of Elasticity, E (MPa)
Heat 1	345	373	441	449	206,800
Heat 2	332	353	435	438	200,400
Heat 3	339	357	440	439	197,400
Mean	339	361	438	442	201,500

3.5 Residual Stresses

Residual stresses were measured once, for the W410×85 sections from Heat 1, using the sectioning method (Ziemian 2010), which measures residual stresses through the release of stresses in a strip which is cut out of the 0.762 m long segment. The residual stress in the longitudinal direction of the girder can then be calculated by measuring the change in length of the strip. Ziemian (2010) recommends, for residual stress specimens cold-sawed from the original 40 ft long W410×85 segment, that the length of the specimen should be cut to a minimum length of three times the largest transverse dimension, plus the gauge length, plus 50 mm to avoid disturbing the residual stress pattern which is originally locked into the central portion of the specimen. In the case of the

W410×85 section and a gauge length of 100 mm, the minimum recommended length of the residual stress specimen is therefore 1.401 m. However, since the original girder used for the full-scale tests was 12.192 m (40 ft) long and was then cut to a length of 11.430 m (37.5 ft) to be used in the full-scale tests, the only length of girder available for the residual stress tests was the remaining 0.762 m (2.5 ft), which is slightly more than half of the recommended length by Ziemian (2010). Furthermore, as the residual stress measurements were only taken for an ancillary girder from one heat of steel, residual stress data is only available for 8 out of 14 girders.

Prior to cutting, the flanges of the ancillary girder are defined into 15 mm × 300 mm strips and the web is defined into 25 mm × 300 mm strips, as shown in Figure 3-16. Eight strips were taken from each flange, and 13 strips were taken from the web. Due to the curve of the fillets, the area near the web–flange junction was not accessible for measurements since the digital length-measuring device could not fit in this area while remaining perpendicular to the surface, and therefore would not give an accurate reading of the change in length of the strip. Therefore, change in length measurements were only attainable for the portion of the flanges and web further than 30 mm away from web–flange junction. Since this is known to be an area of high tensile residual stress in the flange, it is expected that the overall residual stress pattern obtained from these measurements reflects a higher summation of compressive forces compared to tensile forces.

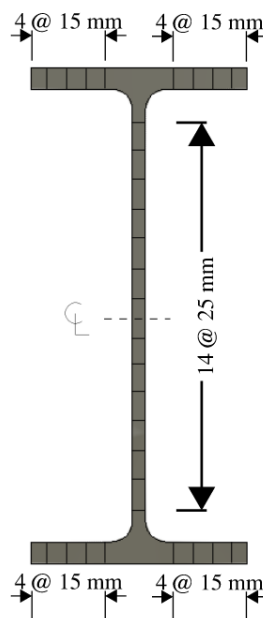


Figure 3-16: Cutting locations for residual stress measurements for W410×85

A line is scribed at mid-width of each strip, and punch marks are then made along this scribe with a 100 mm gauge length. As punch marks leave a large diameter and shallow hole, they are not accurate enough to read length measurements off and serve only to guide the drill bit of a handheld drill. A drill bit of 0.0625 in. diameter, the smallest diameter which can fit in the handheld drill, was used to drill a hole where the punch marks were made on each strip, taking special care to ensure the drill is held perpendicular to the surface being drilled. A Matest digital demec, with a gauge length of 100 mm and precision of 0.001 mm, was used to measure the initial longitudinal spacing (or gauge length) between these drilled holes for each strip. The demecs were zeroed on a reference bar prior to measuring, and three measurements were taken for each gauge length in order to obtain a mean value. The measurements taken by the demec on the drilled holes consistently gave repeatable values for each of the three measurements taken, indicating high precision of the demec and well-drilled holes. For each strip, holes were drilled and measurements were taken on both sides, which negated the need to correct for bowing of the strip following cutting as the mean change in length of both sides was used to calculate the strain (Ziemian 2010).

The 15 mm × 300 mm and 25 mm × 300 mm strips were then cold-sawed from the sectioning piece, as shown in Figure 3-17. The final longitudinal distances between the drilled holes were then measured again, once again taking three measurements for each gauge length. The temperature in the lab at the time of taking initial and final measurements remained consistent, not deviating more than 1.3 degrees Celsius, and therefore the change in length due to temperature change is negligible. The change in the gauge length after cold-sawing the sectioning pieces divided by the original gauge length is calculated for each side of the strip, and the average of both sides (to correct for curvature) is then interpreted as the value of residual strain present in that section prior to removal from the specimen. These strains are converted to stresses using the mean modulus of elasticity measured for the first heat of steel of 206,800 MPa.

In addition to the 100 mm gauge length measurements, holes were also drilled and measured for a 200 mm gauge length in an attempt to have two sets of comparable measurements. However, the measurements obtained from the 200 mm gauge, which used a different measuring device than that used for the 100 mm holes, resulted in a residual stress distribution which was not in

equilibrium when looking at the overall compressive and tensile forces, even after extrapolating the data to account for the portion of the fillets in tension. The distribution obtained from the 200 mm measurements was therefore deemed unreliable.

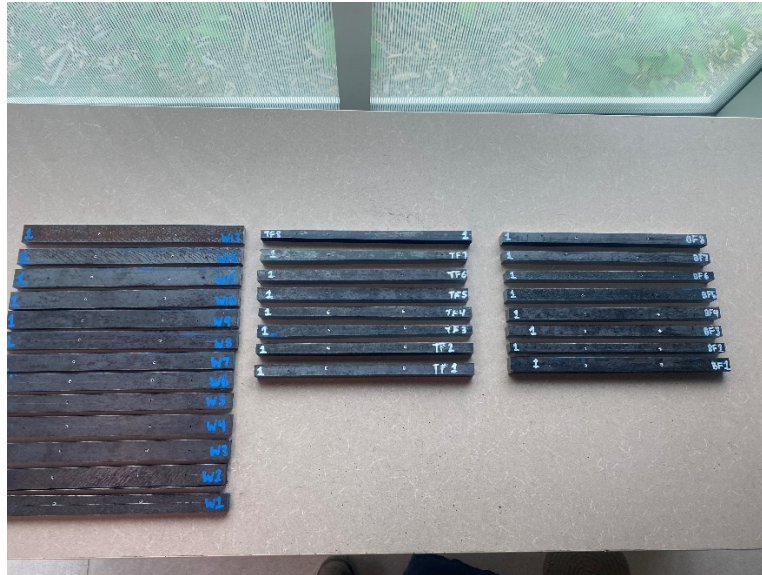


Figure 3-17: Sections for residual stress measurements after cold-sawing

Figure 3-18 shows the residual stress, σ , distribution of the measured girder with the 100 mm gauge readings, where tension and compression are indicated by positive and negative stress values, respectively. For Heat 1, the mean flange and web yield stresses were 345 MPa and 373 MPa, respectively. The web of the section is seen to have tensile residual stresses near the web–flange junction, with compressive residual stresses seen up to about $0.27F_y$ at the middle of the web. The flange tips possessed compressive residual stresses of up to $0.12F_y$, and the sections nearest to the web–flange junction were in tension, with a maximum measured tensile residual stress of about $0.23F_y$. Overall, the measured residual stresses agree with those measured by previous researchers for rolled sections with relatively wide flanges (Essa and Kennedy 1993, Kitipornchai and Trahair 1975).

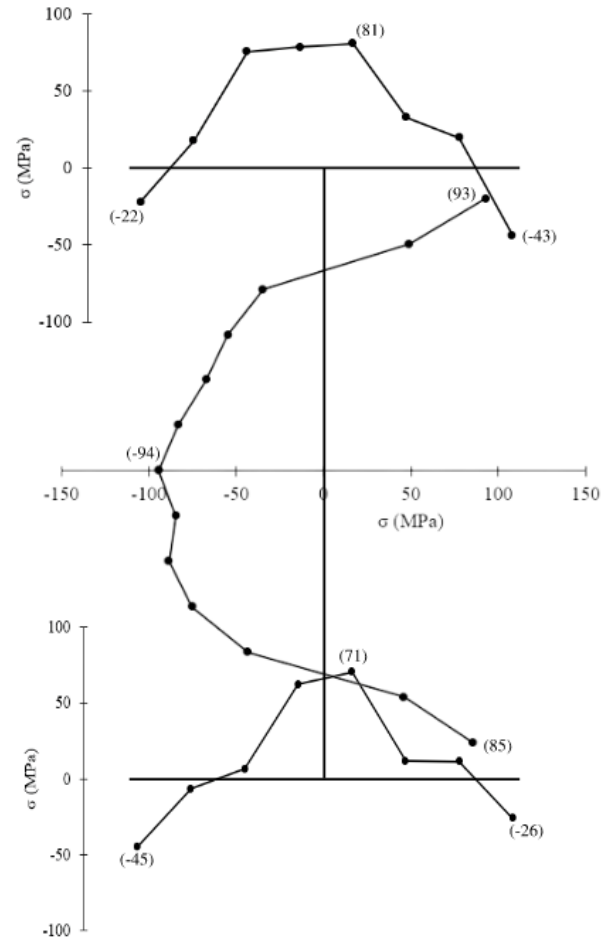


Figure 3-18: Residual stress distribution of W410×85

4 EXPERIMENTAL PROGRAM

To investigate the stability of steel cantilevered girders, an experimental study was developed for 14 full-scale girders in a single overhanging configuration and tests were conducted in the I.F. Morrison Structural Engineering Laboratory at the University of Alberta. This chapter presents the development of the test setup including loading, restraints, and boundary conditions, as well as the instrumentation plan and test procedure.

4.1 Test Setup

The test setup was designed to accommodate the expected girder deflections and rotations according to finite element (FE) simulations done by Esmaeili et al. (2021) and was based largely on recommendations of the Structural Stability Research Council (SSRC) Technical Memorandum No. 9 on flexural testing (Ziemian 2010). Models were prepared in *Revit* (Autodesk Inc. 2022) for each of the five loading and restraint condition (LRC) groups, and a model of the test setup for the C(U)–B(TB) group (LRC 4) is shown in Figure 4-1. The test specimen is shown in blue, and the load frame, bracing system and supports are shown in grey. A plan view of the test setup is shown in Figure 4-2, which also shows the directions referenced in this section. This section describes the loading, support, and bracing details of the test setup to simulate those anticipated in a typical Gerber system while conforming to the laboratory restraints and safety measures.

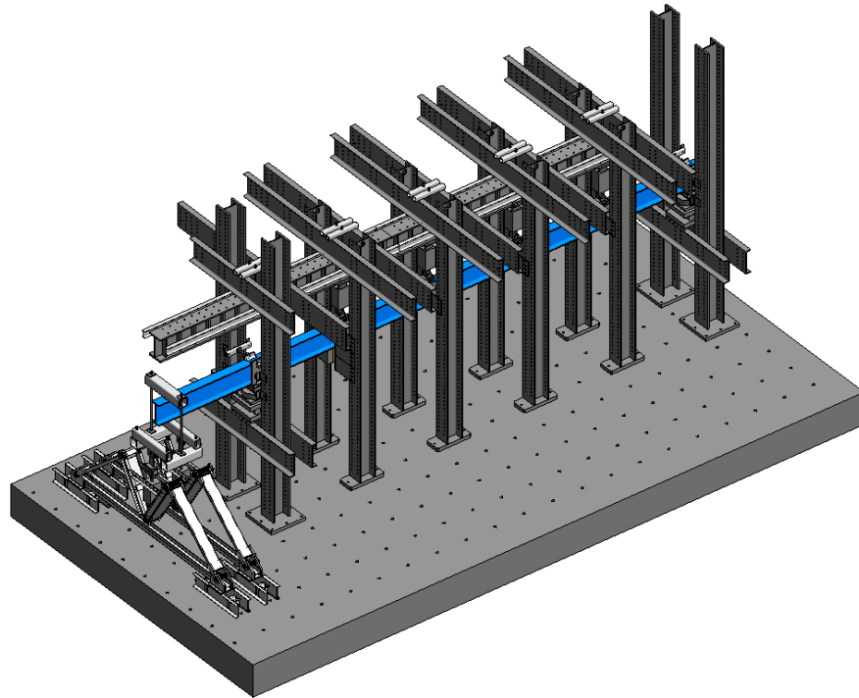


Figure 4-1: Model of experimental test setup (test specimen shown in blue)

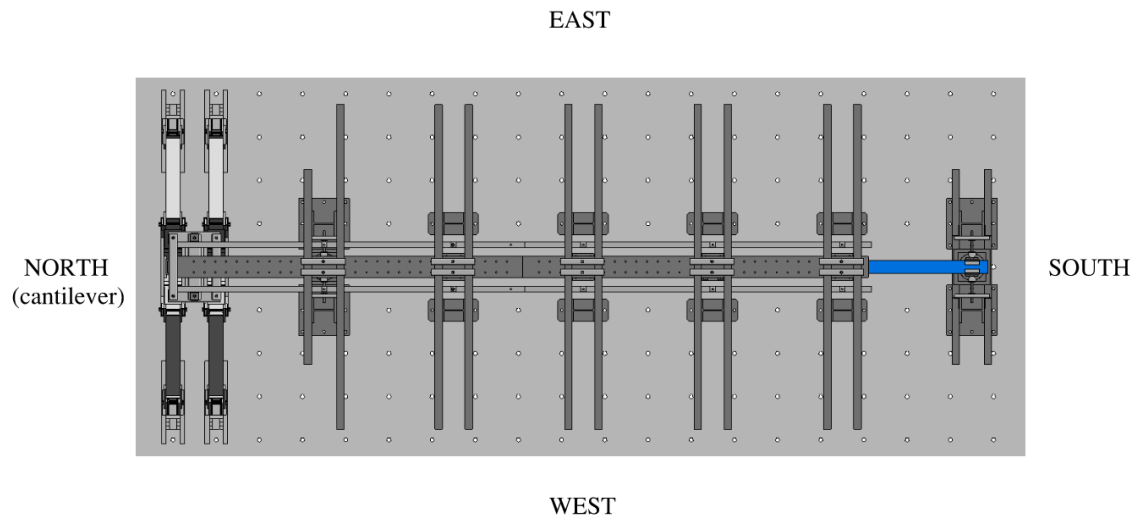


Figure 4-2: Cardinal directions on plan view of test setup

4.1.1 Gravity Load Application

Since the cantilever tip can be either laterally braced or unbraced, two gravity load mechanisms are used in the tests. In the first mechanism, used at load points where the girder is restrained from moving laterally and shown in Figure 4-3, the gravity load is applied using a hydraulic actuator

which generates the concentrated load on the test specimen.

On the top end, the hydraulic actuators are pin-connected to a stiff reaction frame which distributes the reaction load to the laboratory strong floor through high-strength steel anchor rods. The reaction frame is composed of a distributing beam connected to MC460×86 channels through a pair of HSS and Grade 8 threaded rods, which subsequently span across two Meccano columns on either side of the girder. All components of the reaction frame were analyzed under the maximum expected loads obtained from FE simulations to ensure yielding of the fixtures does not occur during a test.

At the bottom end, the actuator is pin-connected to a semi-cylindrical bearing with its axis aligned with the longitudinal axis of the girder which sits on the top flange of the girder, therefore accommodating cross-section twist while maintaining a stable mechanism with the pin-ended hydraulic actuator.

At the start of the test, the hydraulic actuators on the back span are fully retracted. For installation purposes, there was a gap of about 25 mm between the top flange of the girder and the bottom of the semi-cylindrical bearing when the hydraulic actuators were fully retracted at the start of the test, deviating slightly based on the extent of the initial camber of a given girder. As the hydraulic actuator extended, it first cleared the initial gap then pushed down on the top flange of the girder, delivering a downward concentrated force. Although the full stroke of the hydraulic actuators is 150 mm, only about 130 mm could be used to accommodate the downward vertical deflection of the test specimen after the initial gap was cleared. While all the load points on the back span were expected to deflect downward, the cantilever tip was able to move either up or down depending on the load ratio being investigated. Therefore, the hydraulic actuator at the cantilever tip, in the cases where the cantilever tip was laterally restrained, was 70 mm extended at the start of the tests in order to allow the cantilever tip to deflect upward, using the retracting stroke of the actuator, or downward, using the extending stroke of the actuator. Since the hydraulic actuator at the cantilever tip was initially extended, spacer plates were placed at the load points on the back span above the load application point in order to maximize the useable stroke of the hydraulic actuators.

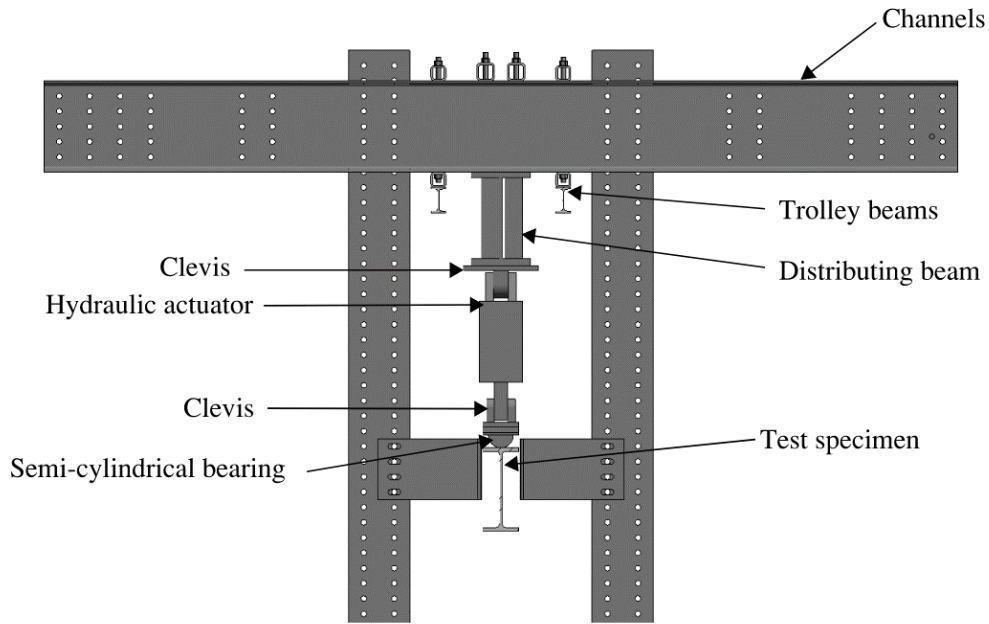


Figure 4-3: Gravity load mechanism at laterally braced load points

Figure 4-4 shows the test frame when viewing the back span from the north support. An addition made to the test frame to facilitate the easy installation and removal of test girders between tests was a trolley-and-chain-fall system. Two trolley beams of S130×15 were installed, one on either side of the distributing beam, as visible in Figure 4-3. Short HSS89×89×9.5 sections with a 1-inch diameter hole drilled through them were welded to the top flange of the trolley beams at 1.83 m spacings, coinciding with the locations of channels in the test frame. The trolley beams were then connected to the channels of the test frame in a manner similar to that used for the distributing beam, using a pair of HSS and Grade 8 threaded rods. Two chain falls were installed on each trolley beam, each with 1-ton load carrying capacity, allowing them to glide down the trolley beams. Consequently, the chain falls could carry and move the test girders into and out of the test frame between tests without the need to disassemble the entire frame.

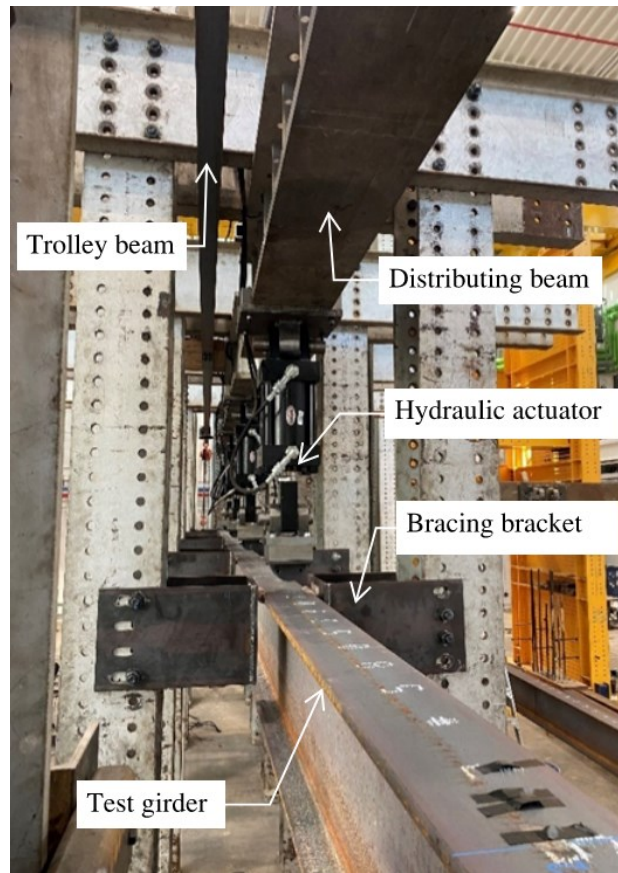


Figure 4-4: Test frame setup

The second gravity load mechanism, used at the cantilever tip when it is laterally unbraced, is composed of three pivot pin-connected components: (1) gravity load simulator (GLS), (2) hydraulic actuator, and (3) load collar, as illustrated in Figure 4-5. At the beginning of the test, the hydraulic actuator is 76 mm extended, accommodating either upward or downward vertical deflection. As it retracts, the hydraulic actuator pulls on the load collar, which delivers a downward concentrated force to the top flange of the test girder. Cross-section twist is accommodated by the load collar, which includes a hemispherical bearing on the top flange. A hemispherical bearing is used as part of the load collar assembly, as opposed to a semi-cylindrical bearing, to allow for the girder to undergo in-plane bending without the use of pin-ended hydraulic actuators. Details of the components of this gravity load mechanism are described in the following sections.

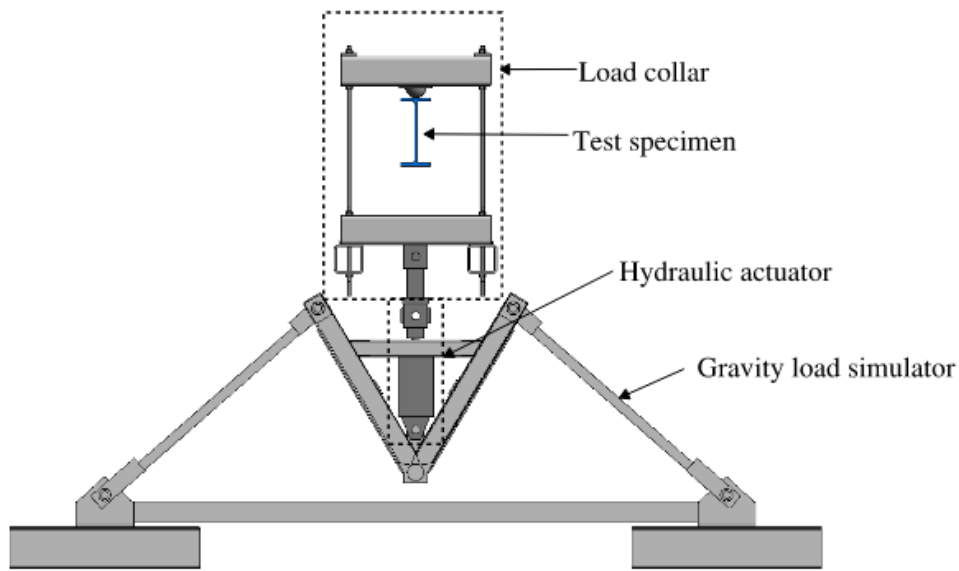


Figure 4-5: Gravity load mechanism at unbraced cantilever tip

4.1.1.1 Gravity Load Simulator

One challenge in flexural testing is maintaining a vertical point load on a test specimen while allowing it to undergo lateral movement without causing the load to become eccentric on the member. The solution employed in this test setup at the cantilever tip, when it is laterally unrestrained, is the gravity load simulator (GLS)—a pin-jointed mechanism used for testing structures that undergo sidesway under vertical loads (Yarimci et al. 1967).

The GLS is capable of displacing freely from its equilibrium position in either direction up to 400 mm, while maintaining a point load that remains approximately vertical and has an in-plane load capacity of 360 kN (Ji et al. 2019, Driver, et al. 1997). While the maximum expected lateral deflection at buckling of 23 mm could easily be accommodated by the 400 mm deformation capacity, the maximum load expected in the tests is 394 kN, which exceeds the capacity of a single GLS. Therefore, two GLSs are employed at the cantilever tip and ganged together using HSS sections, as shown in Figure 4-6. That way, only half the load applied at the cantilever tip can be applied through each GLS, resulting in the full load being transferred through the load collar and to the top flange of the girder without exceeding the in-plane load capacity of each individual GLS.

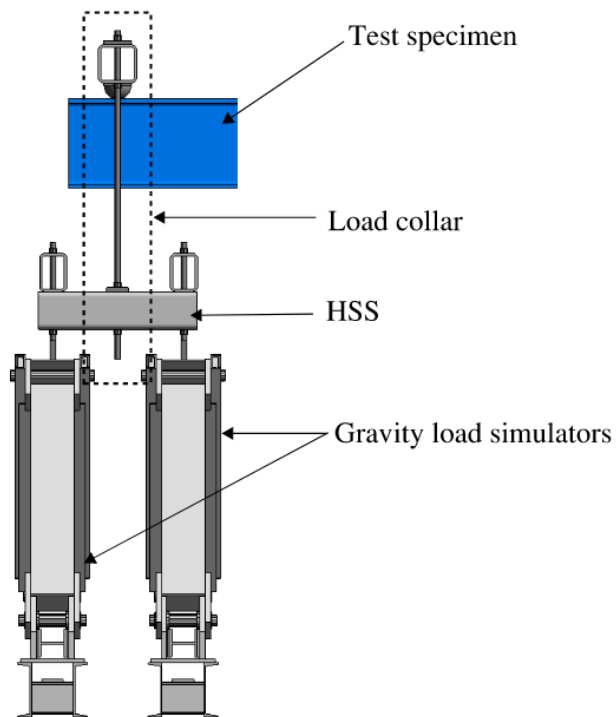


Figure 4-6: GLS and load collar setup at the cantilever tip.

4.1.1.2 Hydraulic Actuator

The GLS provides a connection location for hydraulic actuators, which generate the concentrated load applied to the tip of the cantilever in the tests where the cantilever tip is unbraced. All four hydraulic actuators on the back span are connected to the same manifold, operating at the same pressure. The actuator at the cantilever tip is on a separate manifold, applying a higher load than those on the back span. The actuators on the back span are always using the push (extending) capacity of the actuator, while the actuators connected to the GLS use its pull (retracting) capacity (when the cantilever tip moves down) to apply a downward load on the top flange through the load collar. In cases where the cantilever tip is laterally restrained, the push capacity of the hydraulic actuator at the cantilever tip is used.

At the maximum allowable operating pressure of 21 MPa (3000 psi), the actuators have a load capacity of 385 kN in pull and 514 kN in push. At the cantilever tip, the maximum expected push load at buckling is 403 kN, while the maximum expected pull load is 394 kN. Although the

maximum expected pull load slightly exceeds the capacity of a single hydraulic actuator of 385 kN, two hydraulic actuators act at the cantilever tip in that case due to the ganging of GLSs. This means that the cantilever tip can be loaded up to 770 kN without exceeding the capacity of each individual hydraulic actuator. However, this is limited by the capacity of the GLS, as mentioned previously. The maximum expected vertical deflection at buckling along the back span is 106 mm, which is accommodated by the 130 mm stroke of the hydraulic actuator while allowing for the observation of further deflection in the post-buckling response. As discussed previously, the cantilever tip is anticipated to deflect either upward or downward depending on the load ratio being tested; the maximum expected upward deflection at buckling is 43 mm, while the maximum expected downward deflection is 38 mm, both accommodated by the 76 mm stroke available in either direction in the initial extended position of the actuator.

4.1.1.3 Load Collar

The load generated by the hydraulic actuators at the tip of the cantilever is transferred to the top flange of the test girder through a load collar assembly, shown in Figure 4-7. The top part of the load collar consists of one HSS178×178×13 section and two Grade 8 (ASTM A354 Grade B4) threaded rods. An HSS178×127×13 section is then connected to a yoke and tension rod, which is subsequently connected to the hydraulic actuator in the GLS. Two more HSS178×127×13 sections (light grey in Figure 4-7) then connect the two GLS assemblies together. Additionally, a hemispherical bearing was bolted to the top HSS of the load collar, which sits on the top flange of the test girder and accommodates twist during the tests as shown in Figure 4-7.

HSS members of the load collar under flexure were designed to remain elastic during the tests. To ensure that the nuts bearing against the HSS sections at the connections of the load collar do not yield the thin HSS wall, yield line theory was used. It was concluded that 19 mm plate washers should be added to the top of the HSS sections for the nuts to bear against, as visible in Figure 4-7.

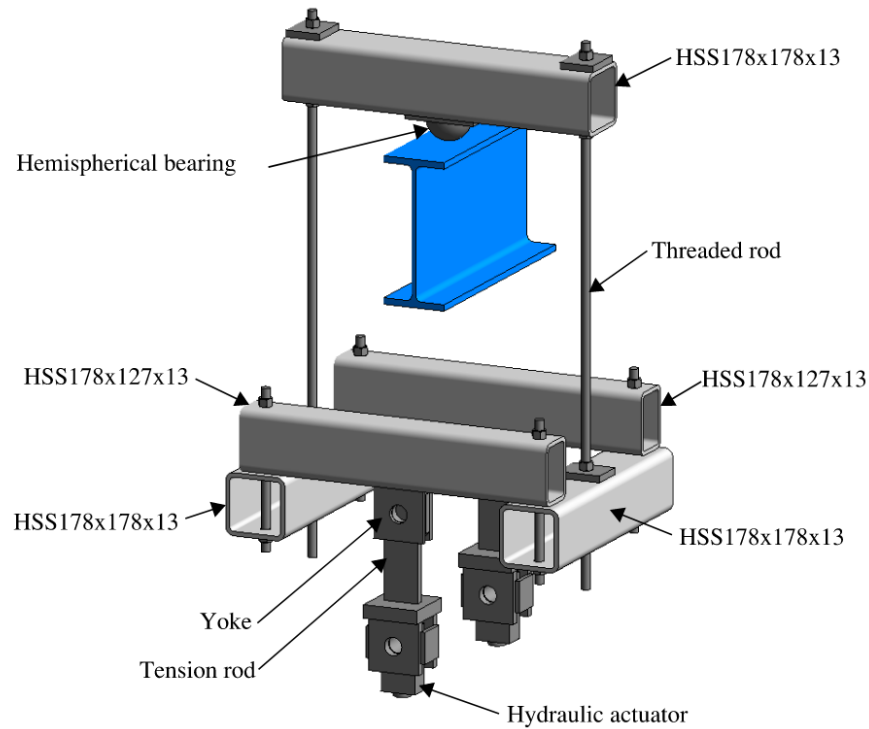


Figure 4-7: Load collar components

4.1.2 Boundary Conditions

Column locations in a typical Gerber frame are simulated in this experimental test setup at the supports. Identical configurations are used at the support fixtures at each end of the back span, creating a simply supported girder where the specimen is free to displace longitudinally and not prevented from warping, but is prevented from twisting and displacing laterally or vertically. This support condition is achieved by having the specimen rest on a set of rollers, a load cell, and a knife edge, as shown in Figure 4-8. The detail of the support, as seen in the test setup, in the longitudinal direction of the girder can be observed in Figure 4-9. The rollers allow the girder to undergo longitudinal displacement to a maximum of 65 mm in either direction. To simulate flexural buckling allowing loading to continue past buckling and into the post-buckling stage, only the roller at the south end remained unlocked throughout the tests. The roller at the north end, closest to the cantilever, was locked to create a pin to allow no more than 5 mm of longitudinal displacement. The knife edge allows the girder to pivot in-plane. The load cell is used to measure the vertical reaction forces at the supports. These elements sit on a pair of MC460×86 channels

spanning between two Meccano columns situated on either side of the girder. Additionally, a chain was fastened across the columns at each end of the girder for added safety.

In order to allow the girder to warp, while simultaneously preventing it from twisting at the supports, four lateral braces are brought in at each vertical support. The braces are composed of Grade 5 fully-threaded rods and are equipped with rollers at the end, visible in Figure 4-9. Two of these braces, one at the top flange and one at the bottom flange, bear against a steel plate hanging off either side of the girder to provide a larger bearing area. These are meant to prevent cross-section twist and lateral movement of the girder, while the rollers allow the girder to warp and displace longitudinally. The strength and stiffness requirements specified in Appendix 6 of AISC 360-22 (AISC 2022) for girder point bracing, as well as the expected maximum brace force at buckling, are used to design the braces. The braces were designed to resist a compressive force of 76 kN, which exceeds the maximum expected brace force at buckling of 22 kN, and exhibited a stiffness of 427 kN/mm, exceeding the requirement specified by AISC 360-22 of 12.8 kN/mm.

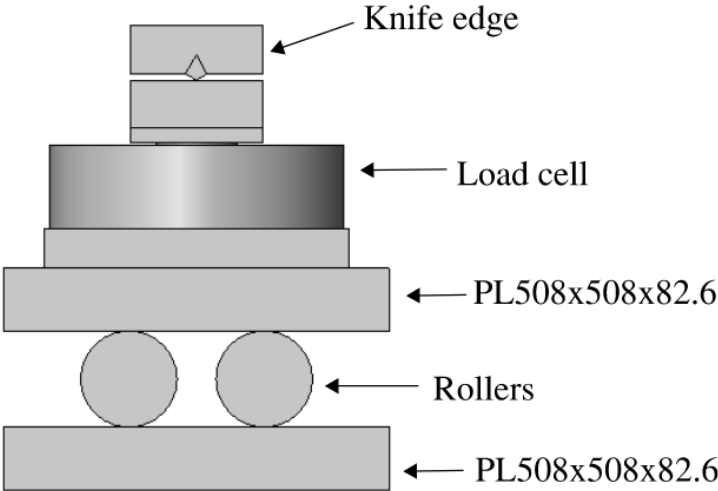


Figure 4-8: Vertical support detail

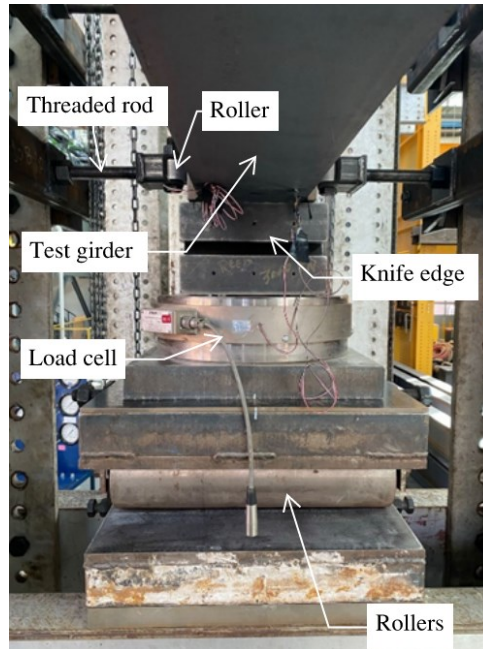


Figure 4-9: Vertical support in the longitudinal direction

4.1.3 Lateral Bracing Conditions

Lateral bracing is used in flexural testing of girders to prevent out-of-plane movement, a simulation of a restraint provided by open web steel joists in a typical Gerber frame. Since the test girder is expected to deflect vertically along the back span and cantilever, it is of crucial importance to use a lateral bracing mechanism that allows for free vertical movement, while simultaneously restraining movement in the direction perpendicular to the girder web in order to avoid incidental restraint. Therefore, a conventional threaded rod, such as that used at the supports and discussed previously, would not be appropriate for use at the load points as the brace would lose contact with the top or bottom flange as the girder deflects vertically. The solution uses a U-shaped bracing bracket, shown in Figure 4-10, bolted to the Meccano columns on either side of the girder where lateral bracing is required. The brackets come equipped with an Acetal sheet attached to the front plate. Acetal is a mixture of Polytetrafluorethylene (PTFE), commonly referred to as TeflonTM, which has a very low coefficient of friction, and Polyoxymethylene (POM), commonly referred to as Delrin[®], which adds hardness to prevent the sheet from deforming significantly under load. The coefficient of friction of the Acetal against steel provided by the manufacturer is 0.21.

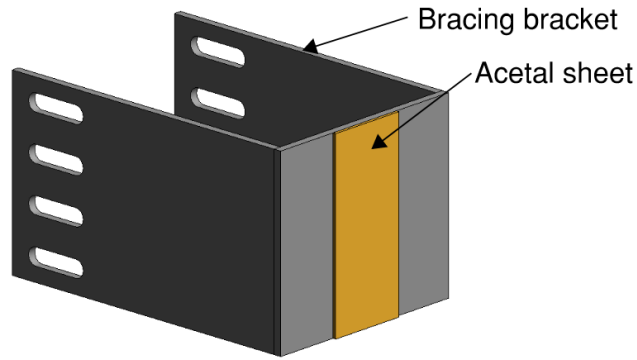


Figure 4-10: Bracing bracket used at load points with Acetal sheet

To further minimize the friction between the sliding surfaces, a cylindrical Acetal bearing is also placed on the flange of the girder which results in Acetal-on-Acetal action at the lateral bracing points, shown in Figure 4-11, and both pieces of Acetal have a coat of grease applied to them. Slotted holes on the side plates of the U-shape allow for adjustability to ensure the Acetal sheet bears against the top flange of the girder. The brackets and cylindrical pieces of Acetal can be seen as part of the test setup in Figure 4-12. As the girder deflects vertically, it is then restrained at the top flange from moving horizontally while undergoing negligibly small vertical frictional forces due to sliding against the greased Acetal sheet.



Figure 4-11: Cylindrical Acetal on test girder flange

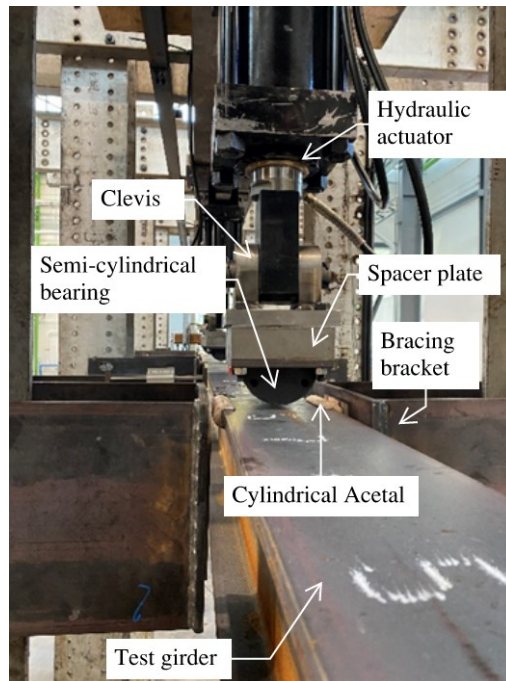


Figure 4-12: Bracing detail

When only the top flange is to be braced, only one of the U-shaped brackets is bolted to the Meccano columns on either side of the test girder to bear against the top flange. The vertical length of the U-shaped brackets is 305 mm, allowing for a maximum vertical deflection of 265 mm, therefore accommodating the maximum expected vertical deflection at buckling of 106 mm without restraining the bottom flange. The maximum rotation that can be safely accommodated by the 305 mm long bracket, without having the web of the girder collide with the front plate, is 16 degrees, which is able to accommodate the expected maximum rotation at buckling along the back span of 4.8 degrees while allowing for post-buckling response to be observed.

When both the top and bottom flanges are braced, three of these U-shaped brackets are bolted underneath one another on the columns on either side of the girder, resulting in a total length of 915 mm. This accommodates the full depth of the girder in the undeflected position of 417 mm, as well as an extra 498 mm of space for the girder to deflect vertically while keeping both the top and bottom flanges bearing against the front Acetal sheet. The maximum expected vertical deflection at buckling of 106 mm is easily accommodated when using this bracing configuration.

While the back span is expected to undergo larger vertical deflections than the cantilever tip, the cantilever tip is expected to rotate about the longitudinal axis more than the back span at buckling, specifically for LRC 2 where only the top flange is braced. Therefore, the U-shaped bracket is bolted one hole higher (76 mm) on the column at the cantilever tip in these tests where the cantilever tip is expected to undergo larger rotations and smaller vertical deflections, which results in a bracket length of 229 mm as opposed to the full 305 mm. Shortening the bracket allows for a smaller maximum vertical deflection of 175 mm and a larger maximum rotation of 25 degrees, which is important in order to investigate the post-buckling response of the girder without having the web of the girder at the cantilever tip collide with the front side of the U-shaped brackets.

As discussed previously, the cantilever tip is expected to deflect either up or down under the different load ratios being tested. Therefore, for the tests where the cantilever tip is expected to deflect upward (i.e., specimens tested under a load ratio of 0.80), the U-shaped brackets are bolted higher on the column in order to continuously keep the top flange laterally restrained as it deflects.

4.2 Instrumentation

To measure the global and local responses of the specimens, including applied loads, reactions, deflections and strains, during the experiments, a plan consisting of six pieces of instrumentation was implemented as shown schematically on an LRC 3 (C(U)–B(TB)) girder in Figure 4-13. Load cells with 2200 kN compressive capacity were placed at each support to measure the reaction forces. To monitor the applied force at each load point, pressure transducers were installed on the hydraulic lines of the actuators, which allowed for a pressure measurement. The applied force can then be calculated using this pressure by multiplying the applied hydraulic fluid pressure by the nominal area of the actuator piston head surface. A redundant measurement of forces allowed for the use of statics to confirm that the reaction forces agree with the total applied loading during the tests, indicating negligible frictional losses.

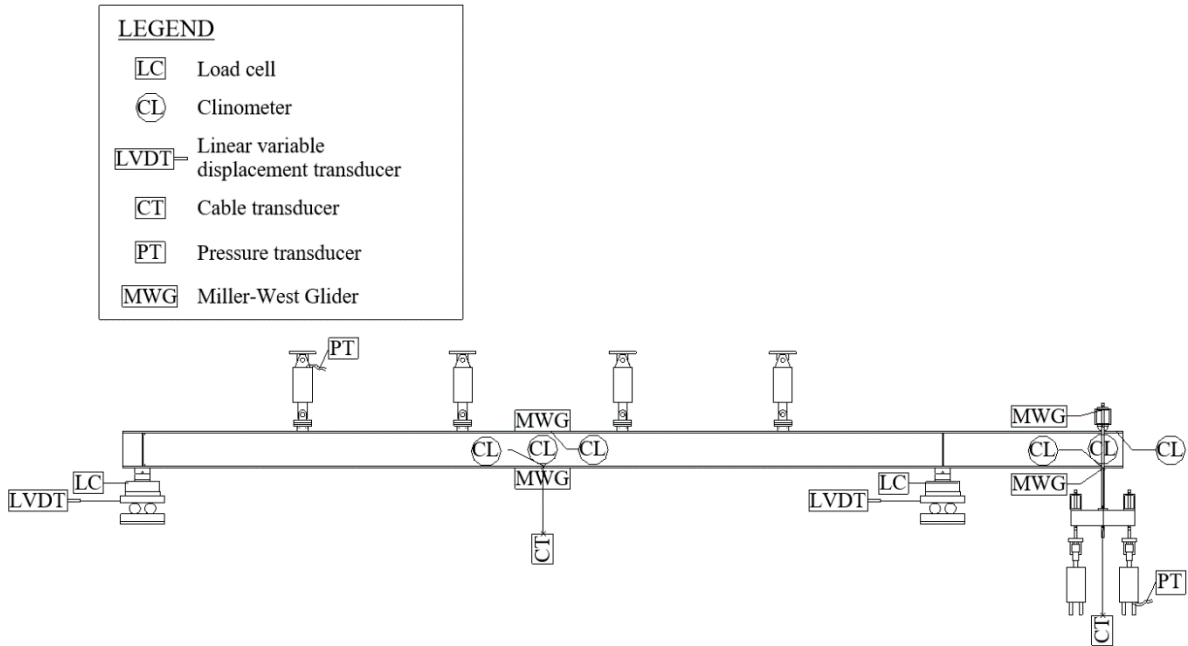


Figure 4-13: Instrumentation plan (LRC 1 and 4 shown)

Two locations were chosen to record lateral deflections, vertical deflections and rotations: at the tip of the cantilever and at the midspan of the back span. Lateral deflections were measured at the top and bottom flange of the girders using Miller-West Gliders, which is a device used to isolate lateral deflections from rotations or vertical deflections which may occur simultaneously as the girder moves laterally. The device is composed of a spring-loaded bar which allows for 220 mm of vertical deflection and bears on the flange of the girder. In the tests where the GLS is employed at the cantilever and both the top and bottom flanges are unbraced, the bar bears on the top HSS of the load collar (which displaces with the top flange) as the top flange of the girder is not accessible. The bar is able to move only horizontally in either direction, remaining in contact with the flange tip as it displaces laterally and vertically, and is able to accommodate up to 110 mm of lateral deflection in either direction. Each Miller-West glider is equipped with a cable transducer that measures the movement of the bar. Figure 4-14 shows the components of a Miller-West Glider at the midspan of the back span as seen in all tests.

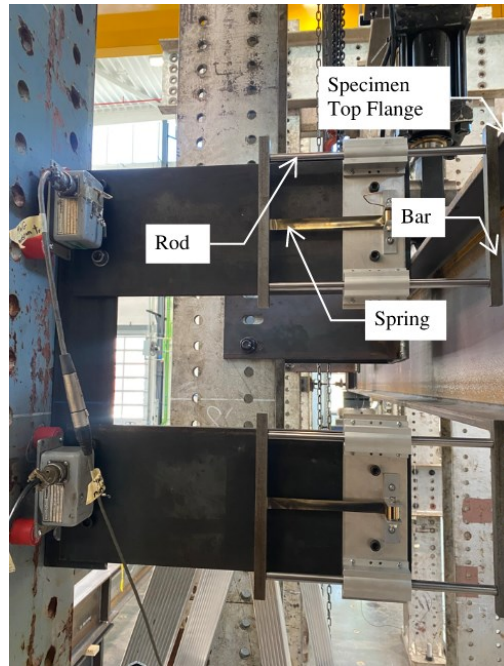


Figure 4-14: Miller-West Glider

The instrumentation setup at the midspan of the back span and the cantilever tip are seen in Figure 4-15 and Figure 4-16, respectively. Three clinometers were installed at the top flange, bottom flange, and web to measure cross-section twist at the cantilever tip and the midspan of the back span. At these same locations, the girder's vertical deflection is also measured using cable transducers mounted to the bottom flange of the girder. At the midspan of the back span, the clinometers on the top flange and web were unobstructed and able to be placed at the exact location. The bottom flange clinometer was placed 25 mm (1 inch) to the south of the midspan of the back span, since the cable transducer was placed at the exact location. At the cantilever tip, the bottom flange and web clinometers were similar to those at the midspan of the back span, but the exact location at the top flange was obstructed by the semi-cylindrical or hemispherical bearing used for loading. Therefore, the top flange clinometer was placed approximately 90 mm south of the cantilever tip in order to clear the bearing.

One linear variable displacement transducer (LVDT) is placed at each support, mounted to the top roller plate of the support assembly, in order to capture the longitudinal displacement of the girder at each support. All instrumentation parts were calibrated before first use and verified prior to each

test to determine if recalibration is necessary.

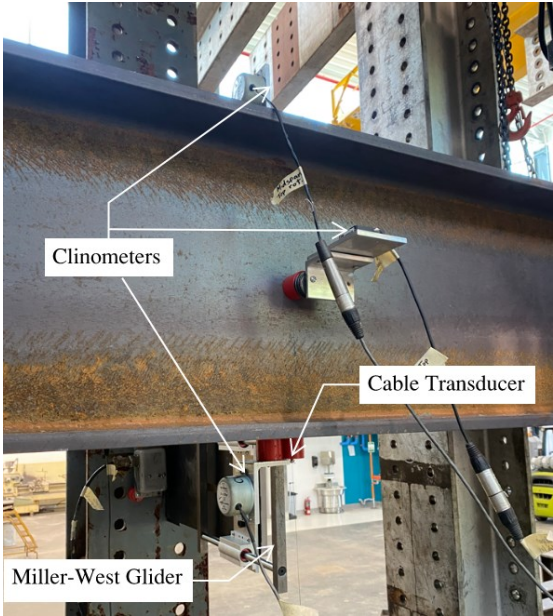


Figure 4-15: Instrumentation setup at midspan of back span

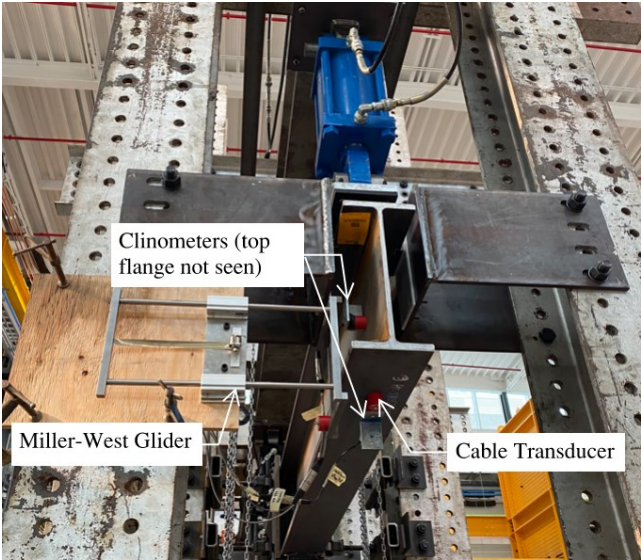


Figure 4-16: Instrumentation setup at cantilever tip for LRC 2

Under the loading expected in the tests based on FE simulations, the girder is expected to experience first yielding at one of two locations: the support at the fulcrum or the second load point

from the south support on the back span, which correspond to the locations of theoretical maximum negative and positive moments, respectively. To capture the stresses at these locations, two strain gauges are mounted to the top flange at the back span, one to the top flange at the fulcrum support, and four to the bottom flange at the fulcrum support. Since both flanges are expected to be in compression under the applied loading (top flange being the compression flange on the back span and bottom flange being the compression flange at the fulcrum support), yielding of the flange tips at these locations will constitute whether elastic or inelastic LTB has taken place (Nethercot 1974). Therefore, the two strain gauges on the back span are mounted longitudinally with one placed at each of the compression flange tips, as shown in Figure 4-17. Since the exact load location on the back span is not accessible to place a strain gauge due to the placement of the cylindrical Acetal at the flange tips, the strain gauges are placed 100 mm to the north (closer to the midspan of the back span) away from the centre of the semi-cylindrical bearing at the load point. At the fulcrum support, since the knife edge bears on the bottom flange of the girder, two strain gauges are instead placed on either side of the knife edge at the flange tips, for a total of four strain gauges on the bottom flange at this location, as shown in Figure 4-18. Additionally, one strain gauge is placed on the top flange at the fulcrum support at the web-flange junction as shown in Figure 4-19, where the highest tensile stresses are expected to occur.



Figure 4-17: Strain gauges mounted to top flange at second load point on back span

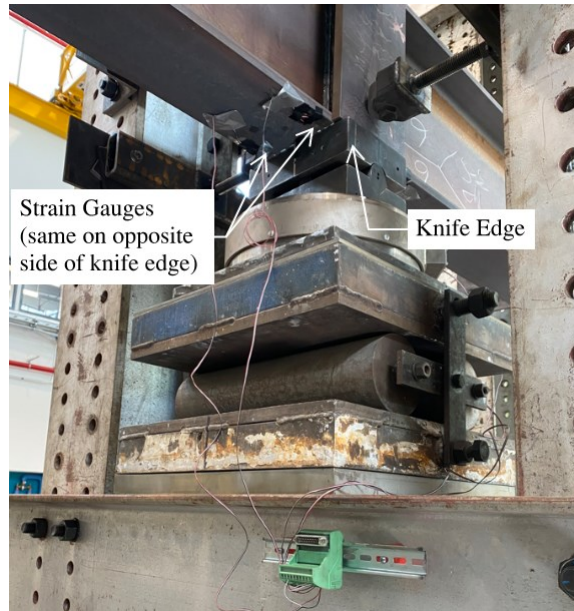


Figure 4-18: Strain gauges mounted to bottom flange at fulcrum support



Figure 4-19: Strain gauge mounted to top flange at fulcrum support

4.3 Girder Installation and Test Procedure

To install the test specimens, the girder was first lifted with a crane and brought close enough to the test setup such that the chain falls were able to attach to the girder, after which the chain falls were used to glide the girder down the test frame so that it was placed over the supports. Markings were made on the bottom flange of the test girder to indicate the location of the knife edge, and the rollers were unlocked and positioned such that the knife edge was in its correct position. The bottom flange of the girder was centered on the knife edge either by lifting or lowering the chain falls on either side of the girder as needed. Once the girder was positioned on the supports, the lateral braces at the supports were installed to secure the girder. The Acetal on the U-shaped brackets were re-greased as needed and were then installed at each load point, and the bolts for each bracket were pre-tensioned using a pneumatic torque wrench to ensure the brackets do not slip in their slotted holes during a test. In the tests where the GLS was used, the top HSS of the load collar was lowered onto the top flange and the load collar was made square by ensuring that the lengths of the threaded rods on either side of the girder were equal before tightening the nuts. The instrumentation was then installed onto the girder, verifying individual calibrations before each test. The hydraulic actuators were then brought down to close the gap, having the bearings rest on the top flange of the girder. Afterward, the hydraulic pressures were allowed to settle. The self-weight was then read off the load cells to account for the dead load from the load collar and hydraulic actuators.

For safety reasons, the rollers at the supports remained locked and nuts were placed in the knife edges, which prevented them from pivoting, when a test was not taking place. A turnbuckle was also used on the GLS to prevent sudden movement and was unlocked only for the duration of a test. Pieces of timber were clamped to the GLS in order to hold the hydraulic actuators vertically while they were not applying load, and the load collar did not have sufficient tension for the actuators to stand vertically on their own under the pin connections. The timber pieces were removed and turnbuckles were released when the applied load on the cantilever reached approximately 15 kN, which allowed for enough tension to remove the timber without seeing significant lateral deflection.

A project hazard assessment and risk form was completed prior to beginning the setup of the test

frame, which outlined existing and potential hazards and the controls which were implemented to address them. During a test, all observers were required to stand away from the test setup behind caution tape.

The loading of the test girders was controlled manually. The four actuators on the back span were connected to a single manifold, and therefore remained at the same pressure throughout a test. The actuator on the cantilever tip was connected to a separate manifold, thus applying a different (larger) load compared to that applied on the back span. Since one of the defining aspects of each individual test was the ratio of the load applied on the back span to the load applied on the cantilever tip, it was of crucial importance to ensure that this load ratio was maintained throughout the course of a test. The load on the back span was first increased while monitoring the load ratio. Once the load ratio became a hundredth higher than intended load ratio, the load on the cantilever was then increased to bring the ratio back down. In the tests where the cantilever tip deflected upward, the pressure at the tip of the cantilever was momentarily released after each increment to allow the cantilever tip to deflect in the desired direction. This procedure was repeated throughout the whole test, applying the loads in increments of 5-10 kN in the linear stage of loading and slowing down near the onset of buckling.

In order to identify when the girder was close to buckling, the load at the cantilever tip was plotted against the vertical and lateral deflections at the midspan of the back span and the cantilever tip. After each increment of load, the load was held for about a minute until all readings of deflection stabilized, and the summation of downward loads from the pressure transducers was compared to the summation of reaction forces from the load cells to ensure negligible frictional losses. When the plot of the load–deflection curves began to show a change in slope, and eventually flattened out into a plateau indicating large deflections for a very small increment in load, the girder was considered to have buckled. Loading continued in order to investigate the post-buckling response of the girder. In the tests where the girder reached its fully plastic moment, the plateau was generally not able to be pushed far enough to see a drop in load without reaching the maximum stroke of the hydraulic actuators. However, in the tests where failure was categorized as buckling, the load–deflection curve captured a drop in load as deflections continued to increase. A test was stopped when either the full stroke of the hydraulic actuators was reached, or the lateral deflections or twists reached a predetermined maximum value based on geometric constraints in the test setup.

5 EXPERIMENTAL RESULTS AND DISCUSSION

The experimental results of the full-scale buckling tests of single-overhanging girders are presented in this chapter. The influence of the parameters used to compose the test specimen matrix, such as lateral bracing conditions and loading conditions, are also discussed. The last two influential parameters identified in Chapter 3, namely cross-sectional properties and configuration (single or double overhang) are not realized directly through this experimental program, since it included only one cross-section and only single overhanging girders. However, the influence of these parameters will be explored in future tests to be conducted at the University of Alberta as part of the larger research project on the stability of overhanging girders.

5.1 Experimental Girder Capacities

The peak loads applied at the cantilever tip during the tests are shown in Table 5-1. The first test specimen, which was intended to be subjected to a ratio of 0.80 of the load on the back span to the load on the cantilever, actually ended up having a 0.75 load ratio due to nuances in figuring out the loading scheme in the laboratory.

It should also be noted that LRC1-0.38 had to be retested due to an inconsistency in the load applied in the first test. For all GLS tests, a fair amount of the lateral movement of the girders was accommodated by the threaded rods of the load collar tilting in the direction out of plane of the girder rather than movement of the GLS. Furthermore, the threaded rods also tilted in-plane of the girder to continue loading the girder as it also bent in-plane. In an attempt to minimize this tilting, in LRC1-0.38, shorter threaded rods were used in the load collar such that the threaded rods were connected to the top HSS with a nut on the bottom wall of the HSS rather than the top, therefore bringing the load point closer to the bearing on the top flange, as shown in Figure 5-1. This required switching to a semi-cylindrical bearing rather than a hemispherical bearing to ensure the loading mechanism remained stable without engaging the stiffness of the additional length of threaded rod. However, upon performing the test, a load much higher than anticipated was obtained as the peak load. It was concluded that the semi-cylindrical bearing provided additional restraint to the tip of the cantilever when it was used as part of the GLS assembly, since the semi-cylindrical bearing

does not allow for the additional degree of rotation that allows for in-plane bending. This was not an issue, however, for the tests performed with the semi-cylindrical bearing connected to the reaction frame (i.e., when GLSs were not used), for the pin-connected hydraulic actuators provided this degree of rotation. Therefore, LRC1-0.38 was retested on a new girder using a hemispherical bearing at the tip of the cantilever; its results are reported herein as LRC1-0.38 Retest.

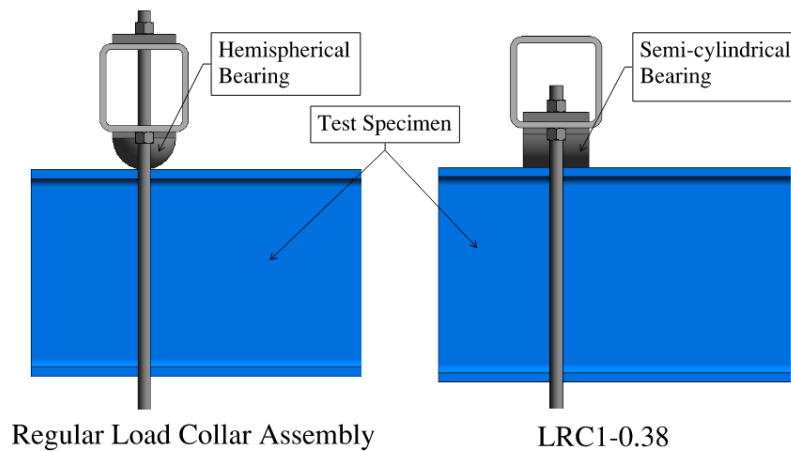


Figure 5-1: Load collar assembly change in LRC1-0.38

Table 5-1 summarizes the peak loads applied at the cantilever tip and back span load point locations, P_{max} and P_b , respectively, the local maximum bending moment along the back span, M_{max}^L , the bending moment at the fulcrum support, M_{Fmax} , as well as the moment capacities normalized to the plastic moment for the back span and fulcrum. The maximum loads and moments reported were calculated using the reaction forces obtained from the load cells, considering the self-weight of the girder and the weight of the load collar at the cantilever tip, which weighed approximately 3.9 kN. The plastic moments were calculated using measured cross-sectional dimensions and yield stresses, with flange and web separated, as reported in Chapter 3.

Table 5-1: Experimental girder capacities

Specimen ID	Max. Load at Cantilever, P_{max} (kN)	Max. Load at Back Span, P_b (kN)	Local Max. Moment on Back Span, M_{max}^L (kN·m)	Max. Moment at Fulcrum, M_{Fmax} (kN·m)	M_{max}^L/M_p	M_{Fmax}/M_p
LRC1-0.80	172	138	644	334	1.01	0.52
LRC1-0.38	332	126	479	619	0.78	1.01
LRC1-0.38 Retest	315	120	473	574	0.77	0.93
LRC1-0.25	300	75	218	544	0.36	0.90
LRC2-0.75	188	141	635	409	1.01	0.65
LRC2-0.38	319	121	473	592	0.74	0.93
LRC2-0.25	330	83	211	608	0.33	0.95
LRC3-0.80	172	138	636	331	1.01	0.53
LRC3-0.25	372	93	263	686	0.42	1.10
LRC4-0.80	167	137	624	333	1.02	0.54
LRC4-0.38	301	114	409	552	0.66	0.89
LRC4-0.25	303	76	209	554	0.34	0.90
LRC5-0.80	172	138	641	332	1.00	0.52
LRC5-0.25	371	93	280	693	0.44	1.09

5.1.1 Experimental Range of Inelastic Behaviour

CSA S16-19 classifies inelastic buckling as buckling that occurs with an M_{max}/M_p value greater than 0.67, but less than 1.00. According to this definition, girders LRC2-0.38, LRC2-0.25, LRC4-0.38, LRC4-0.25, LRC1-0.38 Retest and LRC1-0.25 experienced inelastic buckling, while the rest

reached their full cross-sectional capacity. Nethercot (1974) suggested a classification of the range of buckling which includes the residual stresses seen on the girder; the classification of the girders tested is presented according to this definition in Section 5.3. The obtained range of inelastic behaviour, which saw M_{max}/M_p values falling between 0.89 to 1.10, was significantly higher than the intended range of 0.65 to 1.04. A factor that had a major influence on these results was the degree of warping restraint provided at the fulcrum. There are two main sources of this partial restraint, apart from the internal warping restraint due to the continuity between the cantilever and back span: 1) the rotational restraint about the vertical axis present at the fulcrum due to the support assembly which the girder sits on; 2) the side plates used at the supports for lateral bracing, specifically at the fulcrum support, which is located only 1.83 m away from the cantilever tip, which inhibited warping. Due to the close proximity of the support to the segment of the girder which undergoes the largest deflections at buckling, the girder's capacity becomes extremely sensitive to additional restraint provided at the fulcrum support location, where significant warping deformations are expected at buckling. Additional restraint provided by the fixtures in the support assembly would result in peak loads higher than expected if there were no warping restraints whatsoever; this is explained in further detail in Section 5.4. Furthermore, it should be noted that an M_{max}/M_p value higher than 1.00 is possible due to material strain hardening effects, where the girder experiences an increase in strength as it is subjected to plastic deformation, therefore allowing the maximum moment experienced to slightly exceed the plastic moment of the section.

5.1.2 Effect of Residual Stresses

The residual stress distribution of the W410×85 section used in the experiments, as seen in Figure 3-18, displays tensile stresses at the junction between the flange and the web, transitioning into compressive stresses at the flange tips. The web of the section progresses from tensile residual stresses at the web-flange junction to compressive residual stresses at the middle of the web. As Bjorhovde (1980) stated that residual stresses play a major role in the inelastic LTB strength of laterally unsupported girders, it is important to consider the effects of these residual stresses on the results presented herein. The residual stress distributions observed for the W410×85 section in this experimental investigation compare well with findings by previous experimental programs, such as Essa and Kennedy (1993) and Kitipornchai and Trahair (1975). For comparison, Essa and

Kennedy (1993) found the maximum tensile residual stress at the web-flange junction of the W310×39 section to be $0.21F_y$, while the maximum tensile stress of the W410×85 section studied herein was found to be $0.23F_y$.

While residual stress data is available only for girders from Heat 1, and the effect of residual stresses on the capacities of girders with different residual stress patterns is therefore not realized directly by this investigation, it is known from previous investigations (Essa and Kennedy 1993) that the compressive residual stresses seen at the flange tips of the girders in Heat 1 are expected to reduce the lateral stability of the girder. This is due to the compressive residual stresses present initially in the compression flange, accelerating compressive yielding at this flange and therefore triggering lateral instability. Essa and Kennedy (1993) and Kitipornchai and Trahair (1975)'s numerical investigations of the opposite phenomenon, where tensile residual stresses are present at the flange tips, showed that early yielding of the tension flange has a negligible effect on the lateral stability of the girder.

5.1.3 *Effect of Lateral Bracing*

The effect of a bottom chord extension can be seen by analyzing the results for the five LRCs, first considering only the load case of $0.25P_{max}$ applied at each of the back span load locations. Test specimen LRC1-0.25 (C(U)–B(T)) was the least restrained of the five LRCs, with the cantilever tip left unbraced laterally and lateral restraints provided only to the top flange of the back span load locations. The maximum negative moment ratio seen for this test specimen was an M_{Fmax}/M_p of 0.90. The effect of an additional lateral brace applied to the bottom flange of the back span load location closest to the fulcrum support, simulating a bottom chord extension, can then be observed from the results of LRC4-0.25 (C(U)–B(TB)), which had an identical M_{Fmax}/M_p ratio of 0.90. This indicates that the additional lateral brace on the bottom flange of the back span did not have any effect on the capacity of the girder when the cantilever tip remained unbraced. Furthermore, comparing LRC4-0.38 and LRC1-0.38 Retest, the observed M_{Fmax}/M_p ratios were 0.89 and 0.93, respectively, indicating an increase in capacity of approximately 4% due to the removal of the lateral brace at the bottom flange on the back span. This indicates that the addition of a bottom flange on the back span adjacent to the fulcrum does not enhance the moment capacity of the

girder, and may in fact be slightly detrimental on the capacity. Further research may be useful in understanding this phenomenon and the consequences of adding a bottom flange brace on the back span while leaving the cantilever tip unbraced.

LRC2-0.25 (C(T)–B(T)) was the next critical bracing condition investigated, with a brace provided to the top flange only at the tip of the cantilever and the back span load location closest to the fulcrum support. This bracing condition resulted in an M_{Fmax}/M_p value of 0.95, corresponding to a 6% increase in capacity compared to LRC1-0.25. This is larger than the increase in capacity when a bottom flange lateral restraint was instead added to the bottom flange on the back span while keeping the cantilever tip unbraced in LRC4-0.25, suggesting that bracing the top flange of the cantilever is more effective at increasing the capacity of a single-overhanging girder under the given loading condition compared to adding a bottom chord extension on the back span.

LRC3-0.25 (C(TB)–B(T)) saw the cantilever tip braced at both the top and bottom flanges, with no bottom chord extension on the back span. Compared to LRC1-0.25, this provided a 22% increase in capacity, and a 16% increase in capacity compared to LRC2-0.25 (identical to LRC3-0.25 excluding the bottom chord extension on the cantilever tip). Unlike LRC1-0.25 and LRC2-0.25, LRC3-0.25 was able to reach its fully plastic moment capacity rather than failing due to inelastic LTB. The addition of the bottom flange lateral restraint at the cantilever tip proved to be very effective in increasing the capacity of the girder under the given loading.

Lastly, LRC5-0.25 (C(TB)–B(TB)) was the most restrained test specimen group of the five groups, with bottom chord extensions at both the cantilever tip and the back span load location closest to the fulcrum. Compared to the least restrained test specimen, the M_{Fmax}/M_p ratio of 1.09 exceeds LRC1-0.25's ratio of 0.90 by 21%. This is similar to the increase in capacity seen for LRC3-0.25, since both bracing conditions provided sufficient restraint to the girder such that it was able to reach its full cross-sectional strength (and continue to undergo strain hardening, leading to a moment ratio exceeding 1.00).

Comparing LRC1-0.25, LRC4-0.25, and LRC3-0.25, the effect of providing additional restraint to the more critically loaded segment (i.e., the segment which has a higher distributed load

magnitude, indicated by the κ_1'' ratio of the distributed load on the back span to that on the cantilever segment) of the overhanging girder can be observed. For this loading condition (0.25 load ratio), the load applied on the cantilever tip is much higher than the load applied on the back span, and therefore the cantilever either buckles or reaches its full cross-sectional capacity at the fulcrum. The back span, on the other hand, provides additional restraint to the cantilever segment due to the continuity of the girder at the fulcrum support and the flexural stiffness of the back span. LRC1-0.25 included an unbraced cantilever tip and no bottom chord extension on the back span. When a bottom chord extension was added to the back span in LRC4-0.25, the capacity remained the same. However, when the cantilever tip was braced at the top and bottom flanges instead in LRC3-0.25, the capacity increased by 22%, resulting in a change in failure mode from inelastic LTB seen in LRC4-0.25 and LRC1-0.25 to full cross-sectional strength reached in LRC3-0.25. Therefore, it can be concluded that restraining the more critically loaded segment is more effective in increasing the capacity of the system compared to restraining the adjacent segment.

It should be noted that experimental errors in load application have the ability to influence capacities; therefore, relatively small changes in capacity between various tests (in the range of approximately 4% or lower) should be considered with potential errors in mind. Such potential errors are discussed in Chapter 5.4.

5.1.4 Effect of Loading Condition

The effect of various loading conditions can be observed by analyzing the capacities for the three loading conditions within each of the LRCs. The experimental results show that changing the load magnitude on the back span with respect to that on the cantilever tip has the ability to change the failure mode of the girder. A load ratio of 0.80, where a relatively low load was applied on the cantilever compared to the total load applied on the back span, resulted in the back span reaching the plastic moment of the cross-section at the second load point from the south support (the location of maximum positive moment). For girders tested under load ratios of 0.38 or 0.25, the critically loaded segment was the cantilever rather than the back span due to the relatively high load applied on the cantilever. The failure mode in these girders was either inelastic LTB or reaching the plastic moment, depending on the extent of lateral bracing provided to the girder.

In the most heavily braced LRC groups (LRCs 3 and 5), testing a girder under a load ratio of 0.80 resulted in a bending moment distribution at failure which saw the second load point from the south support reaching a maximum positive moment of M_p (or slightly higher due to strain hardening effects), while the fulcrum experienced a maximum negative moment of 0.52-0.54 M_p . This led to excessive lateral deformations and twist at the midspan of the back span since the exact point of maximum positive moment was a load point and was therefore laterally restrained. On the other hand, girders tested under a load ratio of 0.25 were subjected to a much higher load applied on the cantilever tip compared to the loads applied at each of the back span load locations. These girders saw the fulcrum moment reach M_p , resulting in excessive lateral deformations and twist at the cantilever, while the maximum positive moment experienced on the back span was between 0.42 and 0.44 M_p .

Test specimens in the remaining LRC groups (LRCs 1, 2 and 4) loaded under load ratios of 0.25 and 0.38 experienced inelastic buckling of the cantilever, with the maximum negative moment at the fulcrum ranging between 0.89 and 0.95 M_p . The maximum positive local bending moment experienced by the back span was much higher for load ratios of 0.38 due to the higher load applied on the back span compared to 0.25 ratios. On the other hand, girders tested under a load ratio of 0.80 in these LRC groups saw much higher loads on the back span and, consequently, reached its full cross-sectional strength and exhibited large deformations on the back span.

When comparing load ratios of 0.25 and 0.38, it was observed that changing the load ratio while the magnitude of the distributed load on the cantilever remained larger than the load on the back span (κ_1'' values less than 1.00) has a very small impact on capacity, increasing the M_{Fmax}/M_p ratio by only 1% for LRC4-0.25 compared to LRC4-0.38 and by 2% when comparing LRC2-0.25 to LRC2-0.38. LRC1-0.38 Retest saw a 3% increase compared to LRC1-0.25. This agrees with the predictions seen in Figure 3-6 which showed that for κ_1'' values less than 1.00 the capacity does not change much with changing load ratios.

5.2 Displacement Results

During the tests, girder deflections were monitored at both the cantilever tip and the midspan of the back span. This was an important aspect of the tests in order to control the deformations as the girder reached its buckling load and entered the post-buckling stage, where deformations can progress quickly. When the deflection of a girder continued increasing while the load remained constant, buckling was considered to have been reached, and the load was held constant in order to examine the post-buckling response until either the vertical deflection or rotation limits of the bracing brackets was reached, or hydraulic actuators reached their maximum stroke.

Figure 5-2 shows LRC4-0.80 at the end of the test, with large downward vertical deflections of up to 134.9 mm evident along the back span and upward deflection up to 45.5 mm seen at the tip of the cantilever. Figure 5-3 shows the cantilever segment at the end of the test in LRC5-0.25, which was laterally braced at both the top and bottom flanges at the cantilever tip and therefore experienced large downward vertical deflections of up to 110 mm at this location under the 0.25 load ratio. The cross-sectional view of the cantilever end of LRC2-0.38, which had lateral bracing only at the top flange and exhibited large twist of up to 13.6 degrees (measured at the web) at the end of the test, is shown in Figure 5-4.

Table 5-2, Table 5-3, Table 5-4 and Table 5-5 summarize the deflections measured for each girder at both measurement locations, both at the peak load and immediately before unloading (i.e., the maximum post-buckling response observed). These measurements are reported with the following sign convention, as seen previously in Figure 4-2: positive vertical deflection is upward; positive lateral deflection is movement to the west; positive cross-sectional twist is clockwise rotation when looking at the girder from the south end; positive rotation about a vertical axis is counter-clockwise rotation when looking at the plan view of the girder; and positive longitudinal displacement is movement to the north. Results are unavailable for the post-buckling vertical deflection of LRC2-0.25 due to the cable transducer measuring this deflection malfunctioning during the test. The Miller-West Gliders at the cantilever tip bottom flange and midspan top flange were also not functioning properly throughout LRC4-0.80's test, so data is unavailable for those deflections.



Figure 5-2: Downward deflection on back span and upward deflection at cantilever for LRC4-0.80 at the end of the test

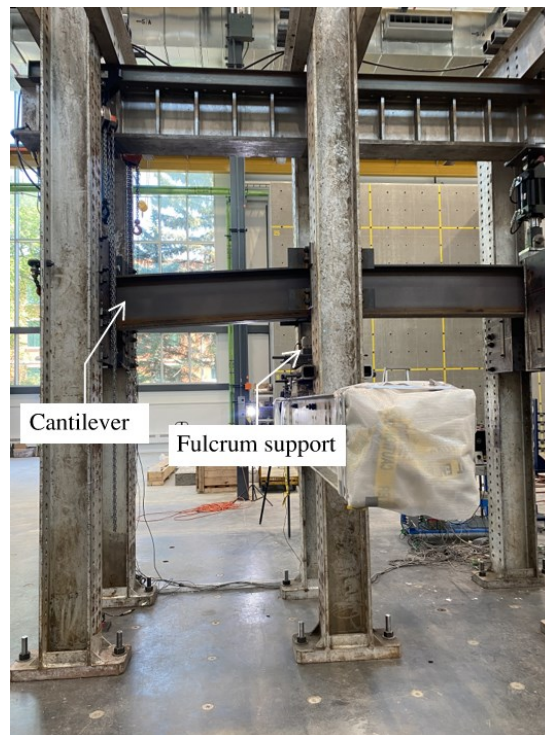


Figure 5-3: Downward deflection at cantilever for LRC5-0.25 at the end of the test



Figure 5-4: Cross-sectional view of cantilever tip at end of LRC2-0.38 test

5.2.1 *General Observations on Displacement*

In the first four tests, the longitudinal rollers were unlocked at both the north and south supports. In LRC2-0.38 and LRC2-0.25, the load ratio resulted in a relatively high load applied at the cantilever compared to each of the back span loads, and therefore loading could be applied in a stable manner while keeping both support rollers unlocked. However, for LRC2-0.75 and LRC3-0.80, the high loads applied on the back span combined with the additional load applied at the cantilever tip resulted in the girder suddenly displacing in the longitudinal direction. This occurred shortly after reaching the load–deflection plateau for LRC2-0.75, and the girder was unloaded afterwards. For LRC3-0.80, the girder jumped longitudinally just prior to reaching the load–deflection plateau, but loading was continued in order to reach the plateau and continue pushing the girder to observe its plastic deformations. Since LRC2-0.75 was unloaded right after it jumped longitudinally, deformations were not able to be obtained much further than those obtained when the peak load was reached. In all subsequent tests, the north support was locked in the longitudinal direction to create a more stable loading mechanism and allow for further investigation of the girders’ post-buckling response. The maximum possible north support displacement after locking the roller was 5 mm in either direction.

Table 5-2: Deflections at midspan of back span at peak load

Specimen ID	Vertical Deflection	Lateral Deflection		Cross-sectional Twist			Longitudinal Displacement	
		Top Flange	Bottom Flange	Top Flange	Web	Bottom Flange	South End Support	Fulcrum
	(mm)	(mm)	(mm)	(deg)	(deg)	(deg)	(mm)	(mm)
LRC1-0.80	-117.5	5.3	2.8	-0.2	-0.2	-0.2	-19.8	-1.5
LRC1-0.38	-54.1	-2.6	9.7	2.0	2.0	1.9	-5.7	0.9
LRC1-0.38 Retest	-55.8	-2.7	11.5	2.2	2.2	2.2	-6.6	0.3
LRC1-0.25	-17.5	-0.1	8.0	1.3	1.3	1.2	-0.6	0.5
LRC2-0.75	-103.1	4.9	-4.4	-1.1	-1.1	-1.3	-15.1	-0.3
LRC2-0.38	-48.3	7.7	-25.8	-4.7	-4.8	-4.7	-7.6	-2.6
LRC2-0.25	-16.7	3.2	-27.3	-4.4	-4.4	-4.4	-4.5	-4.7
LRC3-0.80	-118.4	13.6	-11.7	-3.2	-3.2	-3.2	38.1	46.1
LRC3-0.25	-20.7	3.4	-19.1	-3.3	-3.2	-3.2	-1.2	-0.3
LRC4-0.80	-121.6	-	3.8	1.1	0.9	1.0	-22.4	-3.9
LRC4-0.38	-42.4	0.8	-2.5	-0.4	-0.4	-0.4	-7.2	-2.3
LRC4-0.25	-14.2	-0.9	2.7	0.6	0.5	0.5	-1.1	-1.1
LRC5-0.80	-119.3	9.1	-1.5	-1.1	-1.2	-1.1	-22.1	-3.3
LRC5-0.25	-21.1	-2.4	2.7	0.8	0.9	0.8	1.5	-2.1

Table 5-3: Deflections at cantilever tip at peak load

Specimen ID	Vertical Deflection (mm)	Lateral Deflection		Cross-sectional Twist		
		Top Flange (mm)	Bottom Flange (mm)	Top Flange (deg)	Web (deg)	Bottom Flange (deg)
LRC1-0.80	40.9	-4.8	1.2	0.7	0.8	0.7
LRC1-0.38	-13.6	-31.5	-0.6	3.6	4.4	3.7
LRC1-0.38 Retest	-6.6	51.1	-15.5	-7.4	-8.9	-7.2
LRC1-0.25	-17.1	58.3	-17.1	-7.3	-8.4	-6.8
LRC2-0.75	32.6	0	0.8	-0.3	0.2	0.1
LRC2-0.38	-30.5	0	60.7	8.7	8.9	7.5
LRC2-0.25	-56.9	0	52.1	6.8	7.6	6.4
LRC3-0.80	44.5	0	0	0.5	0.2	0.2
LRC3-0.25	-69.6	0	0	0.8	0.7	0.5
LRC4-0.80	40.5	1.1	-	-0.4	-0.6	-0.6
LRC4-0.38	-21.3	-23.7	10.3	4.2	4.9	3.8
LRC4-0.25	-37.2	-38.6	6.3	4.5	5.6	4.7
LRC5-0.80	40.7	0	0	1.4	1.1	0.8
LRC5-0.25	-87.0	0	0	-0.8	-0.9	-0.7

Table 5-4: Deflections at midspan of back span at post-buckling

Specimen ID	Vertical Deflection (mm)	Lateral Deflection		Cross-sectional Twist			Longitudinal Displacement	
		Top Flange (mm)	Bottom Flange (mm)	Top Flange (deg)	Web (deg)	Bottom Flange (deg)	South End Support (mm)	Fulcrum (mm)
LRC1-0.80	-121.6	6.7	2.5	-0.4	-0.5	-0.5	-20.4	-1.6
LRC1-0.38	-54.8	-2.0	8.0	1.7	1.6	1.5	-5.9	0.9
LRC1-0.38 Retest	-55.9	-3.0	13.1	2.4	2.5	2.4	-6.5	0.3
LRC1-0.25	-18.8	-0.3	10.7	1.7	1.6	1.6	-0.7	0.5
LRC2-0.75	-122.2	9.9	-7.3	-2.1	-2.3	-2.4	-25.2	-6.0
LRC2-0.38	-52.9	9.5	-34.2	-6.2	-6.2	-6.1	-8.0	-2.9
LRC2-0.25	-16.4	4.1	-43.2	-6.8	-6.9	-6.8	-4.3	-5.7
LRC3-0.80	-122.6	13.7	-10.8	-3.0	-3.1	-3.1	37.2	46.6
LRC3-0.25	-20.8	3.5	-20.5	-3.5	-3.4	-3.4	3.7	2.0
LRC4-0.80	-134.9	-	3.9	0.9	0.9	0.8	-23.9	-4.0
LRC4-0.38	-42.4	0.8	-2.5	-0.5	-0.4	-0.5	-7.2	-2.3
LRC4-0.25	-14.2	-0.5	1.6	0.4	0.3	0.3	-1.0	-1.2
LRC5-0.80	-123.0	10.3	-1.8	-1.3	-1.4	-1.3	-22.9	-3.5
LRC5-0.25	-21.4	-2.6	1.9	0.8	0.8	0.7	6.1	0.6

Table 5-5: Deflections at cantilever tip at post-buckling

Specimen ID	Vertical Deflection (mm)	Lateral Deflection		Cross-sectional Twist		
		Top Flange (mm)	Bottom Flange (mm)	Top Flange (deg)	Web (deg)	Bottom Flange (deg)
LRC1-0.80	42.2	-4.7	1.6	0.8	0.9	0.7
LRC1-0.38	-14.4	-54.1	8.9	7.5	8.8	7.4
LRC1-0.38 Retest	-7.2	62.1	-20.2	-9.2	-11.0	-8.9
LRC1-0.25	-30.4	78.3	-24.9	-10.4	-12.1	-9.9
LRC2-0.75	40.0	0	2.8	-0.1	0.4	0.5
LRC2-0.38	-60.2	0	87.7	12.8	13.6	11.5
LRC2-0.25	-	0	96.5	12.5	14.4	12.1
LRC3-0.80	51.4	0	0	0.5	0.2	0.2
LRC3-0.25	-73.6	0	0	0.8	0.7	0.5
LRC4-0.80	45.5	1.1	-	-0.4	-0.6	-0.7
LRC4-0.38	-22.3	-57.0	17.7	8.4	9.7	8.0
LRC4-0.25	-40.0	-87.4	18.4	11.2	13.5	11.3
LRC5-0.80	43.8	0	0	1.4	1.1	0.8
LRC5-0.25	-110	0	0	-1.0	-1.0	-0.9

For girders tested under a load ratio of 0.80, the combined loading on the back span was relatively high compared to the single point load acting on the cantilever tip. This caused significant downward vertical deflections along the back span and caused the cantilever to deflect upward. Due to the large vertical deflections along the back span, the stroke of the hydraulic actuators on the back span was often reached shortly after the peak load, specifically the stroke of the two interior actuators on either side of the midspan of the back span (which saw the highest amount of vertical deflection). Due to this, the response of the girders tested under a load ratio of 0.80 was not able to be investigated much further than the peak load. The maximum vertical deflection observed at the midspan of the back span for each of the girders tested under a load ratio of 0.80 ranged between 121.6 and 134.9 mm, which corresponds to the remaining stroke of the hydraulic actuators upon clearing the initial gap in the test frame. On the other hand, girders tested under a load ratio of 0.38 or 0.25 experienced larger downward vertical deflections at the cantilever tip, and the stopping criteria for these tests were large rotations seen on the cantilever tip.

LRC1-0.38 Retest and LRC1-0.25 were the two least restrained test specimens, with a completely unbraced cantilever tip and no bottom flange bracing on the south side of the fulcrum support, while simultaneously having relatively high loads applied at the cantilever tip compared to the back span loads. Due to the lack of bottom flange bracing on the back span, warping deformations were evident at the fulcrum in these two tests. This was confirmed by two rotary variable displacement transducers (RVDTs) which were placed on the top and bottom flanges of the girder at the centerline of the fulcrum support for these two tests, measuring the rotation of the flanges about a vertical axis. The RVDT readings showed that the bottom flange of the girder rotated clockwise in both tests, while the top flange rotated counterclockwise, consistent with warping. The top flange was also seen to rotate about the vertical axis more than the bottom flange at the onset of buckling.

The maximum top flange lateral deflection experienced at buckling at the cantilever tip was 58.3 mm, and the minimum was 1.1 mm (looking only at the tests with an unbraced top flange at the cantilever tip). At buckling for LRC 1 and LRC 4 girders tested under load ratios of 0.38 and

0.25, the amount of lateral deflection of the top flange of the cantilever tip was always larger than the amount of downward vertical deflection at the cantilever tip. Conversely, girders which reached their full cross-sectional capacity at either the back span or fulcrum support experienced much larger vertical deflection compared to the lateral deflection of either flange at peak load. For all tests where both the top and bottom flange of the cantilever were unbraced, the top flange exhibited lateral deflection which was larger and in the direction opposite to that of the bottom flange.

At the midspan of the back span, the rotations of the top flange, web, and bottom flange at peak load were extremely close, with a maximum deviation of 0.2 degrees. This deviation also held true as the girder underwent plastic deformations. At the cantilever tip, however, the rotations of the web and bottom flange differed by a maximum of 1.6 degrees at buckling, seen in LRC1-0.25, which could be a sign of combined distortional buckling and LTB. In this test, which was the least restrained but most highly loaded girder at the cantilever, web distortion was also visible at the tip of the cantilever near the end of the test, at which time the difference in web and bottom flange rotations had increased to 2.2 degrees. It should be noted that the top flange clinometer at the cantilever tip was placed 90 mm south of the centerline of the load applied at the tip in order to clear the semi-cylindrical or hemispherical bearings used for loading and may therefore have read rotations which were smaller than those experienced at the true tip.

5.2.2 Load–Deflection Behaviour

Load–lateral deflection curves for the top and bottom flanges of the tests for LRC1-0.80 and LRC1-0.25 are shown in Figure 5-5 and Figure 5-6, respectively, with lateral deflection measured at the midspan of the back span and the load depicting the load applied at the tip of the cantilever. Similar curves for the lateral deflection at the cantilever tip are shown in Figure 5-7 and Figure 5-8 for LRC1-0.80 and LRC1-0.25, respectively. As evident from the curves, lateral deflections were relatively small at the beginning, increasing slowly then more rapidly as the girder got closer to reaching its peak load. The onset of buckling was considered to occur when the load–deflection curve ceased to increase, reaching a horizontal asymptote. The load was then held close to constant to investigate the post-buckling behaviour.

At the midspan of the back span for LRCs 1, 2, 3 and 4, the bottom flange exhibited larger lateral deflection than the top flange for girders tested under load ratios of 0.38 and 0.25, where buckling occurred at the cantilever. This is because the top flange of the girder is braced at 0.914 m on either side of the midspan of the back span. For LRC5-0.25, the lateral deflections of the top and bottom flanges were similar in magnitude, due to the bracing of both the top and bottom flange on the back span load location closest to the fulcrum support. Under a load ratio of 0.80 for all LRCs, where the girder reached the plastic moment at the back span, the midspan of the back span exhibited larger lateral deflections of the top flange compared to the bottom flange. Similarly, under load ratios of 0.38 and 0.25 for LRCs 1 and 4, where the failure was categorized by buckling of the cantilever tip, much larger lateral deflections were observed for the top flange of the cantilever tip compared to the bottom flange. For example, LRC1-0.38 Retest exhibited 51.1 mm and -15.5 mm of top flange and bottom flange lateral deflection at buckling, respectively. While LRC2-0.38 and LRC2-0.25 also underwent buckling at the cantilever, the top flange was braced laterally for these tests, leading to larger bottom flange deflections at buckling of 60.7 mm and 52.1 mm in LRC2-0.38 and LRC2-0.25, respectively.

LRC3-0.80 saw the largest top flange lateral deflection at the midspan of the back span of 13.6 mm at the peak load. The largest cantilever tip top flange lateral deflection at buckling of 58.3 mm was seen for LRC1-0.25, which had an unbraced cantilever tip and no bottom chord extension on the back span. When a bottom flange lateral restraint was added to the back span load location closest to the fulcrum (simulating a bottom chord extension) in LRC4-0.25, the top flange lateral deflection at buckling decreased to 38.6 mm. The bottom flange lateral deflection was also smaller, decreasing from 17.1 mm at buckling for LRC1-0.25 to 6.3 mm for LRC4-0.25. A significant beneficial effect on the lateral stiffness of the cantilever segment is therefore observed due to the addition of a bottom chord extension on the back span when the cantilever tip is left unbraced.

Figure 5-9 and Figure 5-10 show the load–vertical deflection curves of LRC1-0.80 and LRC1-0.25, respectively, depicting vertical deflections at both the midspan of the back span and the cantilever tip. Compared to the lateral deflection, relatively large vertical deflections are evident

from the start of the test and continue to increase as loading is increased. While the back span always deflects downward, upward vertical deflections are seen at the cantilever tip in girders tested under a load ratio of 0.80, due to the larger ratio of the loading on the back span compared to the single point load applied at the cantilever tip. The largest upward vertical deflection at buckling was exhibited by LRC3-0.80, which deflected by approximately 44.5 mm upward. In comparison, LRC5-0.25 deflected by 87.0 mm downward at the cantilever tip. It should be noted that the maximum vertical deflections at peak load exhibited for LRCs 3 and 5 were higher than those for other LRCs since LRCs 3 and 5 reached the fully plastic moment and continued to deform while the capacity increased slightly past the fully plastic capacity due to strain hardening. This means that the maximum vertical deflections reported for LRCs 3 and 5 were taken further on the load–deflection curve plateau, where the true maximum load was observed, than for LRCs 1, 2, and 4, which failed by LTB and exhibited a load drop shortly after the buckling load was reached. Similarly, the largest downward back span vertical deflection at midspan is seen when a load of 0.80 is applied at the back span load locations; for example, LRC4-0.80 deflected downward at the midspan by 121.6 mm at buckling, LRC4-0.38 deflected downward by 42.4 mm, and LRC4-0.25 deflected downward by 14.2 mm. Load–deflection curves for all test girders can be found in Appendix C.

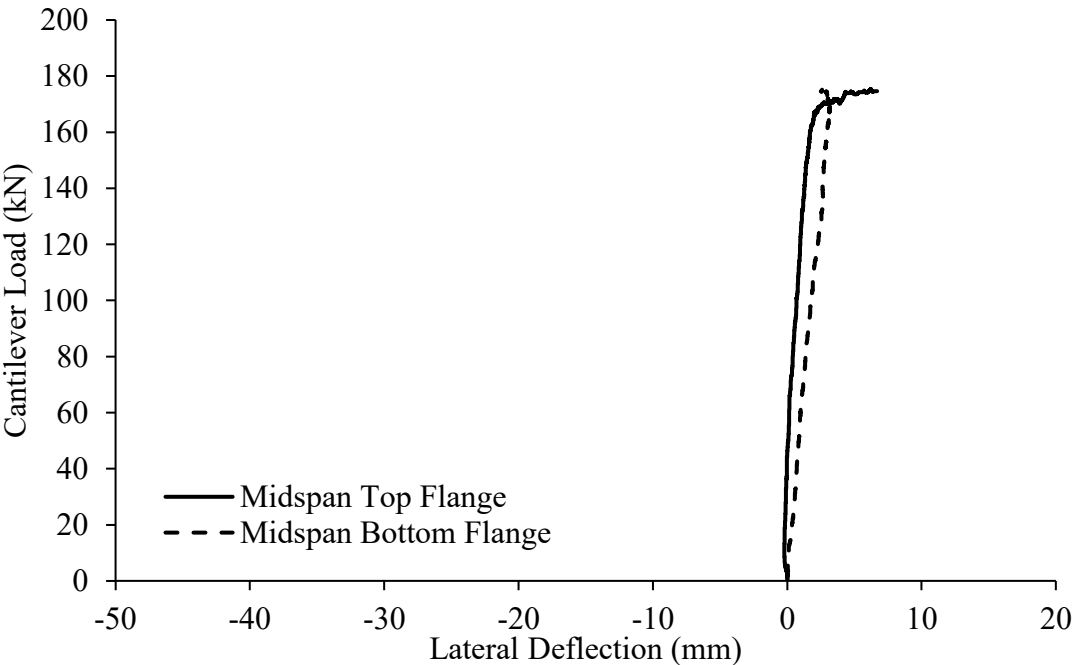


Figure 5-5: Load–lateral deflection curve at midspan of back span for LRC1-0.80

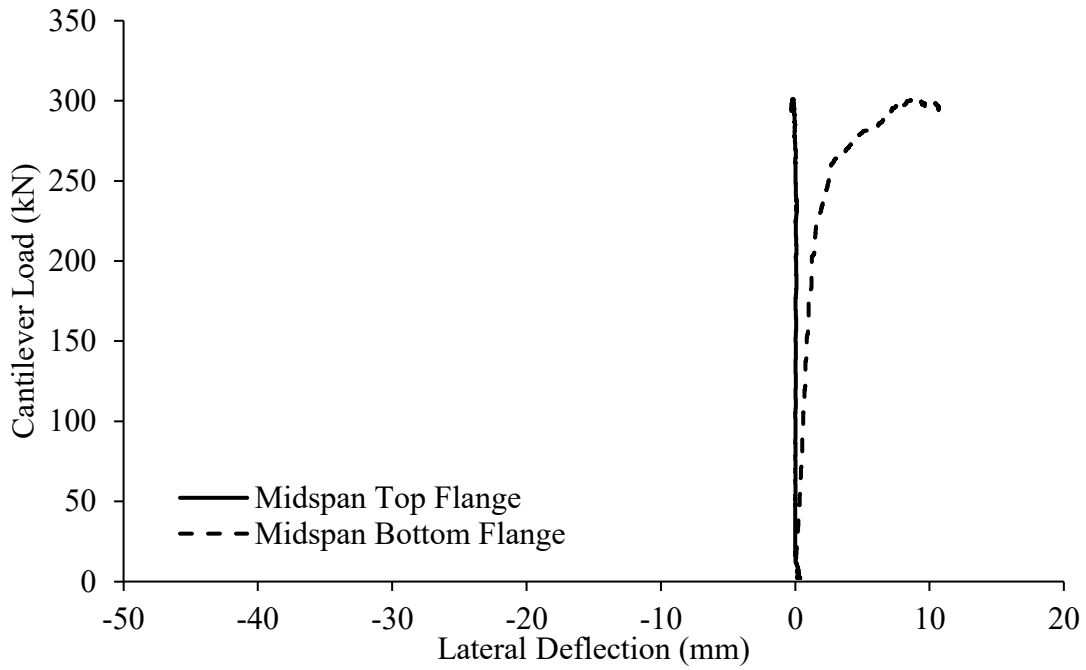


Figure 5-6: Load-lateral deflection curve at midspan of back span for LRC1-0.25

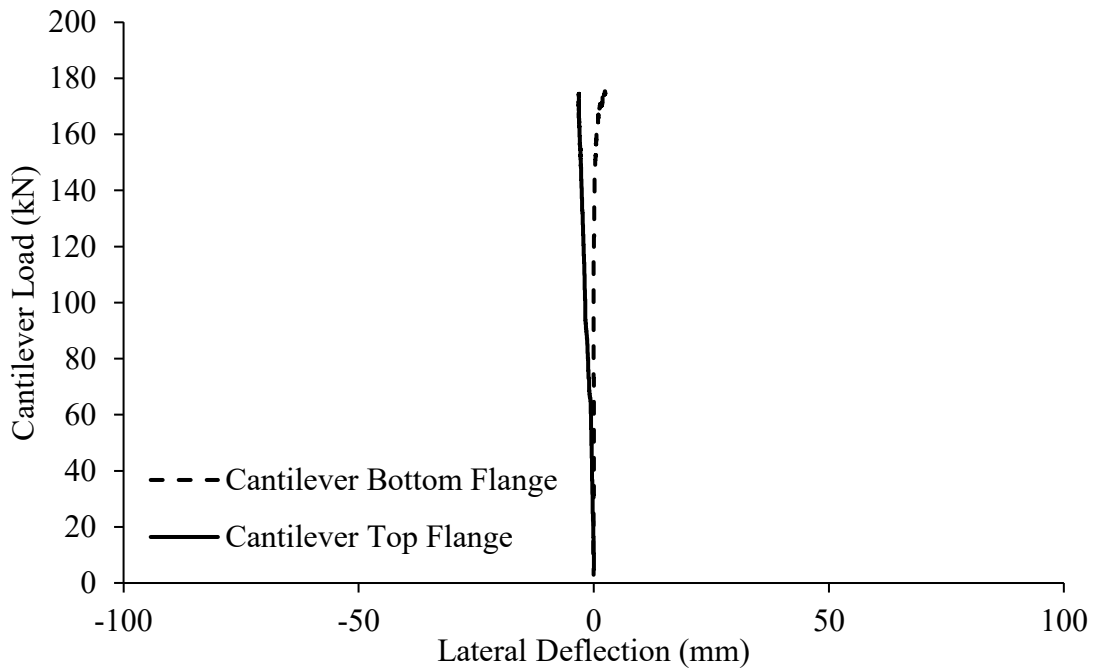


Figure 5-7: Load-lateral deflection curve for cantilever tip for LRC1-0.80

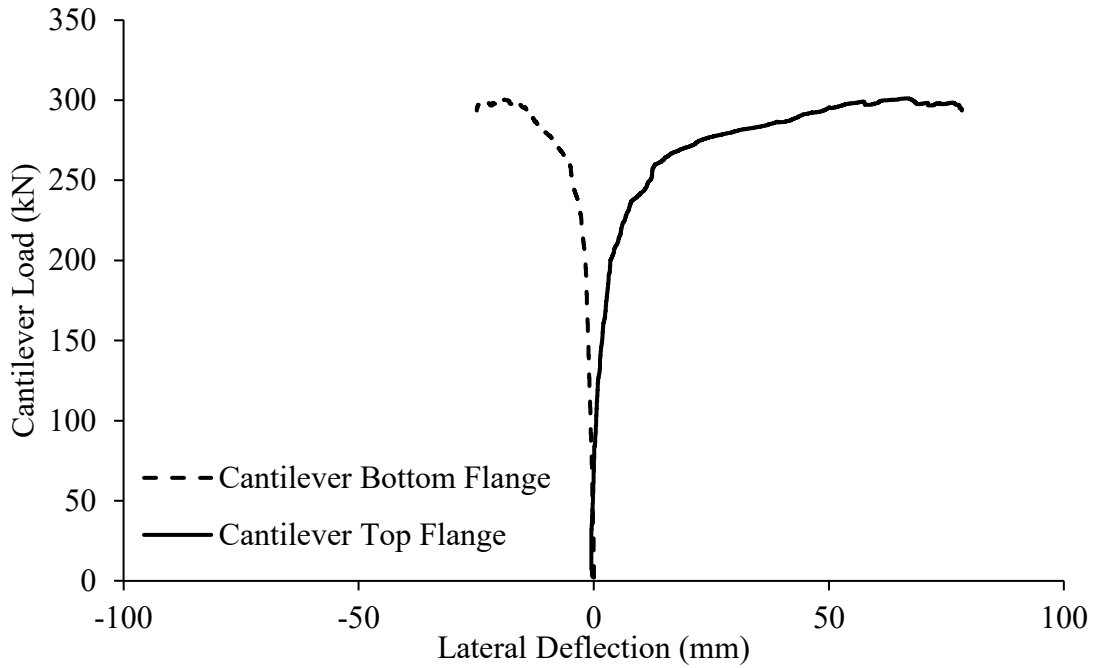


Figure 5-8: Load-lateral deflection curve for cantilever tip for LRC1-0.25

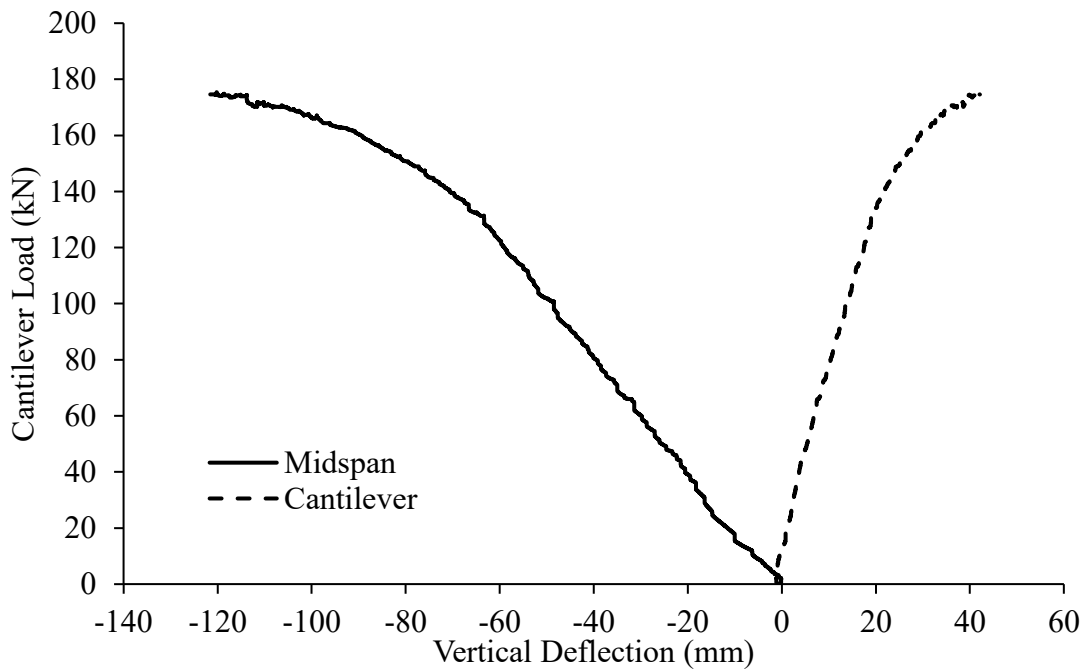


Figure 5-9: Load-vertical deflection curves for LRC1-0.80

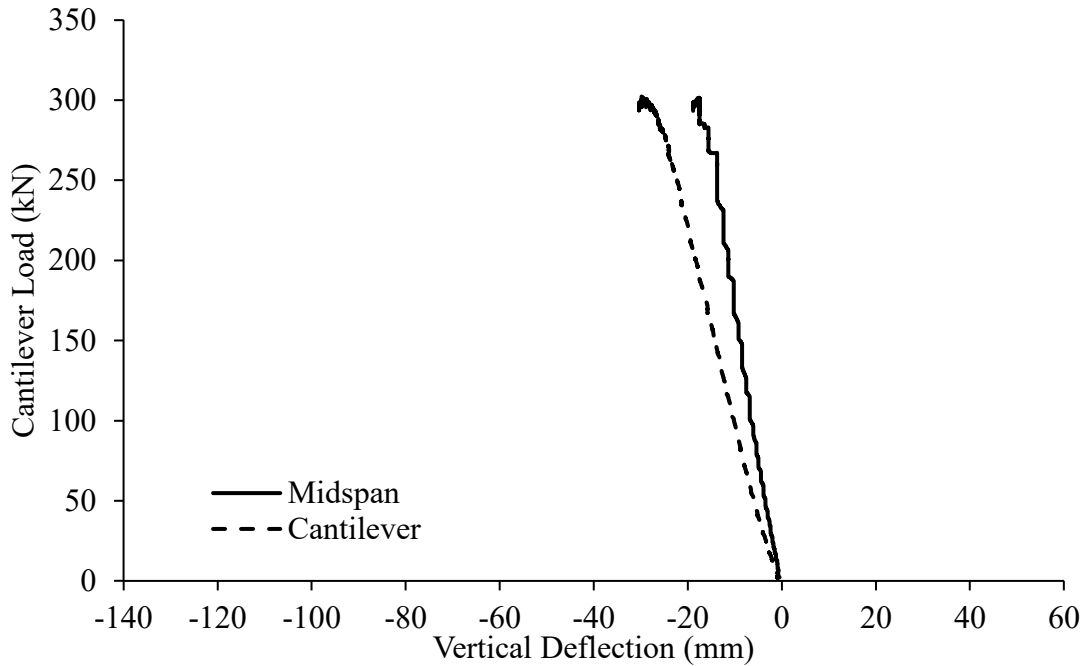


Figure 5-10: Load-vertical deflection curves for LRC1-0.25

5.2.3 Effect of Initial Geometric Imperfections on Deflection

Initial imperfections were measured for each of the test girders as outlined in Chapter 3, as the magnitude of lateral deflection and rotation at buckling are known to be sensitive to these imperfections. The results for the maximum sweep (lateral out-of-straightness) of the top flange and initial twist at the cantilever tip are compared in Table 5-6 to the maximum lateral deflection of the top flange and cross-section twist at the cantilever tip at buckling, for the tests that failed by inelastic LTB. While the sweep distributions presented in Chapter 3 were measured relative to a line running through the centreline of the flange at the cantilever tip and the south support, these values were adjusted to obtain the initial sweep of the cantilever tip relative to the north support.

As shown in Table 5-6, LRC4-0.25 exhibits the largest initial geometric imperfections of the six girders which failed by inelastic LTB. However, this specimen exhibited smaller lateral deflection and twist at buckling compared to LRC1-0.25, which was tested under the same load ratio. This indicates that the bracing provided to the girder played a more vital role on the deflection of the girders compared to the amplitude of initial imperfections, since LRC4-0.25 had an additional

lateral brace applied to the bottom flange on the back span.

LRC4-0.25 and LRC1-0.25 both exhibited lateral deflections of the top flange at buckling in the same direction as the initial sweep of the top flange, while LRC4-0.38 and LRC1-0.38 Retest displaced in the opposite direction to the initial sweep of the top flange. LRC4-0.25 and LRC1-0.25 also exhibited larger lateral deflections at buckling, which could be attributed to the larger load applied on the tip of the cantilever in these tests as well as the fact that the top flange of the girder moved in the same direction as its initial imperfections, rather than first returning to its neutral position of zero lateral deflection before continuing to buckle in the opposite direction as exhibited by LRC4-0.38 and LRC1-0.38 Retest. This observation may have also caused LRC1-0.38 Retest's capacity to increase, resulting in an identical capacity to LRC2-0.38, whereas LRC1-0.25 exhibited a 6% lower capacity compared to LRC2-0.25.

The cross-section twist of LRC4-0.25, LRC1-0.25 and LRC1-0.38 Retest exhibited at buckling aligned with the initially measured twist for these specimens. On the other hand, LRC2-0.38, LRC2-0.25 and LRC4-0.38 twisted in the direction opposite to the initial twist. The initial twist values, however, were relatively small compared to the sweeps and did not have a notable impact on the different magnitudes of twist exhibited by the girders at buckling.

The results in Table 5-6 show that larger initial bottom flange imperfections do not greatly influence the deflections experienced by the bottom flange at buckling. For example, LRC4-0.25, which had the largest initial bottom flange sweep and a higher load applied on the tip of the cantilever compared to LRC4-0.38, exhibited a smaller lateral deflection of the bottom flange at buckling compared to LRC4-0.38.

Table 5-6: Comparison of lateral deflection and twist at cantilever tip at buckling to initial sweep and twist for girders which failed by LTB

Specimen ID	Lateral Deflection		Cross-Section Twist			Initial Sweep		Initial Twist (°)
	Top Flange (mm)	Bottom Flange (mm)	Top Flange (°)	Web (°)	Bottom Flange (°)	Top Flange (mm)	Bottom Flange (mm)	
LRC1-0.38 Retest	51.1	-15.5	-7.4	-8.9	-7.2	-3.1	-5.4	-0.4
LRC1-0.25	58.3	-17.1	-7.3	-8.4	-6.8	3.7	3.1	-0.1
LRC2-0.38	0	60.7	8.7	8.9	7.5	4.2	2.2	-0.3
LRC2-0.25	0	52.1	6.8	7.6	6.4	4.2	2.5	-0.5
LRC4-0.38	-23.7	10.3	4.2	4.9	3.8	4.8	3.9	-0.5
LRC4-0.25	-38.6	6.3	4.5	5.6	4.7	-7.6	-6.9	0.5

5.3 Stress Results

Nethercot (1974) suggested that LTB can only be classified as inelastic if the stress at the compression flange tips reaches the yield stress of the member prior to buckling, taking into account any residual stresses present at the flange tips. The web–flange junction of the tension flange may have experienced significant yielding prior to the instance when the compression flange tips reach the yield stress; however, this does not affect the lateral stability of the girder and therefore does not qualify the girder to have experienced inelastic buckling (Nethercot 1974). Nethercot’s definition of inelastic buckling is used to define the range of buckling experienced, determined by analyzing the strains measured at the top (compression) flange of the back span for girders tested under a load ratio of 0.80 and bottom (compression) flange at the fulcrum support for girders tested under load ratios of 0.38 or 0.25, using longitudinal strain gauges and combining these with the residual stresses measured for the section. If the net stress at the compression flange tips were found to reach the yield stress of the section, obtained from material property results in Chapter 3, the girder is classified as having buckled in the inelastic range.

Figure 5-11 shows the placement of the four strain gauges on the bottom (compression) flange at the fulcrum support along with the cardinal directions in the lab. The test specimen is shown in blue, knife edge in grey, and strain gauges in red. From here forth, these four strain gauges are referred to as Fulcrum Northwest, Northeast, Southwest and Southeast. Figure 5-12 shows the placement of the two strain gauges on the top (compression) flange on the back span, placed 100 mm north of the centreline of the second load point from the south support, referred to as Back Span West and East. The test specimen is shown in blue, semi-cylindrical bearing in grey, and strain gauges in red.

Nethercot (1974)’s definition of inelastic buckling can only be applied to test girders from Heat 1, since residual stress data is unavailable for girders from Heats 2 and 3. The only two test girders from Heat 1 which exhibited LTB prior to reaching their fully plastic moment were LRC2-0.38 and LRC2-0.25. For the other 12 test girders, the stresses are analyzed to ensure yielding of the compression flange tip occurred prior to buckling or reaching the full cross-sectional capacity,

while assuming the same residual stress pattern as Heat 1.

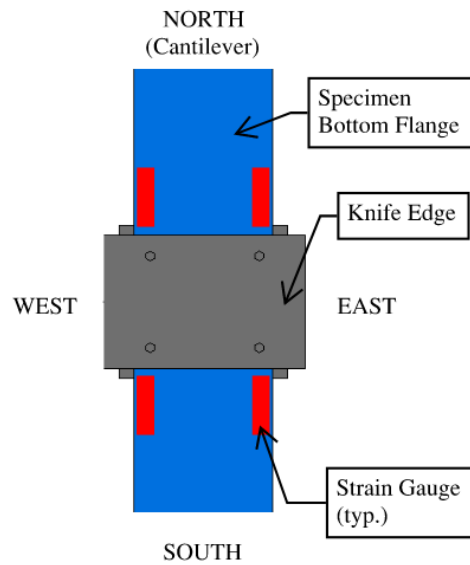


Figure 5-11: Strain gauges on bottom flange of fulcrum support (strain gauges shown in red)

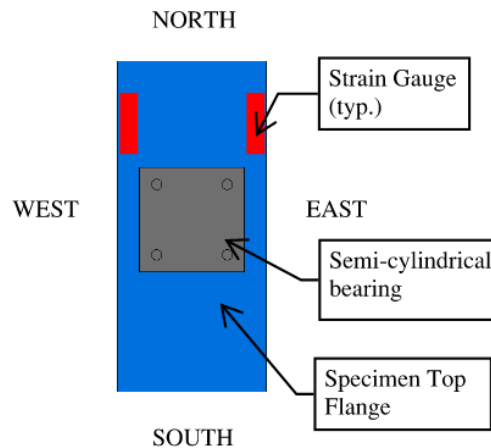


Figure 5-12: Strain gauges on top flange of back span (strain gauges shown in red)

Figure 5-13 shows, for LRC2-0.38, the load applied at the cantilever tip, P_{max} , during the test plotted against the longitudinal microstrains, $\mu\epsilon$, obtained from the Fulcrum Northwest and Northeast strain gauges. Figure 5-14 shows a similar plot for LRC2-0.25, except the Fulcrum Southeast strain gauge was plotted due to the Northeast strain gauge malfunctioning during the test.

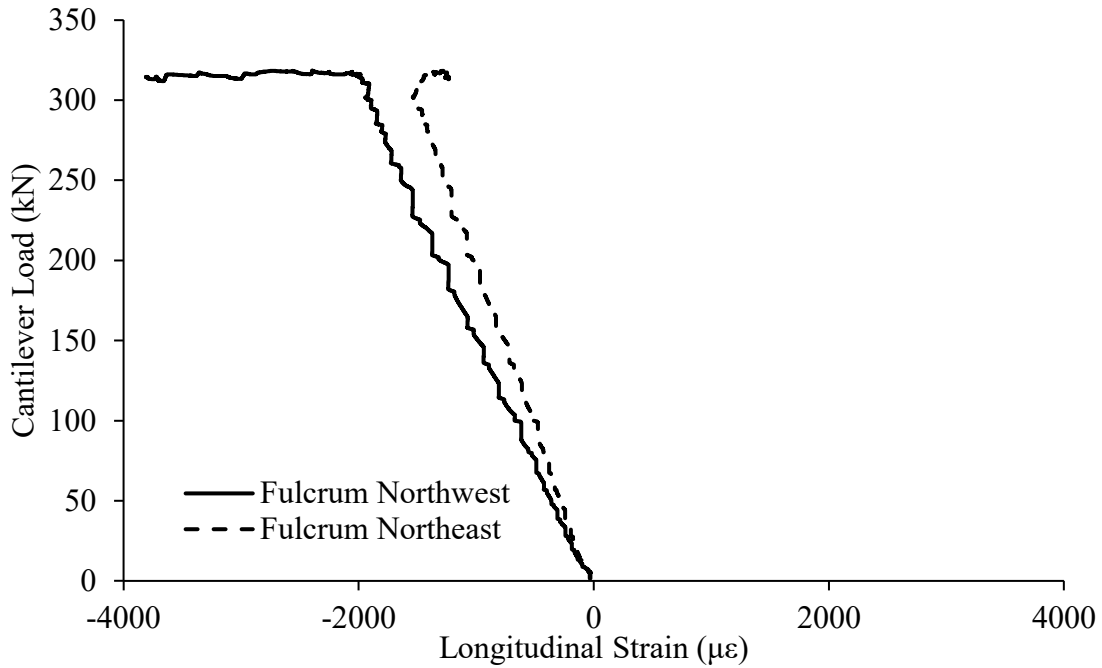


Figure 5-13: Load applied at cantilever tip versus longitudinal flange strains at bottom flange at fulcrum support for LRC2-0.38

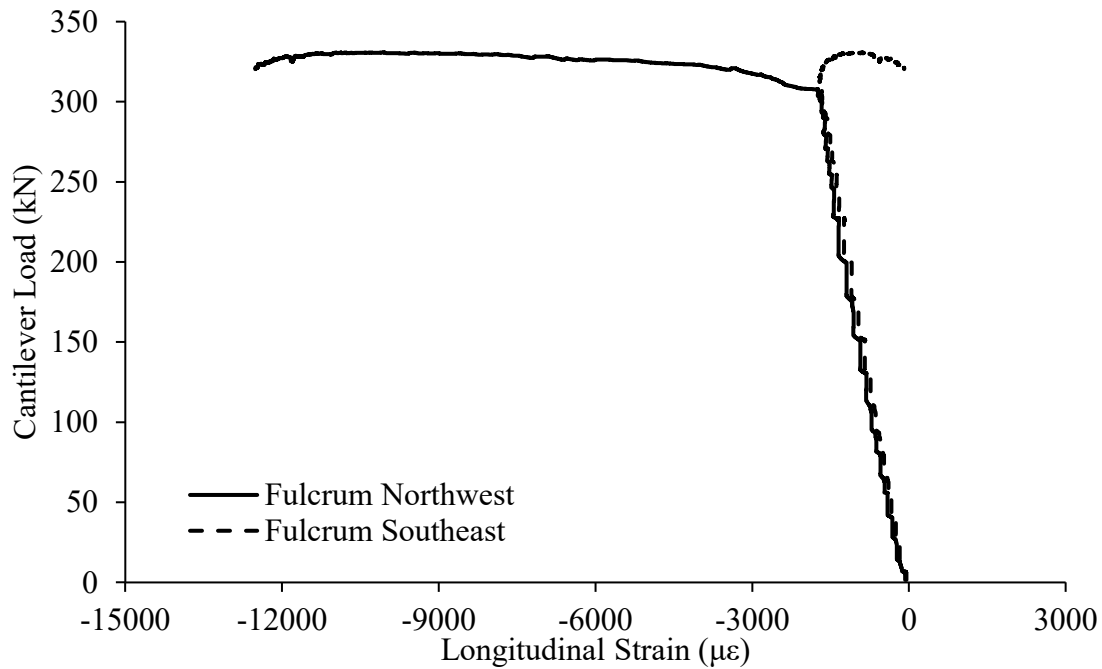


Figure 5-14: Load applied at cantilever tip versus longitudinal flange strains at bottom flange at fulcrum support for LRC2-0.25

The stress corresponding to the strain at peak load measured using the strain gauges can be

obtained using the stress–strain curves obtained from tension coupon tests for each heat. Table 5-7 presents the longitudinal stress obtained at buckling from the strain gauges at the compression flange tips at the two measurement locations, where negative stress indicates compression. These stresses are presented as normalized by the measured flange yield stress of each of the girders, σ_y . An asterisk (*) indicates the value coming from the Fulcrum Southeast strain gauge due to the Fulcrum Northeast strain gauge malfunctioning during the test.

The normalized stresses presented in Table 5-7 show that one side of the flange (east or west) often exhibits higher compressive stresses than the opposite side. In comparison with the lateral deflections seen at buckling at the midspan of the back span and the cantilever tip (Table 5-2 and Table 5-3, respectively), it can be concluded that the side to which the top flange of the girder displaced at buckling at the midspan of the back span for girders tested under a load ratio of 0.80 is the side that experienced higher compressive strains on its top (compression) flange at the second load point from the south support, which is laterally braced, although this comparison is not seen directly in the stress ratios since both the west and east strains corresponded to the yield stress for girders tested under this load ratio. Similarly, the side to which the bottom flange of the girder displaced at buckling at the cantilever tip is the side that experienced higher compressive stresses on its bottom (compression) flange at the fulcrum. For example, LRC2-0.38 saw a bottom flange lateral deflection to the west at buckling and exhibited a longitudinal stress ratio of -1.0 on the west side of the bottom flange and -0.80 on the east side. This phenomenon is evident in all girders tested under load ratios of 0.38 and 0.25, except for LRC1-0.38 Retest and LRC1-0.25. For these two tests, warping deformations at the fulcrum support were significant due to the lower degree of lateral restraint provided to the girder (specifically the lack of the bottom flange lateral bracing at the load location to the south of the fulcrum support) as well as the relatively high load applied at the tip of the cantilever compared to the back span. As mentioned in Section **Error! Reference source not found.**, these two girders exhibited clockwise bottom flange rotation about a vertical axis when looking at the girder in plan view such as in Figure 4-2. In this plan view, a clockwise rotation of the bottom flange at the fulcrum support puts the west side of the flange in “compression” and the east side in “tension”. This resulted in the west side of the bottom flange at the fulcrum support experiencing higher compressive stresses than the east side for LRC1-0.38

Retest and LRC1-0.25. The side of the compression flange which sees additional compressive action due to lateral bending is the side which will have a higher σ/σ_y value, and this side is used to determine the range of buckling which occurred according to Nethercot's (1974) hypothesis.

Table 5-7: Summary of compression flange longitudinal stresses at buckling

Specimen ID	Longitudinal Stress Ratio, σ/σ_y (MPa)			
	Back Span East	Back Span West	Fulcrum Northeast	Fulcrum Northwest
LRC1-0.80	-1.0	-1.0	-0.6	-0.6
LRC1-0.38	-0.8	-0.7	-1.0	-1.0
LRC1-0.38 Retest	-0.7	-0.7	-0.8	-1.0
LRC1-0.25	-0.4	-0.4	-0.9	-1.0
LRC2-0.75	-1.0	-1.0	-0.8	-0.5
LRC2-0.38	-0.8	-0.6	-0.8	-1.0
LRC2-0.25	-0.4	-0.3	-1.0*	-1.0
LRC3-0.80	-1.0	-1.0	-0.7	-0.7
LRC3-0.25	-0.4	-0.4	-1.0*	-1.0
LRC4-0.80	-1.0	-1.0	-0.4	-0.7
LRC4-0.38	-0.6	–	-0.9	-1.0
LRC4-0.25	-0.4	-0.3	-0.9	-1.0
LRC5-0.80	-1.0	–	-0.6	-0.6
LRC5-0.25	-0.4	-0.6	-1.0*	-1.0

* Fulcrum Southeast reading

As shown in Table 5-7, all girders exhibited flexural yielding at buckling at the compression flange tips of the strain measurement location which buckled or reached its full cross-sectional capacity first, according to strain gauge readings. Since the residual stress results for girders from Heat 1 showed that the tips of the flange were under compressive residual stresses, the net stress present at the compression flange tips at buckling exceeds the compressive stress obtained from the longitudinal strain gauges. Furthermore, all girders which failed by LTB exhibited experimental M_{max}/M_p values exceeding 0.67, as shown in Table 5-1. Therefore, in the case of girders with the residual stress pattern from Heat 1, Nethercot's (1974) definition of inelastic buckling is consistent with the definition from CSA S16-19, which classifies inelastic buckling as girders showing experimental M_{max}/M_p values exceeding 0.67.

For girders tested under a load ratio of 0.80, the elastic stiffness according to the load–vertical deflection curve for the cantilever tip is in good agreement with the calculated values according to linear elastic theory, with slopes in the linear region differing by no more than 1.3 kN/mm. For girders tested under a load ratio of 0.25, the load–vertical deflection curve at the cantilever tip agrees well with linear elastic theory up to around 200 kN, when the web–flange junction of the top (tension) flange experienced first yielding at the fulcrum according to the strain gauge reading (taking tensile residual stresses into account). Beyond this point, the test girders began deflecting vertically at a rate faster than predicted by linear elastic theory as expected. For girders tested under a load ratio of 0.38, the slope of the load–vertical deflection curve in the linear region at the cantilever tip observed in the tests was significantly lower than that predicted by linear elastic theory. This could be attributed to the fact that, for a given cantilever tip load, the downward vertical deflection at the cantilever tip under a load ratio of 0.38 was small compared to that under load ratios of 0.80 and 0.25, which exhibited large upward and downward vertical deflections at the cantilever tip, respectively. The smaller deflections for the same value of load correlate to a high stiffness which is sensitive to small errors in vertical deflection measurements. Where a small error in the measurement of vertical deflection may have a minimal effect on the stiffness of girders tested under load ratios of 0.80 and 0.25, this error is amplified for girders tested under a load ratio of 0.38, where the downward deflections are already very small.

5.4 Experimental Errors

Various factors may arise in large-scale stability tests of steel girders which contribute to experimental errors. These factors include fixtures in the test setup which do not function as anticipated, unwanted friction or restraint, errors in instrumentation measuring load, and unintentional eccentricity or misplacement in loading.

One major fixture used in the test setup which did not function as anticipated was the load collar used as part of the GLS assembly. The main feature of the GLS which made it ideal for use in the test setup is its ability to sway laterally in either direction, essentially following the lateral movement of the unbraced test girder, while continually applying a vertical downward load on the top flange of the girder. The GLS was employed for test girders in LRCs 4 and 1. In the tests on girders in LRCs 4 and 1 tested under load ratios of 0.38 and 0.25, which experienced LTB at the cantilever and therefore exhibited large lateral deflections at this location, the GLS moved laterally very minimally. While the load remained in the same position on the top flange of the cantilever tip, confirmed by monitoring the location of the hemispherical bearing directly above the pins of the GLS, a large amount of the lateral deflection of the cantilever tip was instead accommodated by the threaded rods of the load collar bending in the direction out of plane of the girder, as seen in Figure 5-15. While the rods have a tensile capacity greatly exceeding the load applied and the loading was therefore not compromised by this bending, the rods were not able to be used for subsequent tests due to the extent of bending affecting the ability to install the rods in the load collar, and new rods had to be ordered for each test. An attempt was made to minimize this bending in LRC1-0.38 by using shorter threaded rods, but this required changing the hemispherical bearing to a semi-cylindrical one, which in turn provided unwanted restraint to the cantilever tip and resulted in LRC1-0.38 needing to be retested (explained previously).

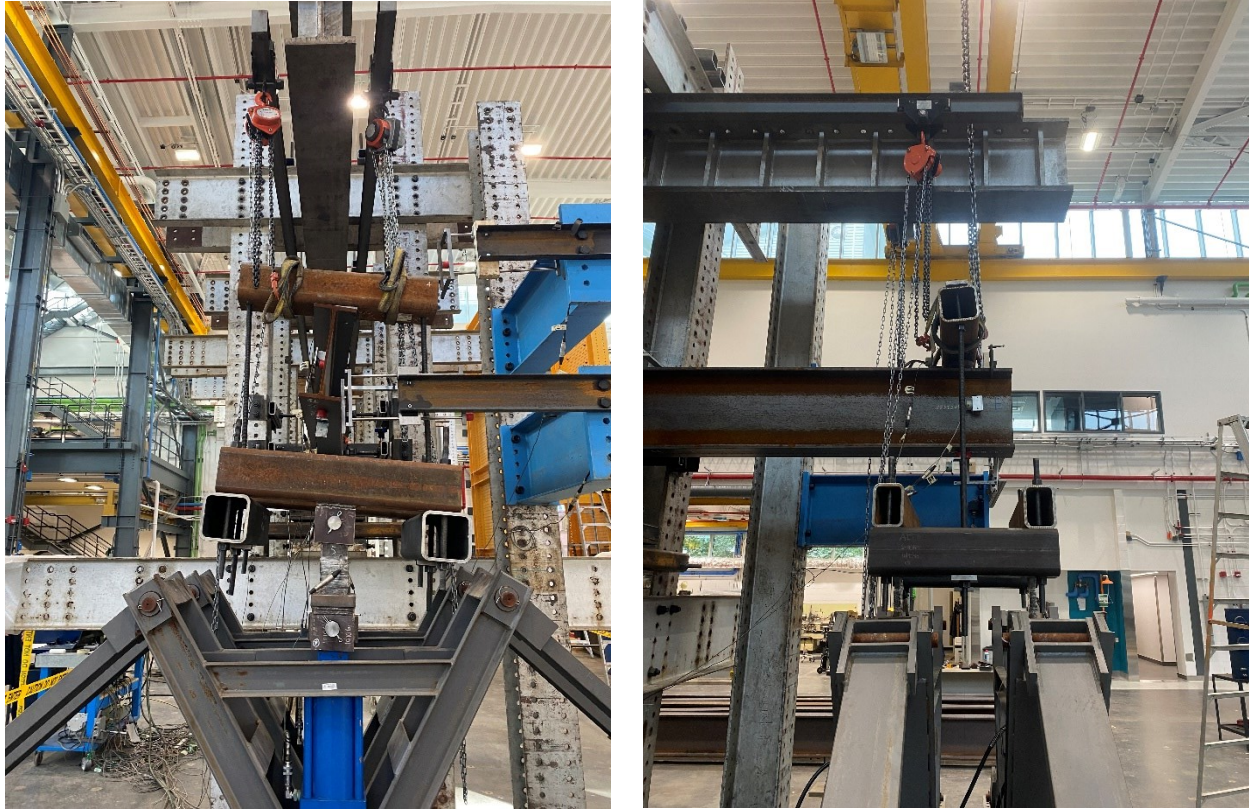


Figure 5-15: Load collar bending during loading LRC1-0.38 Retest

In the first test, the summation of reaction forces (from the load cells at the supports) was monitored along with the summation of downward loads (from the pressure transducers attached to the manifolds of the hydraulic actuators). A difference between these summations of around 30% was observed throughout the test, with the summation of downward forces exceeding the summation of reaction forces, indicating large frictional losses between the steel flange and the Acetal sheet. Two approaches were taken to mitigate this in subsequent tests. The first was the addition of a cylindrical Acetal piece on the flange of the test girder at each lateral brace point, as shown in Chapter 4.1, and a layer of grease was added to both the bracing bracket's Acetal sheet as well as the cylindrical Acetal. This proved to greatly decrease the frictional losses, with a difference between summations of downward and reaction forces reduced to 5% in LRC2-0.38. The second approach taken to reduce the deviation between summation of downward and reaction forces was to investigate the instrumentation used to measure the loads, originally measured as pressures using pressure transducers and converted to load using the area of the piston head of the hydraulic actuators. A test was conducted to determine how much of the difference in load

summations comes solely from the error of the pressure transducers. After the full-scale test of LRC2-0.75 was conducted, the girder was kept in the test setup but the lateral braces at the load points were removed, resulting in the girder being completely unbraced other than at the supports. This was done in an attempt to eliminate the possibility of any frictional losses contributing to the difference in load summations. The back span was then loaded under relatively small loads of up to 30 kN per back span actuator, and the summation of downward and reaction forces was monitored. The difference in summations obtained in this test was around 5%, confirming that almost all frictional losses were eliminated by the addition of the cylindrical Acetal and grease at the lateral brace points. The 5% error in pressure transducer readings remained after recalibrating the pressure transducers. A more reliable measurement of loads was deemed to be obtained using the readings from the load cells at the supports, which was used to calculate the loads applied along the back span and at the cantilever tip using equilibrium.

One possible source of unwanted restraint stemmed from the fixtures at the supports, including the assembly which the girder sits on as shown previously in Figure 4-9, and the side plates used at the supports for lateral bracing. While an identical support configuration has been used by previous researchers in large-scale LTB experiments (Ji et al. 2019, Twizell et al. 2021), the supports in these test setups were placed relatively far from the buckling points on the girder, due to the girders being simply-supported and unbraced along the entire length. Therefore, the effect of the rotational restraint about the vertical axis provided by the support assembly, as well as the torsional stiffness of the side plates, on the girder's ability to undergo warping was minimal, compared to the effect when these side plates were placed at the fulcrum support as seen in this test program, only 1.83 m away from the tip of the cantilever which was meant to undergo large vertical, lateral and twist deformations at buckling. Therefore, it is likely that the support assembly and side plates caused an additional partial warping restraint at the fulcrum support, where significant warping deformations are expected at buckling. This would result in peak loads higher than expected if there were no warping restraints whatsoever.

Another possible source of error is unintentional eccentricities in loading, which may arise due to the semi-cylindrical or hemispherical bearings sitting slightly off-centre on the flange width. The

loads applied using semi-cylindrical bearings attached to hydraulic actuators were centered by ensuring the girder was installed centered on the knife edges at the supports, by measuring the distance between the edge of the knife edge and the edge of the girder flange on either side. Since the hydraulic actuators are centered within the test frame and the girder is laterally braced at the load locations, the semi-cylindrical bearings are effectively centered on the back span. In the tests where the GLS was employed at the cantilever tip, the load collar was lowered onto the top flange of the girder and the distance between the edge of the flange and the centre of the hemispherical bearing was ensured to be equal on either side before securing the load collar. Although care was taken to centre the loads prior to testing, it is possible that the hemispherical bearing at the cantilever tip in the GLS tests may have migrated slightly during testing, causing a very small eccentricity in loading which was not noticeable by inspection.

Accidental misplacement of loading along the length of the girder is another possible source of error in the tests, specifically in those using the GLS. Since the holes drilled in the HSS sections of the load collar are slightly larger than the threaded rods, there was a small amount of slack in the load collar assembly. Although the load collar may have been initially lowered and secured at one position, the assembly may have shifted at the beginning of the test when loading commenced and the load collar assembly was put under tension. The extent of this movement was measured after each test by taking note of the position of a small dent in the top flange left by the hemispherical bearing, which indicates the true position of loading. The two tests with the largest deviations were LRC1-0.38 Retest and LRC1-0.25, the final two tests. While the intended cantilever length was 1.83 m, LRC1-0.38 Retest and LRC1-0.25 were both tested with a cantilever length of 1.80 m, about 2% shorter than intended. However, these shorter cantilever lengths were accounted for in all reported moment resistances.

5.5 Comparison of Test Results with CISC Design Procedure

This section presents a comparison of the results for moment resistance of overhanging girders predicted by the CISC Design Module 8 (Lasby 2019) against the maximum moment obtained from the test results. The proposed method for determining moment resistance for overhanging

girders by CISC requires treating the cantilever and back span segments separately, calculating a moment resistance for each segment. The back span is checked under both maximum positive and negative moments. The check for the maximum positive moment uses the joist spacing as the unbraced length of the segment on the back span subjected to the most critical bending moment gradient, while the critical elastic moment for the back span under maximum negative moment is calculated assuming the entire length of the back span as the unbraced length. The third and final check is for the cantilever under negative bending moment using the Essa and Kennedy (1993) interaction method, which assumes the entire length of the back span is unbraced. While Essa and Kennedy (1993) do not assume the back span is under uniform bending moment in the interaction method, this further conservative assumption is made by CISC based on the recommendation by the SSRC Guide (Ziemian 2010). The interaction factor in the Essa and Kennedy (1993) method takes into account cases of top flange restraint to the cantilever tip and an unbraced tip, as well as both top flange and shear centre loading, but does not provide an interaction factor which accounts for both top and bottom flange bracing at the cantilever tip. Instead, the moment resistance of the cantilever segment is calculated using Schmitke and Kennedy (1985)'s effective length factors for LRCs 3 and 5 (in which the cantilever tip was braced at both the top and bottom flanges). This method was suggested for use for this bracing condition by Essa and Kennedy (1994). In all cases, the moment gradient factor for the back span check is calculated assuming loading is applied at the shear centre.

Moment capacity calculations according to CISC (Lasby 2019) were done using a resistance factor of 1.0, and plastic moments used in the calculations were determined using measured cross-sectional dimensions and yield stresses with the flange and web differentiated. The measured elastic modulus was used, and the moment of inertia about the weak axis was calculated using measured cross-sectional dimensions (taking fillets into account). The torsional and warping constants were estimated for each girder without taking fillets into account.

The nominal moment resistance is calculated using each critical elastic moment by accounting for either elastic or inelastic buckling, and the negative moment at the fulcrum corresponding to the resistance of the back span under positive moment is calculated for comparison with the two other

nominal resistances calculated using the CISC (Lasby 2019) method (one for the back span under negative moment and one for the cantilever). The nominal resistance reported from the CISC method is therefore the minimum of the three nominal moment resistances at the fulcrum. The maximum experimental moment for comparison with the predicted resistances is the fulcrum moment, M_{Fmax} . Table 5-8 provides a comparison of the experimental moment resistances and those predicted by the CISC method, as well as the test-to-predicted ratios and percent error for each test girder. The governing CISC moment resistance is also shown, where ‘C’ indicates the minimum CISC moment resistance was that of the cantilever, ‘B(-)’ indicates back span under negative bending moment, and ‘B(+)’ indicates back span under positive bending moment. Two of these symbols given for a single specimen indicates that these checks give capacities within 1% of each other. A test-to-predicted ratio greater than 1.0, and a positive percent error, indicates that the CISC design method is conservative, whereas a ratio less than 1.0, and a negative percent error, indicates that the design method is unconservative in predicting the moment resistance of a given girder.

A worked example of moment capacity calculations for LRC1-0.25 (C(U)–B(T)) and LRC4-0.25 (C(U)–B(TB)) according to the CISC method is presented. For this load ratio, the bending moment gradient is shown in Figure 5-16.

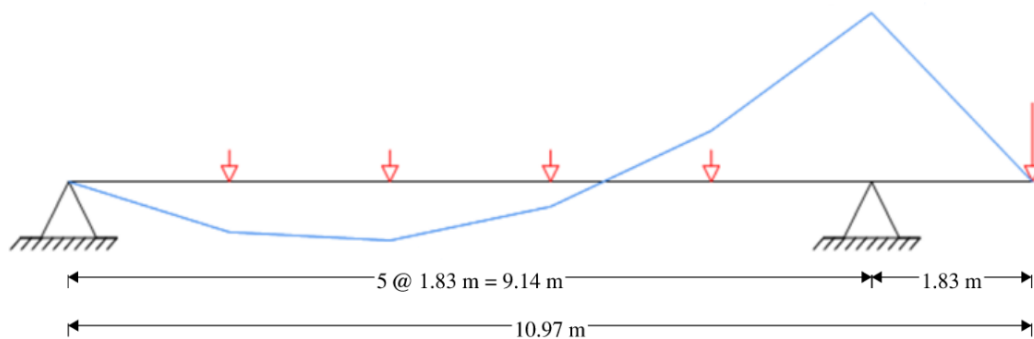


Figure 5-16: Bending moment gradient under a 0.25 load ratio

LRC1-0.25:

Check cantilever:

This check is done using the Essa and Kennedy (1993) method, assuming unrestrained back span,

and assuming uniform bending moment along the 9.14 m long back span as suggested by the SSRC Guide (Ziemian 2010). The assumed bending moment gradient for this check is shown in Figure 5-17.

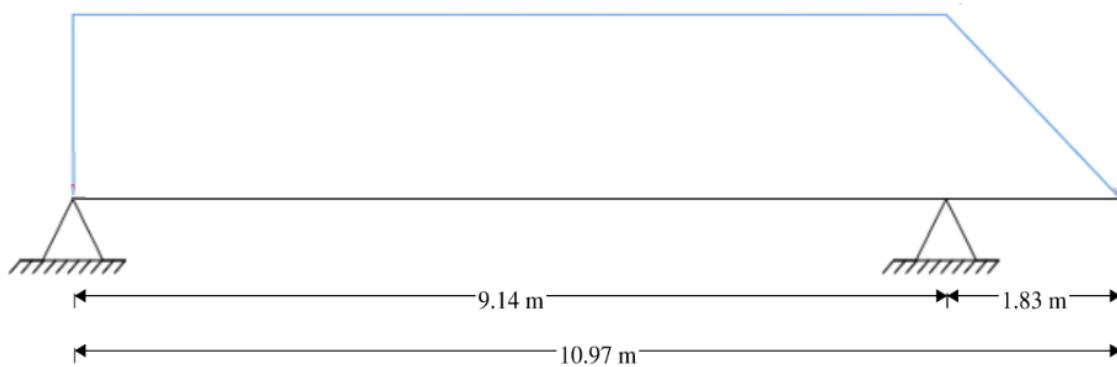


Figure 5-17: Assumed bending moment diagram for cantilever check by CISC method

$$M_{cr} = M_c + I(M_b - M_c)$$

$$\text{For top flange loading: } M_c = 1.5 \frac{GJ}{d} = 1.5 \frac{(77000 \times 903066)}{418} = 249.5 \text{ kNm}$$

$$\begin{aligned} M_b &= \frac{\pi}{L_b} \sqrt{EI_y GJ + \left(\frac{\pi E}{L_b}\right)^2 I_y C_w} \\ &= \frac{\pi}{9144} \sqrt{(200394)(18127141)(77000)(903066) + \left(\frac{\pi(200394)}{9144}\right)^2 (18127141)(7.26 \times 10^{11})} \\ &= 193 \text{ kNm} \end{aligned}$$

Since $M_b < M_c$, $M_{cr,1} = M_c$ (no additional benefit due to interaction). Now, obtaining the resistance:

$$M_p = 605.3 \text{ kNm} \rightarrow 0.67 * M_p = 403.6 \text{ kNm}$$

$$M_{cr,1} < 0.67 * M_p$$

$$\therefore M_{r,1} = 249.5 \text{ kNm}$$

The maximum bending moment on the cantilever occurs at the fulcrum; therefore, $M_{r,1}$ at fulcrum = 249.5 kNm.

Check back span under negative bending moment:

No bottom flange bracing is provided along the back span; therefore, the unbraced length of the back span is 9.14 m. The moment gradient factor can be calculated using moments obtained by

applying a 1 kN load at the cantilever tip and a 0.25 kN load on each of the back span load locations.

$$\omega_2 = \frac{4M_{max}}{\sqrt{M_{max}^2 + 4M_A^2 + 7M_B^2 + 4M_C^2}} \leq 2.5$$

$$= \frac{4(1.83)}{\sqrt{1.83^2 + 4(0.57)^2 + 7(0.46)^2 + 4(0.35)^2}} = 2.8 \rightarrow \omega_2 = 2.5$$

$$M_{cr,2} = \frac{\pi}{L_b} \sqrt{EI_y GJ + \left(\frac{\pi E}{L_b}\right)^2 I_y C_w}$$

$$= \frac{2.5 * \pi}{9144} \sqrt{(200394)(18127141)(77000)(903066) + \left(\frac{\pi(200394)}{9144}\right)^2 (18127141)(7.26 * 10^{11})}$$

$$= 482 \text{ kNm}$$

$$M_p = 605.3 \text{ kNm} \rightarrow 0.67 * M_p = 403.6 \text{ kNm}$$

$$M_{cr,2} > 0.67 * M_p$$

$$M_{r,2} = 1.15M_p \left[1 - \frac{0.28M_p}{M_{cr}}\right] \leq M_p$$

$$= 1.15(605.3) \left[1 - \frac{0.28(605.3)}{482}\right] = 451.4 \text{ kNm}$$

The maximum negative bending moment on the back span occurs at the fulcrum; therefore, $M_{r,2}$ at fulcrum = 451.4 kNm.

Check back span under positive bending moment:

Using the segment between top flange brace points on the back span subjected to the bending moment gradient closest to uniform, which is the second 1.83 m long segment from the end support.

$$\omega_2 = \frac{4M_{max}}{\sqrt{M_{max}^2 + 4M_A^2 + 7M_B^2 + 4M_C^2}} \leq 2.5$$

$$= \frac{4(0.64)}{\sqrt{0.64^2 + 4(0.57)^2 + 7(0.59)^2 + 4(0.62)^2}} = 1.07$$

$$M_{cr,3} = \frac{\pi}{L_b} \sqrt{EI_y GJ + \left(\frac{\pi E}{L_b}\right)^2 I_y C_w}$$

$$= \frac{1.07 * \pi}{1828.8} \sqrt{(200394)(18127141)(77000)(903066) + \left(\frac{\pi(200394)}{9144}\right)^2 (18127141)(7.26 * 10^{11})}$$

$$= 2482.8 \text{ kNm}$$

$$M_p = 605.3 \text{ kNm} \rightarrow 0.67 * M_p = 403.6 \text{ kNm}$$

$$M_{cr,3} > 0.67 * M_p$$

$$M_{r,3} = 1.15M_p \left[1 - \frac{0.28M_p}{M_{cr}}\right] \leq M_p$$

$$= 1.15(605.3) \left[1 - \frac{0.28(605.3)}{2482.8}\right] = 648.6 \text{ kNm} \rightarrow M_{r,3} = M_p = 605.3 \text{ kNm}$$

The maximum positive bending moment on the segment occurs at the second load point from the end support; therefore, finding the equivalent load at the fulcrum by dividing by the ratio of the bending moment on the back span to that at the fulcrum:

$$M_{r,3} \text{ at fulcrum} = \frac{605.3}{0.35} = 1730.9 \text{ kNm}$$

The CISC moment resistance for LRC1-0.25 is the minimum of the three moment resistances calculated at the fulcrum, which is 249.5 kN (governed by the cantilever check).

LRC4-0.25:

Check cantilever:

This check is done using the Essa and Kennedy (1993) method, assuming unrestrained back span, and assuming uniform bending moment along the 1.83 m long back span. The assumed bending moment distribution is similar to that of Figure 5-17, except the back span is 1.83 m long due to the addition of the bottom flange restraint on the back span in LRC 4.

$$M_{cr} = M_c + I(M_b - M_c)$$

$$\text{For top flange loading: } M_c = 1.5 \frac{GJ}{d} = 1.5 \frac{(77000 \cdot 905481)}{417} = 250.8 \text{ kNm}$$

$$\begin{aligned} M_b &= \frac{\pi}{L_b} \sqrt{EI_y GJ + \left(\frac{\pi E}{L_b}\right)^2 I_y C_w} \\ &= \frac{\pi}{1828.8} \sqrt{(197411)(18196956)(77000)(905481) + \left(\frac{\pi(197411)}{1828.8}\right)^2 (18196956)(7.23 \cdot 10^{11})} \\ &= 2281.8 \text{ kNm} \end{aligned}$$

$$\text{For an unbraced cantilever tip: } I = -0.08 + 0.18 \left(\frac{L_b}{L_c}\right) - 0.009 \left(\frac{L_b}{L_c}\right)^2$$

$$= -0.08 + 0.18 \left(\frac{1828.8}{1828.8}\right) - 0.009 \left(\frac{1828.8}{1828.8}\right)^2 = 0.091$$

$$M_{cr} = M_c + I(M_b - M_c) = 250.8 + 0.091(2281.8 - 250.8) = 435.6 \text{ kNm}$$

Now, obtaining the resistance:

$$M_p = 615.3 \text{ kNm} \rightarrow 0.67 * M_p = 410.2 \text{ kNm}$$

$$M_{cr,1} > 0.67 * M_p$$

$$\begin{aligned} M_{r,3} &= 1.15 M_p \left[1 - \frac{0.28 M_p}{M_{cr}}\right] \leq M_p \\ &= 1.15(615.3) \left[1 - \frac{0.28(615.3)}{435.6}\right] = 427.7 \text{ kNm} \end{aligned}$$

The maximum bending moment on the cantilever occurs at the fulcrum; therefore, $M_{r,l}$ at fulcrum = 427.7 kNm.

Check 1.83 m long back span under negative bending moment:

$$\begin{aligned} \omega_2 &= \frac{4M_{max}}{\sqrt{M_{max}^2 + 4M_A^2 + 7M_B^2 + 4M_C^2}} \leq 2.5 \\ &= \frac{4(1.83)}{\sqrt{1.83^2 + 4(0.87)^2 + 7(1.19)^2 + 4(1.52)^2}} = 1.45 \end{aligned}$$

$$M_{cr,2} = \frac{\pi}{L_b} \sqrt{EI_y GJ + \left(\frac{\pi E}{L_b}\right)^2 I_y C_w}$$

$$= \frac{1.45 * \pi}{1828.8} \sqrt{(197411)(18196956)(77000)(905481) + \left(\frac{\pi(197411)}{1828.8}\right)^2 (18196956)(7.23 * 10^{11})}$$

$$= 3305.7 \text{ kNm}$$

$$M_p = 615.3 \text{ kNm} \rightarrow 0.67 * M_p = 410.2 \text{ kNm}$$

$$M_{cr,2} > 0.67 * M_p$$

$$M_{r,2} = 1.15M_p \left[1 - \frac{0.28M_p}{M_{cr}}\right] \leq M_p$$

$$= 1.15(615.3) \left[1 - \frac{0.28(615.3)}{3305.7}\right] = 670.7 \text{ kNm} \rightarrow M_{r,2} = M_p = 615.3 \text{ kNm}$$

The maximum negative bending moment on the 1.83 m long back span occurs at the fulcrum; therefore, $M_{r,2}$ at fulcrum = 615.3 kNm.

Check 7.32 m long segment under negative bending moment:

$$\omega_2 = \frac{4M_{max}}{\sqrt{M_{max}^2 + 4M_A^2 + 7M_B^2 + 4M_C^2}} \leq 2.5$$

$$= \frac{4(0.64)}{\sqrt{0.64^2 + 4(0.55)^2 + 7(0.64)^2 + 4(0.27)^2}} = 1.17$$

$$M_{cr,3} = \frac{\pi}{L_b} \sqrt{EI_y GJ + \left(\frac{\pi E}{L_b}\right)^2 I_y C_w}$$

$$= \frac{1.17 * \pi}{7315.2} \sqrt{(197411)(18196956)(77000)(905481) + \left(\frac{\pi(197411)}{7315.2}\right)^2 (18196956)(7.23 * 10^{11})}$$

$$= 295.5 \text{ kNm}$$

$$M_p = 615.3 \text{ kNm} \rightarrow 0.67 * M_p = 410.2 \text{ kNm}$$

$$M_{cr,3} < 0.67 * M_p$$

$$\therefore M_{r,3} = 295.5 \text{ kNm}$$

The maximum negative bending moment on the segment occurs at the first load point from the fulcrum support; therefore, finding the equivalent load at the fulcrum by dividing by the ratio of the bending moment on the segment to that at the fulcrum:

$$M_{r,3} \text{ at fulcrum} = \frac{295.5}{0.30} = 983.0 \text{ kNm}$$

Check 7.32 m long segment under positive bending moment:

Using the segment between top flange brace points subjected to the bending moment gradient closest to uniform, which is the second 1.83 m long segment from the end support.

$$\begin{aligned} \omega_2 &= \frac{4M_{max}}{\sqrt{M_{max}^2 + 4M_A^2 + 7M_B^2 + 4M_C^2}} \leq 2.5 \\ &= \frac{4(0.64)}{\sqrt{0.64^2 + 4(0.57)^2 + 7(0.59)^2 + 4(0.62)^2}} = 1.07 \end{aligned}$$

$$\begin{aligned} M_{cr,4} &= \frac{\pi}{L_b} \sqrt{EI_y GJ + \left(\frac{\pi E}{L_b}\right)^2 I_y C_w} \\ &= \frac{1.07 * \pi}{1828.8} \sqrt{(197411)(18196956)(77000)(905481) + \left(\frac{\pi(197411)}{1828.8}\right)^2 (18196956)(7.23 * 10^{11})} \\ &= 2450.3 \text{ kNm} \end{aligned}$$

$$M_p = 615.3 \text{ kNm} \rightarrow 0.67 * M_p = 410.2 \text{ kNm}$$

$$M_{cr,4} > 0.67 * M_p$$

$$\begin{aligned} M_{r,4} &= 1.15M_p \left[1 - \frac{0.28M_p}{M_{cr}}\right] \leq M_p \\ &= 1.15(615.3) \left[1 - \frac{0.28(615.3)}{2450.3}\right] = 657.8 \text{ kNm} \rightarrow M_{r,4} = M_p = 615.3 \text{ kNm} \end{aligned}$$

The maximum positive bending moment on the segment occurs at the second load point from the end support; therefore, finding the equivalent load at the fulcrum by dividing by the ratio of the bending moment on the segment to that at the fulcrum:

$$M_{r,4} \text{ at fulcrum} = \frac{615.3}{0.35} = 1759.3 \text{ kNm}$$

The CISC moment resistance for LRC4-0.25 is the minimum of the four moment resistances calculated at the fulcrum, which is 427.7 kN (governed by the cantilever check).

Table 5-8: Comparison of moment resistances from experimental results and CISC (2019)

Specimen ID	Maximum Experimental Moment, M_{Fmax} (kN·m)	CISC (2019) Moment Resistance (kN·m)	Governing CISC Resistance	Test/Predicted	% Error
LRC1-0.80	334	254	B(-)	1.31	24.0
LRC1-0.38	619	246	C	2.52	60.3
LRC1-0.38 Retest	574	252	C	2.28	56.1
LRC1-0.25	544	250	C	2.18	54.0
LRC2-0.75	409	244	C, B(-)	1.68	40.3
LRC2-0.38	592	249	C	2.38	57.9
LRC2-0.25	608	251	C	2.42	58.7
LRC3-0.80	331	245	B(-)	1.35	26.0
LRC3-0.25	686	458	B(-)	1.50	33.2
LRC4-0.80	333	307	B(+)	1.08	7.8
LRC4-0.38	552	434	C	1.27	21.4
LRC4-0.25	554	428	C	1.29	22.7
LRC5-0.80	332	321	B(+)	1.03	3.3
LRC5-0.25	693	635	C, B(-)	1.09	8.4

As indicated by the test-to-predicted ratios, the moment capacities predicted by the CISC (2019) method are conservative for all test girders. The under-estimation of capacity is especially significant for girders tested under load ratios of 0.38 and 0.25 which failed by inelastic LTB. The mean percent error between the test and predicted capacities for girders which failed by LTB was 45%, while the mean percent difference for girders that reached their full cross-sectional capacity was lower at 20%. There are three major differences between the assumptions made in the design method and the circumstances encountered in the tests which must be acknowledged when making

this comparison: bracing conditions on the back span; warping restraint at the fulcrum; and load height effect for loads on the back span.

While the CISC (Lasby 2019) method for predicting the capacity of the cantilever segment takes the restraint of the cantilever tip into account, the method for predicting the back span capacity under maximum negative moment assumes that the top flange is unrestrained along the entire length of 9.14 m (except for LRCs 4 and 5, which had an additional brace provided to the bottom flange at the back span load location adjacent to the fulcrum, and therefore the length of the unrestrained back span was 7.32 m). The test girders, however, all had lateral restraint provided to the top flange of the back span at 1.83 m intervals. Since compression flange bracing is known to greatly increase the buckling capacity, the assumption of CISC's method that the compression flange of the back span is completely unbraced is therefore conservative, especially under bending moment gradients where the majority of the back span experiences the top flange under compression.

The extent of warping restraint provided at the fulcrum is also an important factor when comparing the test results to the predictions based on CISC (Lasby 2019)'s method for overhanging girders. In the checks for both the cantilever and the back span segments, the methods used by CISC (Lasby 2019) assume that the section is free to warp at the fulcrum for the cantilever segment and both simple supports for the back span segment. However, as discussed previously, the girders in the experiments were subjected to a certain degree of warping restraint at the supports stemming from three possible sources: the rotational restraint about the vertical axis provided by the support assembly; the torsional stiffness of the side plates used at the supports; and the internal warping restraint due to the continuity between the cantilever and back span. The warping restraint experienced at the fulcrum is especially influential on the obtained flexural capacity of the girder, due to its close proximity to the cantilever tip, which undergoes large deformation at buckling under certain loading and restraint conditions. This warping restraint would cause the capacity of the tested girders to be higher than if the section was free to undergo warping at the fulcrum, as assumed by the CISC method.

While the effect of load height is taken into account when obtaining the capacity of the cantilever segment in the method used by CISC (Lasby 2019), the capacity of the back span is obtained using a moment gradient factor that assumes loading is applied at the shear centre. Since the test girders were tested under top flange loading on the back span, which causes a destabilizing effect on the section compared to loading at the shear centre, the capacity of the girder would be overestimated by assuming shear centre loading. The extent of this overestimation, however, is not realized directly through the comparison presented herein due to the seemingly more dominant effects of back span lateral restraint and warping restraint at the fulcrum, the combination of which lead to the conclusion that the CISC (Lasby 2019) method for determining the capacity of overhanging girders is conservative for the specimens tested here, especially those that fail by LTB.

6 CONCLUSIONS AND RECOMMENDATIONS

6.1 Summary

Cantilever-suspended-span construction, also known as the Gerber system, is a prevalent approach for steel roof framing in large single-storey buildings in North America. This system comprises three key components: the back span, cantilever, and drop-in segments. Despite its widespread use and benefits in steel buildings across North America, current steel design standards in Canada (CSA 2019) and the United States (AISC 2022) offer limited guidance on the design of Gerber systems. Recent structural failures have emphasized the need for a reassessment of the stability response of these systems, particularly in terms of lateral–torsional buckling (LTB) resistance and the exploration of various bracing strategies.

To investigate the effect of various parameters, such as loading and bracing conditions, on the stability response of the steel Gerber system, a full-scale physical testing program was developed in this M.Sc. research project. The experimental study consisted of 14 ASTM A992 W410×85 (Class 1) single-overhanging girders, with back span and cantilever lengths of 9.14 m and 1.83 m, respectively. At both the end and fulcrum supports, the test girders were simply-supported in-plane and torsionally pinned. Four point loads were applied at 1.83 m intervals along the back span, and a single point load was applied at the tip of the cantilever. All test girders were predicted to exhibit a failure mode of either inelastic LTB or reaching the full cross-sectional capacity. The major objectives of the research project comprised four parts: developing a test matrix that includes the most influential parameters on the LTB capacity of overhanging girders, designing an experimental test setup, performing 14 full-scale girder tests, and analyzing the experimental results.

To aid in the development of the test specimen matrix, numerical simulations conducted by Esmaeili et al. (2021) were used to evaluate the influence of various parameters on the LTB capacity of steel cantilevered girders. The parameters with the highest influence on the stability response of steel overhanging beams according to the numerical simulations, including the lateral bracing conditions, loading conditions, cross-sectional properties, and number of overhangs, were

considered in selecting the test specimens. The design of the test setup was based largely on preliminary finite element (FE) simulations of the test specimens, which provided the anticipated loads and deflections in the tests. Initial geometric imperfections and material properties were measured for all test specimens prior to testing, and residual stresses were measured for the heat of steel which supplied 8 out of 14 test girders.

The experimental results for capacity and deflection of each test girder were analyzed, considering the effect of influential parameters such as loading and bracing conditions, residual stresses, and initial geometric imperfections. Through the placement of five strain gauges at the fulcrum support and two strain gauges at the location of local maximum moment on the back span, stresses were analyzed to ensure yielding of the compression flange tip occurred prior to buckling, considering residual stresses. Lastly, the moment resistances obtained from the experiments for each test girder were compared against resistances predicted by the CISC (2019) design procedure.

6.2 Conclusions

The following conclusions are made from this M.Sc. research project:

- The residual stress distribution measured for the W410×85 section showed compressive stresses at the flange tips.
- The relatively large initial geometric imperfections compared to previous experimental studies measured in this study suggest the importance of these measurements in full-scale testing programs.
- When the cantilever tip is left unbraced, the addition of a bottom flange lateral brace at the back span load location closest to the fulcrum support has minimal effect on the moment resistance of the girder; however, the addition of this brace leads to a significant beneficial effect on the lateral stiffness of the cantilever tip.
- Bracing the top flange of the cantilever tip is more effective at increasing the capacity of a single-overhanging girder compared to adding a bottom flange brace on the back span and leaving the cantilever unbraced.
- The addition of a bottom flange lateral brace at the cantilever tip was particularly effective

in increasing the capacity of the girder.

- For κ_1'' (ratio of the distributed load magnitude on the back span to that on the cantilever) values less than 1.00, the change in capacity with changing load ratios is minimal.
- When the cantilever tip is unbraced and the girder experienced LTB, the amount of lateral deflection of the top flange exceeds the amount of downward vertical deflection at the cantilever tip. On the other hand, girders, which reached their full cross-sectional capacity experienced much larger vertical deflection compared to lateral deflection of either flange at peak load.
- The capacity of overhanging girders is very sensitive to the extent of warping restraint provided to the girder at the fulcrum support, due to the close proximity of the fulcrum to the cantilever tip (which undergoes large deformations at buckling), evident by the higher range of capacities obtained than intended as predicted by FE simulations.
- The CISC (Lasby 2019) design method for overhanging girders underestimates the capacity of all single-overhanging girders investigated in this study due to its conservative assumptions associated with bracing conditions on the back span and warping restraints at the fulcrum.

6.3 Recommendations for Further Research

While the experimental study presented herein provides insight into the stability response of steel cantilevered girders, further investigation of certain aspects would be beneficial for improving the understanding of these systems. This will be instrumental in the introduction of a practical and efficient design method for these systems. These aspects include:

- Cross-sectional properties, as well as an additional cantilever segment seen in double-overhanging girders, were identified alongside loading and lateral bracing conditions as influential parameters which affect the capacity of overhanging girders. While these parameters were not investigated in this study, physical testing which includes this data is necessary to understand their effect on the stability response of overhanging girders.
- The degree of warping restraint provided at the support, particularly the fulcrum support, was identified as a factor which the capacity of overhanging girders is greatly sensitive to.

Further physical testing which eliminates the warping restraint at the fulcrum to a further extent would be useful to help with understanding the effect of this restraint on the capacity of overhanging girders.

- Drop-in segments, including the connection of this segment to the cantilever tip, as well as the bracing stiffness provided by open-web steel joists, are important aspects of Gerber systems, the investigation of which through physical testing would be beneficial in further understanding the behaviour of these systems.

REFERENCES

- AISC. (2022). *ANSI/AISC 360-22 Specification for Structural Steel Buildings*. American Institute of Steel Construction, Chicago, IL.
- AISC. (1986). *Load and resistance factor design specification for structural steel buildings*. American Institute of Steel Construction, Chicago, IL.
- AISI. (1986). *AISI-Specifications for the Design of Cold-Formed Steel Structural Members*. American Iron and Steel Institute, Washington, DC.
- Andrade, A., Camotim, D., and Providencia e Costa, P. (2007). "On the evaluation of elastic critical moments in doubly symmetric I-section cantilevers." *Journal of Constructional Steel Research*, 63, 894–908.
- ASTM International. (2023). *A370-23 Standard Test Methods and Definitions for Mechanical Testing of Steel Products*. American Society for Testing and Materials, West Conshohocken, PA.
- ASTM. (2020). *ASTM A992/A992M-20 Standard Specification for Structural Steel Shapes*. American Society for Testing and Materials, West Conshohocken, PA.
- Autodesk Inc. (2022). *Revit Architecture 2022 User's Guide*. Version 2022, San Rafael, CA.
- Baker, K. A., and Kennedy, D. J. L. (1984). "Resistance factors for laterally unsupported steel beams and biaxially loaded steel beam columns." *Canadian Journal of Civil Engineering*, 11(4), 1008–1019.
- Bjorhovde, R. (1980). "Research needs in stability of metal structures." *ASCE Journal of Structural Division*, 106(12), 2435–2442.
- CISC. (1989). "Roof Framing with Cantilever (Gerber) Girders & Open Web Steel Joists." Canadian Institute of Steel Construction, Willowdale.
- Closkey, Dan J. (1988). "Report of the Commissioner Inquiry Station Square Development." Province of British Columbia, Burnaby, BC.
- CSA. (2019). *CSA S16-19 Design of Steel Structures*. Canadian Standards Association, Toronto, ON.
- CSA. (2014). *CSA S16-14 Design of Steel Structures*. Canadian Standards Association, Toronto, ON.
- CSA. (2013). *CSA G40.20-13/G40.21-13 (reaffirmed 2023) General requirements for rolled or welded structural quality steel/Structural quality steel*. Canadian Standards Association, Toronto,

ON.

CSA. (1984). *CAN3-S16-M84 Steel Structures for Buildings (Limit States Design)*. Canadian Standards Association, Toronto, ON.

Dassault Systèmes. (2017). *Abaqus/Standard User's Manual*. Version 2017, Vélizy-Villacoublay, France.

Dibley, J. E. (1969). "Lateral torsional buckling of I-sections in Grade 55 steel." *Proceedings of the Institution of Civil Engineers*, 43(4), 599–627.

Driver, R. G., Kulak, G. L., Elwi, A. E., and Kennedy, D. J. L. (1997). "Seismic behaviour of steel plate shear walls." Structural Engineering Report No. 215, University of Alberta, Edmonton, AB.

Dux, P. F., and Kitipornchai, S. (1983). "Inelastic Beam Buckling Experiments." *Journal of Constructional Steel Research*, 3(1), 3–9.

ECCS. (1981). *Composite structures*. European Convention for Constructional Steelwork, London, New York.

Esmacili, V., Imanpour, A., and Driver, R. G. (2021). "Stability of Gerber Systems with Top-flange Bracing." *Annual Stability Conference*, Structural Stability Research Council, Louisville, KY.

Essa, H. S., and Kennedy, D. J. L. (1994). "Design of Cantilever Steel Beams: Refined Approach." *Journal of Structural Engineering*, 120, 2623–2636.

Essa, H. S., and Kennedy, D. J. L. (1993). "Distortional Buckling of Steel Beams." Structural Engineering Report No. 185, University of Alberta, Edmonton, AB.

Fukumoto, Y., Itoh, Y., and Kubo, M. (1980). "Strength variation of laterally unsupported beams." *ASCE Journal of Structural Division*, 106(1), 165–181.

Galambos, T. V. (1988). *Guide to stability design criteria for metal structures*. 4th Ed., John Wiley & Sons, Inc., New York.

Ji, D., Driver, R.G., and Imanpour, A. (2019). "Large-scale Lateral–torsional Buckling Tests of Welded Girders." Steel Centre Engineering Report No. 015, University of Alberta, Edmonton, AB.

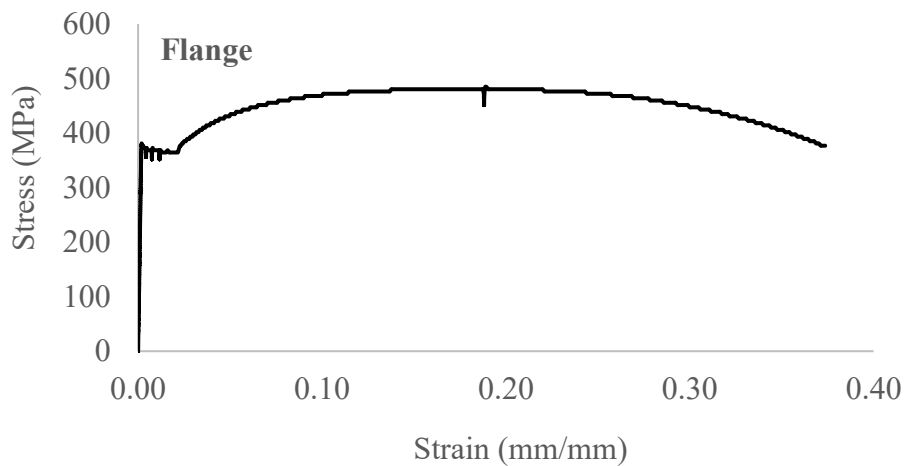
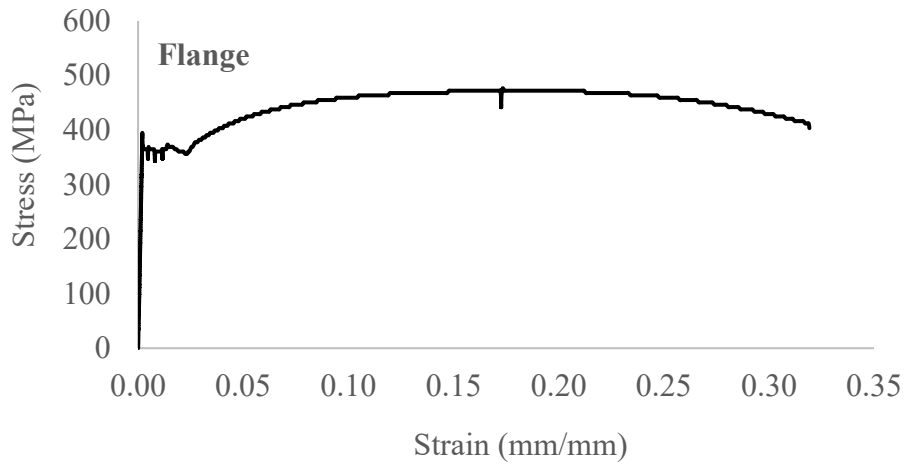
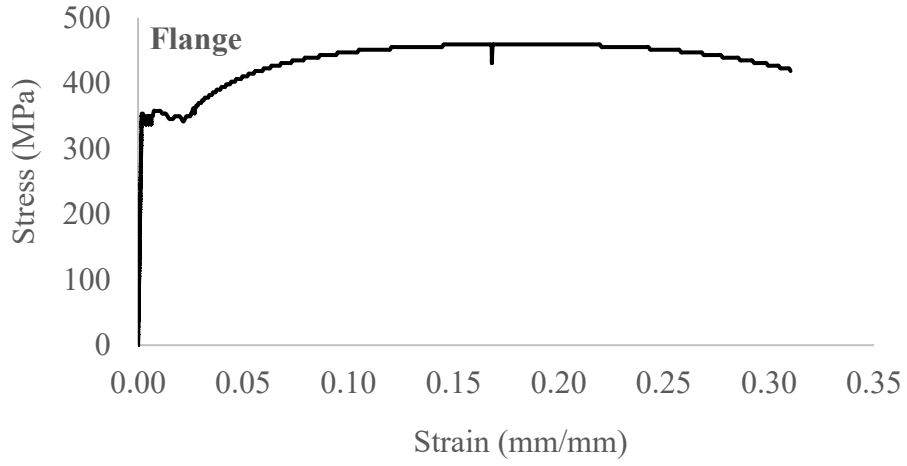
Kirby, P. A., and Nethercot, D. A. (1979). *Design for Structural Stability*. John Wiley & Sons, Inc., New York.

Kitipornchai, S., and Trahair, N. S. (1975). "Inelastic buckling of simply supported I-beams." *ASCE Journal of Structural Division*, 101(7), 1333–1347.

- Kubo, M., and Fukumoto, Y. (1988). "Lateral–torsional buckling of thin-walled I-beams." *Journal of Structural Engineering*, 114(4), 841–855.
- Lasby, R. M. (2019). "CISC Design Module 8 – Single-Storey Building Design." Canadian Institute of Steel Construction, Markham, Ontario.
- Metten, A. (2019). "Structural Design of the Gerber Girder Cantilever System – Filling the Knowledge Gap [Conference presentation]." *The Canadian Steel Conference*, Canadian Institute of Steel Construction, Montreal, Quebec.
- Nethercot, D. A. (1974). "Residual stresses and their influence upon the lateral buckling of rolled steel beams." *The Structural Engineer*, 52(3), 89–96.
- Nethercot, D. A. (1973). "The Effective Lengths of Cantilevers as Governed by Lateral Buckling." *The Structural Engineer*, 51(5), 161–168.
- Roeder, C. W., and Assadi, M. (1982). "Lateral Stability of I-beams with Partial Supports." *Journal of the Structural Division*, 108(8), 1768–1780.
- Rongoe, J. (1996). "Design Guideline for Continuous Beams Supporting Steel Joist Roof Structures." *NASCC Proceedings*.
- Schmitke, C. D., and Kennedy, D. J. L. (1985). "Effective lengths of laterally continuous, laterally unsupported steel beams." *Canadian Journal of Civil Engineering*, 12, 603–616.
- Timoshenko, S. P., and Gere, J. M. (1961). *Theory of Elastic Stability*. McGraw-Hill, New York.
- Trahair, N. S. (1983). "Lateral Buckling of Overhanging Beams." *International Conference on Instability and Plastic Collapse of Steel Structures*, Manchester, Granada Publishing, London.
- Trahair, N. S. (1963). "The Effective Lengths of Simply Supported Rolled Steel Joists." *Journal of the Institution of Engineers Australia*, 35(6), 121–128.
- Twizell, S., Driver, R.G., and Imanpour, A. (2021). "Lateral–Torsional Buckling Response of As-built and Heat-straightened Welded Steel Girders." University of Alberta, Edmonton, AB.
- Venter, S. H. (2016). "Effect of the Adjacent Span on the Lateral–torsional Buckling Capacity of Overhang Beams." Department of Civil Engineering, University of Pretoria, Pretoria, South Africa.
- Yarimci, E., Yura, J. A., and Lu, L-W. (1967). "Techniques for testing structures permitted to sway." *Experimental Mechanics*, 7(8), 321–331.
- Yura, J. A., and Helwig, T. A. (2010). "Buckling of Beams with Inflection Points." *Proceedings of the Annual Stability Council*, Structural Stability Research Council, Florida.

Ziemian, R. D. (2010). *Guide to Stability Design Criteria for Metal Structures*. 6th Ed., John Wiley & Sons, Inc., Hoboken, NJ.

APPENDIX A: MATERIAL PROPERTY PLOTS



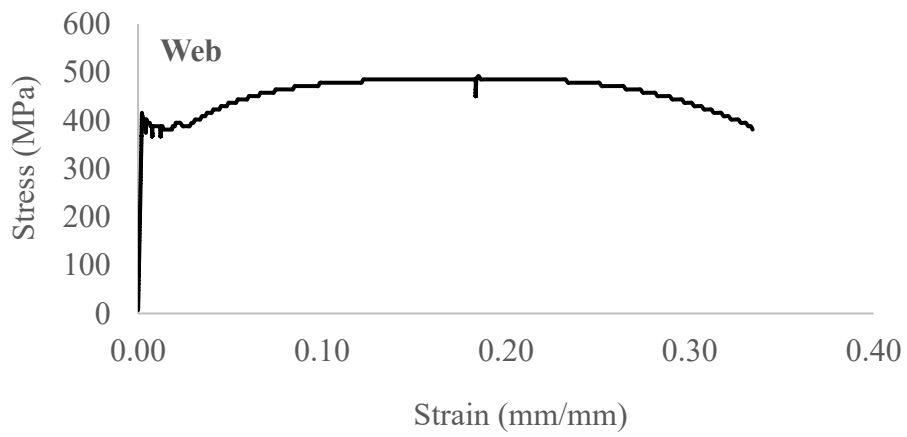
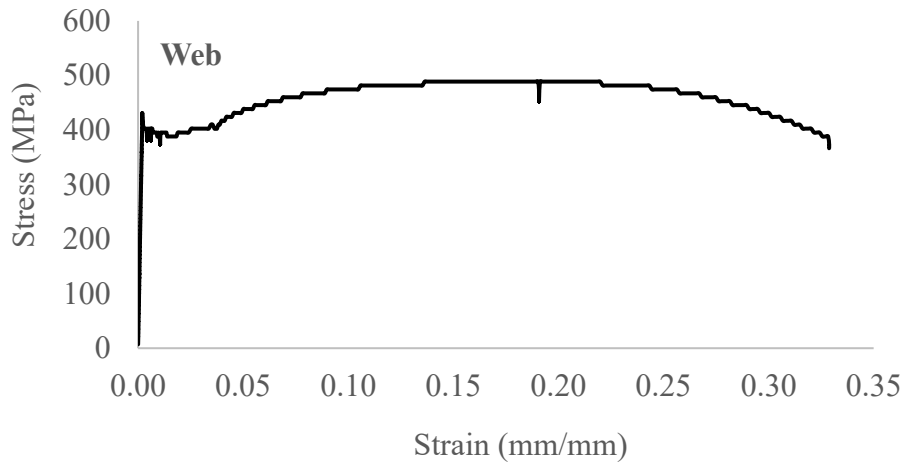
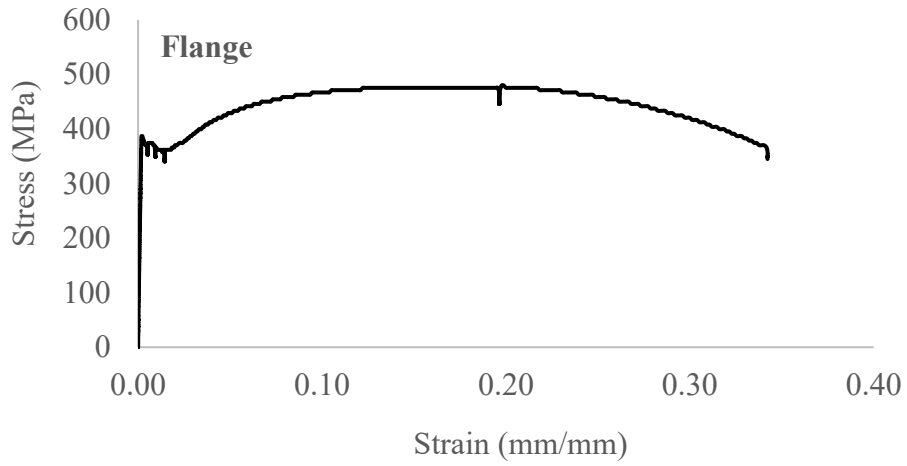
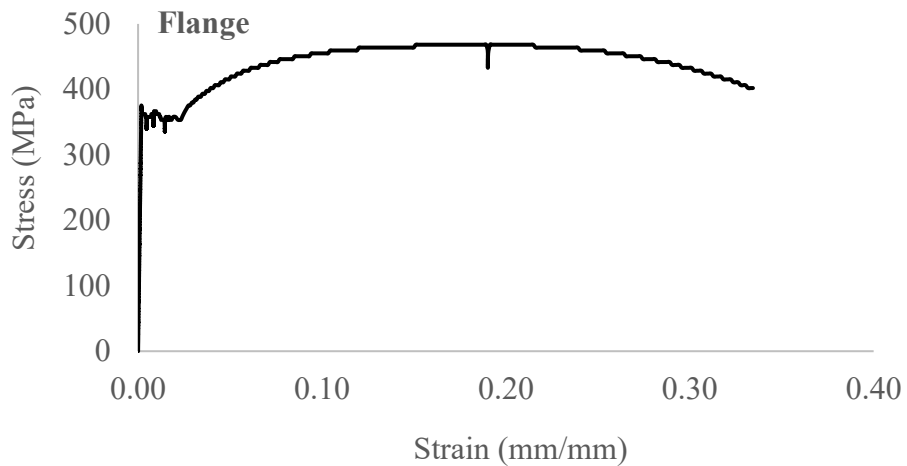
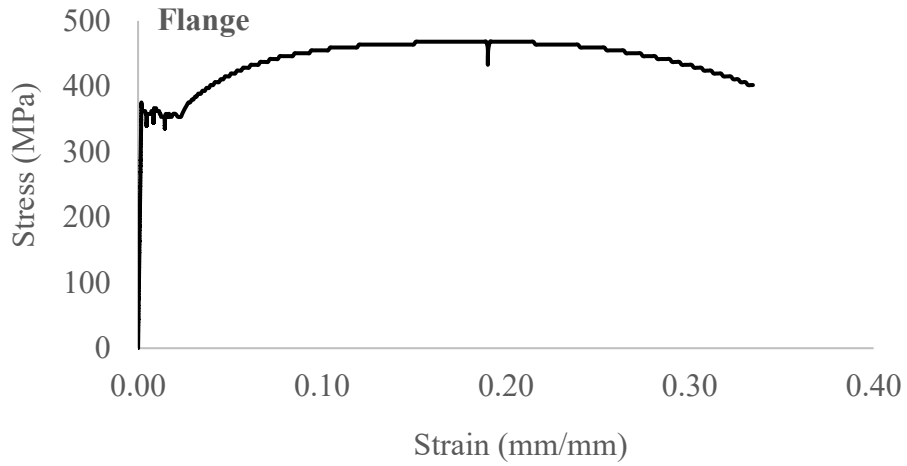
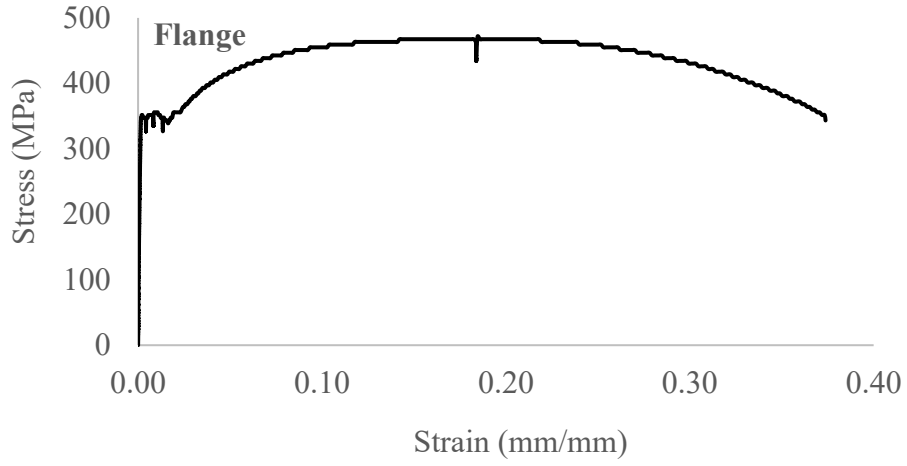


Figure A-1: Engineering stress-strain results for Heat 1



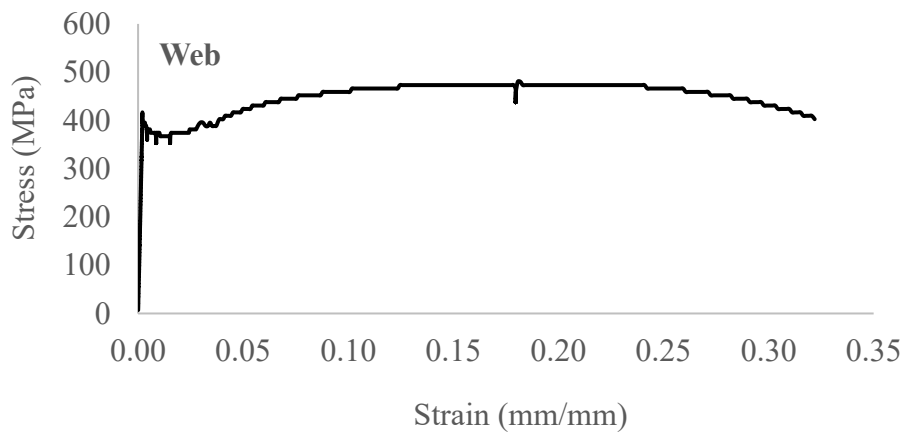
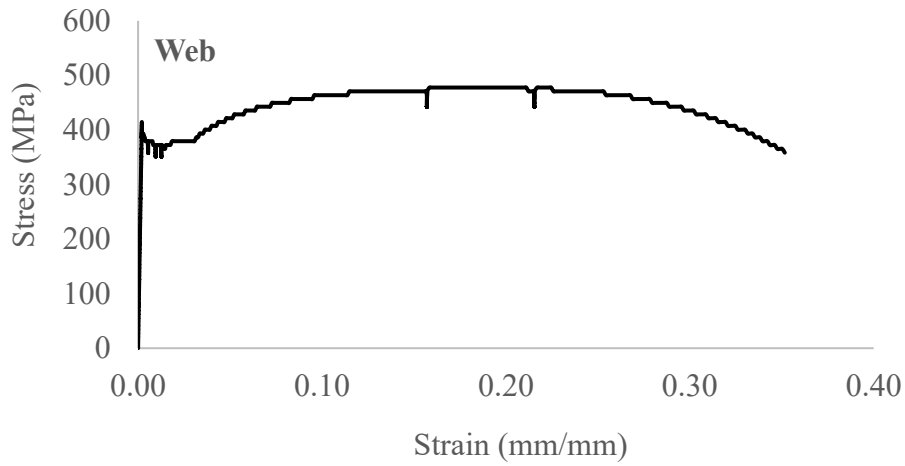
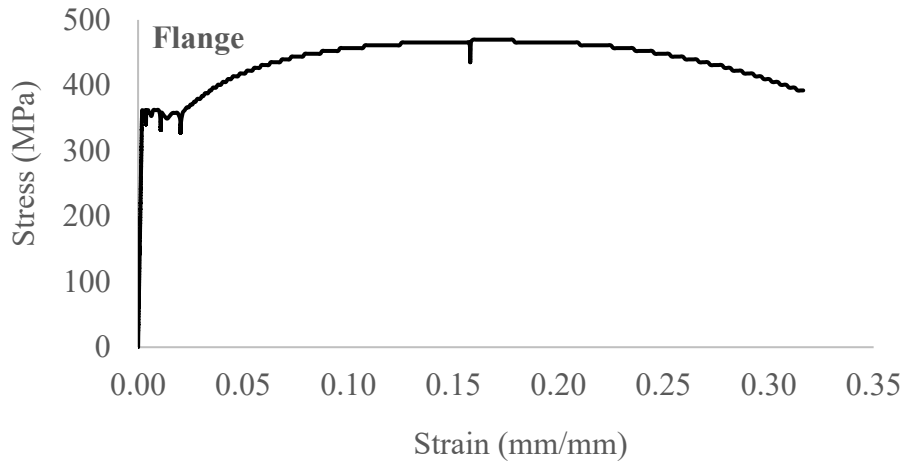
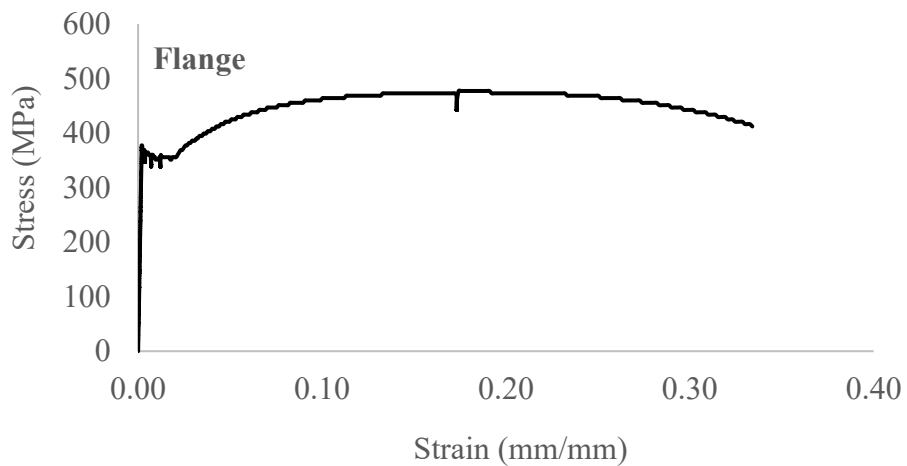
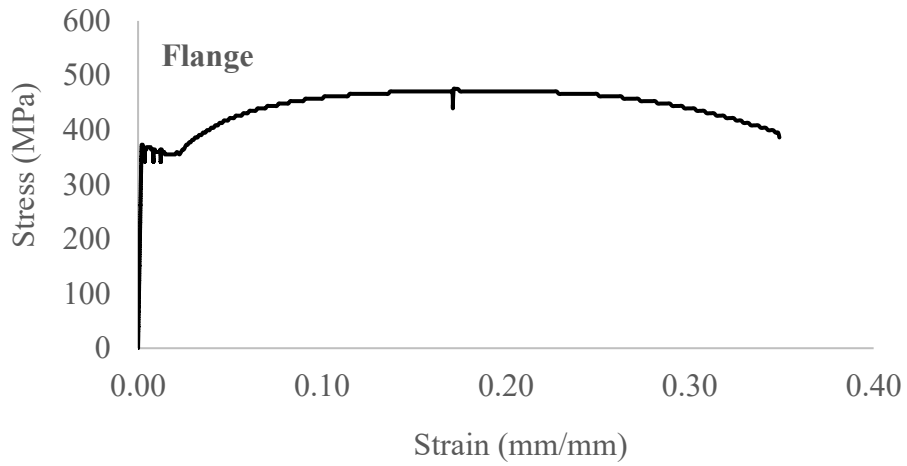
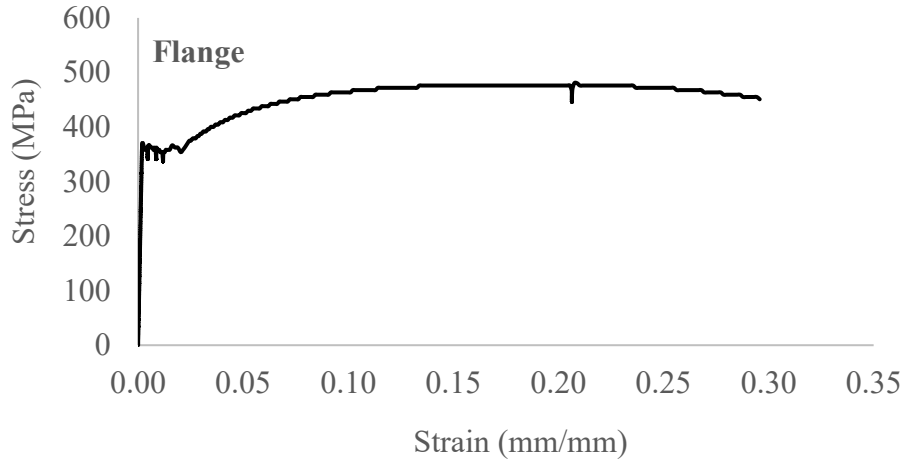


Figure A-2: Engineering stress-strain results for Heat 2



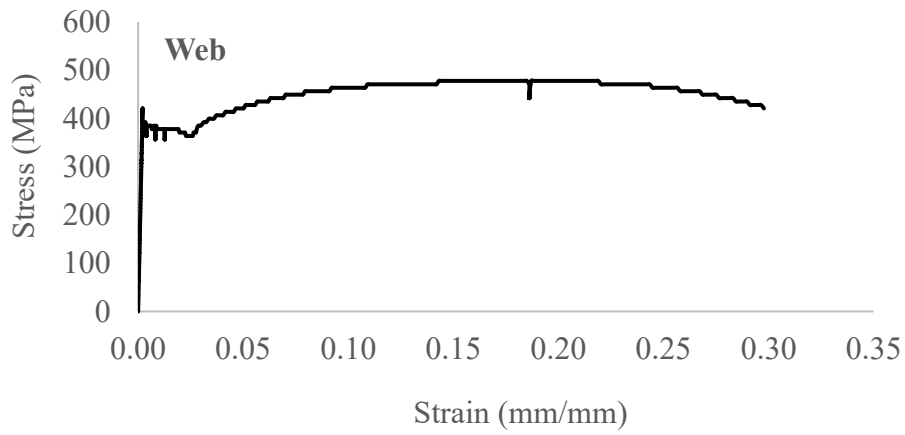
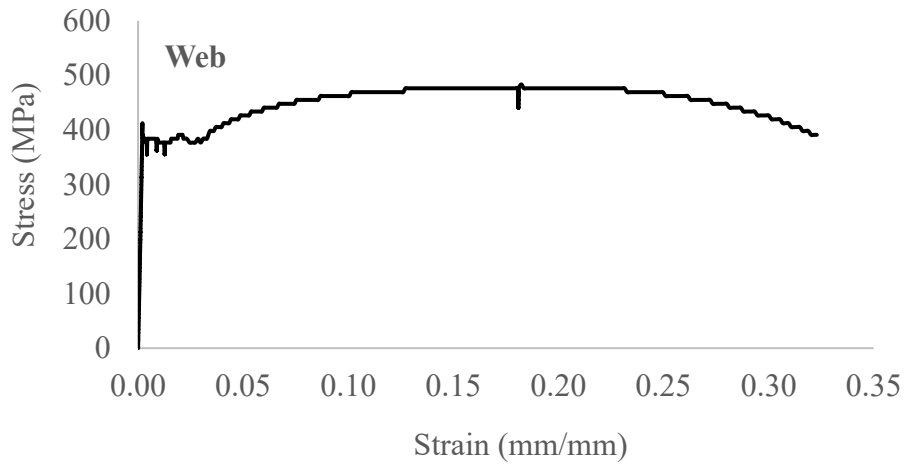
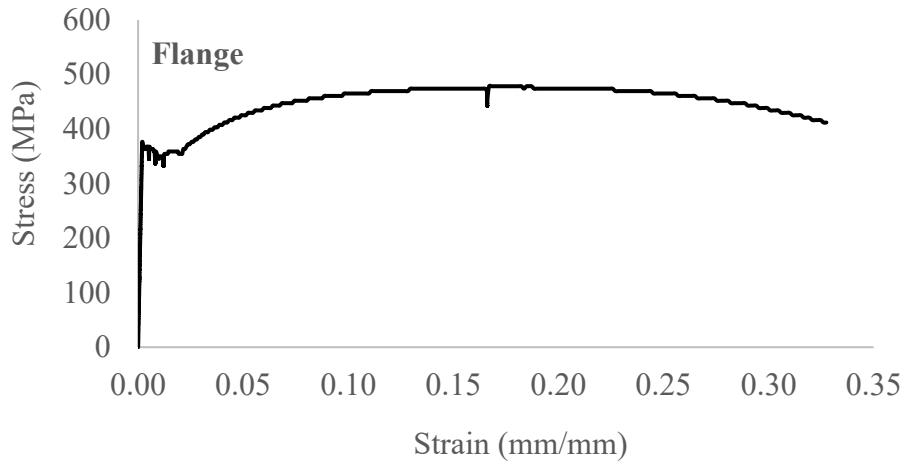


Figure A-3: Engineering stress-strain results for Heat 3

APPENDIX B: MEASURED INITIAL GEOMETRIC IMPERFECTIONS

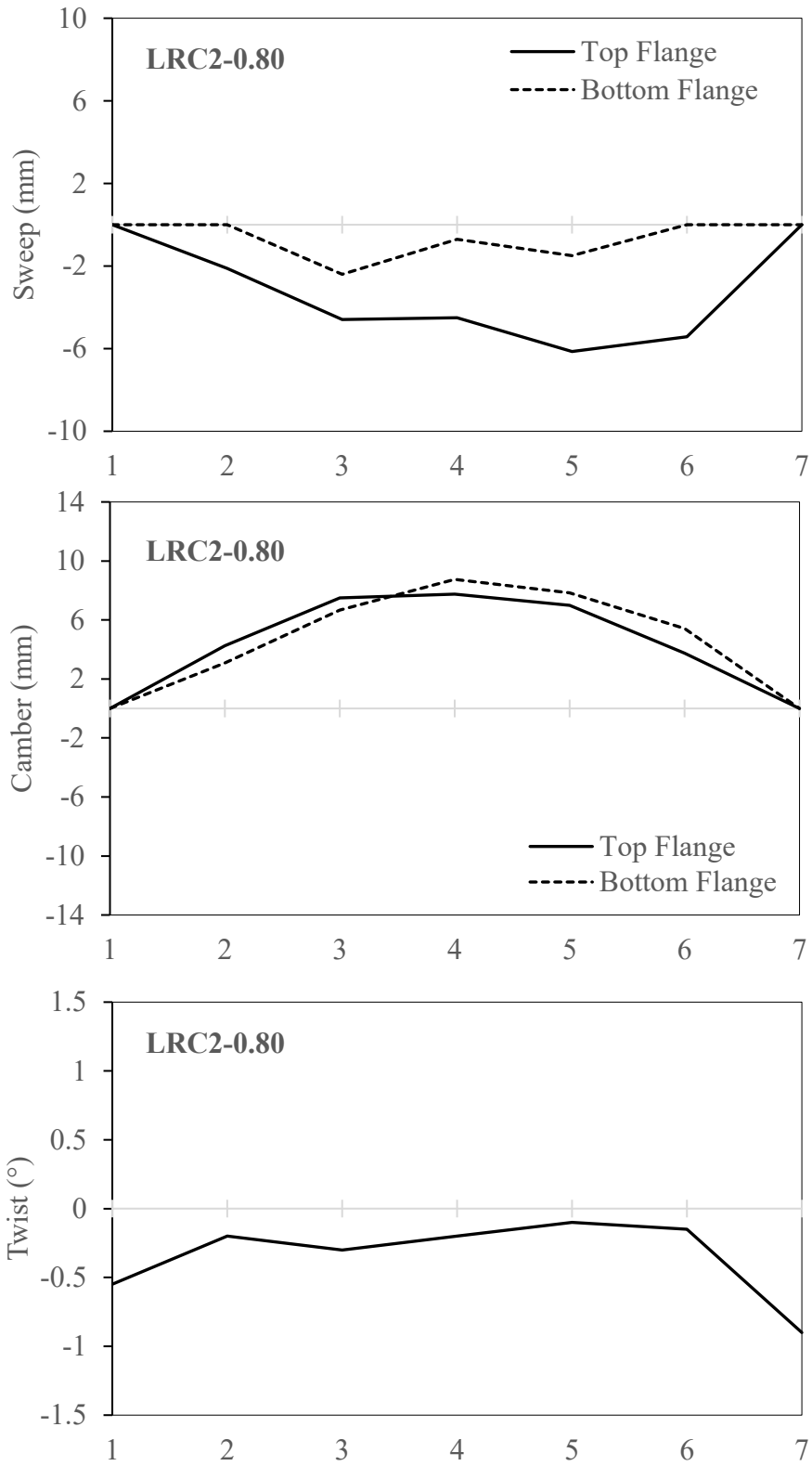


Figure B-1: Initial geometric imperfections for LRC2-0.80

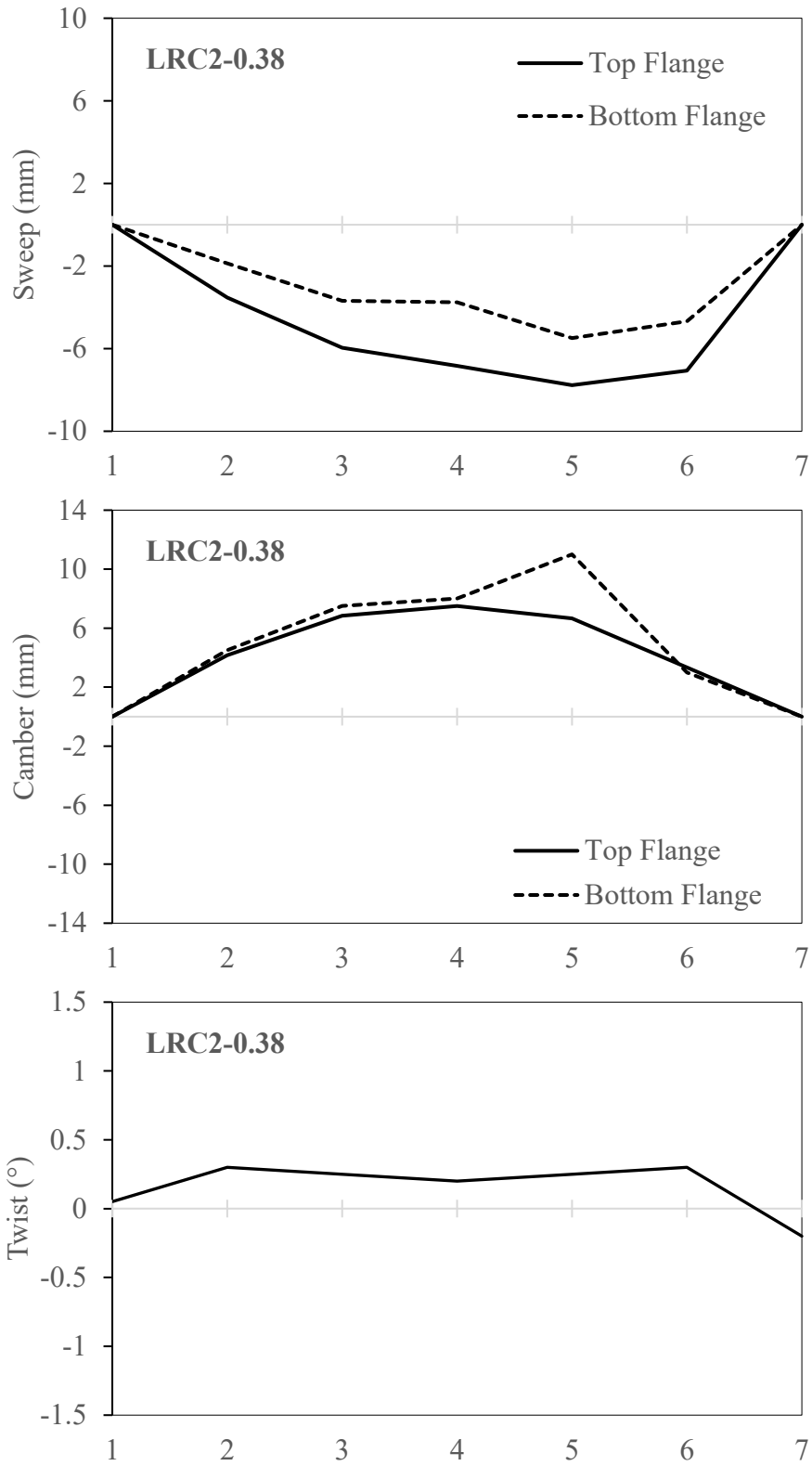


Figure B-2: Initial geometric imperfections for LRC2-0.38

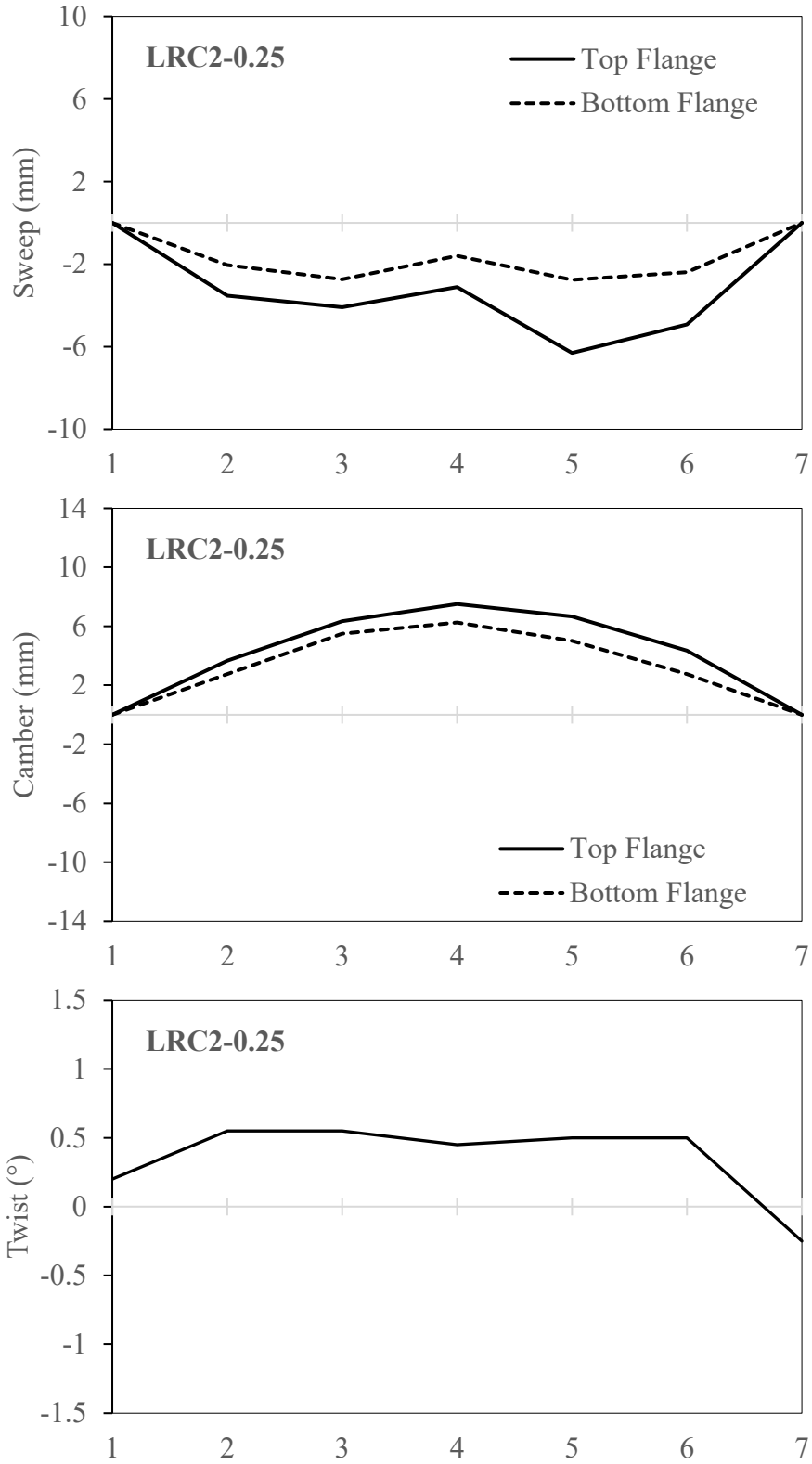


Figure B-3: Initial geometric imperfections for LRC2-0.25

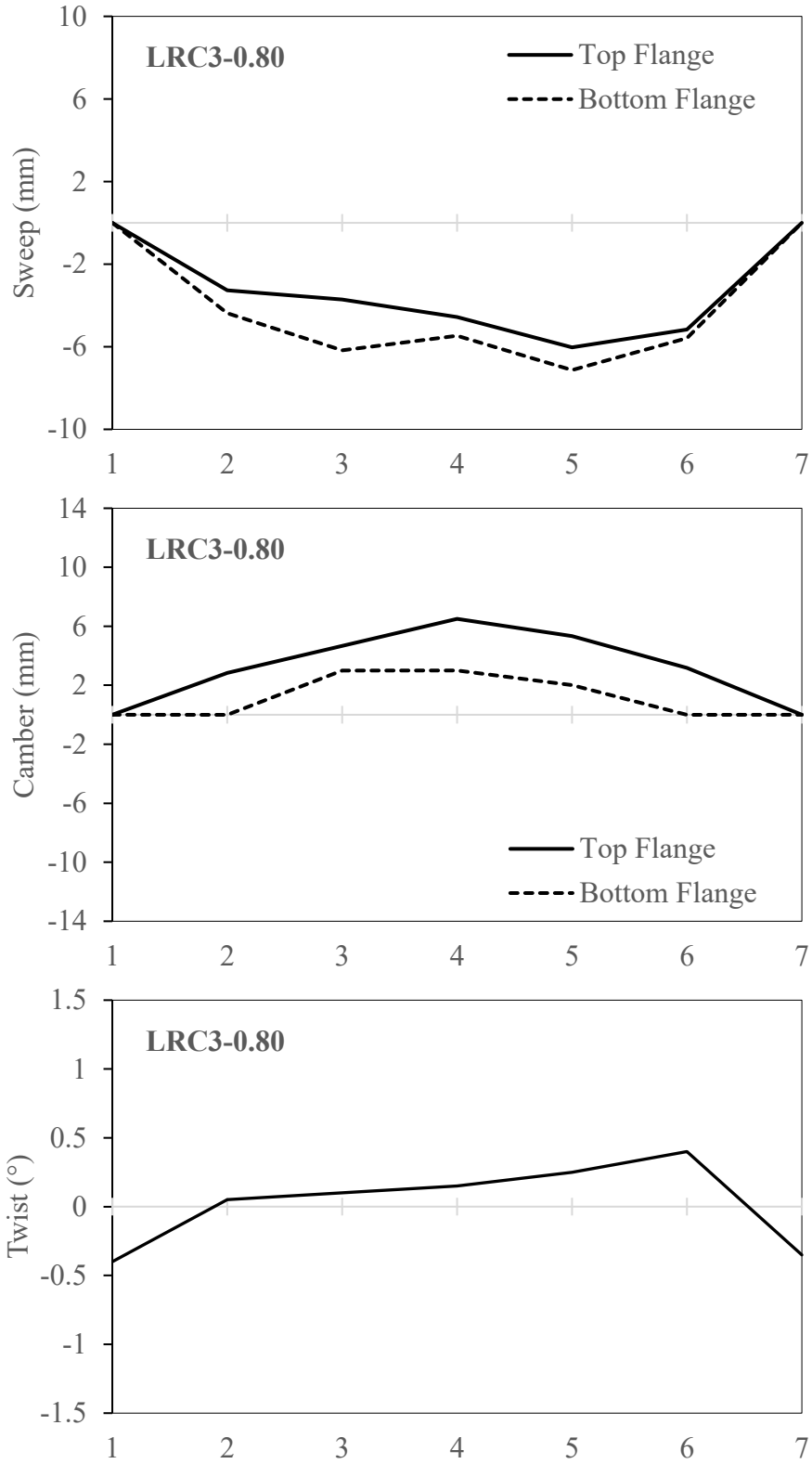


Figure B-4: Initial geometric imperfections for LRC3-0.80

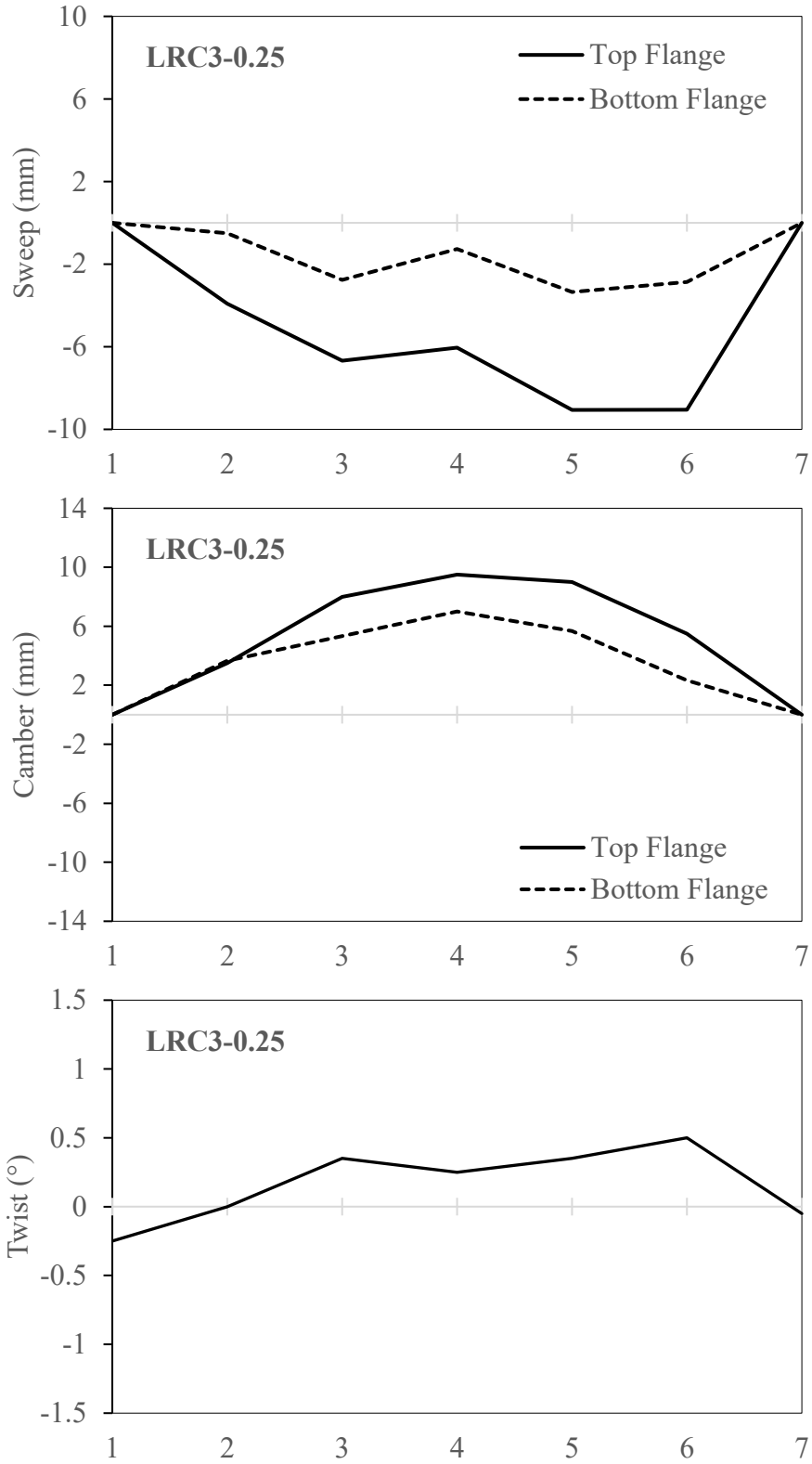


Figure B-5: Initial geometric imperfections for LRC3-0.25

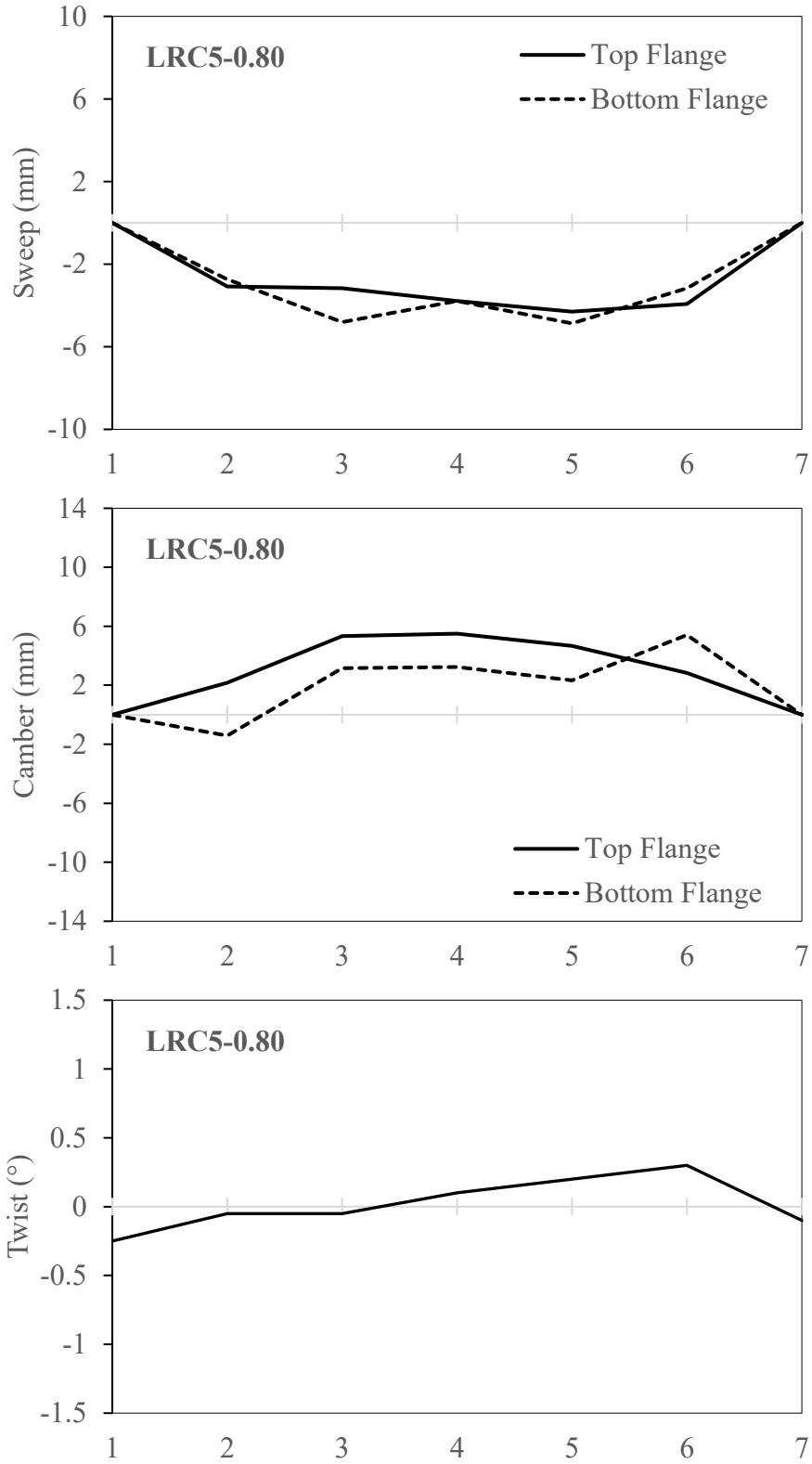


Figure B-6: Initial geometric imperfections for LRC5-0.80

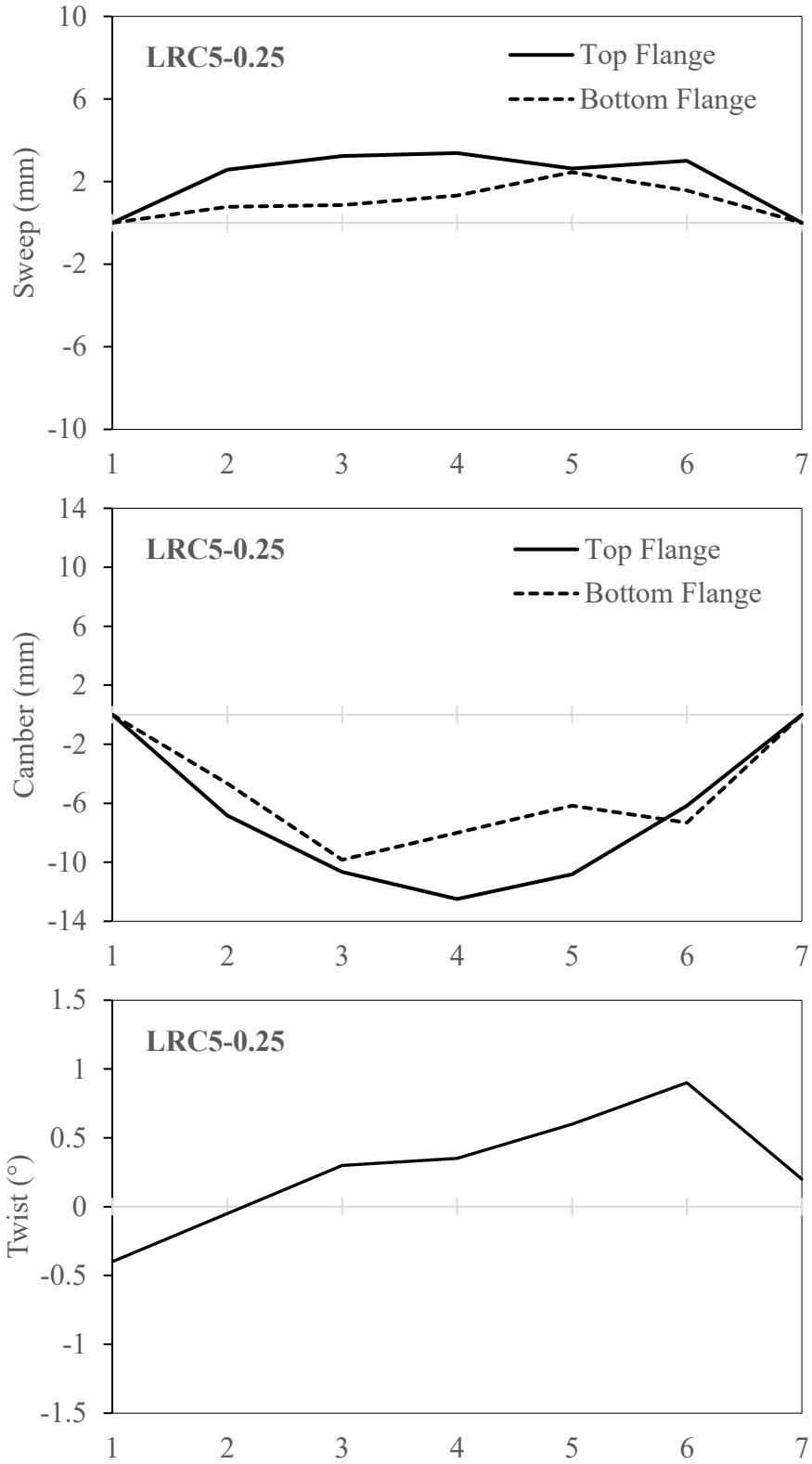


Figure B-7: Initial geometric imperfections for LRC5-0.25

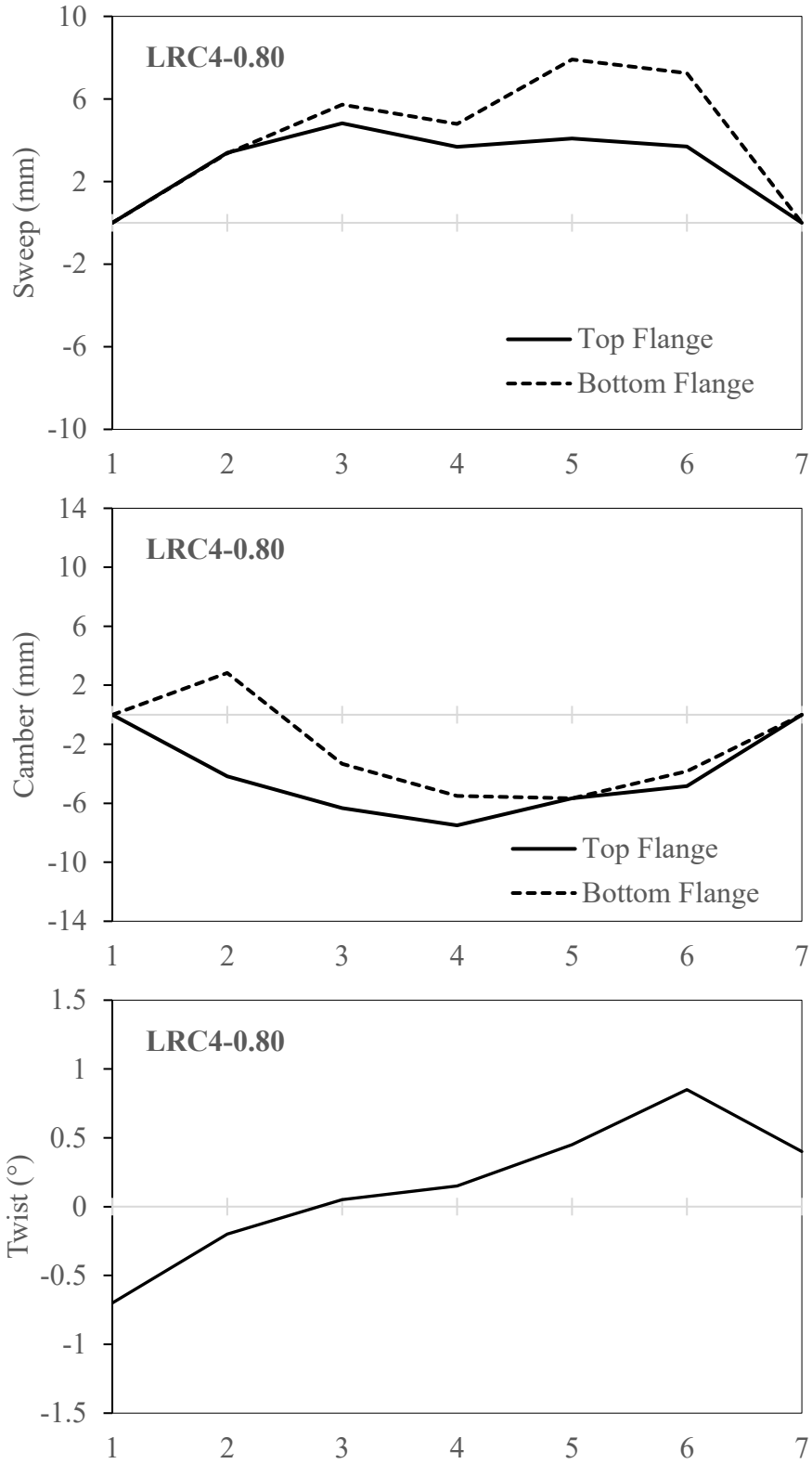


Figure B-8: Initial geometric imperfections for LRC4-0.80

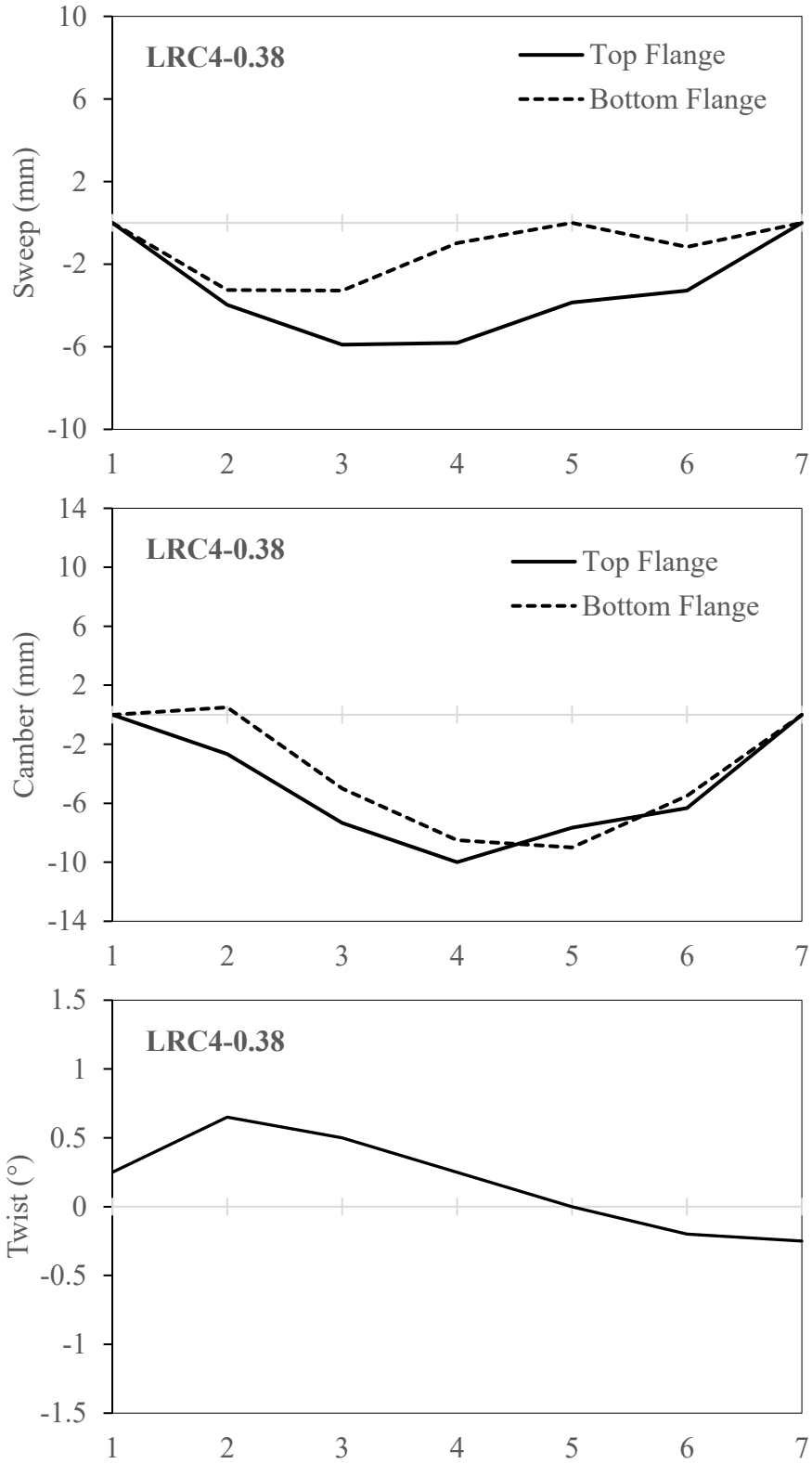


Figure B-9: Initial geometric imperfections for LRC4-0.38

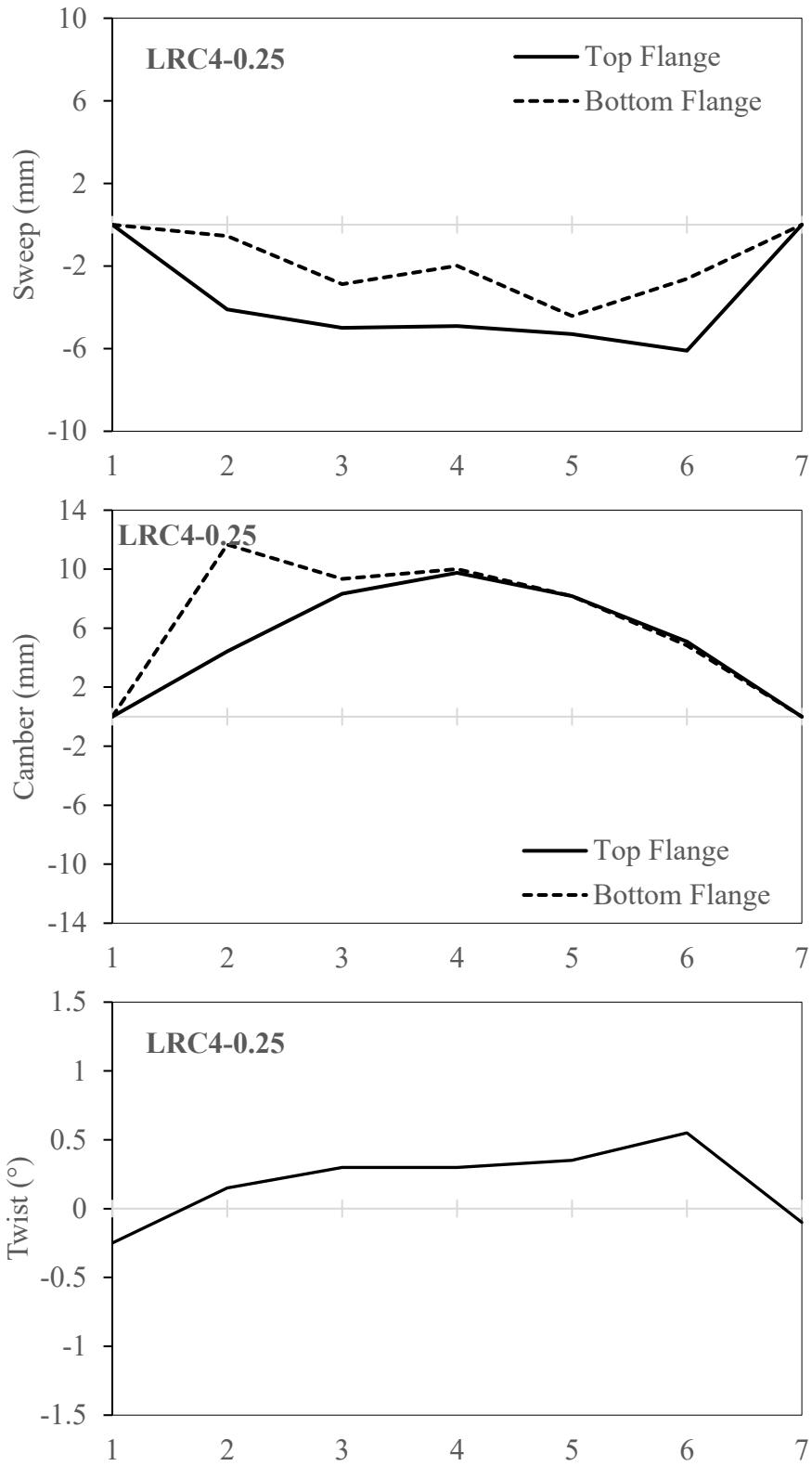


Figure B-10: Initial geometric imperfections for LRC4-0.25

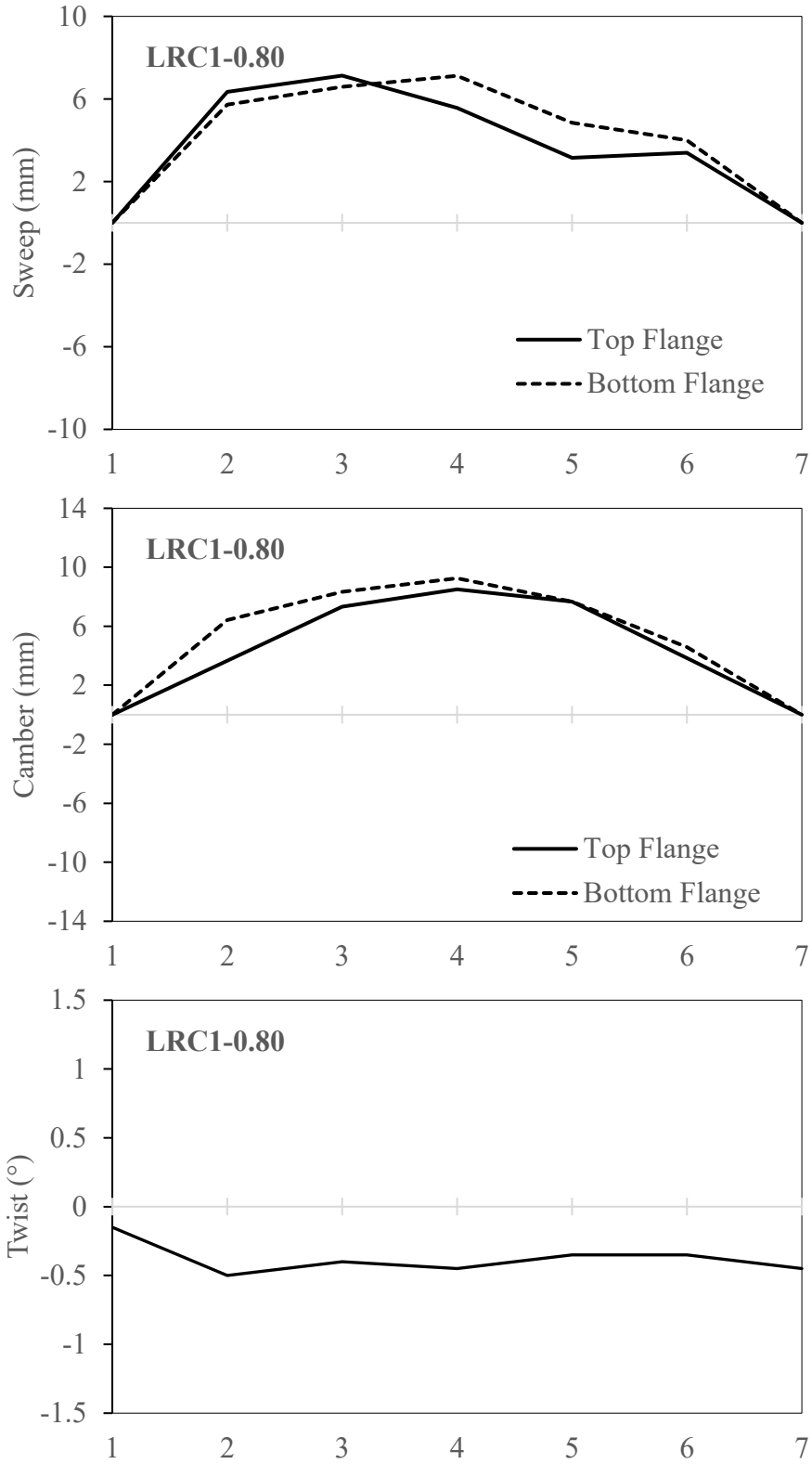


Figure B-11: Initial geometric imperfections for LRC1-0.80

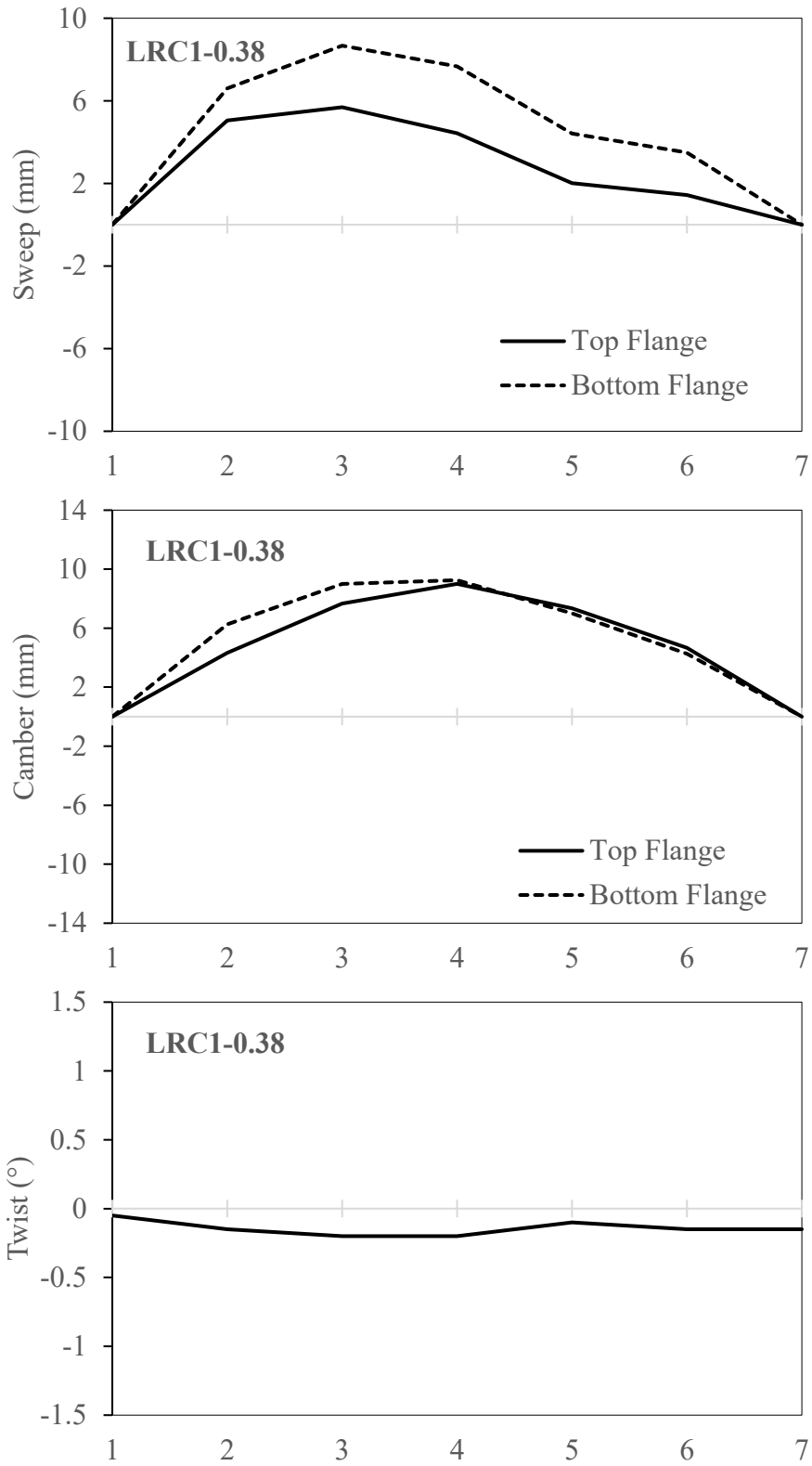


Figure B-12: Initial geometric imperfections for LRC1-0.38

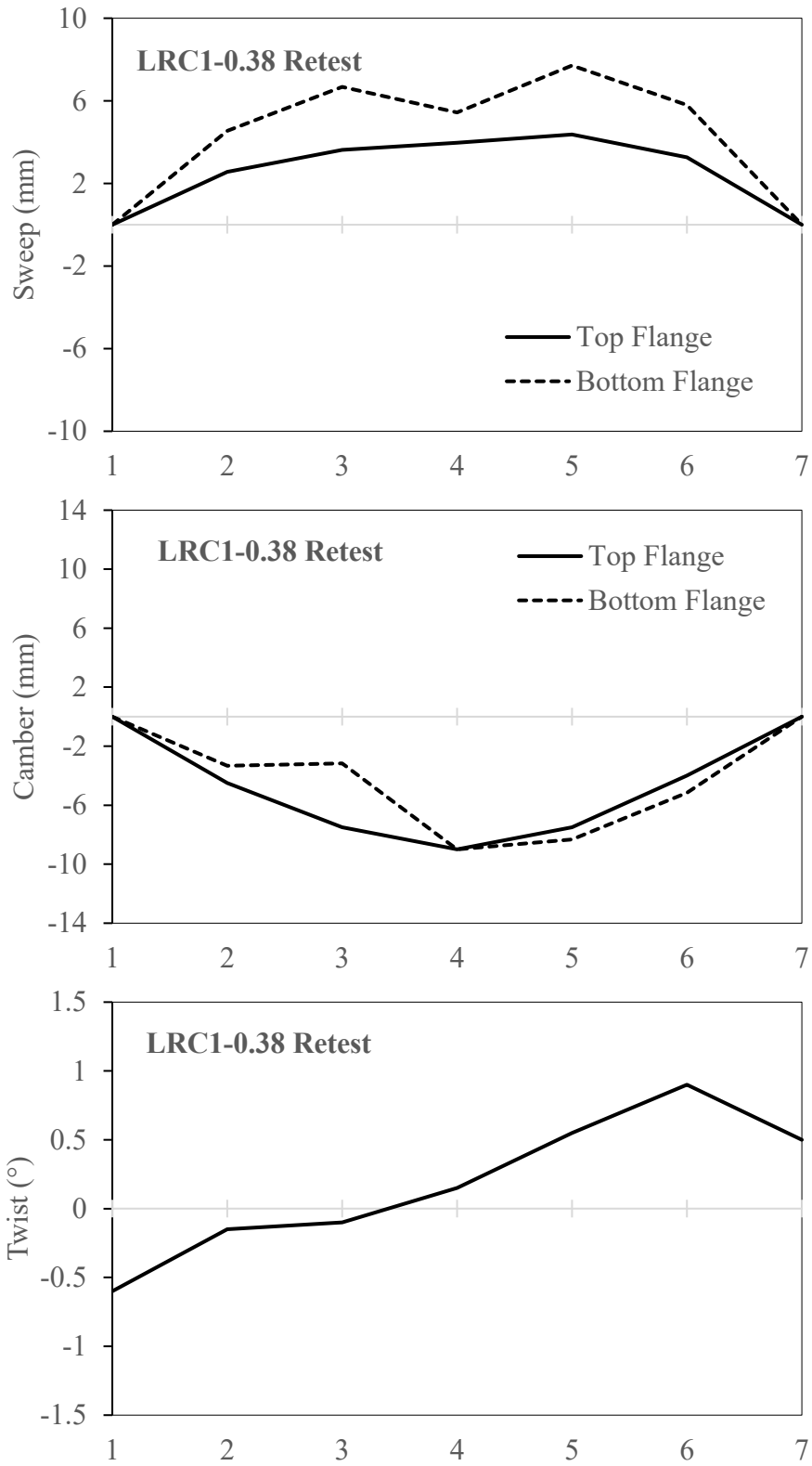


Figure B-13: Initial geometric imperfections for LRC1-0.38 Retest

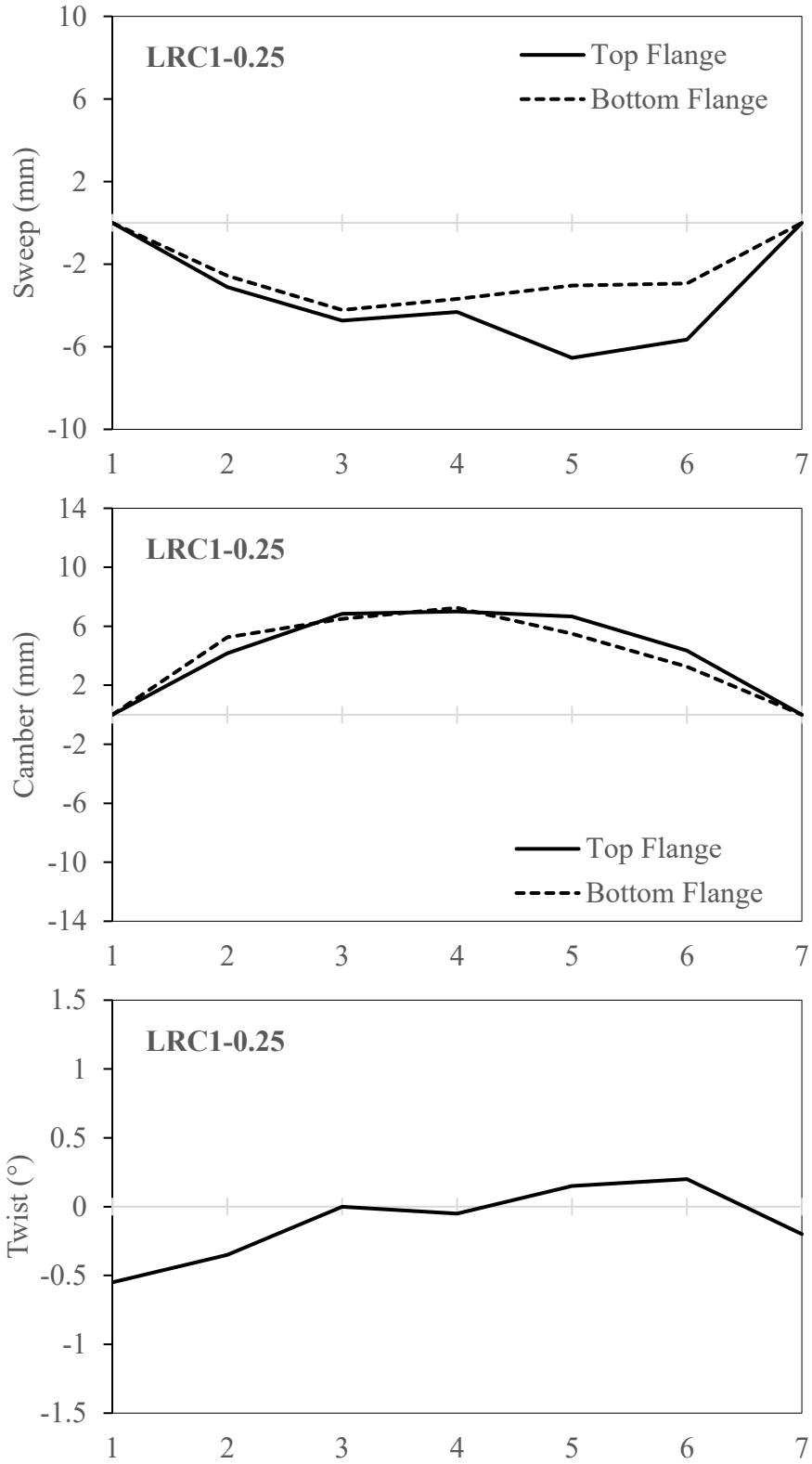


Figure B-14: Initial geometric imperfections for LRC1-0.25

APPENDIX C: EXPERIMENTAL LOAD-DEFLECTION CURVES

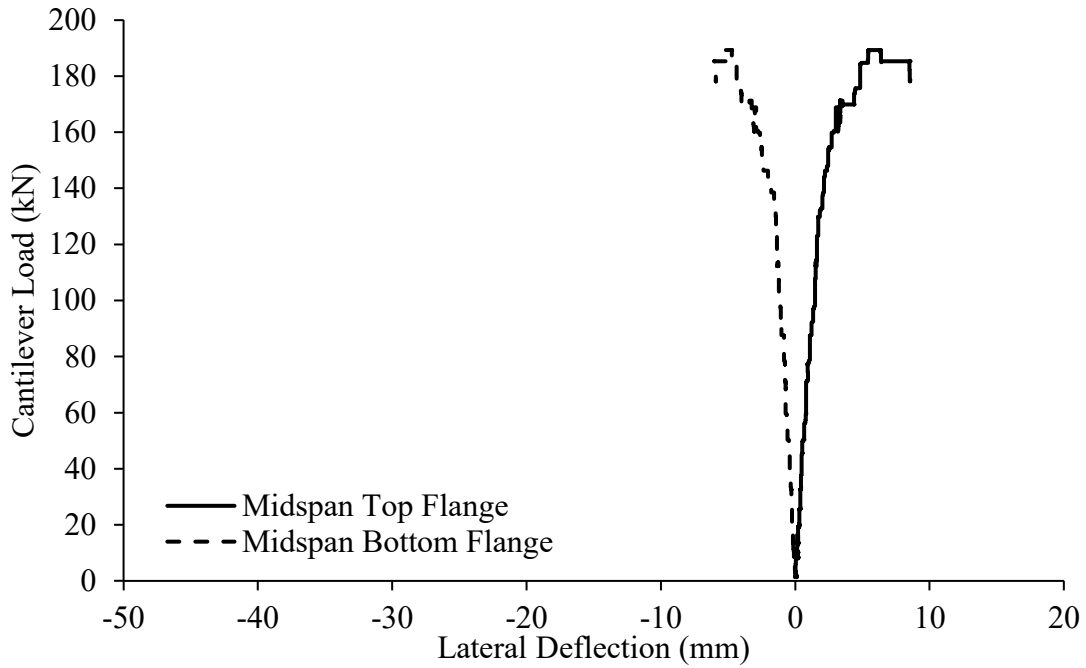


Figure C-1: Load-lateral deflection curves for midspan of back span for LRC2-0.75

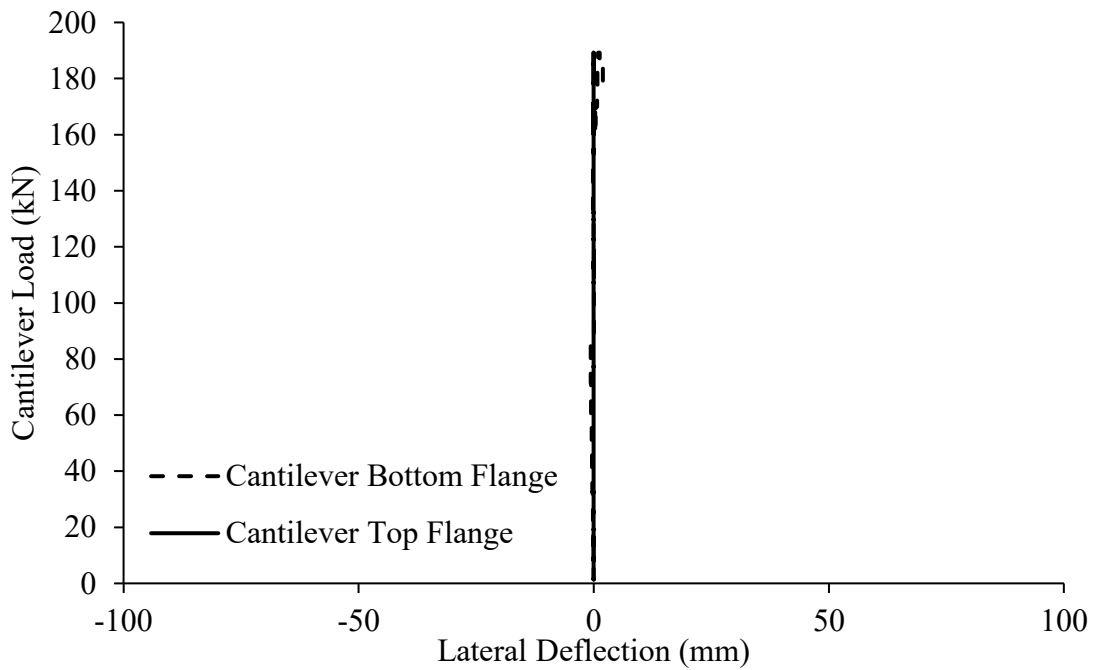


Figure C-2: Load-lateral deflection curves for cantilever for LRC2-0.75

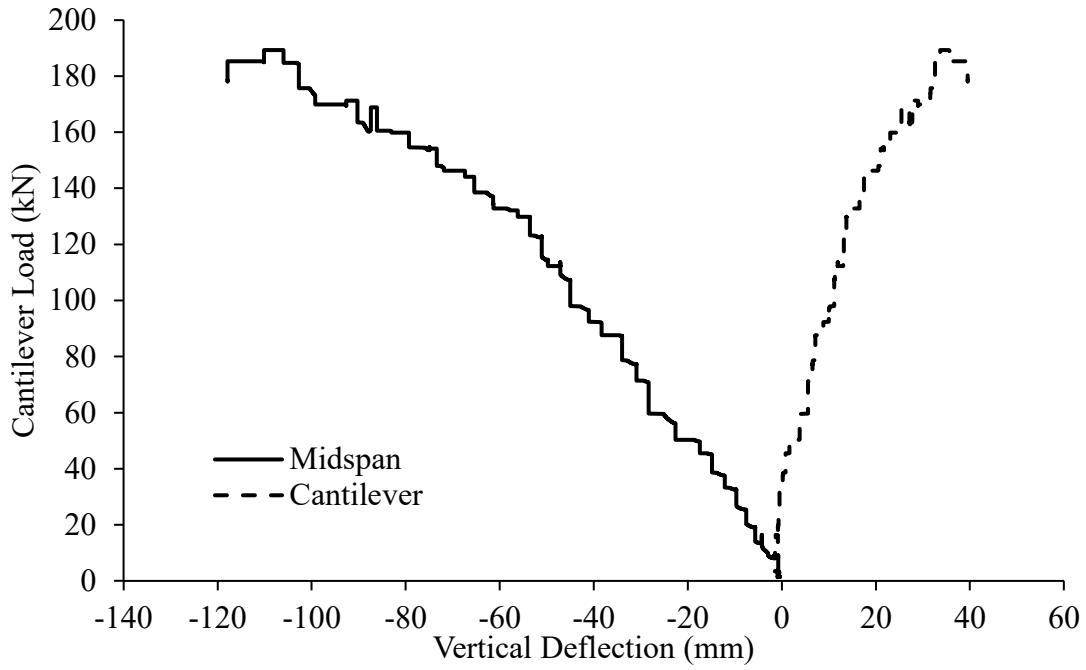


Figure C-3: Load-vertical deflection curves for LRC2-0.75

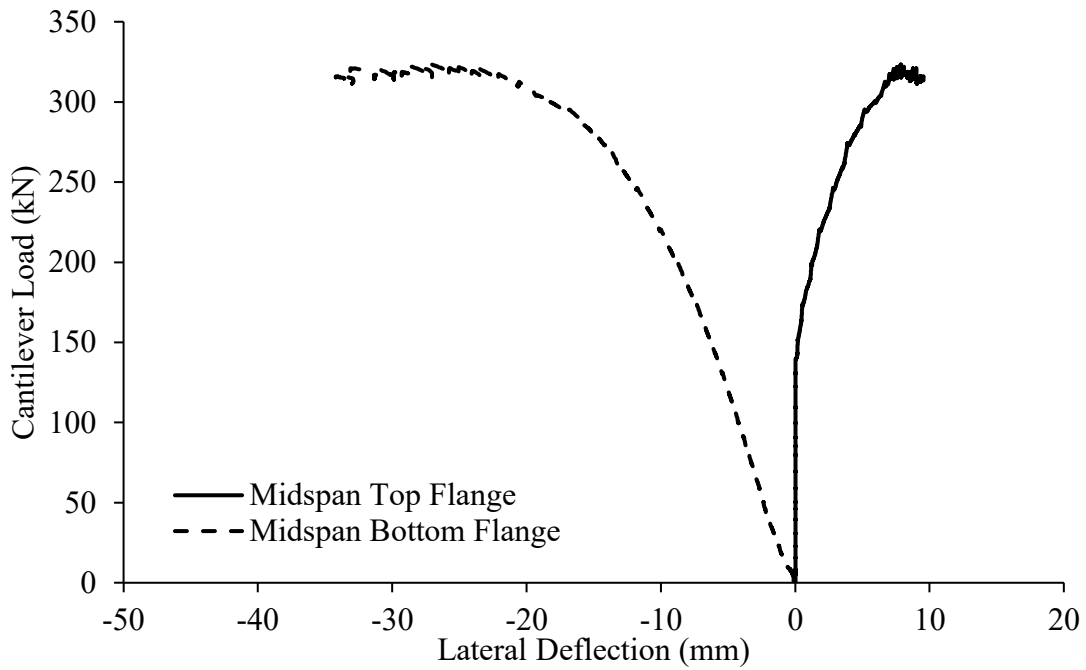


Figure C-4: Load-lateral deflection curves for midspan of back span for LRC2-0.38

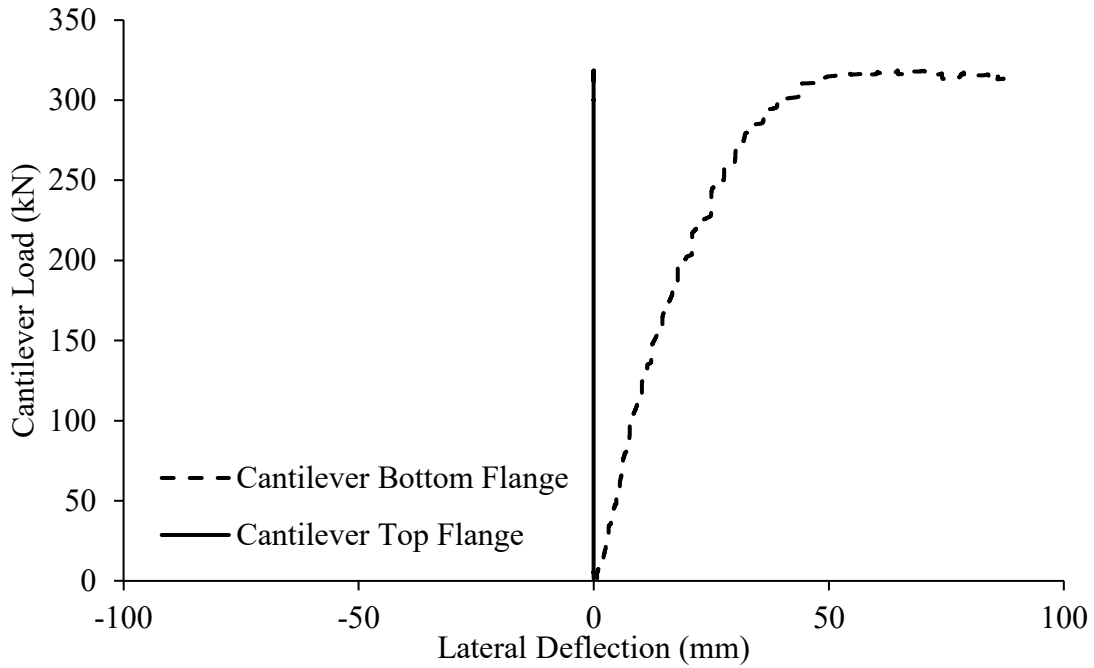


Figure C-5: Load-lateral deflection curves for cantilever for LRC2-0.38

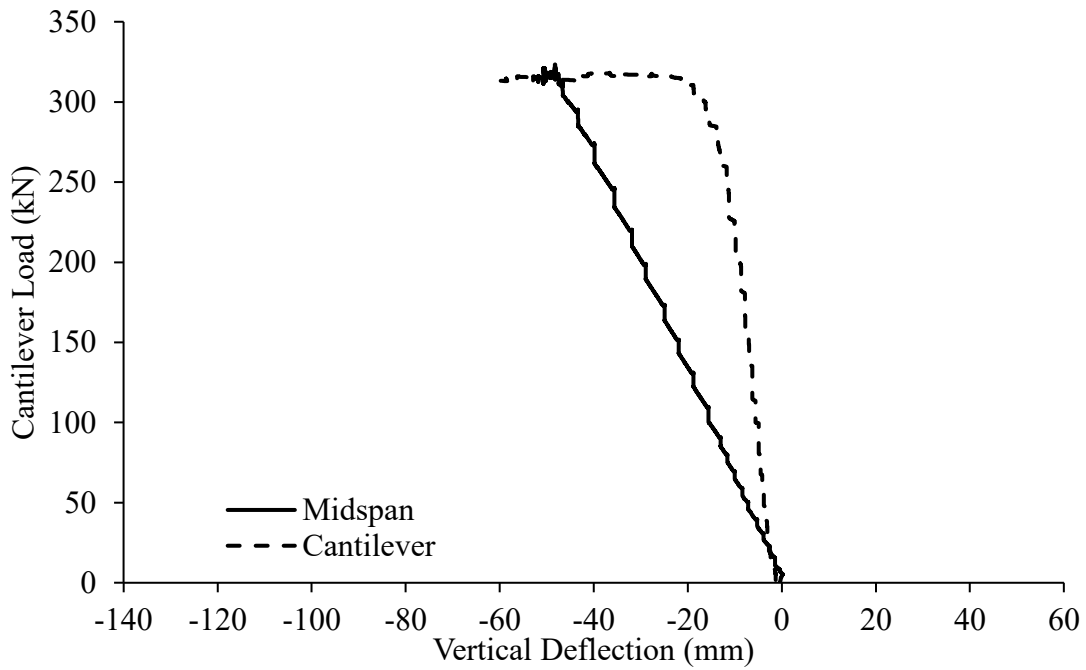


Figure C-6: Load-vertical deflection curves for LRC2-0.38

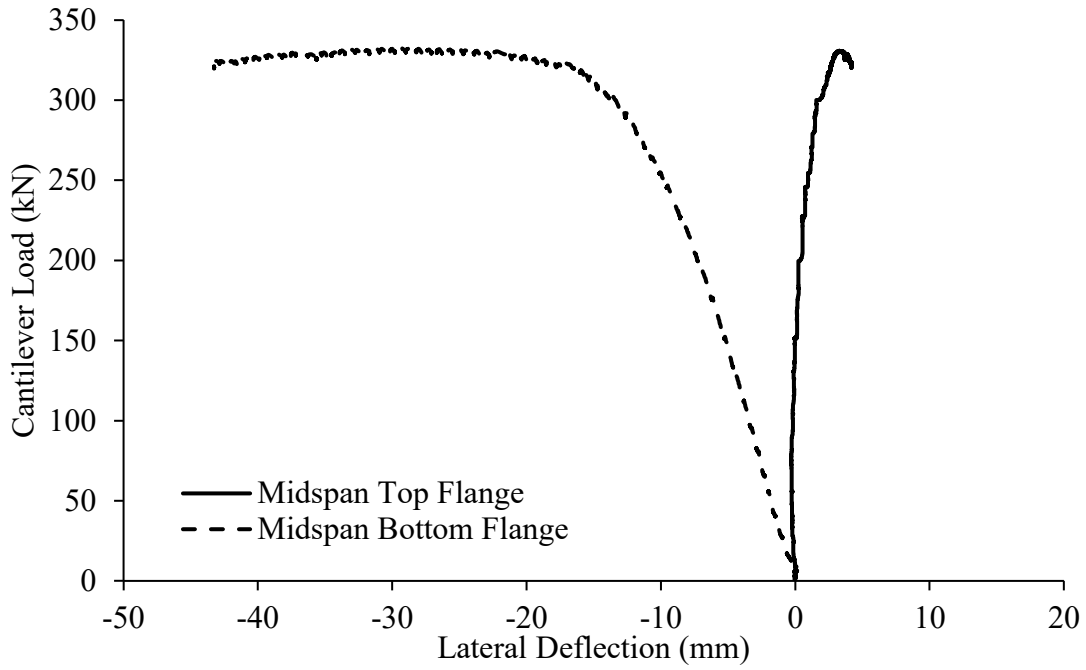


Figure C-7: Load-lateral deflection curves for midspan of back span for LRC2-0.25

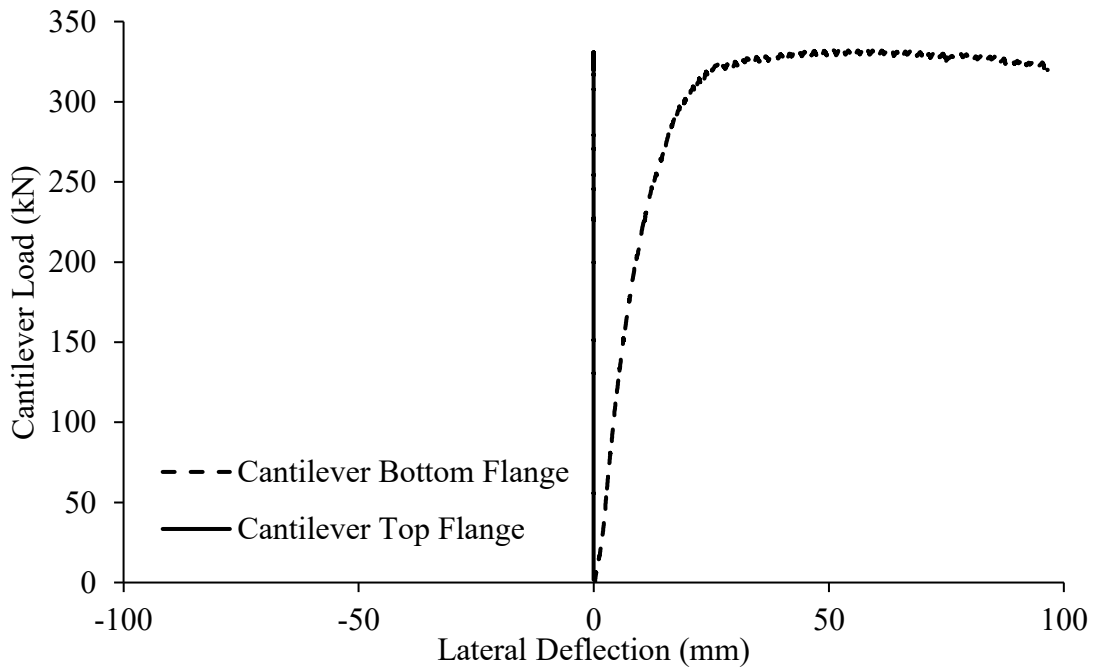


Figure C-8: Load-lateral deflection curves for cantilever for LRC2-0.25

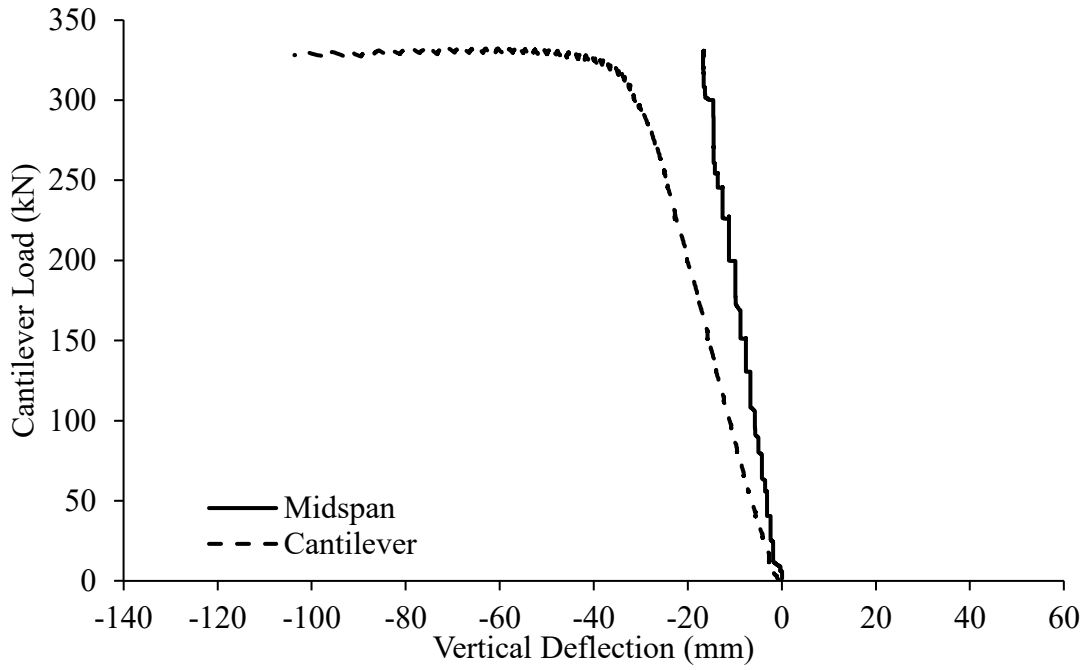


Figure C-9: Load-vertical deflection curves for LRC2-0.25

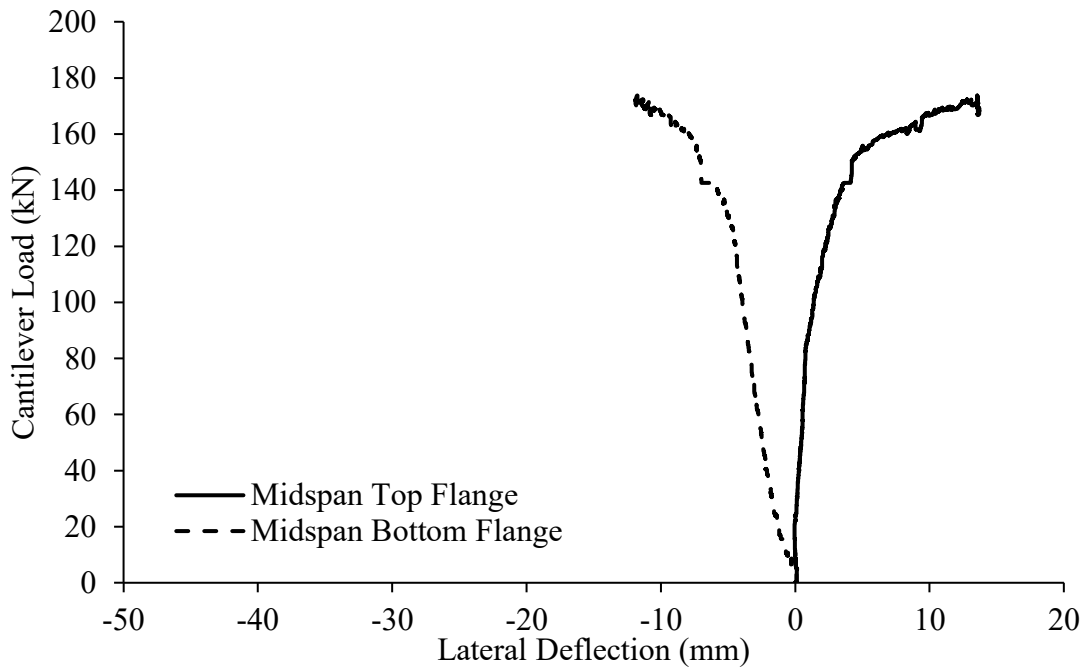


Figure C-10: Load-lateral deflection curves for midspan of back span for LRC3-0.80

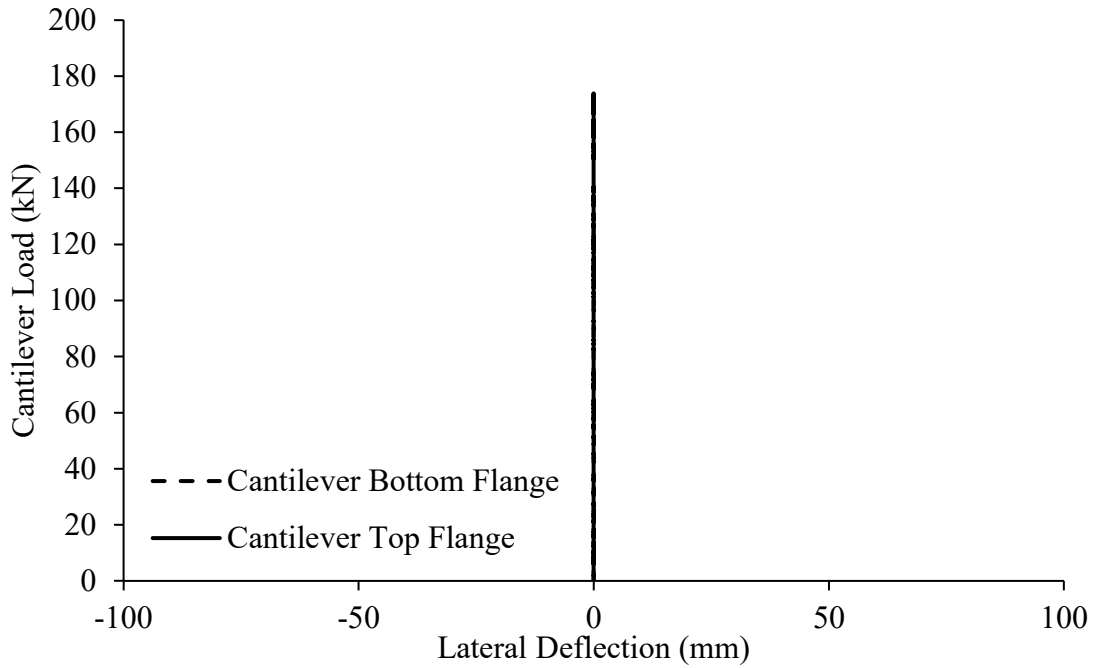


Figure C-11: Load-lateral deflection curves for cantilever for LRC3-0.80

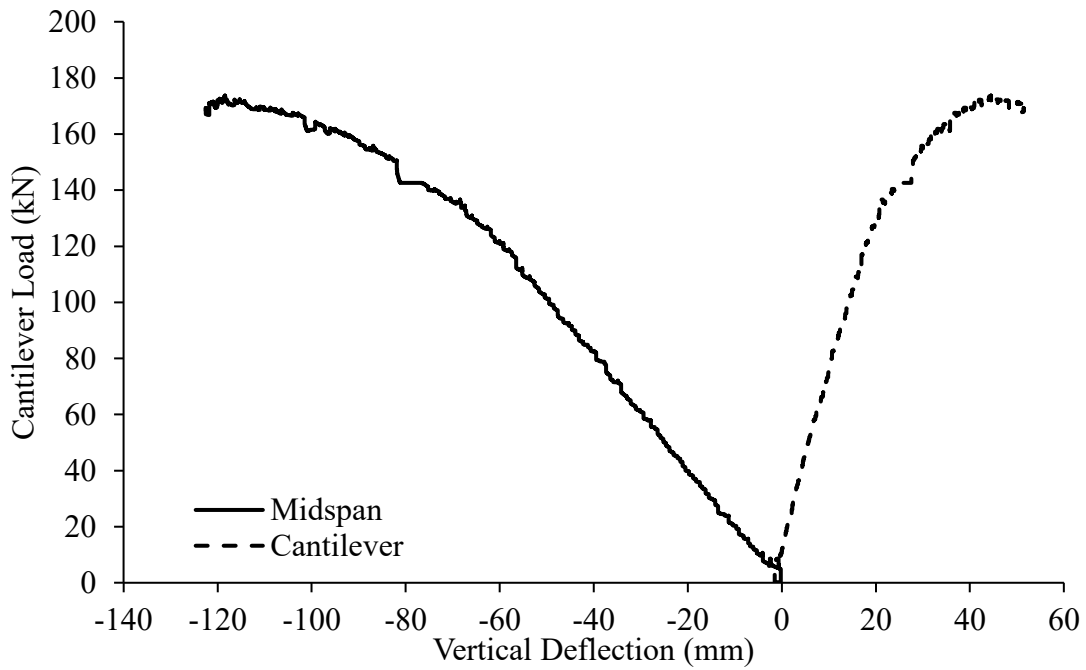


Figure C-12: Load-vertical deflection curves for LRC3-0.80

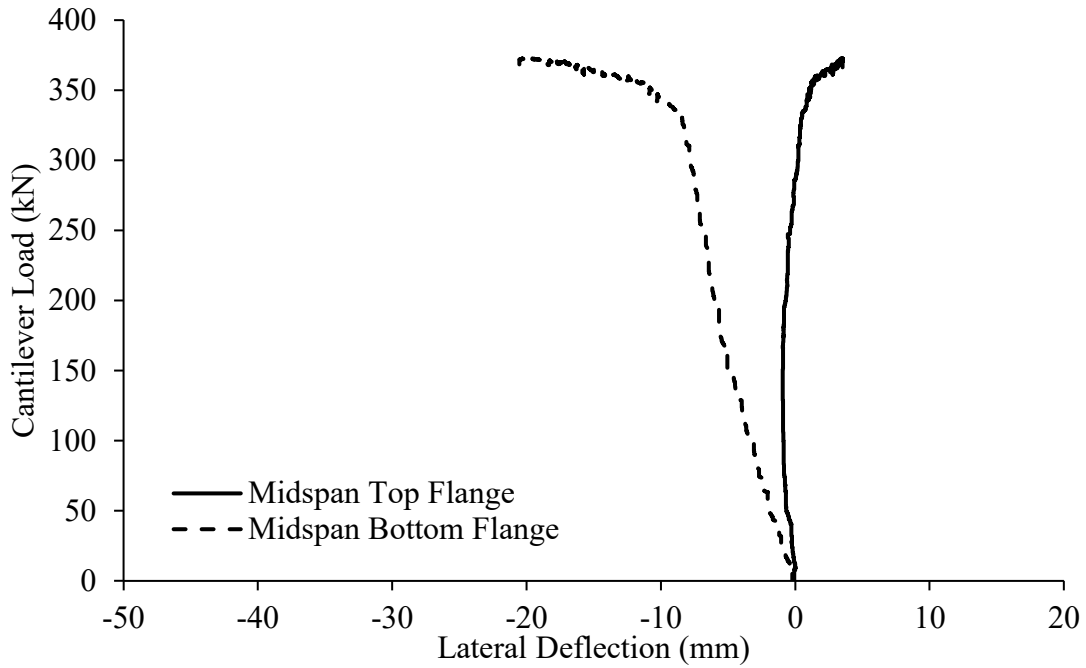


Figure C-13: Load-lateral deflection curves for midspan of back span for LRC3-0.25

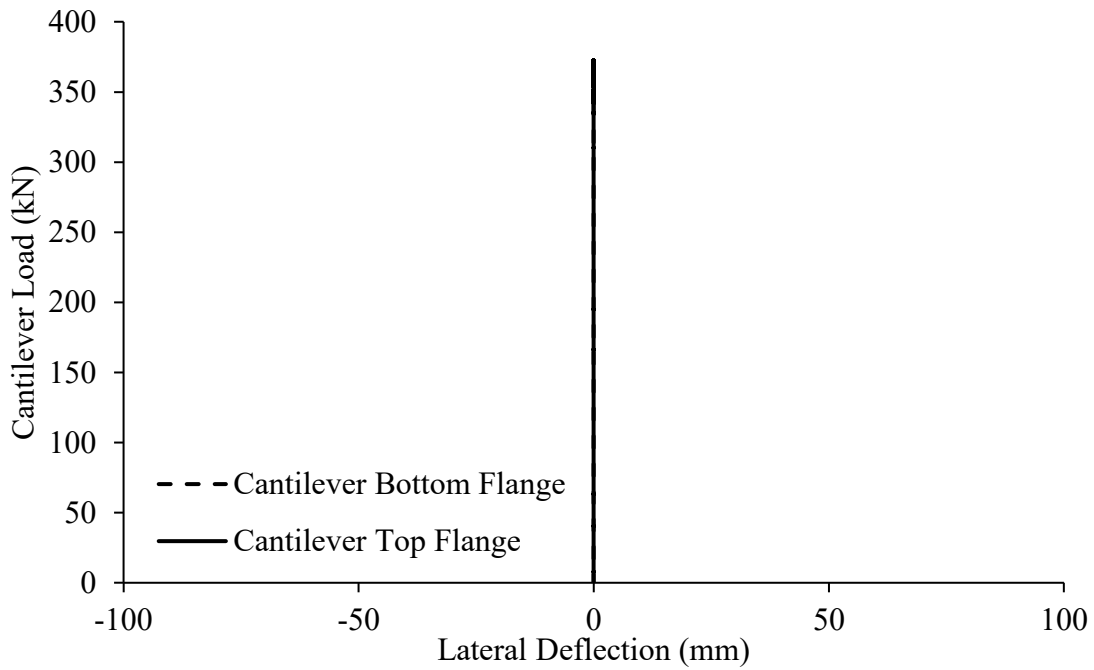


Figure C-14: Load-lateral deflection curves for cantilever for LRC3-0.25

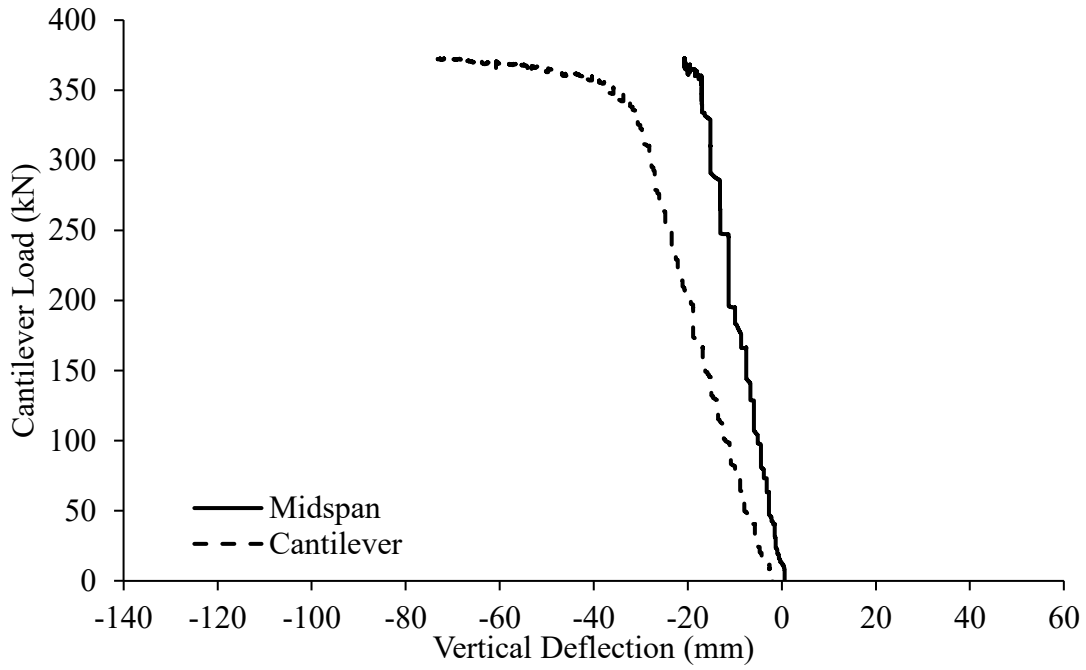


Figure C-15: Load-vertical deflection curves for LRC3-0.25

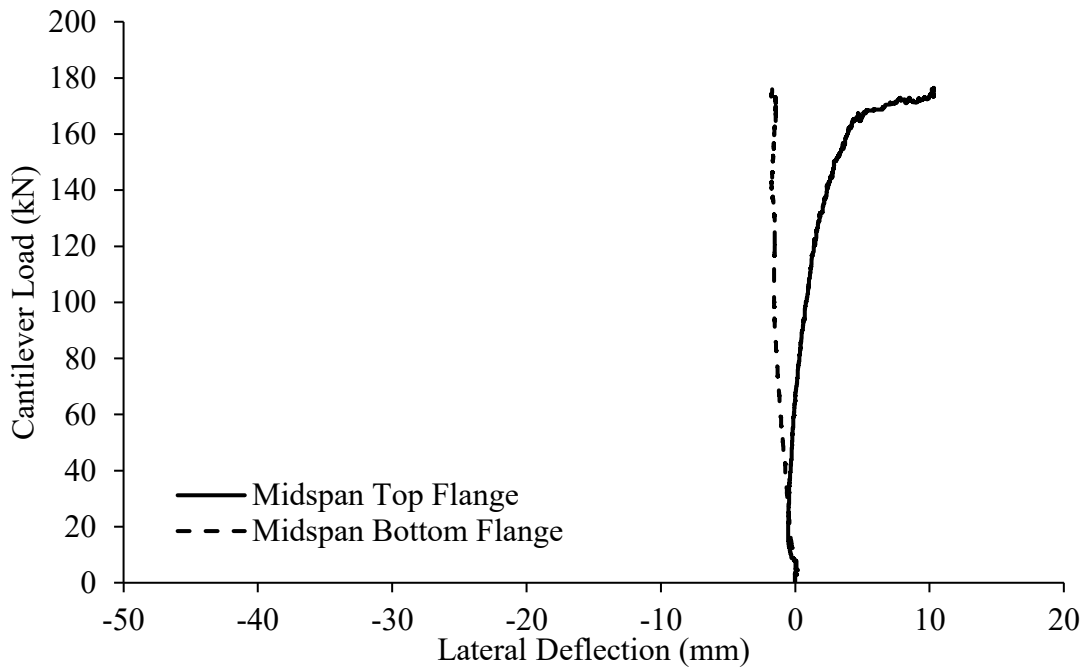


Figure C-16: Load-lateral deflection curves for midspan of back span for LRC5-0.80

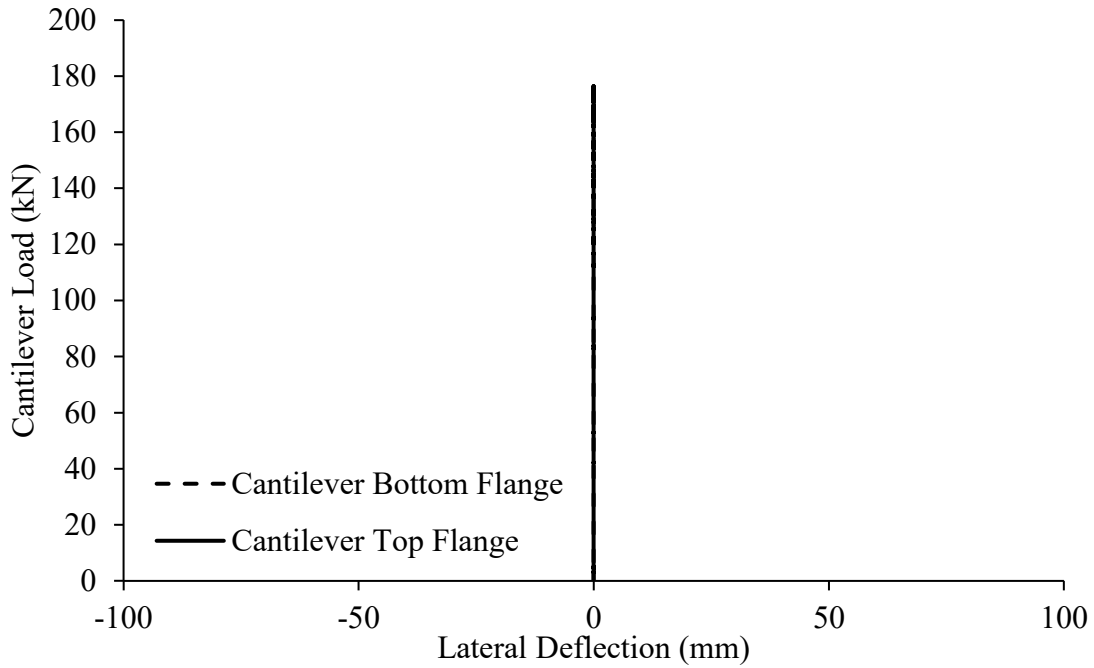


Figure C-17: Load-lateral deflection curves for cantilever for LRC5-0.80

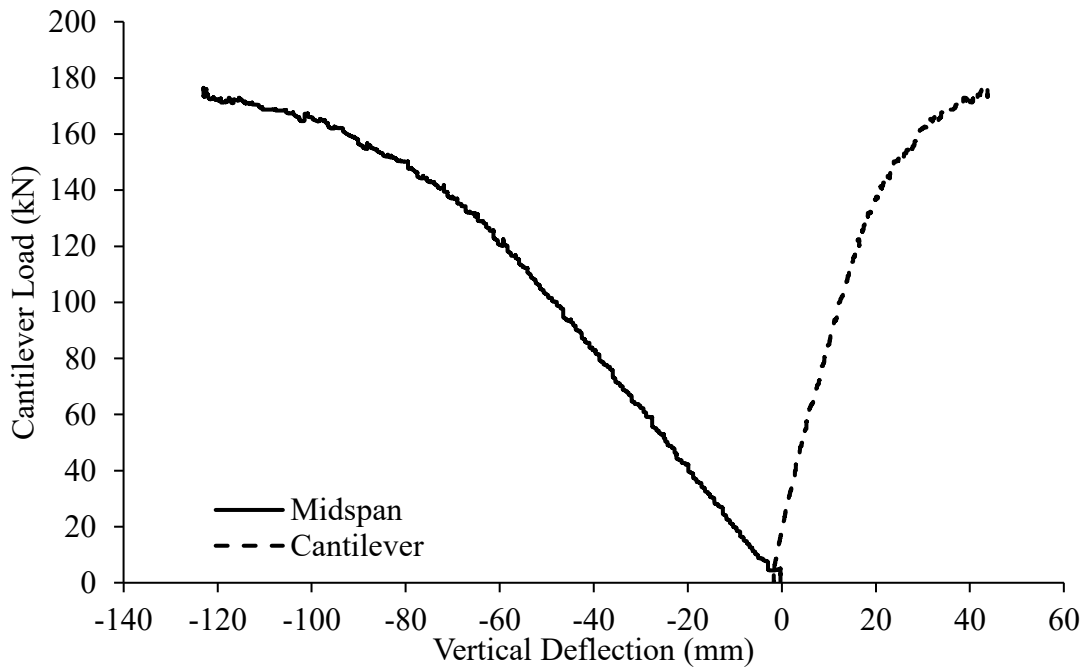


Figure C-18: Load-vertical deflection curves for LRC5-0.80

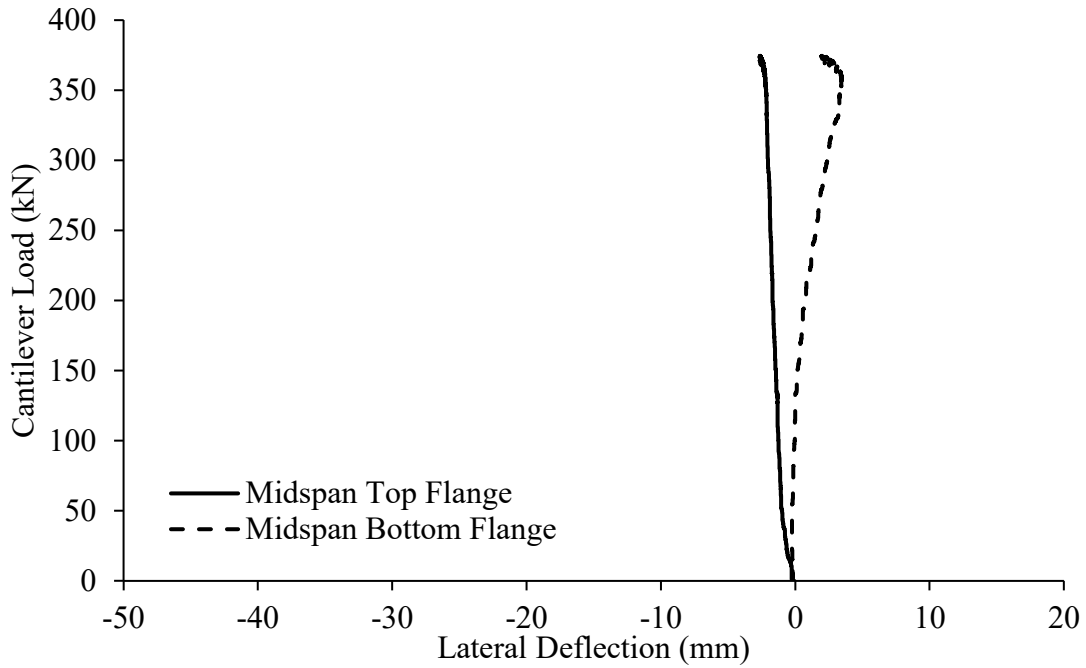


Figure C-19: Load-lateral deflection curves for midspan of back span for LRC5-0.25

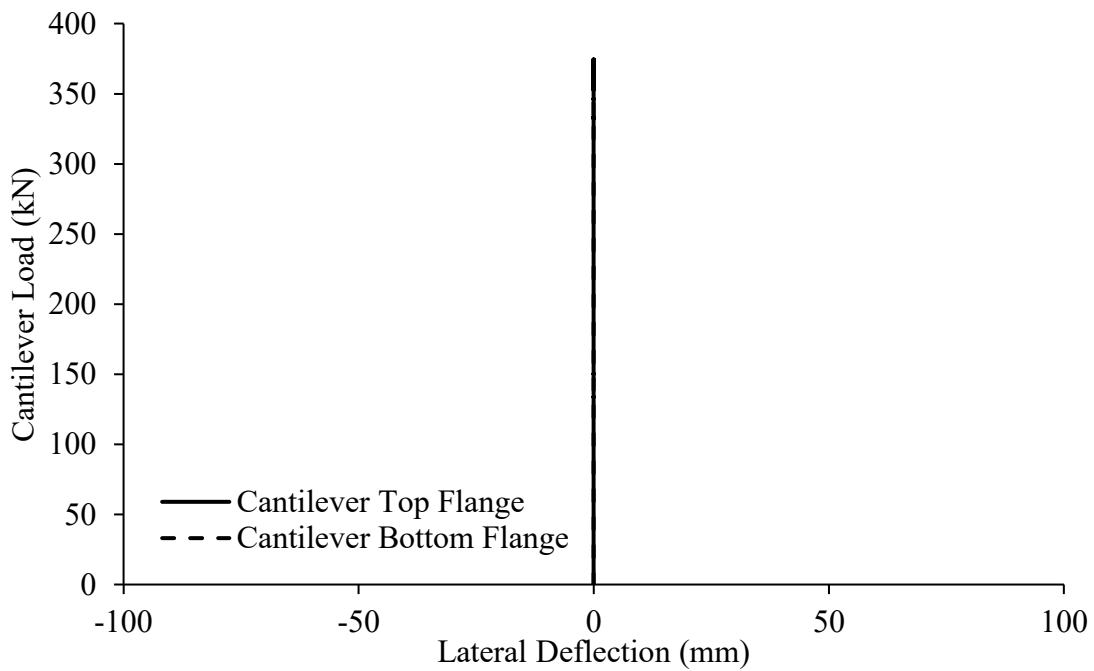


Figure C-20: Load-lateral deflection curves for cantilever for LRC5-0.25

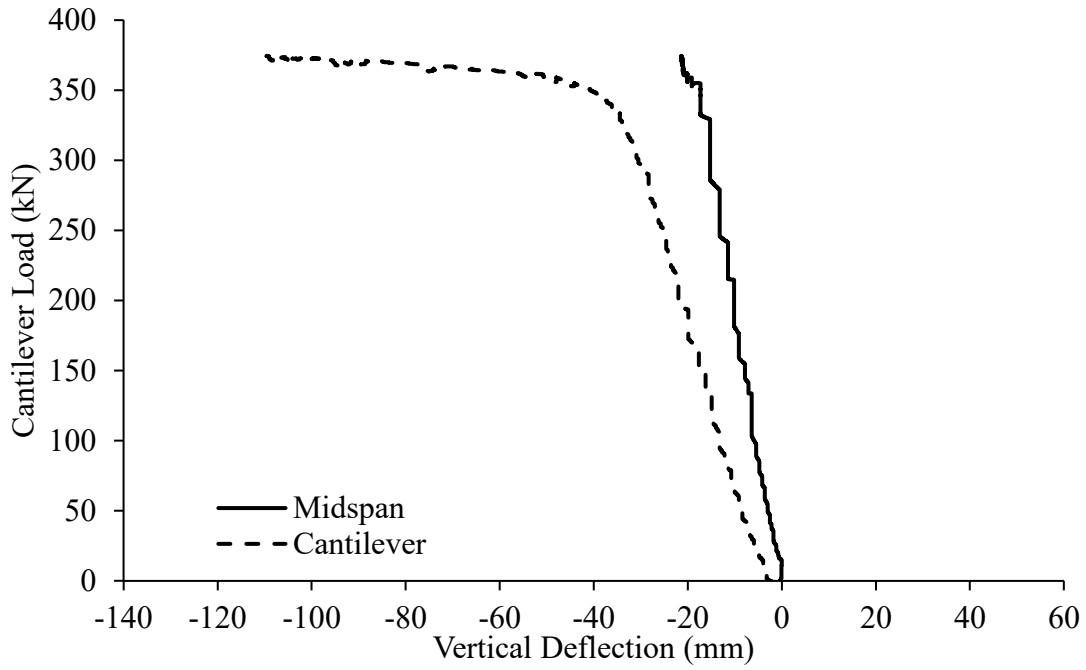


Figure C-21: Load-vertical deflection curves for LRC5-0.25

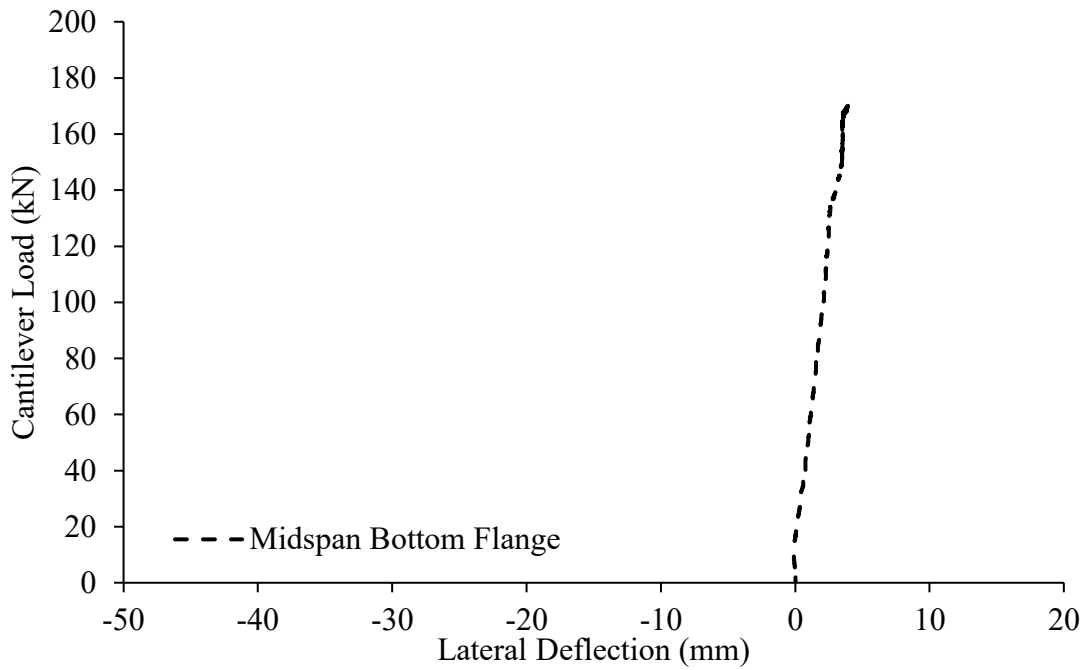


Figure C-22: Load-lateral deflection curves for midspan of back span for LRC4-0.80

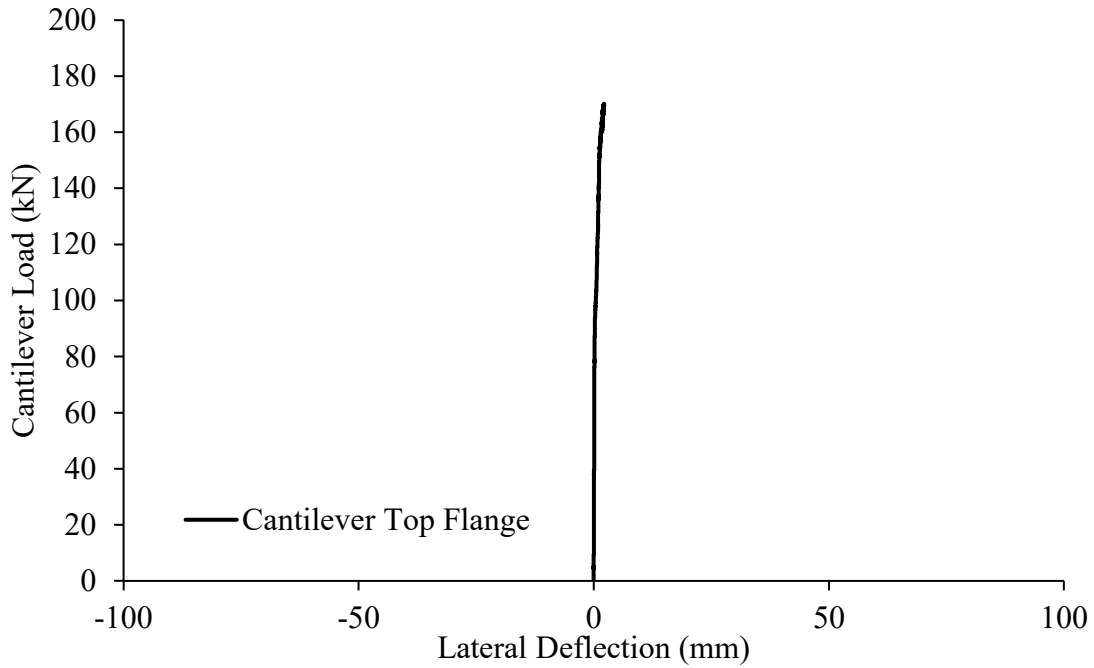


Figure C-23: Load-lateral deflection curves for cantilever for LRC4-0.80

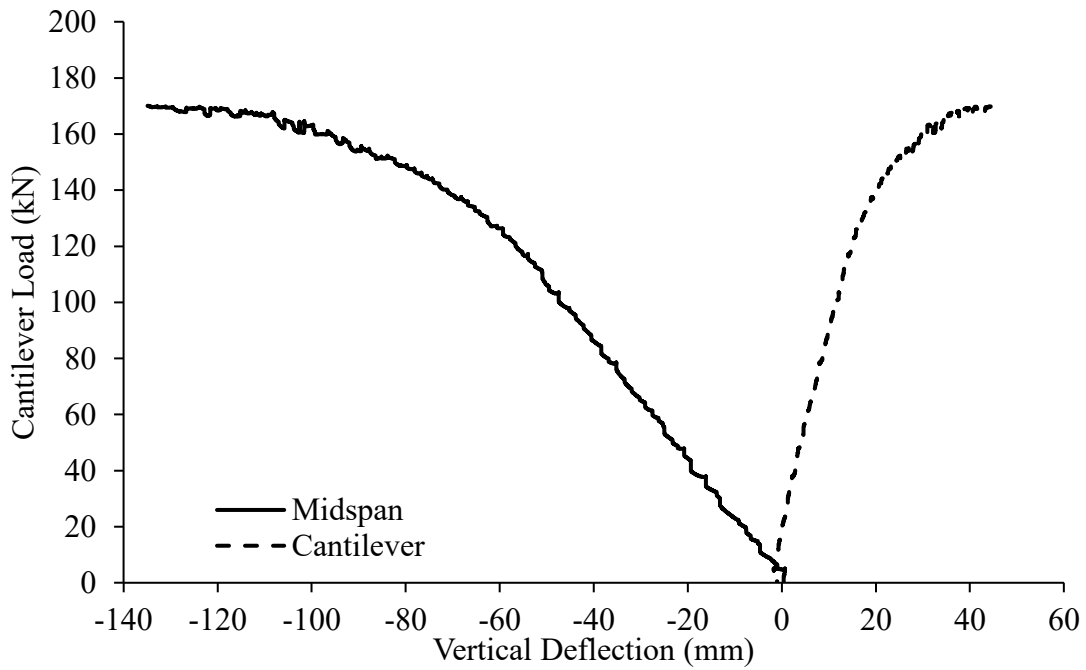


Figure C-24: Load-vertical deflection curves for LRC4-0.80

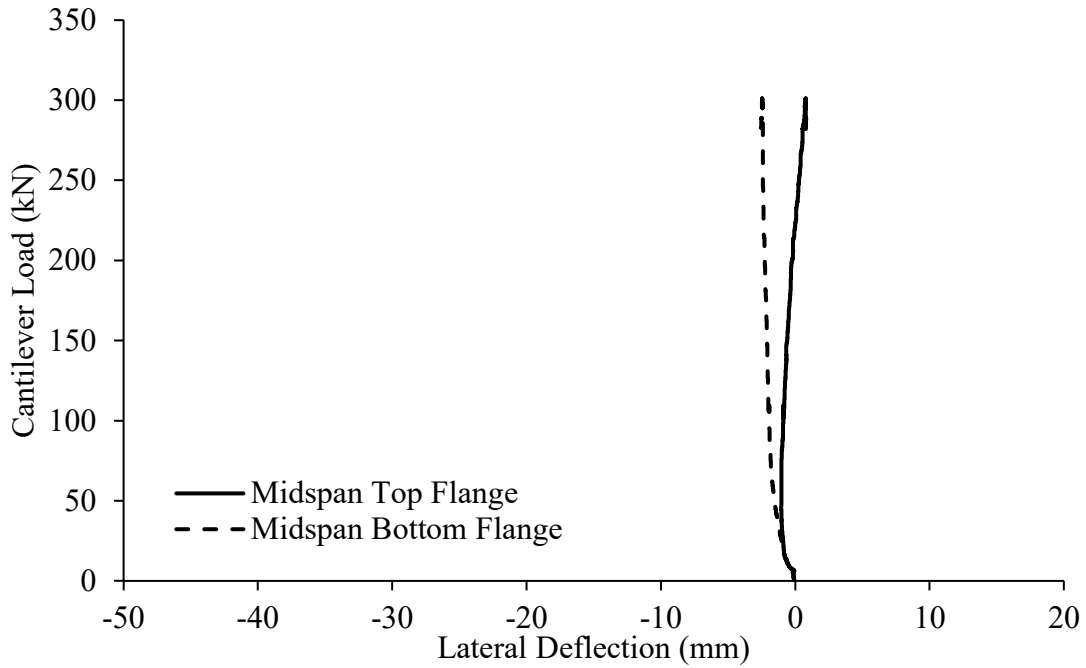


Figure C-25: Load-lateral deflection curves for midspan of back span for LRC4-0.38

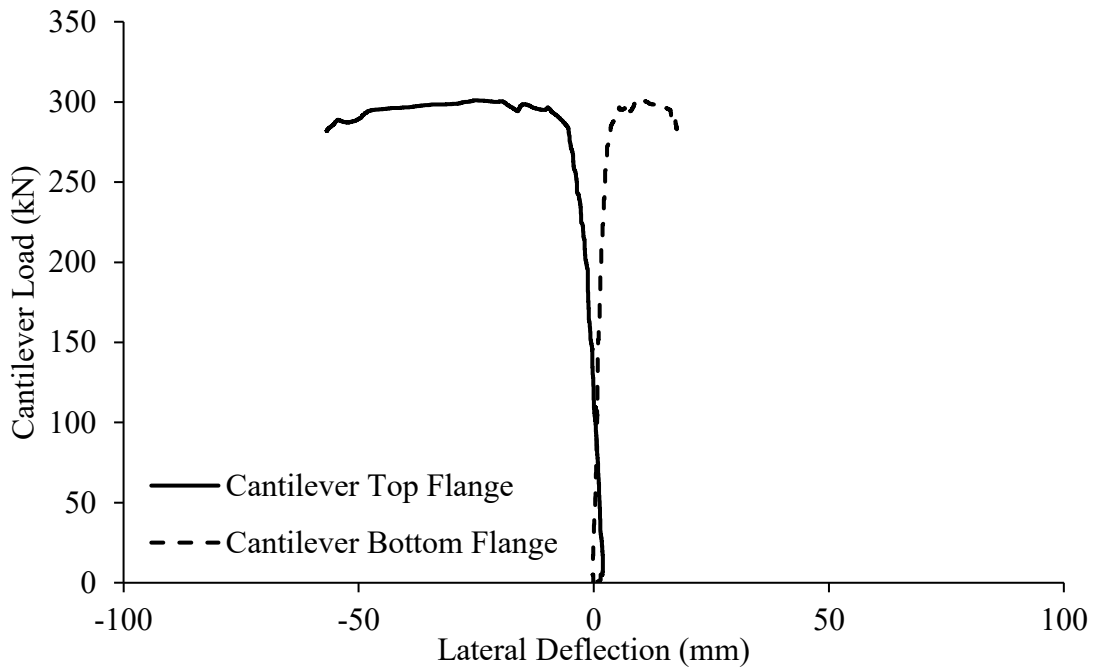


Figure C-26: Load-lateral deflection curves for cantilever for LRC4-0.38

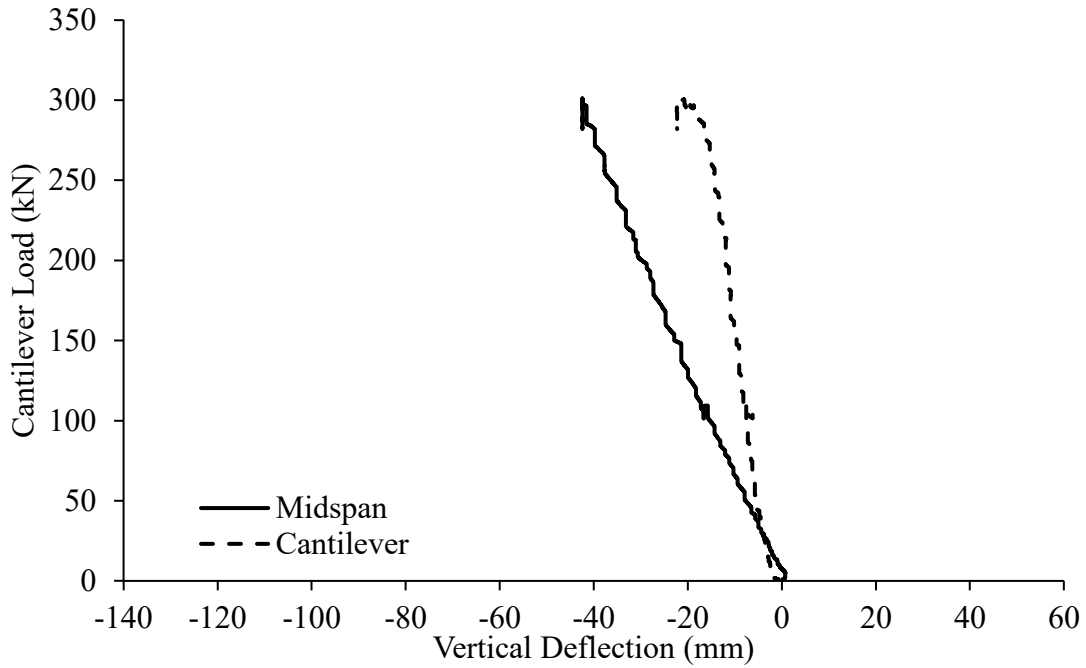


Figure C-27: Load-vertical deflection curves for LRC4-0.38

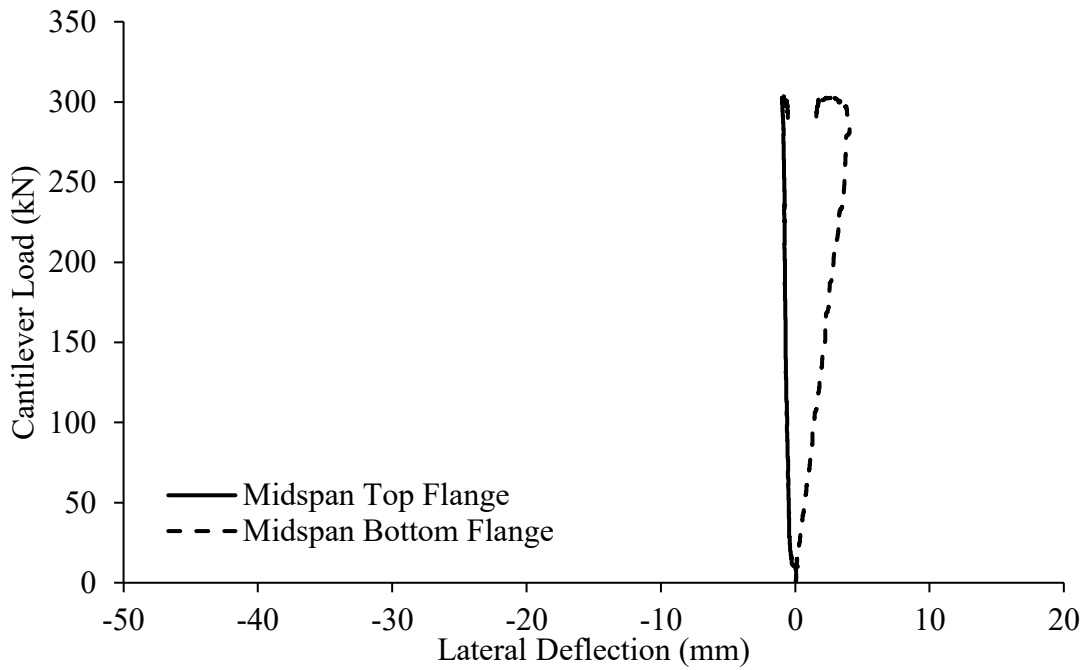


Figure C-28: Load-lateral deflection curves for midspan of back span for LRC4-0.25

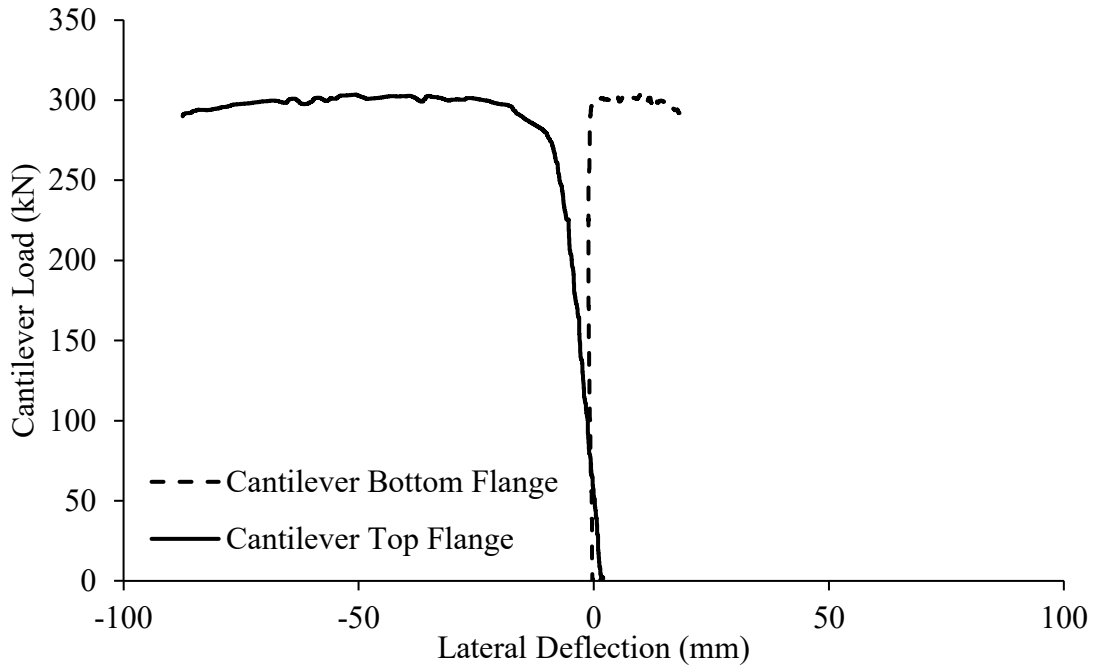


Figure C-29: Load-lateral deflection curves for cantilever for LRC4-0.25

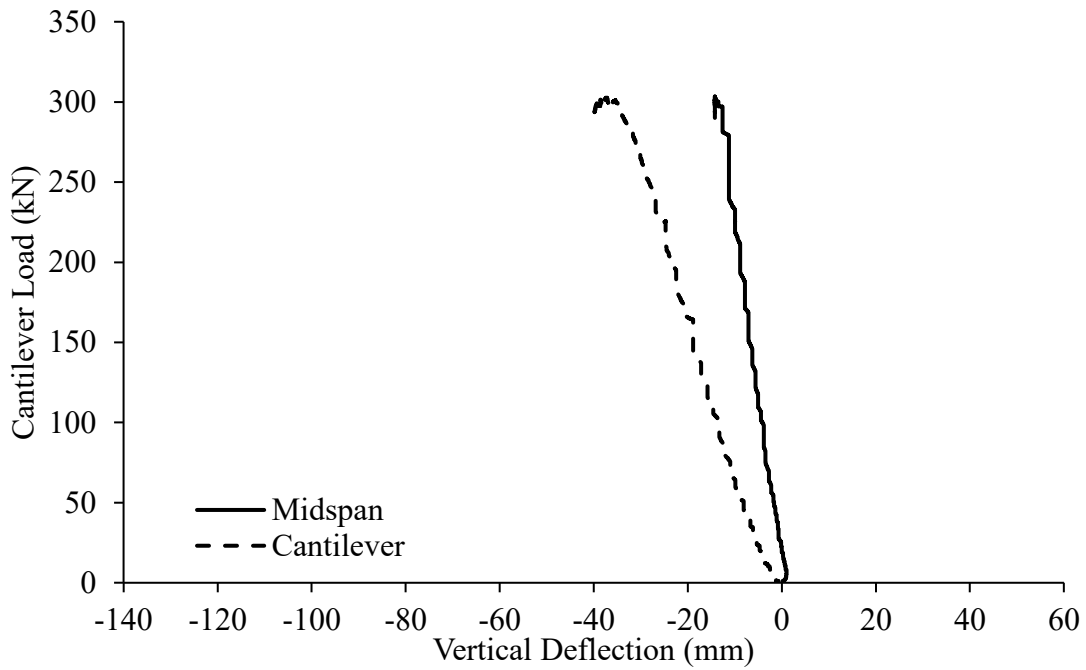


Figure C-30: Load-vertical deflection curves for LRC4-0.25

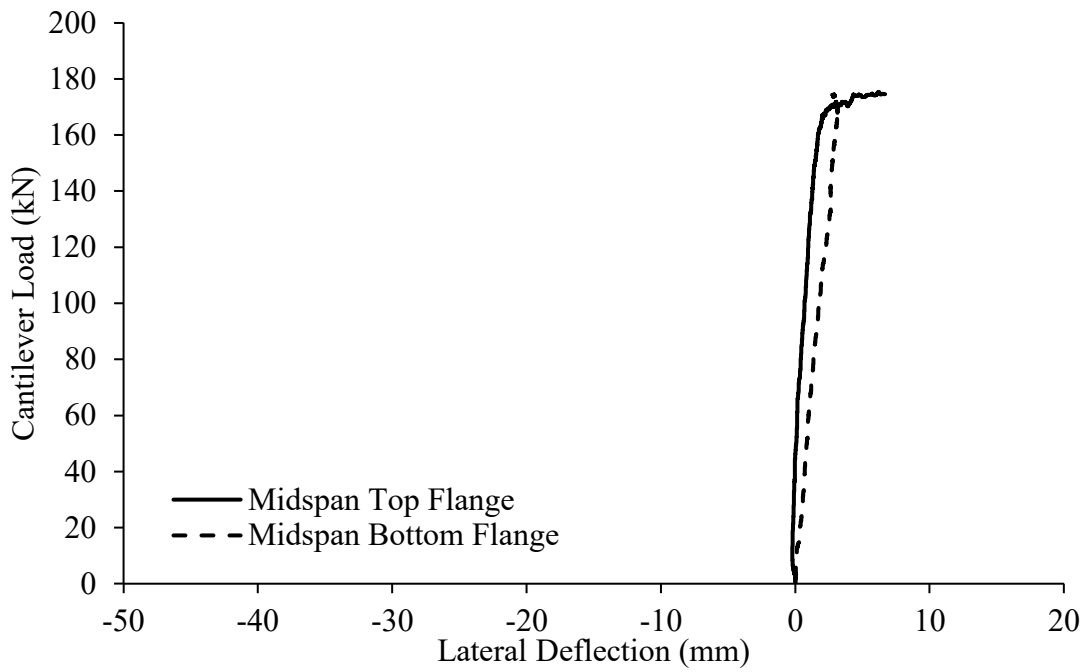


Figure C-31: Load-lateral deflection curves for midspan of back span for LRC1-0.80

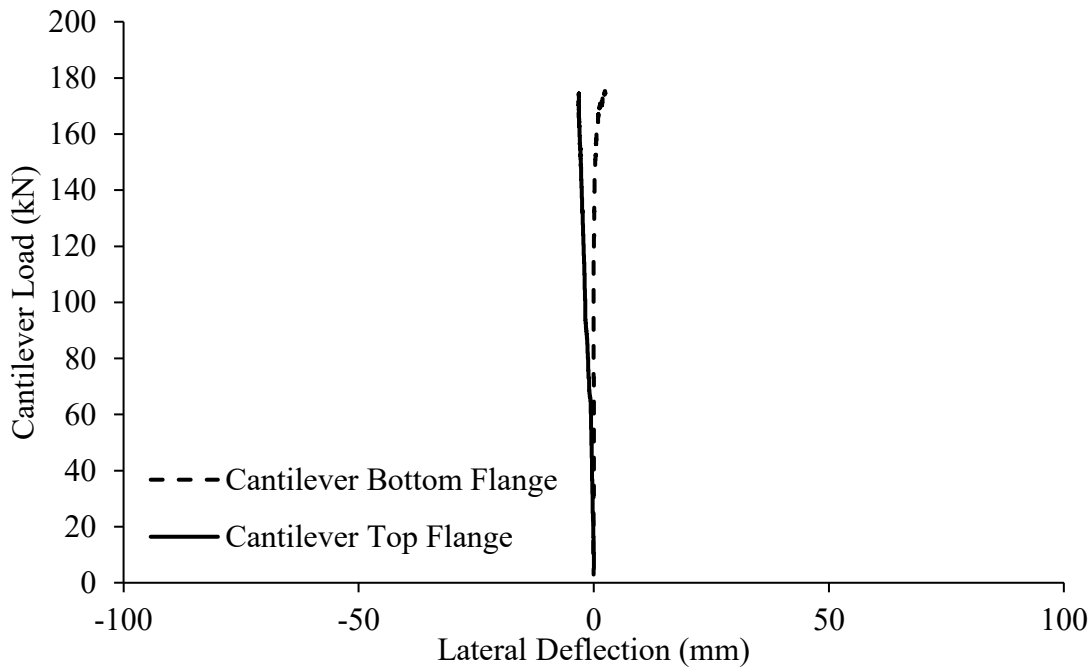


Figure C-32: Load-lateral deflection curves for cantilever for LRC1-0.80

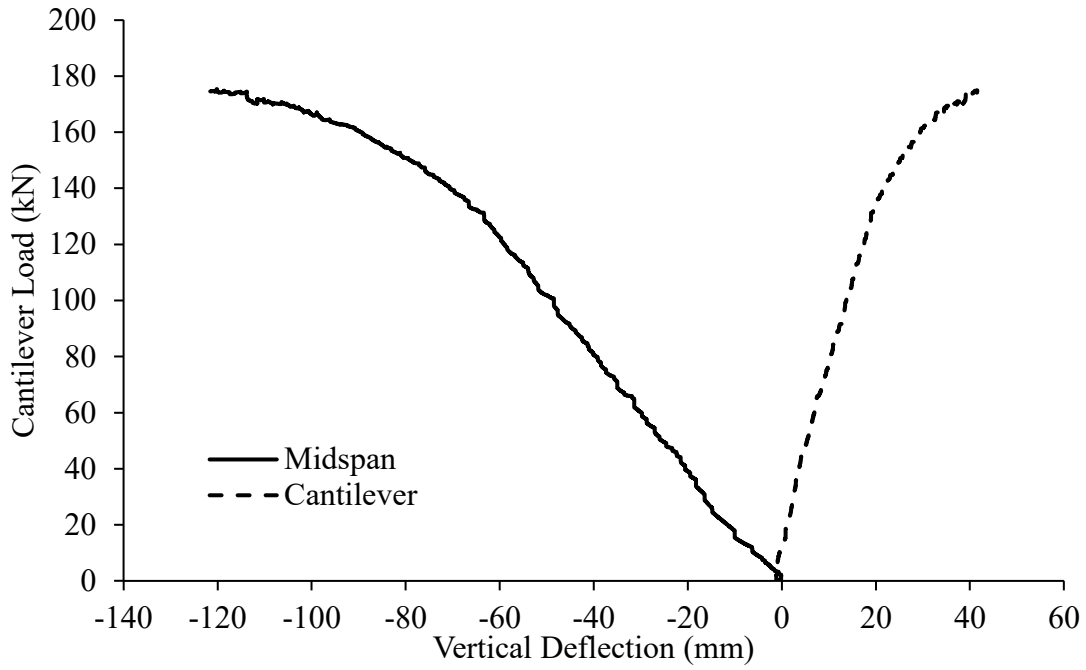


Figure C-33: Load-vertical deflection curves for LRC1-0.80

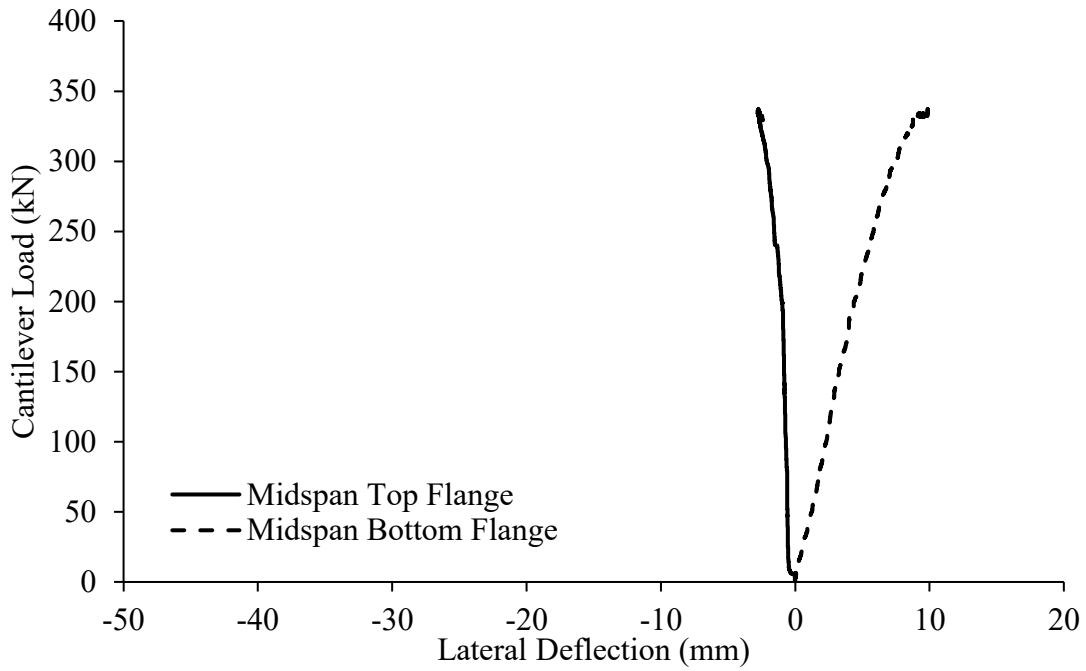


Figure C-34: Load-lateral deflection curves for midspan of back span for LRC1-0.38

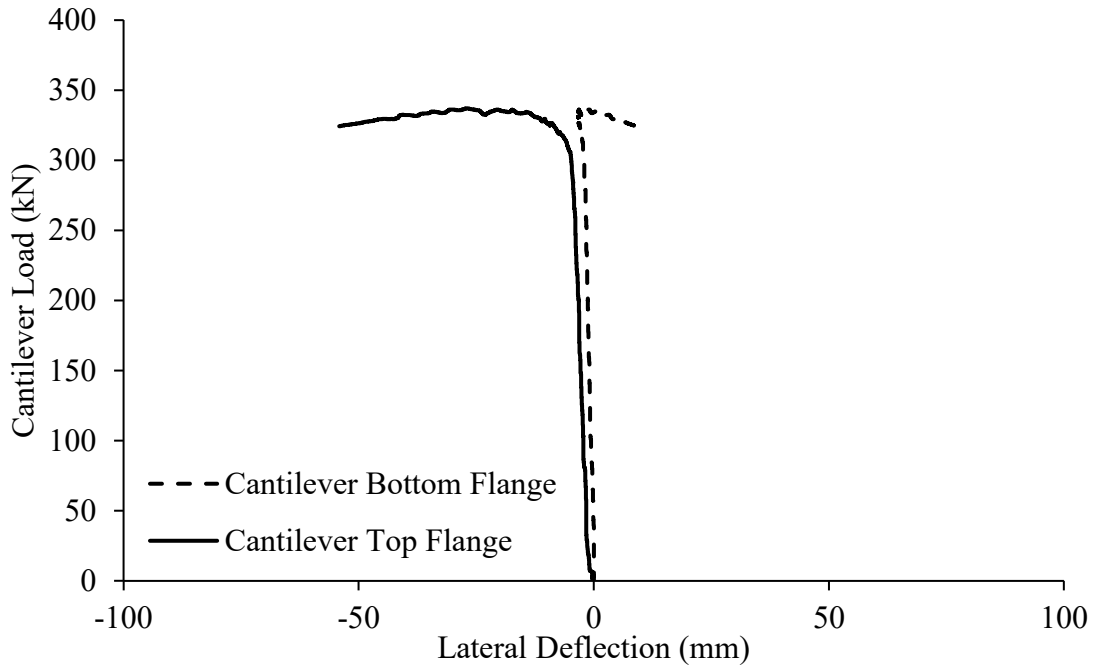


Figure C-35: Load-lateral deflection curves for cantilever for LRC1-0.38

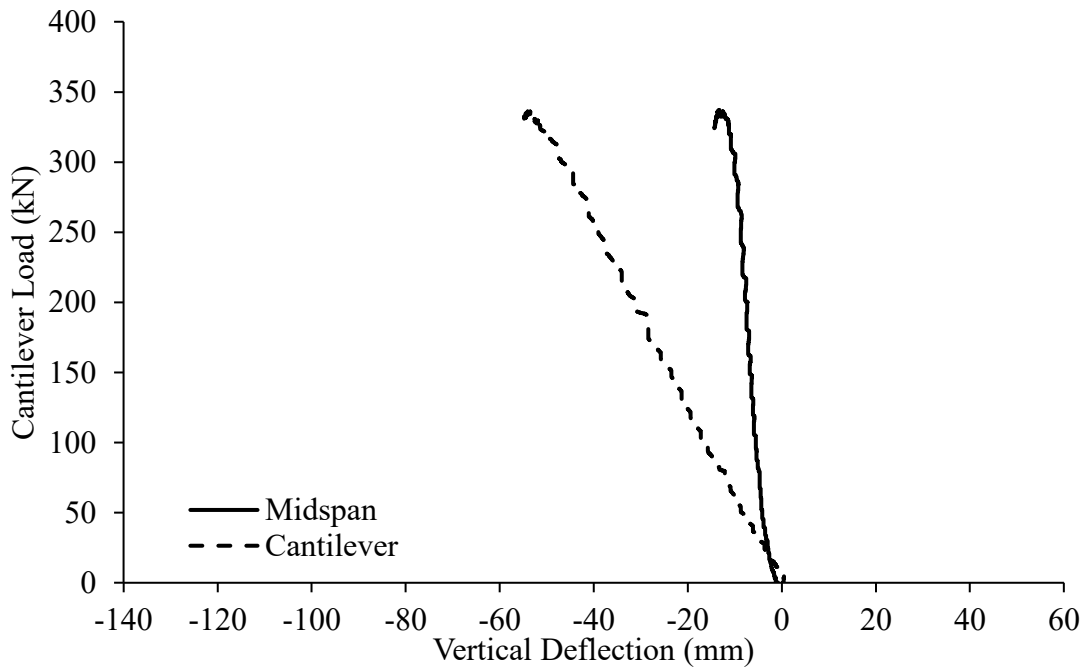


Figure C-36: Load-vertical deflection curves for LRC1-0.38

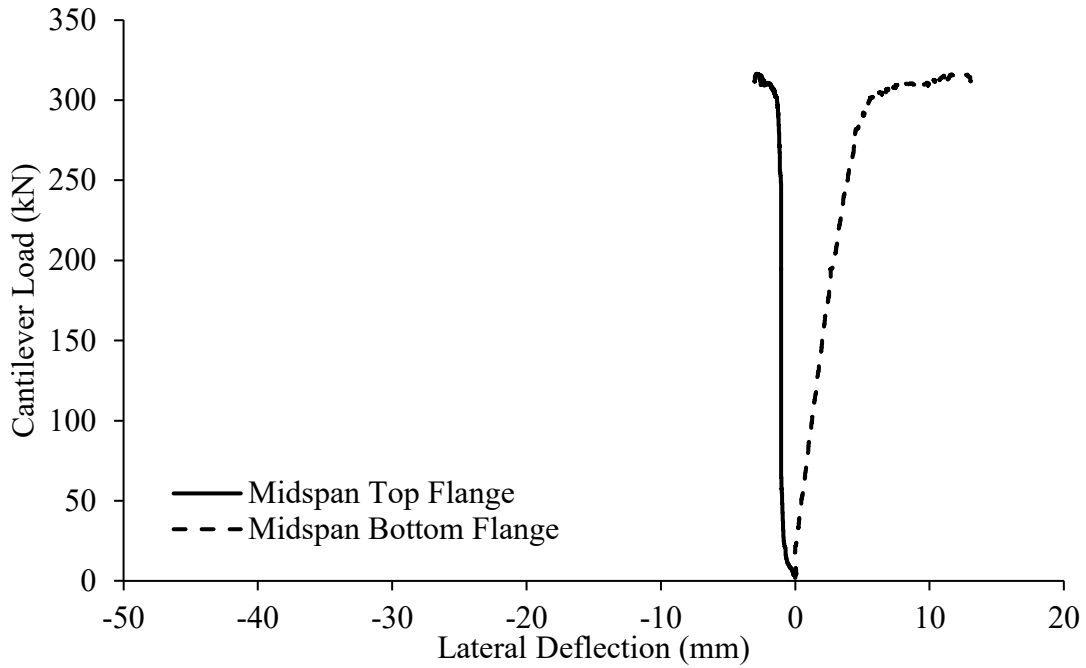


Figure C-37: Load-lateral deflection curves for midspan of back span for LRC1-0.38 Retest

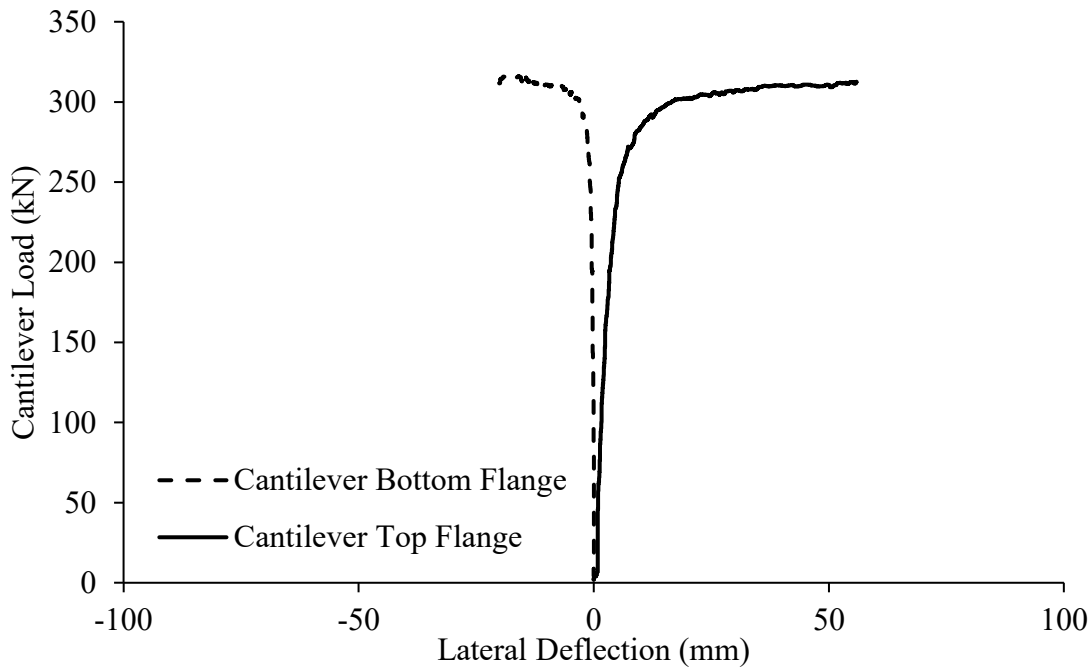


Figure C-38: Load-lateral deflection curves for cantilever for LRC1-0.38 Retest

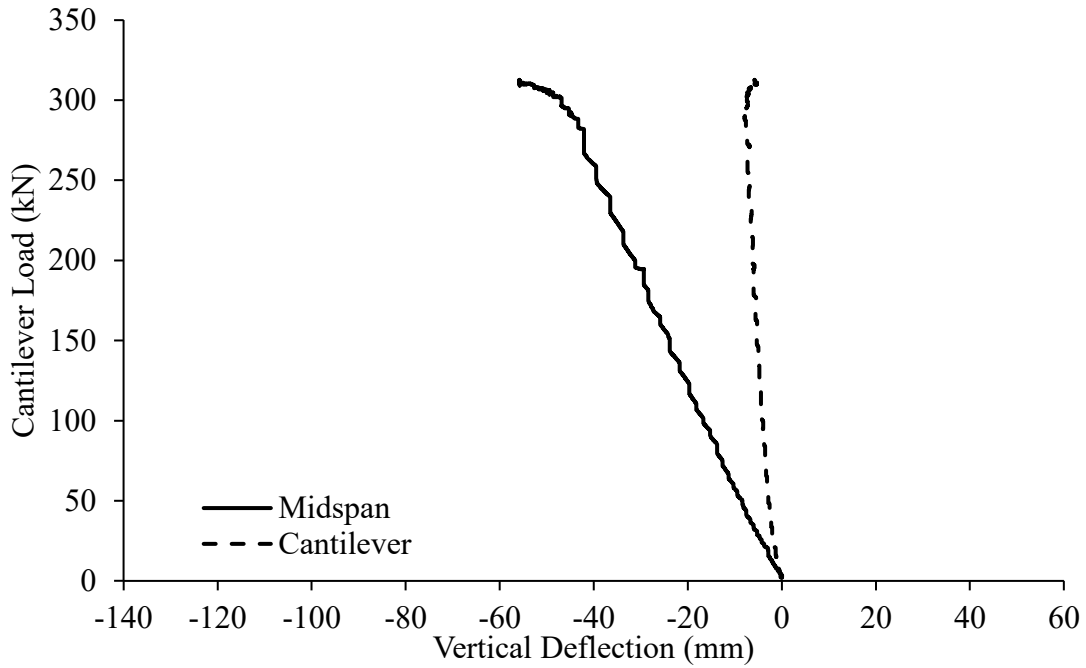


Figure C-39: Load-vertical deflection curves for LRC1-0.38 Retest

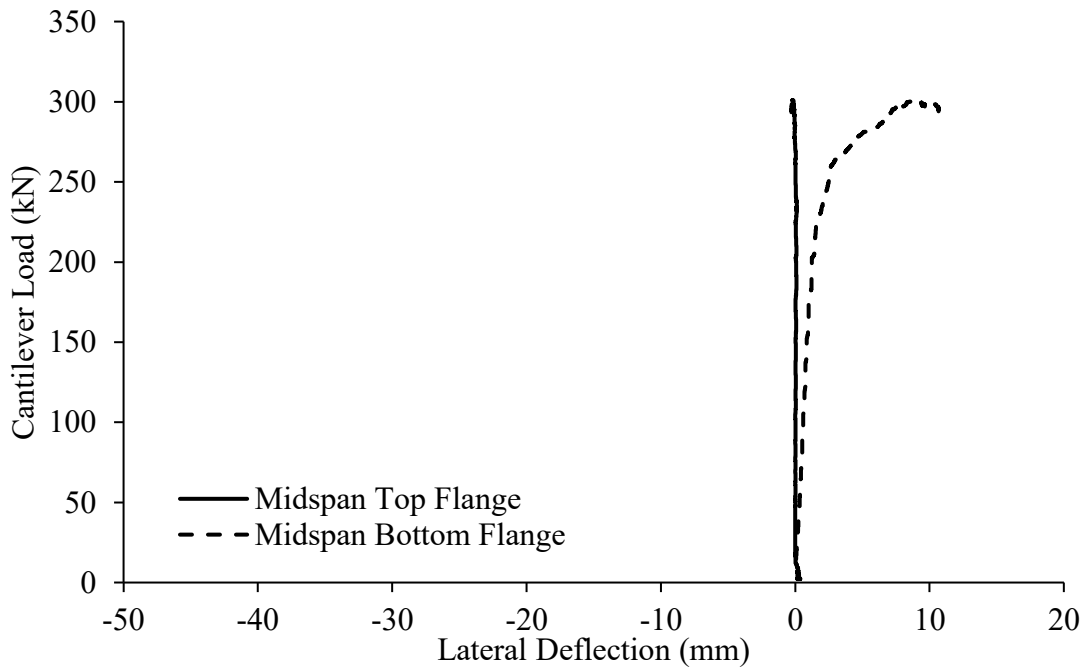


Figure C-40: Load-lateral deflection curves for midspan of back span for LRC1-0.25

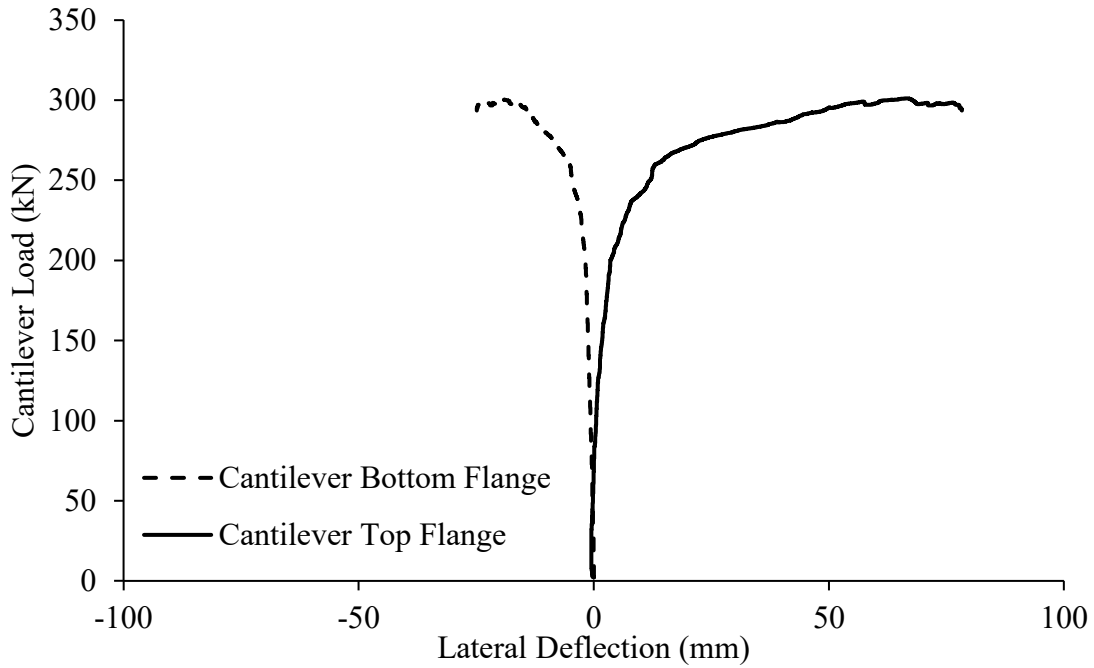


Figure C-41: Load-lateral deflection curves for cantilever for LRC1-0.25

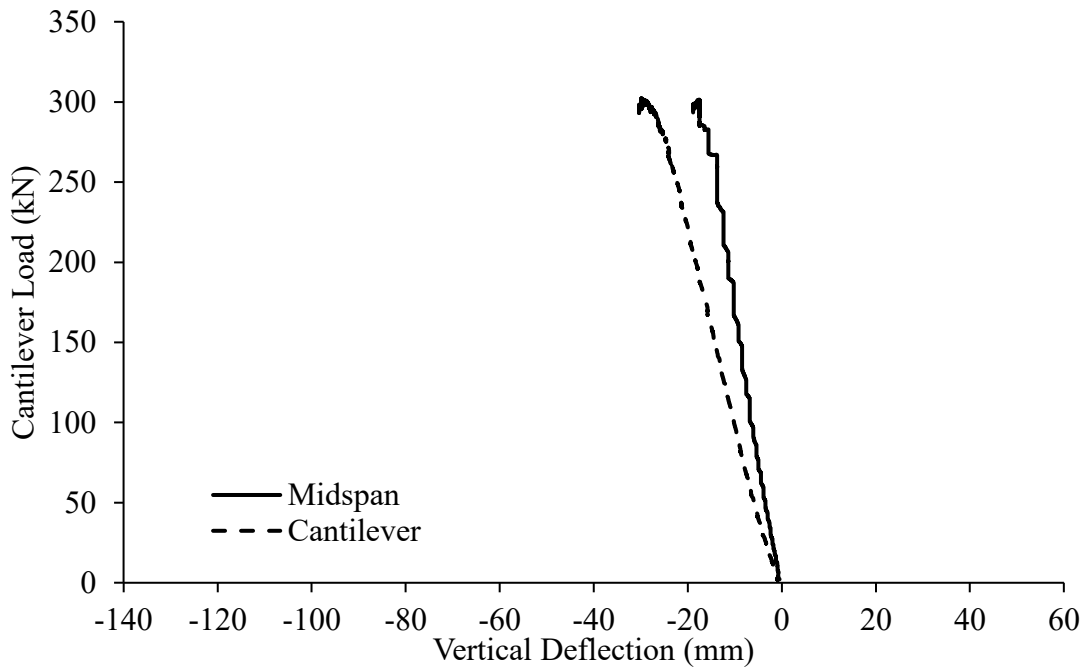


Figure C-42: Load-vertical deflection curves for LRC1-0.25